A steady-state self-consistent computer model of twin stripe double hererostructure semiconductor lasers.

Kumar, Tribhawan

Award date:
1985

Awarding institution:
University of Bath

A STEADY-STATE SELF-CONSISTENT COMPUTER MODEL

OF

TWIN STRIPE DOUBLE HETEROSTRUCTURE SEMICONDUCTOR LASERS

submitted by Tribhawan Kumar
for the degree of PhD
of the University of Bath
1985

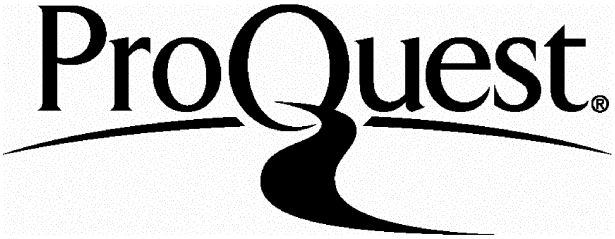

To the memory of my parents

CONTENTS PAGE

SUMMARY

Twin stripe laser structures show great promise in integrated optics systems. It has been demonstrated in the recent years that the optical interaction from such structures produce properties such as beam steering, pulse generation and bistability. The thesis describes a computer model of the lateral behaviour of such a device. The model takes into account current spreading in the p-type confining layer, the effect of lateral diffusion of carriers in the active layer and bimolecular and stimulated radiative recombinations in a self-consistent manner. The device operating below threshold becomes a special case and can be analysed without including the stimulated recombination effect in the full model. The assumptions made in this model are such that the results show the effect of quasi-Fermi level pinning above threshold due to gain saturation. Results for the single stripe laser are presented to compare with other existing models without any extra efforts. The thesis presents results of the optical field distributions of a twin stripe laser found consistent with the carrier density and current density distributions under variety of current injection conditions. The results predict the lateral movement of the optical field under asymmetric drive conditions which produce asymmetric variation of the complex dielectric constant of the active layer. The optical results are accompanied by the corresponding carrier and current distributions found consistently. The thesis also highlights the influence of device geometry and carrier diffusion on the optical behaviour of the device. The effect of stimulated recombination on the current spreading is also pointed out. The results show that the required modifications of the dielectric constant of the active layer to produce the near field shift and hence beam steering can be introduced by monitoring the current through the two electrodes.

ACKNOWLEDGEMENTS

The author wishes to express his gratitude to Dr. R.F. Ormondroyd and Professor T.E. Rozzi for their encouragement and supervision of this research project.

Thanks are also due to Dr. J. Sarma and Dr. K.A. Shore for their helpful discussions during this research programme.

Special thanks are also due to my wife Mrs. Neena Kumar for her moral support and encouragement.

Finally, the financial support which was made available by the university of Bath to the author is highly appreciated.

LIST OF PRINCIPAL SYMBOLS

The principal symbols used in this thesis are given below.

A_{cv}	Transition probability of spontaneous emission of an electron from the conduction band to the valence band
$\underline{a}$	Unit vector along the x axis
B_{cv}	Transition probability of stimulated emission of an electron from the conduction band to the valence band
B_{vc}	Transition probability of stimulated absorption of a photon
$\underline{B}$	Magnetic flux (vector quantity)
b	Normalized propagation constant
$\underline{b}$	Unit vector along the y axis
c	Velocity of light in a vacuum
$\underline{c}$	Unit vector along the z axis
$\underline{D}$	Electric displacement vector
D_e	Diffusion constant of electrons
D_h	Diffusion constant of holes
D_{amb}	Ambipolar diffusion constant
2d	Thickness of the central layer in a three-layer dielectric slab waveguide
e	Electronic charge
$\underline{E}$	Electric field intensity (vector quantity)
E_c'	Energy level within the conduction band of a semiconductor
E_c	Conduction band edge
E_v'	Energy level within the valence band of a semiconductor
E_v	Valence band edge
$E'=(E_c' - E_v')$	Energy difference
ΔE_c, ΔE_v	Conduction band and valence band discontinuities in a heterojunction energy band diagram
E_{g1}, E_{g2}	Energy gaps of the two semiconductors forming a heterojunction
F_o	Fermi level in thermal equilibrium

F_c	Quasi-Fermi level relative to the conduction band
F_v	Quasi-Fermi level relative to the valence band
f_{ce}	Probability of the conduction band level being occupied by an electron
f_{ve}	Probability of the valence band level being occupied by an electron
f_{ch}	Probability of the conduction band level being occupied by a hole
f_{vh}	Probability of the valence band level being occupied by a hole
g	Local gain coefficient
h	Planck's constant
$\underline{H}$	Magnetic field intensity vector
h_x	Horizontal step length in a finite difference mesh
h_y	Vertical step length in a finite difference mesh
I	Intensity of light
I'	Current in amperes
$\underline{J}$	Current density vector
J	Current density magnitude
j	Complex number $\sqrt{-1}$
J_{nom}	Nominal current density
J_o	Dark current in a diode
J_p	Hole current density
J_n	Electron current density
$\underline{k}$	Wave vector
k	Wave vector magnitude
k_B	Boltzmann constant
K	Extinction coefficient or imaginary part of a complex refractive index
L_c	Laser cavity length
L_e, L_h	Diffusion lengths of electrons and holes respectively
m_e, m_h	Effective masses of electrons and holes respectively

n	Refractive index (real quantity)
$\tilde{n}$	Complex refractive index
N	Carrier density
N_i	Normalization constant for the carrier density in numerical calculations
N_c	Density of states of the conduction band
N_v	Density of states of the valence band
n_{i1}, n_{i2}	Intrinsic carrier density in the material 1 and 2 respectively
n_p	Minority electrons in a lower band gap p-type semiconductor in a heterojunction
n_N	Majority electrons in a larger band gap n-type semiconductor in a heterojunction
n_{po}, n_{NO}	Thermal equilibrium electron concentrations in a lower band gap p-type and a larger band gap n-type semiconductors respectively
P	Total optical power
p_N, p_p	Hole concentrations in a larger band gap n-type and a lower band gap p-type semiconductors in a heterojunction
p_{NO}, p_{po}	Hole concentrations under thermal equilibrium in a larger band gap n-type and a lower band gap p-type semiconductors in a heterojunction
$P'(E')$	Density of photons of energy E'
$\underline{r}$	Position vector
R	Coupling parameter between gain and refractive index guidance
$r_{sp}(E')$	Spontaneous emission rate in a semiconductor
$R_{st}(E')$	Stimulated emission rate in a semiconductor
$r_{stim}(E')$	Net stimulated emission rate in a two energy level system
$r'_{stim}(E')$	Stimulated emission rate in a two energy level system
$r_{abs}(E')$	Net rate of absorption in a two energy level system
$r'_{abs}(E')$	Absorption rate in a two energy level system
$r'_{sp}(E')$	Spontaneous transition rate in a two energy level system
R_{mode}	Reflection coefficient of cavity mirrors for a given mode
S_o	Photon density in a laser cavity
S_z	Z component of the optical power

t	Active layer thickness
V	Potential
V_{bi}	Built-in potential
V_{DB}	Potential at the diode boundary
V_{rms}	Root mean square potential
VS_1, VS_2	Applied potentials on the two stripes of a twin stripe laser
v	Normalized frequency
v_c	Cut-off frequency of a mode
W	Stripe width/scaling factor for the field normalization
α	Absorption coefficient
β	Propagation constant (real quantity)
$\tilde{\beta}$	Complex propagation constant
μ	Permeability of a medium
μ_o	Permeability in a free space
ε	Dielectric constant (real quantity)
ε_r	Relative dielectric constant
ε_o	Free space dielectric constant
$\tilde{\varepsilon}$	Complex dielectric constant
ω	Angular frequency
λ	Wavelength in a free space
Γ	Confinement factor
σ	Conductivity of the material
α_{mode}	Cavity loss suffered by a propagating mode
ψ	Unnormalized lateral field profile in the active layer
Ψ	Normalized lateral field profile
θ, θ'	Over-relaxation parameters in numerical calculations
Θ	Under-relaxation parameters in calculations

CHAPTER I

INTRODUCTION

1.1 Introductory Remarks

There has been tremendous growth in the development of optical fibre communications systems since 1970 following the invention of the laser light source in 1958 (1), the semiconductor laser (2 - 4) and the development of low loss optical fibres (5). As part of these developments there is now considerable interest being shown in novel semiconductor lasers which have optical properties such as bistability (6 - 9), short optical pulse generation (10) and beam steering (11). Optical amplification, and optical coupling are also being actively researched. In particular, multi-stripe lasers have been found to exhibit many of the properties listed above. However, the geometry of the multi-stripe laser plays an important part in the ultimate application of the device, and the lateral mode behaviour of the laser is so sensitive to changes in geometry that it becomes essential to develop a computer model of the device in order to fully appreciate its behaviour. This allows a wide range of controlling parameters to be changed systematically to show their relative importance in controlling the modal behaviour of the device, and this allows the design to be optimised in a more efficient way than by the fabrication of a wide range of multi-stripe lasers.

The work reported in this thesis is concerned with the development of a computer model which describes the lateral behaviour of the optical modes of multi-stripe GaAs/AlGaAs double heterostructure lasers. In particular, the oxide isolated single-stripe laser and the closely coupled parallel twin-stripe laser shown in figures (1.1-1) and (1.1-3) respectively, will be considered. In such devices a narrow active region where the recombination of carriers takes place is sandwiched by two larger band-gap AlGaAs semiconductor layers. This restricted width of the active layer by the heterojunctions helps to minimise the threshold current density as shown in figure (1.1-2). A feature of the model is

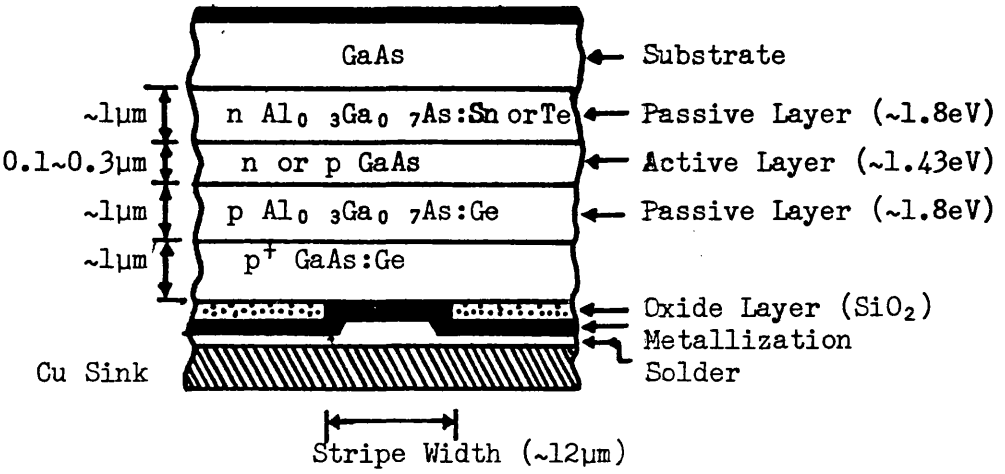

Figure 1.1-1 Single stripe laser mounted on a copper heat sink drawn not to scale.

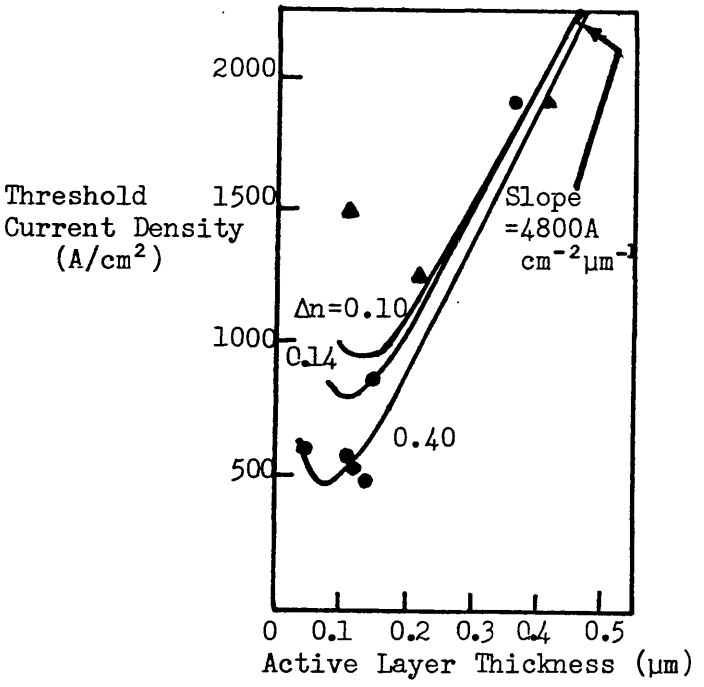

Figure 1.1-2 Threshold current density as a function of active layer thickness. The theoretical curves for the refractive index discontinuities Δn shown. The experimetal points are for Al concentration steps Δx of 0.2 (▲) and 0.65 (●). (Assumed Δn=0.62Δx

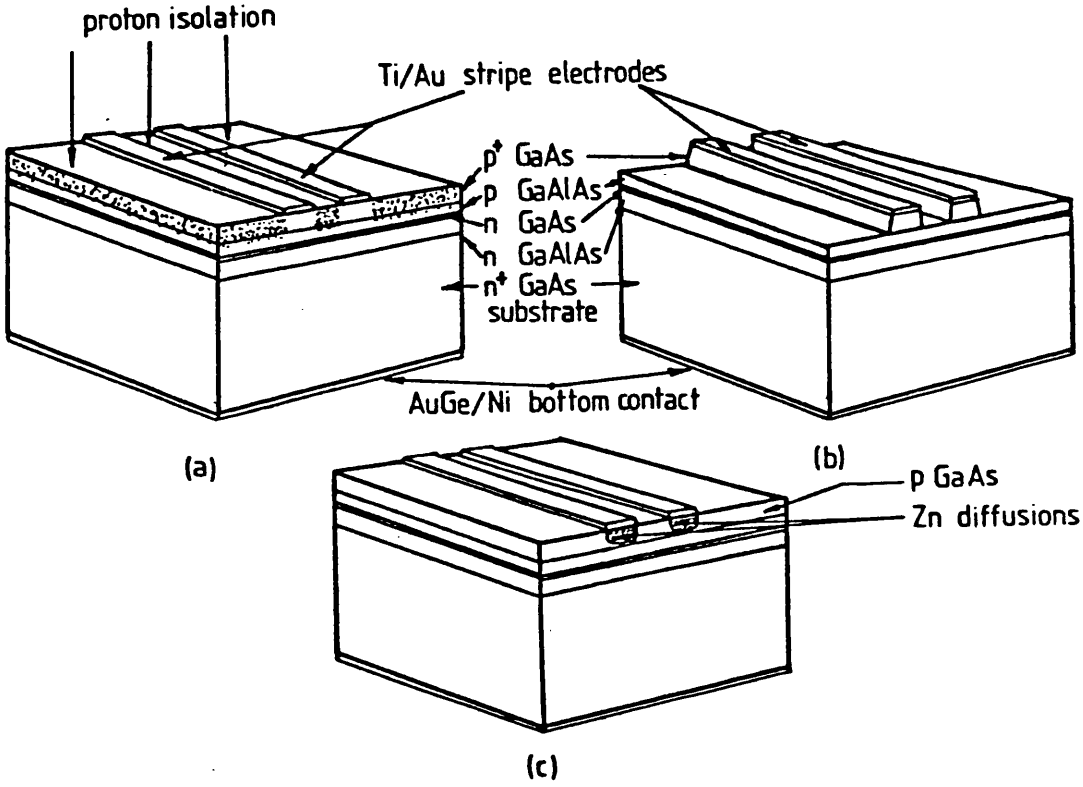

Figure 1.1-3 Twin-stripe laser structures showing how lateral current spreading in the p^+ GaAs capping layer may be minimised

a) Proton isolation

b) Removing unwanted GaAs capping layer

c) Semi-insulating GaAs with diffused stripe contacts

that it solves the carrier distribution in the active layer of the laser in a fully self-consistent way with the interacting optical field, current spreading and carrier diffusion. Because of this a more realistic model of the modal behaviour of lasers has been possible. In particular it has been possible to model the beam steering behaviour of the optical field of the twin-stripe laser structure, which has been the underlying aim of this work. Self-consistent solution of the optical field intensity and carrier density distribution is necessary because the two are linked by the stimulated recombination coefficient, such that a high optical output stimulates a higher level of carrier recombination which in turn reduces the optical gain producing the radiated field.

In the next section of the chapter the historical developments of optical communications systems, and in section (1.3) a brief outline of the thesis will be presented.

1.2 Historical Developments of Optical Systems

The desire to communicate messages over large distances has been of fundamental importance to Man since the earliest times, and he has striven to increase both the rate at which messages are transmitted and the distance over which they are transmitted. To this end, optical techniques were used for over 2000 years. Initially, this was only for sending alarms or announcing specific events via a rudimentary line-of-sight binary channel using beacon fires, the meaning of the signal being prearranged between the sender and receiver. The Greeks were reputed to be the first to use this technique as early as 800 BC. However, by 150BC techniques were being developed to encode the optical signal according to the alphabet to allow any message to be sent. Refinements on the basic idea continued until the end of the 19^{th} century with the development of Bell's photophone. The optical channel was unreliable however relying

upon the human eye and atmospheric effects such as fog and rain.

The development of the telegraph by Morse in 1838 marked the start of a new era in communications - electrical communications, and the widespread use of a telephone system quickly followed. Wire-less communication was demonstrated by Marconi in 1895 and this was a major advance, enabling mobile communications and broadcast communications to be made over wide areas of coverage. Since then an increasingly large proportion of the electromagnetic spectrum has been used for conveying information from one place to another using the technique of modulation; whereby the message to be transmitted is superimposed onto a sinusoidally varying electromagnetic carrier wave. As the need to transmit information has increased, great demands have been placed on wire and cable networks and on the electromagnetic spectrum. Thus, the trend has been to employ progressively higher frequencies in the spectrum, which has the added benefit of allowing larger transmission bandwidths and an increased information capacity.

Since the advent of laser optical sources in the infrared region of electromagnetic spectrum in 1958 and their subsequent realisation (4,12), serious interest in optical communication was rekindled. This device provided highly monochromatic and coherent radiation of a type similar to the radiation produced by a microwave generator, rather than the type produced by a fluorescent light source. It thus appeared that this source capable of handling information over a much wider bandwidth could be modulated at higher rates and used in much the same way as an electrical r.f. sources. Early optical systems were based on line-on-sight communications because of the highly directional nature of the transmitted light. However, it soon became apparent that for widespread communication networks such systems were hopelessly inadequate, and some form of guiding

structure would remove the constraints placed on the line-on-sight systems. (Satellite-Satellite and Satellite-Submarine line-on-sight communication systems are, however, in current development).

Concurrent with these developments was research into optical fibre guides. Despite the high attenuation of early optical fibres, Kuo and Hockman (13) were first persons to realise that optical fibre communication systems were perfectly feasible if the losses could be reduced to 20dB/km. In 1970 this was achieved by Kapron et al (14). Current development of fibres has further reduced the attenuation to 0.2dB/km at 1.55μm. However, to achieve these figures it was necessary to tailor the wavelength of the laser source to match the 'window' of minimum attenuation of the fibre material. The semiconductor injection laser, based on GaAs was developed after the gas laser in 1963 (2 - 4), however the early homojunction lasers had such high threshold currents as to make them impractical for room-temperature operation. The major breakthrough in optical communications systems occurred with the development of the GaAs/$Al_xGa_{1-x}As$ double heterostructure laser which could be operated at room-temperature at much reduced threshold current density.

With the development of the practical double heterostructure laser, and improved fibre technology, the development of optical fibre communications systems gathered momentum and since then there have been a great many significant technological developments in light sources, the fibre and photodetectors. GaAs is now no longer the only useful material from which lasers may be fabricated, but devices based on InP/InPGaAs heterostructures have been developed which covers the wide range of wavelengths 0.92μm - 1.65μm including the wavelength corresponding to the lowest loss and dispersion region of silica fibre.

The result has been the development of a transmission system that has certain inherent advantages over conventional copper wire systems. Now, optical fibres have lower transmission losses and for a wider bandwidths when compared with copper wires. The fibres have a very small cross-section, light-weight and their very wide bandwidths allow very high information rates. Furthermore, the fibres have a high immunity to electromagnetic interference and freedom from electromagnetic pulse problems. They are also electrically isolated and cross-talk between adjacent fibres is low. Finally, silica, the principal material, from which high quality fibres are made, is abundant and inexpensive.

There are now many hundreds of thousands of kilometers of optical fibre telephone, cable TV and data systems in service throughout the world. Nevertheless research into improved optical sources, detectors and fibres and fibre interconnections is continuing at a high pace. Of current interest is the development of a wide range of novel optical sources. Some of these developments have concentrated on producing lasers with a high degree of optical coherence for single mode coherent modulation schemes, such as the external cavity laser (15) and the distributed feedback laser (16). However, there is also a growing interest in optically coupled multi-stripe lasers because of their possible novel applications such as optically and electrically controlled bistability (6 - 9), ultra-short optical pulse generation (10), beam steering (11) and coherent combination of the power of laser arrays (17). Ultimately these developments may lead to an integrated optics system for optical signal processing, optical routing of modulated signals and optical logic applications.

1.3 Outline of the Thesis

A brief introduction to semiconductor injection lasers is presented in chapter II. Here the Einstein coefficients and the necessary conditions

for lasing are derived. The laser gain and its dependence on the doping of the semiconductors are also discussed together with the threshold condition for amplification in a cavity resonator. Heterojunctions, which are formed when two semiconductors with different energy gaps are joined to form a p-n junction, are also introduced in this section and the various properties of heterojunctions, and their advantages over homo-junctions are presented

One of the most important aspects in the understanding of the semiconductor laser is the optical waveguide formed in the active layer which determines the modal behaviour of the device. This is discussed in chapter III. In the double heterostructure laser the active layer is quite thin (0.1μm - 0.3μm) and is sandwiched between cladding layers of material having a lower refractive index, so that a dielectric waveguide is formed perpendicular to the active layer. The idea of effective dielectric constant is also introduced in this chapter. In the lateral direction of the active layer, however, the carriers are free to diffuse laterally. In this direction the complex dielectric constant of the active layer varies as a function of the carrier density. It is explained in chapter III how the complex dielectric constant profile provides a weak guidance of the optical field in the lateral direction. The guidance of the wave in the lateral direction is very important in determining the stability of the device.

In chapter IV the past work of multi-stripe geometry lasers is reviewed and the outline of the model adopted in this thesis is given.

Chapter V presents a simple model of the electrical behaviour of the twin stripe laser. A summary of this work appears in reference (18). This chapter emphasises the need to take into account the effect of

current spreading from the electrodes through the confining layer of a heterojunction laser to the active layer. Current spreading reduces the level of the current injected into the active layer quite considerably, but perhaps more important is the fact that results in a broadening of the current density distribution. In multi-stripe lasers this broadening of the injected current density distribution effectively couples the electrodes, and its effect is particularly important.

The presence of the non-linear heterojunction influences current spreading in the cladding layer. In this chapter the heterojunction is modelled by a series of diodes along the active layer and the two dimensional potential distribution in the cladding layer is found subject to this boundary condition. The chapter considers the current density distribution problem of a twin stripe laser, and examines the effect on the distribution of applied potential, interstripe coupling via the cladding layer and the geometrical factors of cladding layer thickness, electrode width and spacing.

Lateral diffusion of the carriers in the active layer and bimolecular recombination are other important factors in addition to the non-linear heterojunction. In chapter VI the effect of lateral carrier diffusion on the carrier density distribution and the current density distribution is examined. In this chapter the non-linear heterojunction is modelled using the quasi-Fermi level separation in the active layer to calculate the carrier density distribution, rather than via a simple diode model. In this model the current in the cladding layer is coupled to the lateral diffusion equation in the active layer via the quasi-Fermi level separation, however, it is clear that the problem must be solved consistently and the procedure used is outlined in the chapter.

The results give the distribution of spontaneous radiation. However, since the effect of stimulated recombination is not included the model is only valid upto the threshold condition. In chapter VII the effect of stimulated recombination is included in the diffusion equation. This requires the solution of the optical waveguide equation in the lateral direction subject to the condition of a complex dielectric constant profile laterally, from this the optical intensity can be calculated. The optical intensity affects the carrier density which produces the gain, and so it is necessary to solve the optical problem self-consistently with the carrier density distribution and the current spreading problem. The chapter highlights the effects of stimulated recombination on the current spreading and the stability, the effect of gain-guidance and anti-guidance on the stability of the device. The chapter also considers the effect of symmetrical and asymmetrical pumping on mode stability and the shift in the near field of light output.

In the final chapter VIII, the conclusions of the self-consistent model of the twin stripe laser are presented and suggestions for further work are made.

References

1. A. Schwalow and C. Townes: "Infrared and optical masers", Phys. Rev., Vol.112, p1940, 1958.

2. H. Kroemer: "A proposed class of heterostructure injection lasers", Proc. IEEE, Vol.51, p.1782, 1963.

3. R.N. Hall, G.E. Fenner, J.D. Kingsley, T.J. Soltys and R.O. Carlson: "Coherent light emission from GaAs junctions", Phys. Rev. Lett., 9, pp.366-368, 1962.

4. H. Kessel, I. Ladany, M. Ettenberg and H. Lockwood: "Lightwave communications: Light sources", Physics Today, pp.38-47, May 1976.

5. T. Miya et al: "An ultimate low loss single mode fibre at 1.55μm", Electron. Lett., Vol.15, pp.106-108, 1979.

6. T.G. Dziura and D.G. Hall: "Bistable operation of two semiconductor lasers in an external cavity: rate-equation analysis", J. IEEE Quantum Electron. Vol. QE-19, pp.441-448, 1983.

7. K.A. Shore: "Semiconductor laser bistable operation with an adjustable trigger", Opt. and Quantum Electron., Vol. 14, pp.321-326, 1982.

8. P. Glas and R. Muller: "Bistable operation of a GaAs-GaAlAs diode laser coupled to an external resonator of narrow spectral bandwidth", Opt. and Quantum Electron., pp.375-389, 1982.

9. K.A. Shore, N.G. Davies and K. Hunt: "Constant power contours and bistability in twin stripe lasers", Opt. and Quantum Electron., Vol.15, pp.547-548, 1983.

10. I.H. White, J.E. Carroll and R.G. Plumb: "Closely coupled twin-stripe lasers", Proc. IEE, Vol.129, Pt.I, No.6, pp.291-296, 1982.

11. D.R. Scifres, R.D. Burnham and W. Streifer: "Beam scanning with twin stripe injection lasers", Appl. Phys. Lett., Vol.33, pp.702-704, 1978.

12. T.H. Maiman: "Stimulated optical radiation in ruby", Nature, Vol.187, p.493, 1960.

13. K.C. Kao and G.A. Hockman: "Dielectric fibre surface waveguides for optical frequencies", Proc. IEE, Vol.133, p.1151, 1966.

14. F.P. Kapron, D.B. Beck and R.D. Maurer: "Radiation losses in glass optical waveguides", Appl. Phys. Lett., Vol.17, pp.423-425, 1970.

15. K.J. Ebeling, L.A. Coldren, B.I. Miller and J.A. Rentschler, Electron. Lett., Vol.18, p.901, 1982.

16. L.D. Westbrook, A.W. Nelson, P.J. Fiddyment and J.S. Evans, Electron. Lett., Vol.20, p.225, 1984.

17. D.E. Ackley and R.W.H. Engelmann: "High-power leaky-mode multiple-stripe lasers", Appl. Phys. Lett., Vol.39, pp.27-29, 1981.

18. T. Kumar, R.F. Ormondroyd and T.E. Rozzi: "Interstripe coupling and current spreading in a subthreshold double heterostructure twin stripe laser", IEEE J. Quantum Elcetron., Vol. QE-20, pp.364-373, 1984.

CHAPTER II

SEMICONDUCTOR LASER PRINCIPLES

2.1 Introduction

In this chapter the basic principle of a laser system and the necessary conditions required for lasing action to occur, are described. In a simple gas lasing system the gas atoms can be described in two energy states- the ground state and the excited state. An incident photon of correct energy can be absorbed causing an atom in the ground state to go to the excited state. This process is known as stimulated absorption. The excited atom has a tendency to relax back to the ground state emitting a quantum of energy equal to the difference between the two energy states. Emission can occur in two possible ways. Firstly the excited atom can emit a photon spontaneously. Secondly the excited atom can interact with the incident photon and emit the photon of the same frequency and phase as the incident photon. This is called stimulated emission. All these three processes in the two energy level system are shown in figure(2.1).

The laser is an amplifier of stimulated emitted radiation. In thermal equilibrium, according to Boltzmann statistics, there are more atoms in the ground state and therefore an incident photon is most probably absorbed. In order to have net stimulated emission in a system it is essential to have the population of the excited state greater than that of the ground state. In otherwords, population inversion must exist and this is one of the necessary conditions for lasing action. In different lasing systems there are different ways of achieving population inversion. For instance in a gas laser it can be achieved by passing an electric discharge through the gas to excite the bound electrons to the higher level whereas in a semiconductor laser a forward bias p-n junction produces it by injecting minority carriers into both p-type and n-type regions. These excess minority carriers recombine with the majority carriers in each region to produce photons- if the

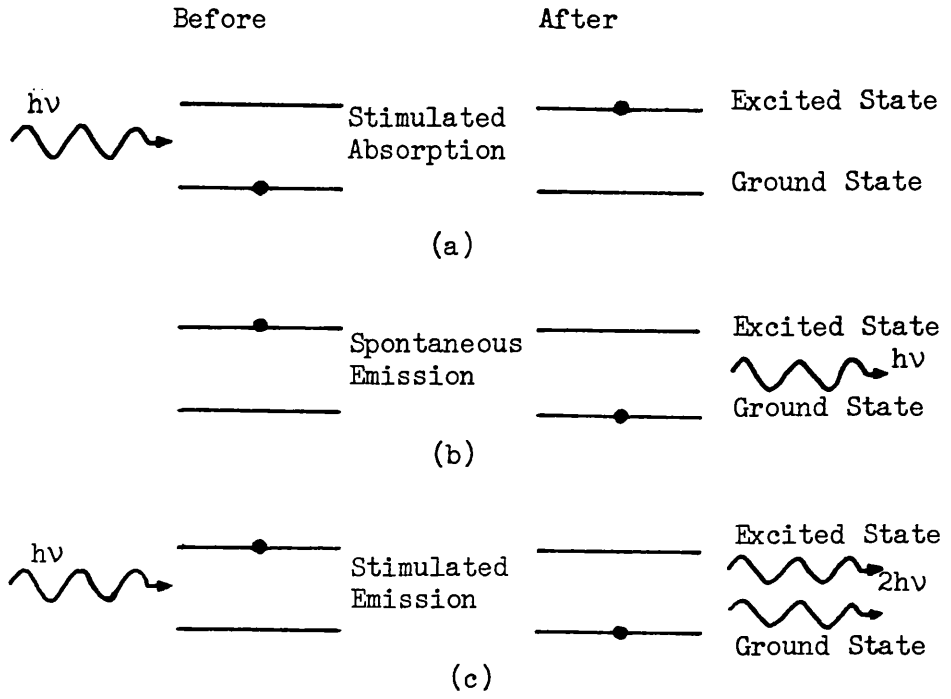

Figure 2.1 Three emission processes (a) stimulated absorption, (b) spontaneous emission and (c) stimulated emission are shown in a two energy level system. A black dot indicates the state of the atom before and after the transition takes place.

recombination process is radiative. Hence, once population inversion is produced in a given system, multiplication of photons via the mechanism of stimulated emission take place. Such devices which provide photon gain are said to be active. In contrast with a passive medium the light travelling in the active medium is amplified.

In order to produce a highly collimated and monochromatic beam, the light beam is allowed to travel in the active medium. Amplification of light travelling a only small distance into the active medium is small, therefore large amplification is achieved by making the light travel a large distance through the active region. In the laser this is achieved by making the light travel many times in the medium by reflections from two mirrors as shown in figure (2.2-2). Such an arrangement, called a cavity resonator, greatly increases the effective distance travelled by the light in the active medium and ensures some coherence to the light because the cavity ensures that only certain wavelengths are amplified.

2.2 Semiconductor Lasers

A simple semiconductor laser consists of a direct band gap semiconductor crystal such as GaAs doped in such a way to give p-type and n-type layers with a p-n junction at the interface. Both the p-type and n-type regions are heavily or degenerately doped. This is necessary because it is then easy to satisfy the lasing condition in the p-n junction under a forward electrical bias, as will be discussed in the following sections (the lasing condition states that the separation of quasi-Fermi levels must be greater than the energy gap of the semiconductor). This condition is evident in figure (2.2-1b). As the forward bias is applied to the junction, electrons and holes flow across the junction to exist as

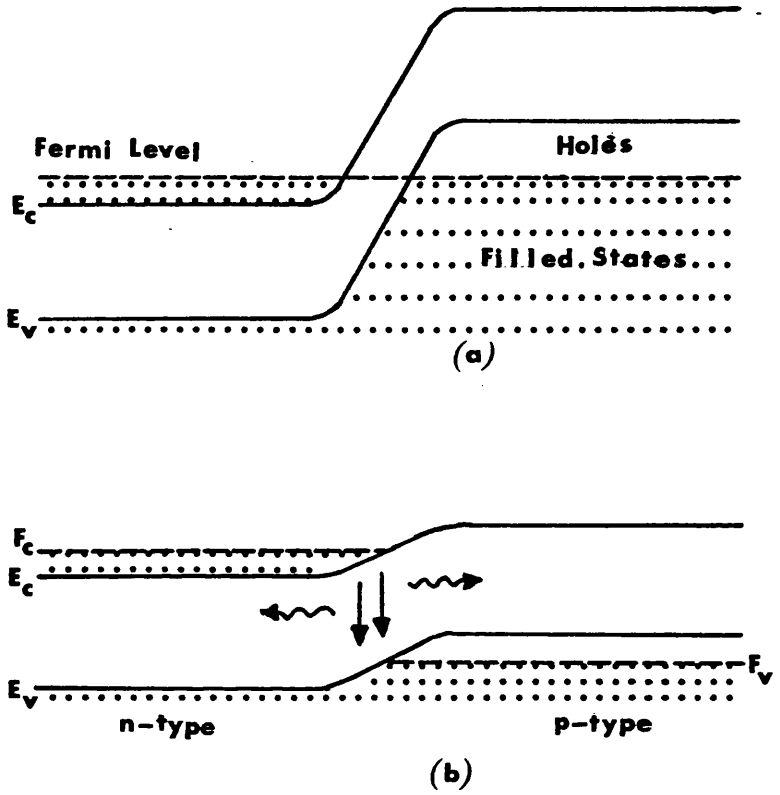

Figure 2.2-1 Energy band diagram of a p-n junction laser. (a) Thermal equilibrium. (b) Forward biased. E_C and E_V denote the band edges of conduction band and valence band respectively. F_C and F_V represent the quasi-Fermi levels. Note that the Fermi levels lie within the bands because of heavily doped junction.

minority carriers in their respective regions. These injected minority carriers are out of thermal equilibrium and therefore recombine radiatively to emit photons. The high density of injected carriers results in population inversion but because of recombination of the injected carriers this is only maintained over a narrow junction region, as shown in the figure (2.2-1b). It is only in this region that the electromagnetic wave will be amplified as it travels along the junction. There is no population inversion in either of the neutral regions of the diode, i.e the p-type or n-type regions away from the junction, and therefore these regions are essentially passive and optically lossy. Unlike gas lasers no external mirrors are required in semiconductor lasers to form the cavity resonator. The cavity resonator in a semiconductor laser is made by cleaving the opposite faces of the p-n junction along the natural crystalline planes (110) as shown in figure (2.2-2). Because semiconductor material such as GaAs has a high value of refractive index 3.5 then the air/ semiconductor interface produces high reflectivity of typically 0.3. Furthermore in semiconductor lasers the transitions take place between the energy bands rather than discrete energy levels as in gas laser systems and therefore a large optical gain in the semiconductor lasers is expected.

2.3 Direct/Indirect Band-Gap Semiconductors

It was stated in the previous section that semiconductor lasers are made from direct band-gap semiconductor such as GaAs and InAs. In order to explain this statement the basic semiconductor band diagrams will be considered in this section. In a semiconductor the band which at absolute zero temperature entirely filled with electrons is called the valence band and the next higher band of allowed states, which is

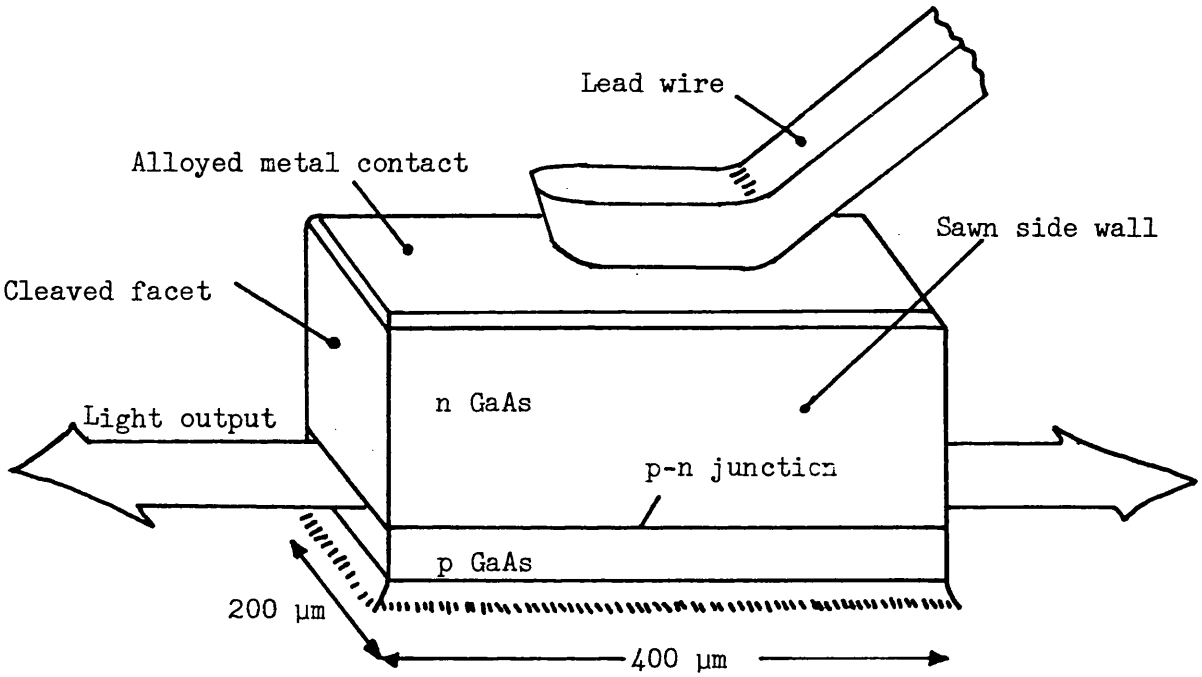

Figure 2.2-2 A homojunction laser in the form of a cavity resonator formed by parallel cleaved facets.

empty at absolute zero, called the conduction band. The valence and conduction bands are separated by a forbidden gap E_g as shown in figures (2.3-1). If the semiconductor is at a temperature sufficiently higher than absolute zero degree, the lattice may impart sufficient energy to the electrons in the valence band causing them to be excited to the conduction band as shown in figures (2.3-1). A thermally generated electron-hole pair is thus created. The reverse process is also equally probable in which the electron in the conduction band loses energy to the lattice and falls back to recombine with the hole in the valence band. These transitions require not only energy conservation but also momentum conservation. In a direct band-gap semiconductor such as GaAs the maximum of the valence band lies exactly below the minimum of the conduction band as shown in figure (2.3-1a). Consequently a direct transition when the recombining electron and hole have the same momentum ($\hbar k_c$) is most probable in the direct band-gap semiconductors. On the other hand in indirect band-gap semiconductors such as Si and Ge, the maximum of the valence band is not located exactly below the minimum of the conduction band, as shown in figure (2.3-1b), and therefore the transition of the electron from the conduction band into the hole in the valence band must be phonon or impurity assisted to conserve the momentum (1). Dumke (2) has shown that in indirect band-gap semiconductors the free carriers absorption is expected to increase more rapidly with high pumping than the optical gain, thus making net stimulated emission impossible. In luminescent devices with a high quantum efficiency such as lasers, it is desired to have a material in which the excess carriers recombine quickly by a dominant radiative mechanism giving rise to a high optical gain. In a direct band-gap semiconductor diode the radiative recombination process is thus dominant when forward bias is applied (no phonons are involved) and consequently a high luminescent efficiency

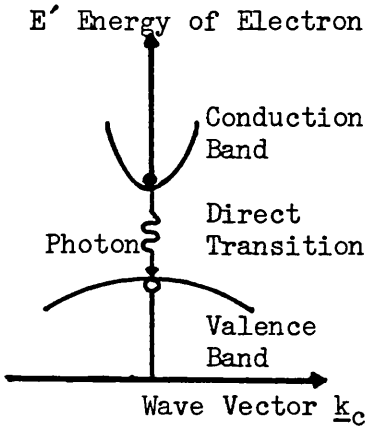

FIG. 2.3-1a

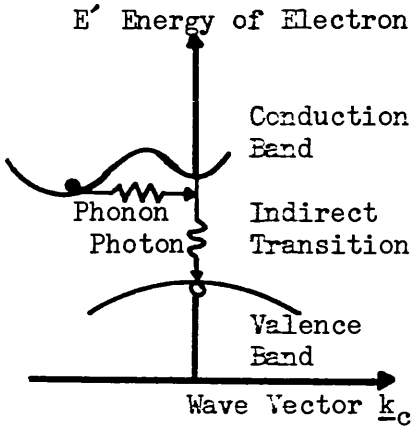

FIG. 2.3-1b

In (a) the lowest point of the conduction band occurs at the same value of $\underline{k}_c$ as the highest point of the valence band. A direct optical transition is drawn vertically with no significant change of $\underline{k}_c$, because the emitted photon has a very small wave vector. The indirect transition in (b) involves both a photon and a phonon because the lowest point of the conduction band is not exactly above the highest point of the valence band in $\underline{k}_c$ space. Therefore involvement of third particle such as phonon is essential to conserve momentum ($\hbar\underline{k}_c$).

is expected (3). In this thesis, attention is therefore paid to the direct band-gap semiconductor GaAs for lasing mechanism.

2.4 The Einstein Relations

The rates of absorption, stimulated emission and spontaneous emission of photons are described by the Einstein relations and these govern the interaction of the radiation field with free-carriers in a semiconductor. At thermal equilibrium, the probability of an energy state, E_o', being occupied in a semiconductor by an electron is given by Fermi-Dirac relation as below:

$$f_o = \frac{1}{\exp\left[(E_o' - F_o)/k_BT\right] + 1} \qquad (2.4\text{-}1)$$

where F_o is the position of the Fermi level, k_B is the Boltzmann constant and T is the temperature. However if thermal equilibrium condition does not exist in the material, the occupation probability of electrons in both the conduction and valence band states can be written in a way similar to the above expression by using two separate quasi-Fermi levels as given by:

$$f_{ce} = \frac{1}{\exp\left[(E_c' - F_c)/k_BT\right] + 1} \qquad (2.4\text{-}2a)$$

$$f_{ve} = \frac{1}{\exp\left[(E_v' - F_v)/k_BT\right] + 1} \qquad (2.4\text{-}2b)$$

where E_c' and E_v' represent energy levels within the conduction and valence bands respectively and F_c and F_v are the corresponding quasi-Fermi levels. The probability that a state is unoccupied by an electron corresponds to the occupation probability of a hole and can be written as follows:

$$f_{ch} = 1 - f_{ce} \qquad (2.4\text{-}3a)$$

$$f_{vh} = 1 - f_{ve} \qquad (2.4\text{-}3b)$$

The spontaneous transition rate from the energy state E_c' in the conduction band to the valence band is determined by the number of electrons available in the conduction band and the number of holes available in the valence band. The probability for this transition is represented by A_{cv}, and the spontaneous emission rate is given below:

$$r_{sp}'(E') = A_{cv} f_{ce} f_{vh} \tag{2.4-4}$$

where the number of electrons and holes in the conduction and valence bands is expressed in terms of their corresponding probabilities. When the density of photons of energy E', $P'(E')$ is incident, it can force the electrons from the conduction band to recombine with a hole in the valence band emitting a photon in phase. If B_{cv} denotes the transition probability, the stimulated transition rate is given by:

$$r_{stim}'(E') = B_{cv} f_{ce} f_{vh} P'(E') \tag{2.4-5}$$

In addition to the downward transition, the incident density of photons $P'(E')$ can cause an electron from the valence band to jump to the conduction band. This is the case of stimulated absorption. The upward transition probability is denoted by B_{vc} and the transition rate is given as follows:

$$r_{abs}'(E') = B_{vc} f_{ch} f_{ve} P'(E') \tag{2.4-6}$$

At thermal equilibrium the total photon generation rate must be equal to the total photon absorption rate. Using the above three equations one gets:

$$r_{stim}'(E') + r_{sp}'(E') = r_{abs}'(E') \tag{2.4-7a}$$

$$B_{cv} f_{ce} f_{vh} P'(E') + A_{cv} f_{ce} f_{vh} = B_{vc} f_{ch} f_{ve} P'(E') \tag{2.4-7b}$$

$$P'(E') = \frac{A_{cv}/B_{cv}}{\{B_{vc}/B_{cv}(f_{ch}f_{ve})/(f_{ce}f_{vh}) - 1\}} \qquad (2.4\text{-}7c)$$

Using equations (2.4-2) - (2.4-3) one can evaluate the expression $(f_{ch}f_{ve})/(f_{ce}f_{vh})$ as below:

$$(f_{ch}f_{ve})/(f_{ce}f_{vh}) = \exp\{(E_c' - E_v')/k_BT - (F_c - F_v)/k_BT\}$$

or

$$(f_{ch}f_{ve})/(f_{ce}f_{vh}) = \exp(E'/k_BT - \Delta F/k_BT) \qquad (2.4\text{-}8)$$

where $E' = E_c' - E_v'$ is the energy difference of the states involved in the transitions and $\Delta F = F_c - F_v$ is the quasi-Fermi level separation which is zero at thermal equilibrium. Substituting $\Delta F = 0$ in equation (2.4-8) one gets:

$$(f_{ch}f_{ve})/(f_{ce}f_{vh}) = \exp(E'/k_BT) \qquad (2.4\text{-}9)$$

In order to derive the Einstein coefficients A_{cv}, B_{cv} and B_{vc}, the above equation may be used with equation (2.4-7c) to write the spectral density $P'(E')$ as:

$$P'(E') = \frac{A_{cv}/B_{cv}}{(B_{vc}/B_{cv})\exp(E'/k_BT) - 1} \qquad (2.4\text{-}10)$$

The spectral density at a specific energy E' has the units of the number of photons per unit volume and unit energy interval. The spectral density at an energy, E', following the black body radiation analysis in a cavity, ignoring the dispersion of the medium is given by (4):

$$P'(E') = (8\pi\, n^3E'^2/h^3c^3)\left\{\frac{1}{\{\exp(E'/k_BT) - 1\}}\right\} \qquad (2.4\text{-}11)$$

where n is the refractive index of the medium, h is Planck's constant and c is the velocity of light in a vacuum. On comparing equations (2.4-10) and (2.4-11) the following Einstein relations can be written:

$$B_{vc} = B_{cv} \qquad (2.4\text{-}12a)$$

$$A_{cv} = (8\pi\, n^3 E'^2/h^3c^3)B_{cv} \qquad (2.4\text{-}12b)$$

The above Einstein relations show that the spontaneous emission probability A_{cv} is related to the absorption and stimulated emission probability.

2.4.1 The stimulated emission condition

In order to have net positive stimulated emission the necessary condition originally derived by Bernard (5) can be written from equations (2.4-5) and (2.4-6) as follows:

$$f_{ce}f_{vh} > f_{ch}f_{ve}$$

or

$$(f_{ch}f_{ve}/f_{ce}f_{vh}) < 1 \qquad (2.4.1\text{-}1)$$

This inequality ensures that there is net positive stimulated transitions. Using the expression (2.4-8) the above inequality reduces to:

$$\exp(E'/k_BT) < \exp(\Delta F/k_BT)$$

$$E' < \Delta F \qquad (2.4.1\text{-}2)$$

Clearly, the necessary condition for stimulated emission states that the separation of the quasi-Fermi levels under pumping conditions must exceed the separation of the states involved. The minimum separation of the transition states in a semiconductor is equal to the forbidden gap $E_g = E_c - E_v$ and therefore the quasi-Fermi levels must lie within the respective bands for stimulated emission to be dominant.

2.4.2 Relation between the absorption coefficient and spontaneous and stimulated emission rates

From equations (2.4-5) and (2.4-6) the net rate of stimulated emission can be calculated as:

$$r_{stim}(E') = B_{cv}P'(E')\{f_{ce}(1 - f_{ve}) - f_{ve}(1 - f_{ce})\}$$

or

$$r_{stim}(E') = B_{cv}P'(E')\{f_{ce} - f_{ve}\} \qquad (2.4.2\text{-}1)$$

In deriving this expression use of expression (2.4-3) is made. By using equation (2.4-11) for $P'(E')$ and the Einstein relation (2.4-12b) the following expression can be written on substitution, of the equation (2.4.2-1):

$$r_{stim}(E') = \frac{A_{cv}(f_{ce} - f_{ve})}{\exp(E'/k_BT) - 1} \qquad (2.4.2\text{-}2a)$$

Defining $r_{st}(E')$ as in equation (2.4.2-2b) below the above equation becomes:

$$r_{st}(E') = A_{cv}(f_{ce} - f_{ve}) \qquad (2.4.2\text{-}2b)$$

$$r_{stim}(E') = \frac{r_{st}(E')}{\exp(E'/k_BT) - 1} \qquad (2.4.2\text{-}2c)$$

$r_{st}(E')$ is called the stimulated emission rate which when multiplied by the number of photons per mode gives the net stimulated emission rate $r_{stim}(E')$. Similarly, the net absorption rate $r_{abs}(E')$ can be written as:

$$r_{abs}(E') = B_{cv}P'(E')\{f_{ve} - f_{ce}\} \qquad (2.4.2\text{-}3a)$$

The net absorption rate $r_{abs}(E')$ is equal to the absorption coefficient multiplied by the photon flux. The photon flux is equal to the spectral density $P'(E')$ multiplied by the velocity of light in a medium of refractive index n. The net rate of absorption ignoring any dispersion

thus becomes:

$$r_{abs}(E') = \alpha(E')P'(E')\{c/n\} \qquad (2.4.2\text{-}3b)$$

Equating (2.4.2-3a) with equation (2.4.2-3b), the following expression is obtained:

$$\alpha(E') = \frac{B_{cv}(f_{ve} - f_{ce})}{\{c/n\}} \qquad (2.4.2\text{-}4)$$

By using the Einstein relation (2.4-12b) and equation (2.4.2-2b) it is readily seen that the numenator in the above equation is simply $- r_{st}(E')\{h^3c^3/8\pi\, n^3E'^2\}$ which allows the above expression to be written as follows:

$$\alpha(E') = - \left\{\frac{h^3c^2}{8\pi\, n^2E'^2}\right\} r_{st}(E') \qquad (2.4.2\text{-}5)$$

This shows that the absorption coefficient and $r_{st}(E')$, the stimulated emission rate are related by a constant prefactor. Further, it is possible to relate the absorption coefficient $\alpha(E')$ with the spontaneous emission rate. From equations (2.4-5) and (2.4-6), the following expression can be written:

$$r_{abs}(E') = B_{cv}P'(E')\{f_{ve}f_{ch} - f_{ce}f_{vh}\}$$

or

$$r_{abs}(E') = B_{cv}P'(E')f_{ce}f_{vh}\{(f_{ve}f_{ch}/f_{ce}f_{vh}) - 1\} \qquad (2.4.2\text{-}6)$$

From equation (2.4-8) the above expression can be written as:

$$r_{abs}(E') = B_{cv}P'(E')f_{ce}f_{vh}\{\exp\{(E' - \Delta F)/k_BT\} - 1\} \qquad (2.4.2\text{-}7)$$

Making use of the Einstein relation (2.4-12b) it becomes:

$$r_{abs}(E') = \left\{\frac{h^3c^3}{8\pi\, n^3E'^2}\right\} r'_{sp}(E')P'(E')\{\exp\{(E' - \Delta F)/k_BT\} - 1\} \qquad (2.4.2\text{-}8)$$

Equating (2.4.4-8) with equation (2.4.2-3b), $r_{sp}'(E')$ can be written as:

$$r_{sp}'(E') = \frac{8\pi n^2 E'^2 \alpha(E')}{h^3 c^2 \{\exp\{(E' - \Delta F)/k_B T\} - 1\}} \qquad (2.4.2\text{-}9)$$

This gives the relation between the spontaneous emission rate and the absorption coefficient. If the value of $\alpha(E')$ is substituted into equation (2.4.2-9) from the equation (2.4.2-4) and $r_{st}(E')$ is used from equation (2.4.2-2b), the following relation can be obtained:

$$r_{st}(E') = r_{sp}'(E')\{1 - \exp\{(E' - \Delta F)/k_B T\}\} \qquad (2.4.2\text{-}10)$$

Therefore (2.4.2-9) and (2.4.2-10) can be used to calculate the spontaneous emission and stimulated emission rates respectively once the value of absorption coefficient $\alpha(E')$ is known. It is seen from equation (2.4.2-4) that the transition probability B_{cv} must be known to calculate the absorption coefficient and hence the other emission rates.

In order to evaluate the transition probability the time dependent perturbation solution of the Schrödinger equation with the Hamiltonian given below in equation (2.4.2-11) must be found. The detailed treatment can be found in references (6 - 7):

$$H^I = H^o + H^t \qquad (2.4.2\text{-}11)$$

where H^o is the Hamiltonian in the unperturbed system and H^t is the time dependent perturbation. The transition probability between the states given by the wavefunctions, $\Psi_c(\underline{r},t)$ and $\Psi_v(\underline{r},t)$ after (6) is given by:

$$B_{cv} = (\pi/2\hbar)\left|\langle\Psi_v^*(\underline{r},t)|H^I|\Psi_c(\underline{r},t)\rangle\right|^2 \qquad (2.4.2\text{-}12)$$

where $\Psi_v^*(\underline{r},t)$ is the complex conjugate of the wavefunction corresponding to the initial state and $\Psi_c(\underline{r},t)$ represents the wavefunction of the

final state. $\underline{r}$ is a position vector in a 3-dimensional space. The matrix element representing the interaction of the Hamiltonian between the initial and final states after (6) is as follows:

$$|\langle\Psi_v^*(\underline{r},t)|H^I|\Psi_c(\underline{r},t)\rangle|^2 = \int_V \Psi_v^*(\underline{r},t)H^I\Psi_c(\underline{r},t)\, d^3\underline{r} \qquad (2.4.2\text{-}13)$$

2.5 Absorption Coefficient And Spontaneous And Stimulated Emissions In Semiconductors

So far the absorption coefficient and its relation with the spontaneous and stimulated emission rates were derived in a simple case when only two discrete energy levels E_c' and E_v' separated by energy $E' = h\nu$ were taking part in transitions. In actual practice the situation in a semiconductor is more complex however, in that carriers taking part in transitions occupy energy bands rather than discrete energy levels. It is convenient to assume that the bands of a semiconductor are parabolic. The density of states for parabolic bands of a semiconductor are derived in various books (8 - 9) and are plotted in figure (2.5-1). E_c and E_v correspond to the conduction band edge and the valence band edge respectively. The upward transition rate between the valence and conduction bands of the semiconductor is proportional to the density of states occupied by electrons in the valence band and the empty, available density of states in the conduction band. Similarly, the downward transition rate is proportional to the density of states occupied by electrons in the conduction band and the empty, available density of states in the valence band. The absorption coefficient which is proportional to the difference between the upward and downward transition rates as seen in section (2.4.2) must take into account all of energy levels of the two bands separated by the energy of photon $E' = h\nu$ taking part in the transitions. The expression for the absorption coefficient therefore becomes:

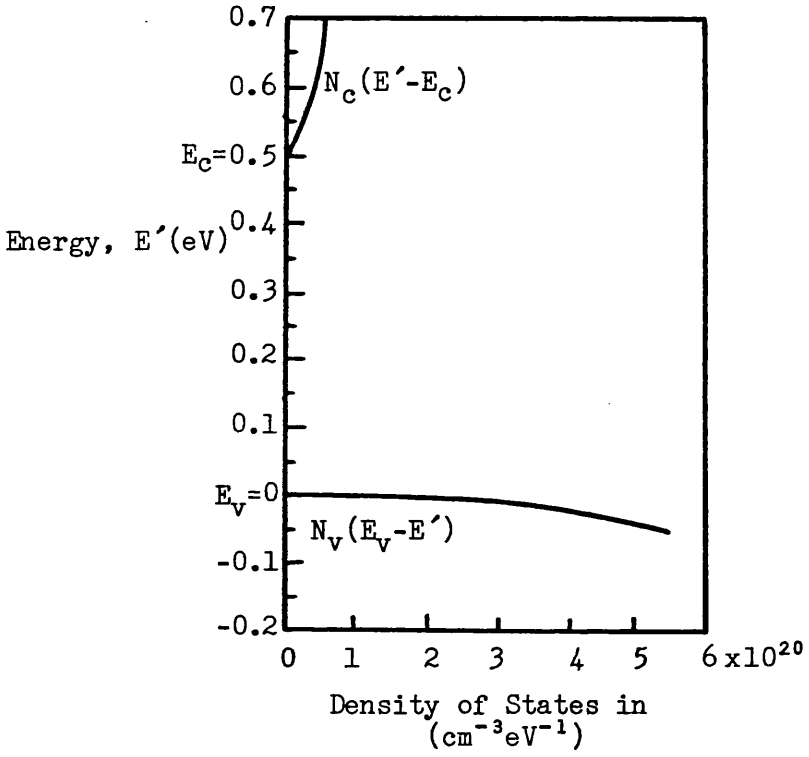

Figure 2.5-1 The variation of the parabolic density of states with energy for $m_e = 0.08m_o$ and $m_h = 0.5m_o$. Energy gap has been taken as 0.5 eV for the convenience of graph plotting.

$$\alpha(E') = \int_{-\infty}^{\infty} \{B_{cv}/(c/n)\} N_c(E_c') N_v(E_c' - E') \{f_{ve}(E_c' - E') - f_{ce}(E_c')\} dE_c' \tag{2.5-1}$$

where the zero energy reference point is chosen at the conduction band edge E_c, E_c' represents an energy state in the conduction band and $(E_c' - E')$ is the corresponding state in the valence band separated by the photon energy $E' = h\nu$. It should be noticed that the above absorption coefficient expression in a semiconductor is much complicated as compared with the absorption coefficient for the case of two energy levels given by equation (2.4.2-4). Further, the distribution functions in equation (2.5-1) given by $f_{ve}(E_c' - E')$ and $f_{ce}(E_c')$ change as the pumping rate changes which is due to the shift in the quasi-Fermi levels in their respective bands. The transition probability B_{cv} can be written in terms of matrix elements in equation (2.5-1) for the electric field travelling wave as (10):

$$B_{cv} = \left(\frac{\pi e^2 \hbar}{m^2 \varepsilon_o n^2 E'}\right) |M|^2 \tag{2.5-2}$$

which then reduces equation (2.5-1) to the following expression after Lasher and Stern (11):

$$\alpha(E') = \left(\frac{\pi e^2 \hbar}{m^2 \varepsilon_o n\, c\, E'}\right) \int_{-\infty}^{\infty} N_c(E_c') N_v(E_c' - E') \{f_{ve}(E_c' - E') - f_{ce}(E_c')\} |M|^2 \, dE_c' \tag{2.5-3}$$

This relation gives the absorption coefficient in the semiconductor taking into account the transitions between the valence and conduction bands instead of the two discrete energy levels. Similarly expressions for spontaneous and stimulated emissions can be written as below:

$$r_{sp}(E') = \left(\frac{4\pi e^2 n E'}{m^2 \varepsilon_o h^2 c^3}\right) \int_{-\infty}^{\infty} N_c(E_c') N_v(E_c' - E') f_{ce}(E_c') \{1 - f_{ve}(E_c' - E')\} |M|^2 \, dE_c' \tag{2.5-4}$$

$$R_{st}(E') = \left(\frac{4\pi\, n\, e^2 E'}{m\, \varepsilon_o h^2 c^3}\right) \int_{-\infty}^{\infty} N_c(E_c') N_v(E_c' - E') \{f_{ce}(E_c') - f_{ve}(E_c' - E')\} |M|^2 \, dE_c' \tag{2.5-5}$$

It should be noted that the band to band recombination time of the carriers is longer than the relaxation time of the carriers within each band and therefore quasi-equilibrium in each band is assumed which allows one to write the carrier distribution by Fermi functions in these expressions. The problem of calculating $\alpha(E')$, $r_{sp}(E')$ or $R_{st}(E')$ becomes one of calculating the density of states $N_c(E_c')$ and $N_v(E_c' - E')$ and the matrix element $|M|^2$. The density states for the parabolic band assumption is given by (10 - 11):

$$N_c(E_c') = (2\pi^2)^{-1}(2m_e/\hbar^2)^{\frac{3}{2}}(E_c')^{\frac{1}{2}} \tag{2.5-6a}$$

$$N_v(E_c' - E') = (2\pi^2)^{-1}(2m_h/\hbar^2)^{\frac{3}{2}}(E_c' - E')^{\frac{1}{2}} \tag{2.5-6b}$$

In the above equations m_e and m_h denote the effective masses of electrons in the conduction band and holes in the valence band respectively. These simple expressions for the density of states are no longer valid if the semiconductor is degenerately doped or the injected carrier density is high. In a heavily or degenerately doped semiconductor the band edges are not sharply defined and the impurity level merges into the band, giving rise to a band tail. Kane (12) has treated the effect of band tailing on the density of states. Kane's model assumes the fluctuations of periodic potential due to ionized impurities alone and the carriers are assumed to have low kinetic energy to follow the fluctuations produced by the ionized impurities. He gives the density of states in n-type semiconductor as:

$$N_c(E_c') = (2\eta_c)^{\frac{1}{2}}\left(\frac{m_e^{\frac{3}{2}}}{\pi^2 \hbar^3}\right) y\left(\frac{E_c' - E_c}{\eta_c}\right) \tag{2.5-7}$$

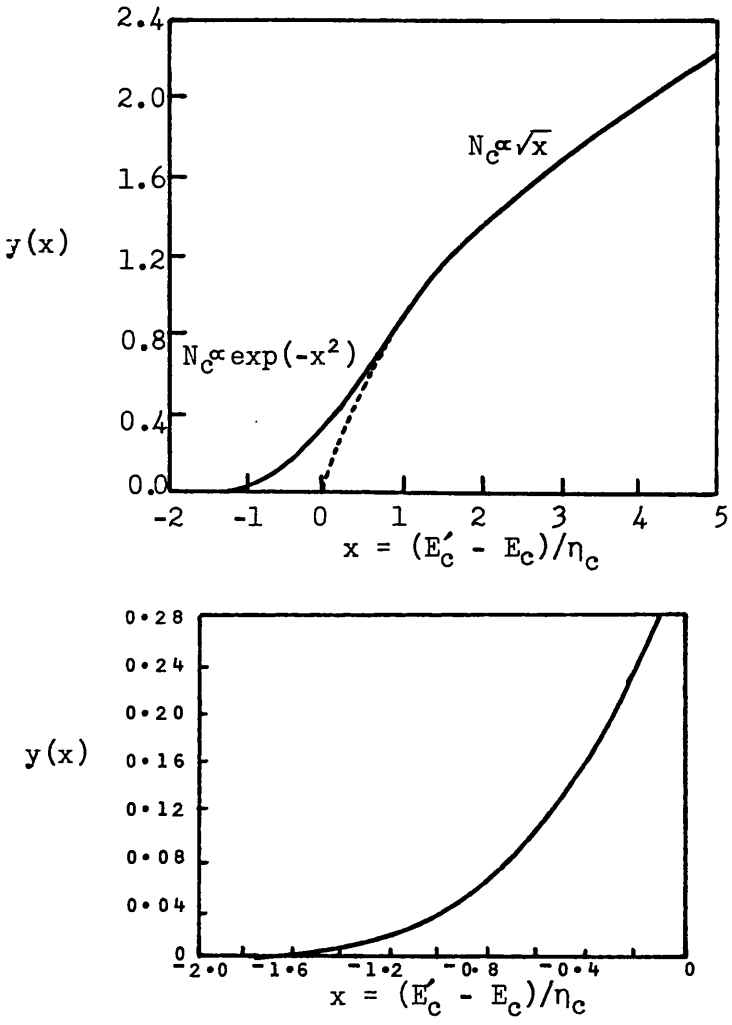

Figure 2.5-2 y plotted as a function of x (After 12).

E_c represents the normal parabolic band edge and $\eta_c = \sqrt{2}\, V_{rms}$, V_{rms} represents the root mean square potential energy fluctuations. The function y(x) with $x = (E_c' - E_c)/\eta_c$ is defined as below:

$$y(x) = 1/\sqrt{\pi} \int_{-\infty}^{x} (x - z)^{\frac{1}{2}} \exp(-z^2)\, dz \qquad (2.5\text{-}8)$$

Figure (2.5-2) shows that N_c varies parabolically at high energy and the variation is of Gaussian form $\exp\{-(E_c' - E_c)^2/\eta_c^2\}$ at low energy. This type of calculation has been performed by several authors, each using different assumptions. For example the Kane model overestimates the band tailing unless the carriers possess a large effective mass which supports the low kinetic energy assumption. Halperin and Lax (13) modified the Kane model by taking into account the kinetic energy of the carriers. Figure (2.5-3) shows that the Halperin and Lax model gives much reduced band tail than the Kane model (after Hwang (14) who did a comparitive study of the two models). In a further modification, Casey and Stern (15) approximated the density of states by the Kane Gaussian function modified to fit the Halperin and Lax results. These results are shown in figure (2.5-4).

Matrix elements also occur in the integrands of the absorption coefficient and emission rates (see equations (2.5-3) - (2.5-5)). If the material is pure then $\underline{k}$ selection rule which simply means the conservation of momentum as seen in section (2.3) rigidly applies in the various transitions between the bands (16). On the other hand if the material is heavily doped, carriers undergo elastic collisions with the impurity atoms and therefore $\underline{k}$ selection rule is relaxed (11). For the simplest parabolic band structure in case of no impurities Kane(17) gives the matrix element as:

$$|M_b|^2 = 1.33\, m_o E_g \qquad (2.5\text{-}9)$$

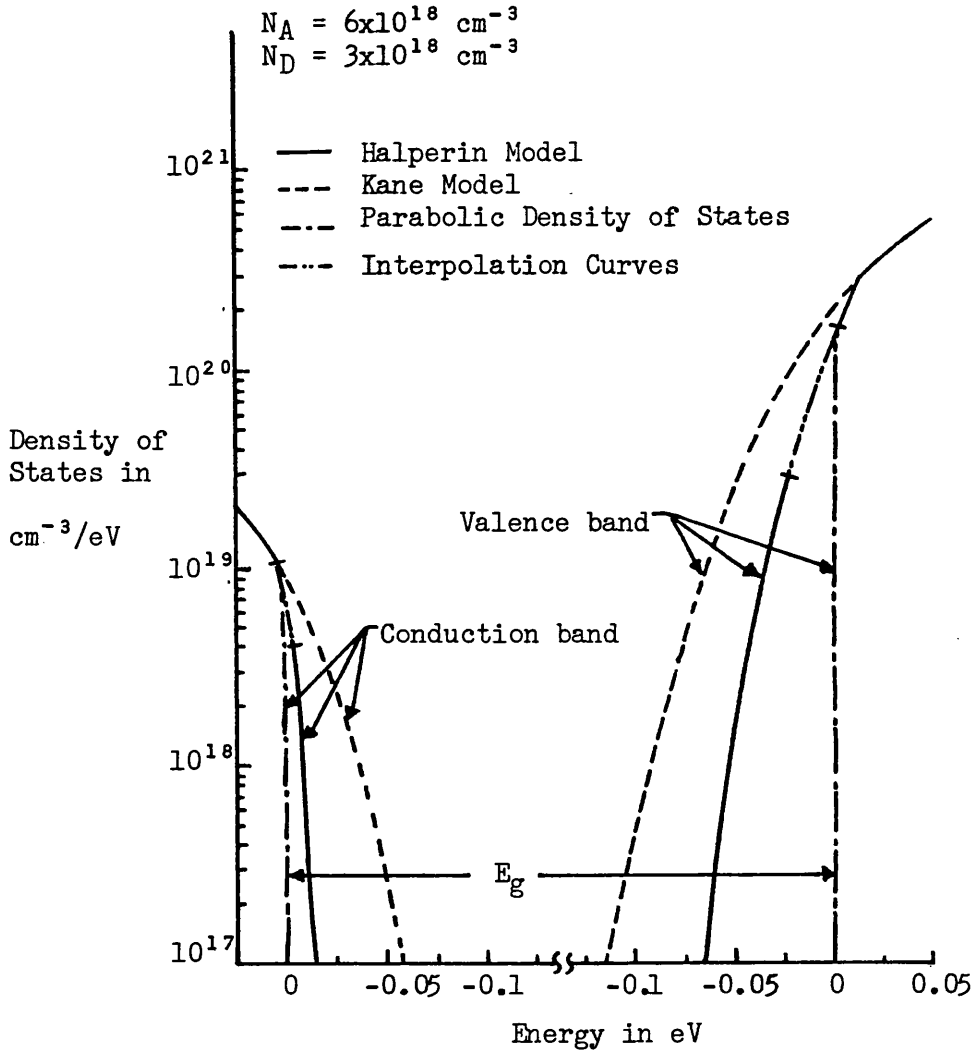

Figure 2.5-3 Comparison of the density of states in the band tails of GaAs obtained from the Kane model and the Halperin model. Curves apply for the labelled doping levels at a temperature of 300K and with the injection level required to give a gain of 100 cm^{-1}(14).

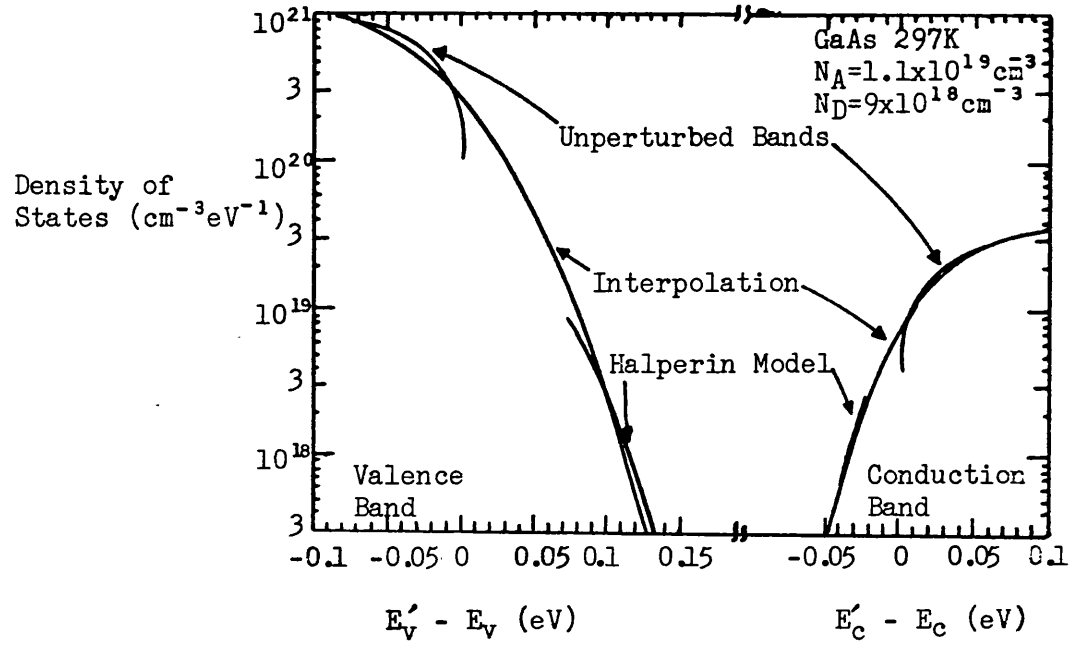

Figure 2.5-4 Densities of states in the conduction and valence band for GaAs with net acceptors $2x10^{18}cm^{-3}$. The lower curves show the densities of states in the band tails as calculated from the Halperin and Lax model and the curves interpolating them to join the upper curves are Kane functions.GHLBT model (15)

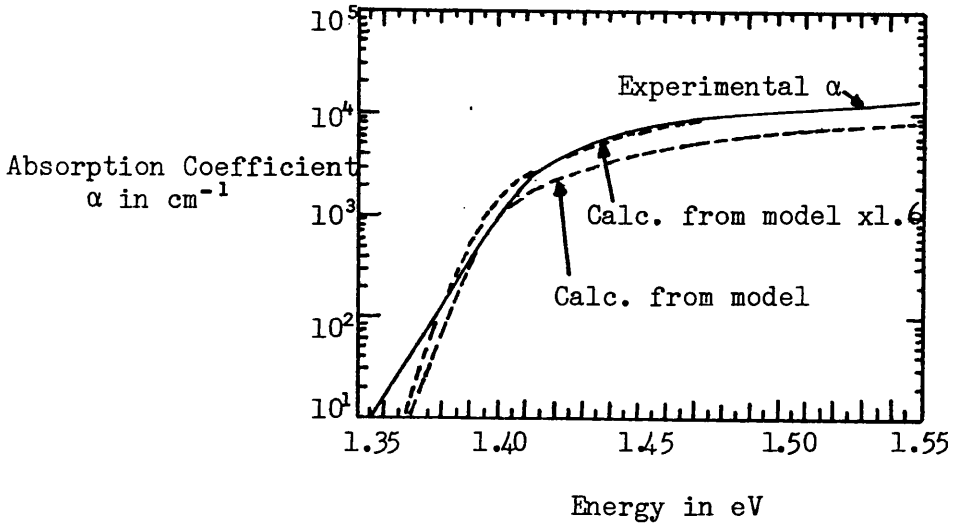

Figure 2.5-5 Comparison of the experimental and calculated absorption coefficient for hole concentration $1.2x10^{18}cm^{-3}$ (15).

where m_o is the free electron mass and E_g is the energy gap of the semiconductor. Casey and Panish (18) give the matrix element calculation for the simplest case of the transition between a shallow acceptor state and a parabolic conduction band. Casey and Stern (15) have carried out more complex analysis of the matrix element included the band tailing effect. Figure (2.5-5) shows the comparison of the absorption coefficient calculated from the equation (2.5-4) after (15). In their analysis they observed that the experimental values of the absorption coefficient in p-type GaAs above the absorption edge exceeded the theoretically expected value by 1.6. They attributed this to Coulomb enhancement (19) of the optical matrix element. Similar results have been confirmed by DeFonzo (20) in a semiconductor laser with pure or lightly doped active layer.

2.5.1 Gain-current relationship

The gain-current relationship in a diode laser is very useful to give the laser threshold condition. When the absorption coefficient in equation (2.5-3) is negative, this corresponds to the condition of optical gain. Just below threshold for quantum efficiency unity, all the injected carriers recombine spontaneously emitting photons. The number of photons per unit volume per second is given by:

$$R_{sp} = \int_0^\infty r_{sp}(E')\, dE' \qquad (2.5.1\text{-}1)$$

Assuming that the recombination occurs within a region of thickness d which is usually taken as unity to define the nominal current density J_{nom}. The nominal current density is related to R_{sp} by the following expression:

$$J_{nom} = eR_{sp} \qquad (2.5.1\text{-}2)$$

J_{nom} is determined by the diode current density per unit thickness of the recombination region. To relate J_{nom} to the gain coefficient $g(E') = -\alpha(E')$, R_{sp} is determined using the expression (2.5-4) to calculate $r_{sp}(E')$ with the appropriate expressions for density of states and matrix element. The gain coefficient is obtained from the expression (2.5-3) using the same density of states function and the matrix element as used in the determination of $r_{sp}(E')$

Figure (2.5.1-1) shows a graph of gain coefficient vs energy of the photons at different values of the nominal current density and temperature after Stern (21). As the current increases quasi-Fermi levels move into their respective bands and peak value of the gain coefficient shifts to higher energy. Furthermore due to the band tailing effect the band edge is not sharply defined and consequently there is not a sharp cut-off at E_g in the gain spectrum. Stern (22) has calculated gain vs nominal current density in a pure material which is close to the situation in a heterojunction laser diode with a lightly doped active or recombination region. For undoped GaAs material, the linear variation of the gain coefficient with nominal current density is predicted at room temperature by Stern (22). More recently these results are confirmed by DeFonzo(20). Figure (2.5.1-2) is reproduced from the reference (21). The peak gain coefficient varies linearly with J_{nom} for $50 \leq g_{max}(E') \leq 400$ cm^{-1}. The zero of $g_{max}(E')$ is offset from $J_{nom} = 0$. For the low gain region super linear behaviour is represented by the following equation (23):

$$g_{max} = 4.7 \times 10^{-6} (J_{nom} - 2 \times 10^3)^2 \qquad (2.5.1\text{-}3)$$

and for the higher gain region as below:

$$g_{max} = 5.0 \times 10^{-2} (J_{nom} - 4.5 \times 10^3) \qquad (2.5.1\text{-}4)$$

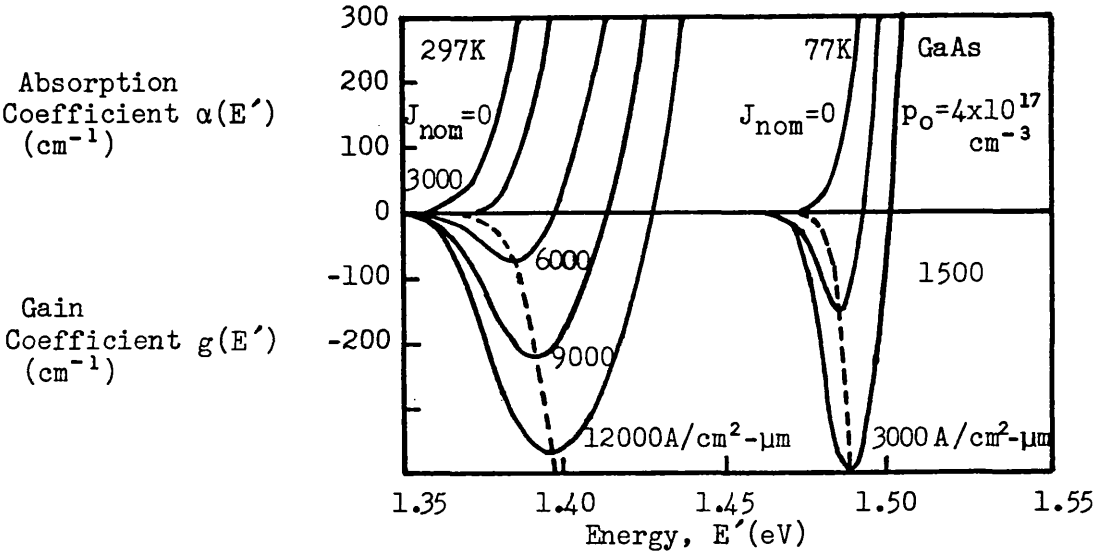

Figure 2.5.1-1 The absorption (gain) coefficient vs. energy of the band gap of GaAs at different values of the excitation given by J_{nom} for two different temperatures (21).

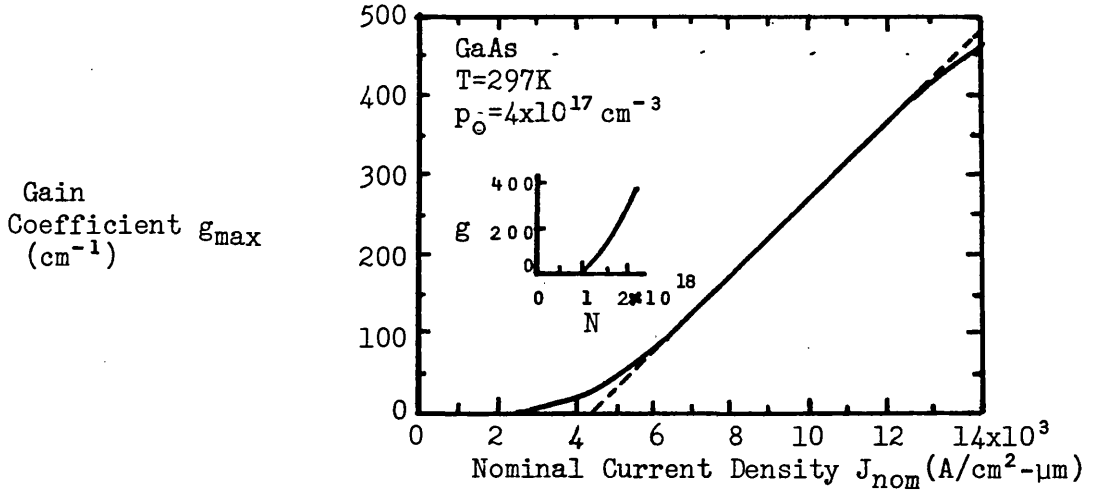

Figure 2.5.1-2 Gain coefficient variation with nominal current density. Inserted figure shows the relationship between the gain coefficient and the injected carrier density. The dashed line represents a linear dependence (Ref. 21).

This linear relationship supports the linear dependency of the gain on the carrier density (23).

2.6 The Cavity Resonator

The lasing condition for a net positive stimulated emission rate was seen in the the last section. When this condition is satisfied the absorption coefficient becomes negative which corresponds to net optical gain. The semiconductor laser oscillator uses the gain of an active material within a Fabry-Perot etalon or cavity to provide a feedback cavity oscillator. The cavity is formed by two reflecting cleaved facets along the crystalline planes (110). An electromagnetic wave travelling in the cavity undergoes constructive interference after suffering reflections from the facets and therefore grows in amplitude because of the optical gain of the active medium. In order to sustain oscillations in the cavity the growing wave must overcome the various losses present in the cavity. The plane wave in the cavity can be described by a complex propagation constant $\tilde{\beta}$ as below:

$$E(z) = E_o \exp(-j\tilde{\beta}z) \qquad (2.6\text{-}1)$$

It will be shown in chapter III that $\tilde{\beta}$ is related to the complex refractive index as below:

$$\tilde{\beta} = (n - jK)k \qquad (2.6\text{-}2)$$

K , called the extinction coefficient, is related to the absorption coefficient. In the active region, however, the net gain $(g - \alpha)$ implies the growth of the wave as it travels through the medium. α, includes the losses of the cavity due to free carrier absorption and scattering of the radiations into the lossy regions etc. The complex propagation constant for the active medium thus becomes:

$$\tilde{\beta} = \{n + j(g - \alpha)/2k\}k \qquad (2.6\text{-}3)$$

The growing wave with the above mentioned propagation constant can be written from equation (2.6-1) as below:

$$E(z) = E_o \exp\{(g - \alpha)z/2\}\exp(-jnkz) \qquad (2.6\text{-}4)$$

The field incident on the two facets is partly reflected and partly transmitted and therefore at the two facets fractions R_1 and R_2 of the incident power are reflected. On reflection at the second facet located at $z = L_c$, the field can be written as:

$$E(L_c) = \sqrt{R_2}\, E_o \exp\{(g - \alpha)L_c/2\}\exp(-jnkL_c) \qquad (2.6\text{-}5)$$

where the term $\sqrt{R_2}$ takes into account the emission losses at the second facet. After reflection from the facet at $z = L_c$ the wave travels back to the first facet at $z = 0$. Just before reflection at the facet at $z = 0$, the field is given by:

$$E(0) = \sqrt{R_2}\, E_o \exp\{(g - \alpha)L_c\}\exp(-2jnkL_c) \qquad (2.6\text{-}6)$$

On reflection at the first facet ($z = 0$) it reduces to:

$$E(0) = \sqrt{R_1 R_2}\, E_o \exp\{(g - \alpha)L_c\}\exp(-2jnkL_c) \qquad (2.6\text{-}7)$$

From equation (2.6-1) at $z = 0$ initially the field was E_o which has now become as given above after travelling a distance $2L_c$ in the cavity. The wave will be self-sustaining if:

$$E(0) = E_o \qquad (2.6\text{-}7a)$$

that is true if the following condition is satisfied.

$$\sqrt{R_1 R_2}\, \exp\{(g - \alpha)L_c\}\exp(-2jnkL_c) = 1 \qquad (2.6\text{-}8)$$

This gives two independent conditions:

- the phase condition which is as follows:

$2nkL_c = 2\pi L$ $\qquad L = 0,1,2,3,4.....$

or

$$L(\lambda/n) = 2L_c \qquad L = 0,1,2,3,4..... \qquad (2.6\text{-}9)$$

- the amplitude condition is as below:

$$\sqrt{R_1R_2}\exp\{(g - \alpha)L_c\} = 1$$

or

$$g = \alpha + (1/2L_c)\ell n\{1/(R_1R_2)\} \qquad (2.6\text{-}10)$$

Assuming the power reflectances R_1 and R_2 of the two facets to be the same (R_{mode}) the above equation (2.6-10) can be further simplified to:

$$g = \alpha + (1/L_c)\ell n(1/R_{mode}) \qquad (2.6\text{-}11)$$

This condition shows that the gain coefficient must make up for the losses in the cavity, α and the transmission of the power through the facets in order to sustain oscillations in the cavity.

The condition (2.6-9) gives the number of nodes L between the facets of the cavity of length L_c and refractive index n. Because of the repeated reflections between the partly reflecting facets, part of the radiation associated with modes determined by the expression (2.6-9) having the highest optical gain coefficient is retained and amplified at each pass. Lasing occurs when the gain is sufficient to overcome losses. The separation between the adjacent longitudnal modes of the cavity can be obtained from equation (2.6-9) by differentiating and using dL = -1 for the adjacent modes as shown below:

$$d\lambda = \frac{\lambda^2}{2nL_c\{1 - (\lambda/n)(dn/d\lambda)\}} \qquad (2.6\text{-}12)$$

The term in the bracket arises from dispersion along the cavity. The longitudnal mode separation is inversely proportional to the cavity

length L_c. Because in a semiconductor laser the cavity length is typically 250 μm - 0.8 mm and is much shorter than for a gas laser, the separation $d\lambda$ between the longitudnal modes in the semiconductor laser is much larger.

2.7 Heterojunctions

In an ordinary junction called the homojunction discussed in section (2.2) the injected electrons and holes diffuse to some distance from the junction depending upon their respective diffusion lengths before recombining. In the homojunction structure therefore there is no mechanism of confining the carriers within the active region to create a high population inversion for a given injection current and there is also no satisfactory means of confining the optical field to the region where the population inversion exists. Consequently the threshold current density in the homostructure laser is very high particularly at and above room temperature. These problems are overcome successfully in a double heterostructure laser.

Kroemer (24) and Alferov and Kazarinov (25) first proposed independently improved operation of an injection laser by sandwiching a lower band-gap semiconductor between the two layers of higher band-gap semiconductor. The main advantages of this structure are:

(i) The step discontinuity in the dielectric constant at the interfaces of the lower and higher band-gap semiconductors forms a waveguide structure which confines the optical field in the active layer.

(ii) The potential barrier at the interface provides injected carrier confinement which increases the optical gain and reduces the threshold current density.

The formation of a single heterostructure junction requires the growth

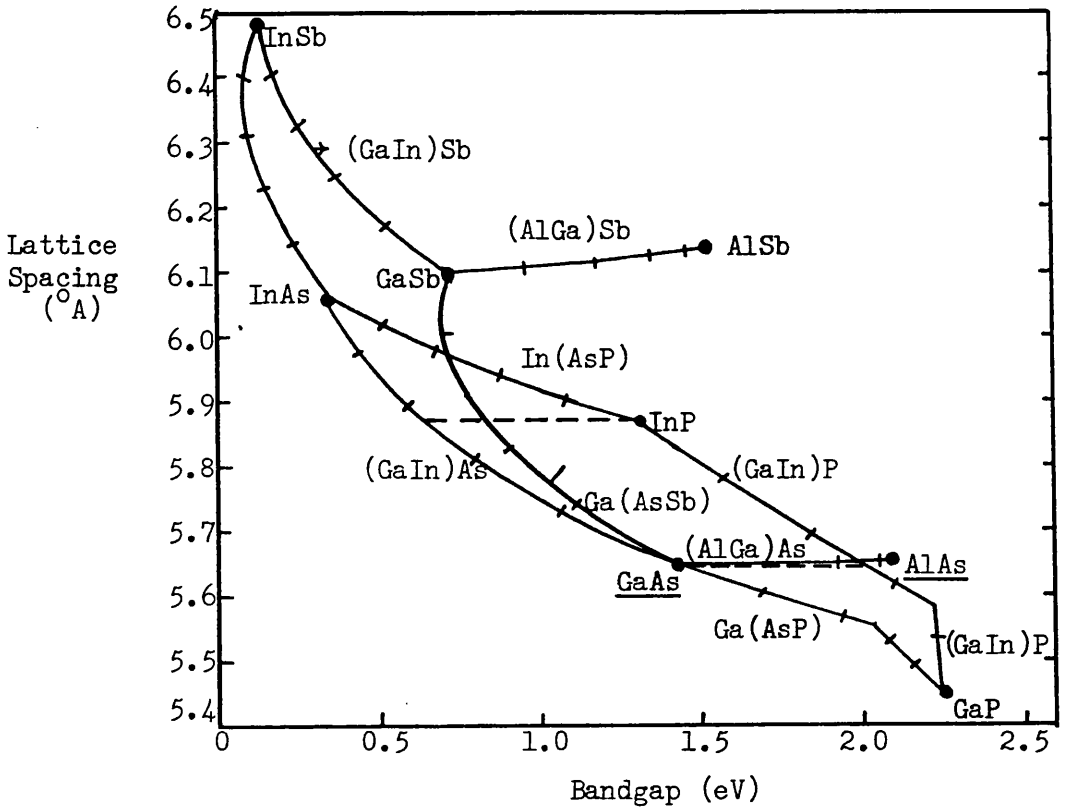

Figure 2.7-1 Relationship between bandgap and lattice spacing in a number of III/V semiconductors containing ternary combinations of Al, Ga, In and P, As and Sb.

of one type of semiconductor material onto another, yet preserving crystallinity. This requires that the lattice constant of the two semiconductor materials is closely matched. Figure (2.7-1) plots the band-gap energy of several compound semiconductors used in optoelectronics as a function of their lattice constant. It is seen from this figure that there is a very good match between GaAs and (GaAl)As for a wide range of Ga concentrations in the $Ga_{1-x}Al_xAs$ alloy. This allows quite a wide change in bandgap between active and confining layers by altering x. Therefore Ga atoms can be replaced by Al atoms in a GaAs structure without causing any significant strain in the structure which could lead to non-radiative recombination centres such as dislocations.

Two types of heterojunction can be formed. In a double heterojunction semiconductor laser both isotype and anisotype junctions are formed on either side of the active region. If the active region is n-type doped the heterojunctions are n-N isotype and n-P anisotype. On the otherhand in p-type active region the heterojunctions are p-P isotype and p-N anisotype. P-type or N-type materials correspond to a large band-gap $Al_xGa_{1-x}As$ layer. Detailed analysis of heterojunctions can be found in references (26 - 28). After Anderson (29) the formation of the abrupt heterojunction is described in the figure (2.7-2). In the figure χ_1 and χ_2 represent the electron affinities of the two semiconductors and ϕ_1 and ϕ_2 are corresponding to their work functions. Electron affinity is defined as the minimum energy required to remove an electron from the bottom of the conduction band to the vacuum level. Work function on the other hand is the minimum energy required to remove an electron from the Fermi level to the vacuum level. After the two materials are"joined" together forming a junction the Fermi level must be constant across the junction of the two materials. The electrons

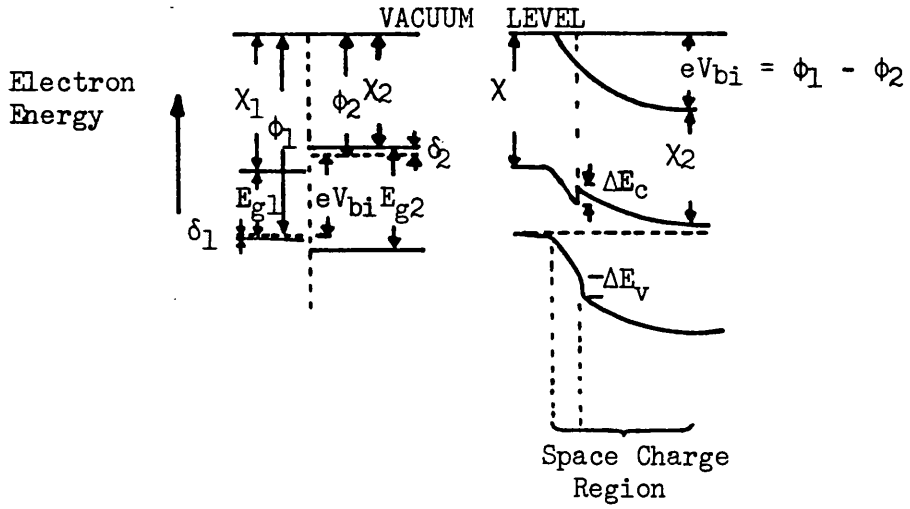

Figure 2.7-2 Energy band diagram of an ideal anisotype p-N heterojunction after Anderson (29).

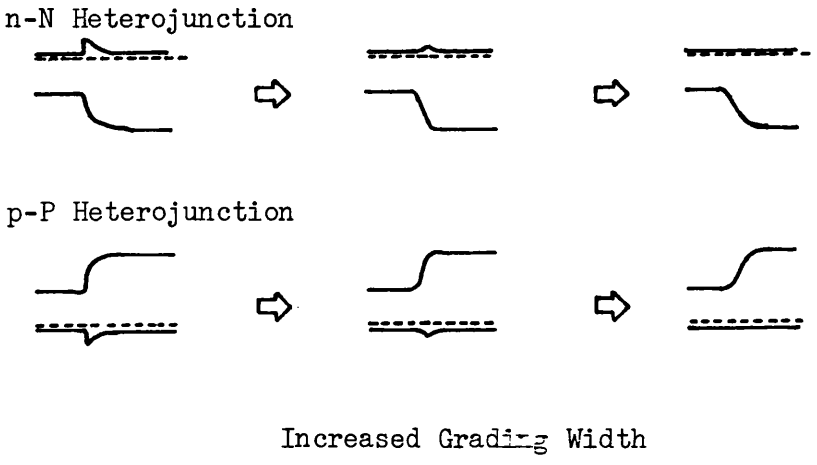

Figure 2.7-3 Band diagrams for graded isotype junctions with increasing bandgap grading in the interface region of the heterojunction.

from the large band-gap N-type material diffuse to the low band-gap p-type material until equilibrium is established. The resulting band diagram is shown in figure (2.7-2). The built-in potential is $eV_{bi} = \phi_1 - \phi_2$. From the figure it can be easily shown that the built-in potential is given by:

$$eV_{bi} = (E_{g1} + \chi_1 - \delta_1) - (\chi_2 + \delta_2) \qquad (2.7\text{-}1)$$

The valence band and conduction band discontinuities of two semiconductors at the abrupt p-N junction are given by:

$$\Delta E_c + \Delta E_v = \Delta E_g \qquad (2.7\text{-}2)$$

The spikes appearing in the energy band diagram (2.7-3) ΔE_v or ΔE_c can be eliminated by a graded formation of the junction. Figure (2.7-4) shows that smaller the concentration on either side of the junction larger the graded region (30). The graded isotype junctions behave like an ohmic contact. To get some idea of injection efficiency in an anisotype junction the homojunction analysis can be used. From the analysis of a simple p-n junction (31 - 32) the density of injected electrons into the p-region from the N-region under a forward bias V is given by:

$$n_p = n_{po}\exp(eV/k_BT) \qquad (2.7\text{-}3)$$

n_{po} represents the thermal equilibrium minority carriers in the p-region. A similar expression for the density of holes injected into the N-region is:

$$p_N = p_{NO}\exp(eV/k_BT) \qquad (2.7\text{-}4)$$

p_{NO} denotes the thermal equilibrium minority carriers in the N-region. If the widths of the p and N regions are much greater than their respective minority carrier diffusion lengths and there is no field

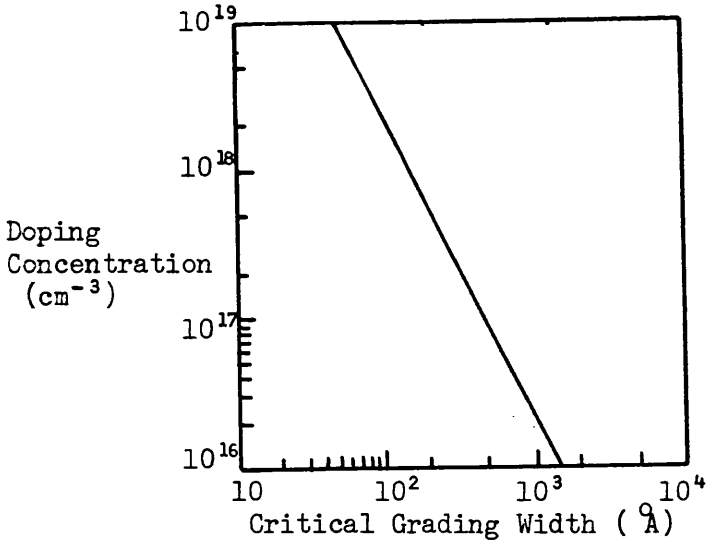

Figure 2.7-4 In an isotype symmetrically doped n-N heterojunction grading width needed to reduce the conduction band spike height from 20 to 1 k_BT (30).

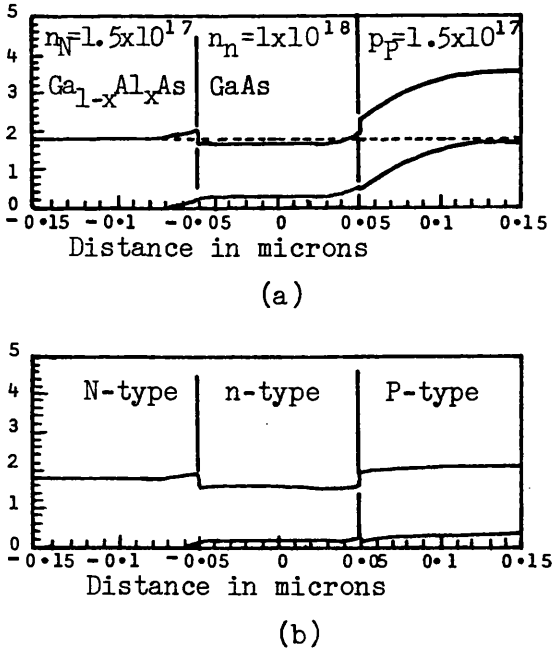

Figure 2.7-5 Energy band diagram for GaAs/$Ga_{0.7}Al_{0.3}As$ N-n-P double heterojunction (a) zero bias and (b) forward bias of 1.43V.

present in them. The ideal diode analysis can be used to solve the diffusion equation of the carriers in each region separately assuming the n_p and p_N approach to n_{po} and p_{NO} respectively at a large distance from the junction. The two diffusion current densities at the edges of depletion region thus become:

$$J_n = -(eD_e/L_e)\{n_p - n_{po}\} \tag{2.7-5}$$

$$J_p = (eD_h/L_h)\{p_N - p_{NO}\} \tag{2.7-6}$$

Substituting the value of n_p and p_N from equations (2.7-3) and (2.7-4) the above equations can be written as:

$$J_n = -\left(\frac{eD_e n_{po}}{L_e}\right)\{\exp(eV/k_BT) - 1\} \tag{2.7-7}$$

$$J_p = \left(\frac{eD_h p_{NO}}{L_h}\right)\{\exp(eV/k_BT) - 1\} \tag{2.7-8}$$

The ratio of the two injected current densities $|J_n|/|J_p|$ can be written as below:

$$|J_n|/|J_p| = \{(D_e n_{po} L_h)/(D_h p_{NO} L_e)\} \tag{2.7-9}$$

By using the law of mass-action $n_{po}p_{po} = n_{i1}^2$ and $p_{NO}n_{NO} = n_{i2}^2$.
It is also known that n_{i1} and n_{i2} are related to the respective band gaps in the two materials as given below:

$$n_{i1}^2 = 2\left(\frac{2\pi\, m_{e1}k_BT}{h^2}\right)^{\frac{3}{2}} 2\left(\frac{2\pi\, m_{h1}k_BT}{h^2}\right)^{\frac{3}{2}} \exp(-E_{g1}/k_BT) \tag{2.7-10}$$

$$n_{i2}^2 = 2\left(\frac{2\pi\, m_{e2}k_BT}{h^2}\right)^{\frac{3}{2}} 2\left(\frac{2\pi\, m_{h2}k_BT}{h^2}\right)^{\frac{3}{2}} \exp(-E_{g2}/k_BT) \tag{2.7-11}$$

By making use of these expressions the ratio of the two current densities can be written as:

$$|J_n|/|J_p| = \left(\frac{m_{e1}m_{h1}}{m_{e2}m_{h2}}\right)^{\frac{3}{2}} \left(\frac{D_e n_{NO} L_h}{D_h p_{po} L_e}\right)\exp\{(E_{g2} - E_{g1})/k_BT\} \tag{2.7-12}$$

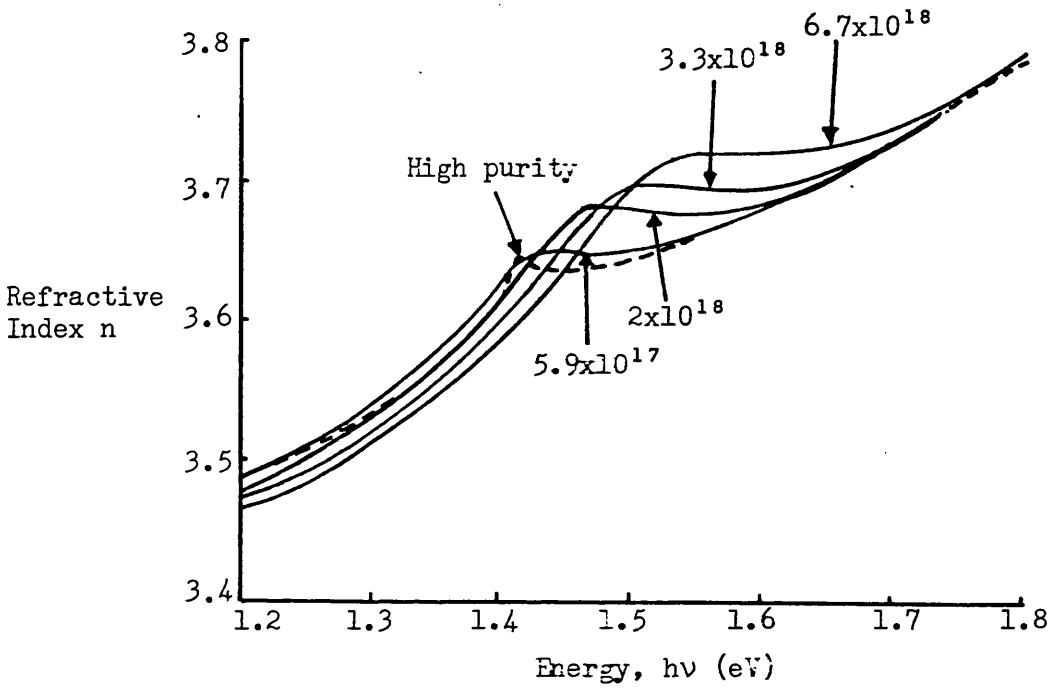

Figure 2.7-6 Refractive index of n-type GaAs as a function of photon energy for various values of n-doping (cm^{-3}) labelled in figure (34).

Clearly $(E_{g2} - E_{g1}) > o$, because E_{g2} energy gap of N-type material is greater than that of p-type material and k_BT is equal to 1/40 eV at room temperature. This shows that even for a small difference of energy gap, the exponetial term is dominant and $|J_n| >> |J_p|$. As mentioned earlier, this gives an advantage of carrier confinement reducing the undesired carrier injection from the p-region to N-region material. In a double heterostructure laser shown in the figure (2.7-5) it is thus concluded that an isotype junction provides a barrier to minority carriers from the low band-gap semiconductor to the higher band-gap semiconductor whereas the built-in potential and the band discontinuity at the anisotype junction provides a barrier to the majority carriers in the central layer. Joyce and Dixon (33) have described the electrical characterisation of heterostructure lasers. Figure (2.7-6) shows the variation of the refractive index with impurity concentration. It is important to know the refractive index variation which is responsible to form an optical waveguide in order to confine the field in the active region.

2.8 Conclusions

In this chapter, the basic principle of semiconductor lasers as well as the necessary condition for stimulated emission have been presented. The relationships between absorption coefficient, stimulated emission and spontaneous emission are given. The necessary threshold gain coefficient for a cavity resonator to sustain oscillations is derived. Comparison of homojunction and heterojunction lasers is given. Advantages of heterojunction lasers are given. It is thus the aim of this chapter to introduce lasers emphasizing on the properties of semiconductor lasers, briefly. A list of references given at the end of this chapter may be useful to expand this chapter in detail.

References

1. W.Shockley and W.T. Read: "Statistics of the recombination of holes and electrons", Phys. Rev., 87, pp.835- , 1952.

2. W.P. Dumke: "Interband transitions and maser action", Phys. Rev., 127, pp.1559- , 1962.

3. W.N. Carr: "Characteristics of GaAs spontaneous infrared source with 40% efficiency", IEEE Trans. Elec. Devices, ED-12,p.531, 1965.

4. H.C. Casey, Jr., and M.B. Panish: "Heterostructure Lasers, Part A: Fundamental Principles", Academic Press, New York, 1978, pp.112-116.

5. M.G.A. Bernard and G. Duraffourg: "Laser conditions in semiconductors", Phys. Status. Solidi, 1, p.699, 1961.

6. R.L. White: "Basic Quantum Mechanics", p.233, McGraw-Hill, New York, 1966.

7. F. Stern: "Solid State Physics", (F. Seitz and D. Turnbull eds.) Vol.15, p.300, Academic Press, New York, 1963.

8. J.S. Blakemore: "Semiconductor Statistic", Pergamon Press, New York 1962, chapter 1 and 2.

9. J.P. Mckelvey: "Solid State and Semiconductor Physics", Harper Publisher, New York, 1966.

10. H.C. Casey,Jr. and M.B. Panish: "Heterostructure Lasers, Part A: Fundamental Principles", p.126, Academic Press, New York, 1978.

11. G. Lasher and F. Stern: "Spontaneous and stimulated recombination radiation in semiconductors", Phys. Rev., 133, A553, 1964.

12. E.O. Kane: "Thomas-Fermi approach to imprure semiconductor band structure", Phys. Rev., 13, p.79, 1963.

13. B.I. Halperin and M. Lax: "Impurity band tails in the high density limit. I minimum counting methods", Phys. Rev., 148, p.722, 1966.

14. C.J. Hwang: "Properties of spontaneous and stimulated emission in GaAs junction lasers. I. Densities of states in the active regions", Phys. Rev. B2, pp.4117-4125, 1970.

15. H.C. Casey, Jr., and F. Stern: "Concentration dependent absorption and spontaneous emission in heavily doped GaAs", J. Appl. Phys., Vol.47, pp.631-643, 1976.

16. C.J. Hwang et al: "Threshold behaviour of (GaAl)As-GaAs lasers at low temperature", J. Appl. Phys., Vol. 49, pp.29-34, 1978.

17. E.O. Kane: "Band structure of Indium Antimonide", J. Phys. Chem. Solids, vol.1, pp.249-261, 1957.

18. H.C. Casey, Jr., and M.B. Panish: "Heterostructure Lasers, Part A: Fundamental Principles", pp.144-147, Academic Press, 1978.

19. W.F. Brinkman and P.A. Lee: "Coulomb effects on the gain spectrum of semiconductors", Phys. Rev. Lett., Vol.31, pp.237-240, 1973.

20. A.P. DeFonzo: "Gain mechanism in an (AlGaAs) double heterostructure laser", IEEE J. Quantum Electron., p.1537, 1983.

21. F. Stern: "Calculated spectral dependence of gain in excited GaAs", J. Appl. Phys., Vol.47, pp.5382-5386, 1976.

22. F. Stern: "Gain-current relation for GaAs lasers with n-type and undoped active layers", IEEE J. Quantum Electron., Vol. QE-9, pp.290-293, 1973.

23. H.C. Casey, Jr., and M.B. Panish: "Heterostructure Lasers, Part B: Materials and Operating Characteristics", p.181, Academic Press, 1978.

24. H. Kroemer: "A proposed class of heterostructure injection lasers", Proc. IEE, Vol.51, p.1782, 1963.

25. Zh.I. Alferov and R.F. Kazarinov: "Author's cerificate number 1032155/26-25", U.S.S.R., 1963.

26. B.L. Sharma and R.K. Purohit: "Semiconductor Heterojunctions", Pergamon Press, Oxford, 1974.

27. A.G. Milnes and D.L. Feucht: "Heterojunctions and Metal-Semiconductor Junctions", Academic Press, New York, 1972.

28. M.S. Lundstrom and R.J. Schuelke: "Modelling semiconductor heterojunctions in equilibrium", Solid State Electr., Vol.25, pp.683-691, 1982.

29. R.L. Anderson: "Experiments on Ge-GaAs heterojunctions", Solid State Electr., Vol.5, p.341, 1962.

30. J. Womac and R.H. Rediker: "The graded gap $Al_xGa_{1-x}As$/GaAs heterojunction", J. Appl. Phys., Vol.43, p.4129, 1972.

31. S.M. Sze: "Physics of Semiconductor Devices", Wiley (Interscience), New York, 1967.

32. A.G. Grove: "Physics and Technology of Semiconductor Devices", Wiley, New York, 1967.

33. W.B. Joyce and R.W. Dixon: "Electrical characterization of heterostructure lasers", J. Appl. Phys., Vol.49, pp.3719-3728, 1978.

34. H.C. Casey, Jr., D.D. Sell and M.B. Panish: "Refractive index of $Al_xGa_{1-x}As$ between 1.2 and 1.8 eV", Appl. Phys. Lett., Vol.24, p.63, 1974.

CHAPTER III

OPTICAL WAVEGUIDES

3.1 Introduction

In this chapter the waveguiding theory of stripe geometry double heterostructure lasers is reviewed, starting with a treatment of an ordinary three layer dielectric waveguide. This is then extended further to explain the waveguiding properties of semiconductor lasers (1 - 9). The natural starting point is with the basic Maxwell equations from which the wave equations may be derived. Electromagnetic processes in a medium are described by the following set of Maxwell equations:

$$\nabla \times \underline{H} = \underline{J} + \partial \underline{D}/\partial t \qquad (3.1\text{-}1)$$

$$\nabla \times \underline{E} = - \partial \underline{B}/\partial t \qquad (3.1\text{-}2)$$

$$\nabla . \underline{D} = \rho \qquad (3.1\text{-}3)$$

$$\nabla . \underline{B} = 0 \qquad (3.1\text{-}4)$$

Equations of state for an isotropic medium are given below:

$$\underline{D} = \varepsilon \underline{E} \qquad (3.1\text{-}5)$$

$$\underline{B} = \mu \underline{H} \qquad (3.1\text{-}6)$$

$$\underline{J} = \sigma \underline{E} \qquad (3.1\text{-}7)$$

In these equations $\underline{E}$ is the electric field intensity vector in volt/m, $\underline{H}$ is the magnetic field intensity vector in amp/m, $\underline{D}$ is the electric displacement vector in coulomb/m^2, $\underline{B}$ is the magnetic flux density in tesla, $\underline{J}$ is the current density in amp/m^2 and ρ is the charge density in coulomb/m^3. ε and μ are the dielectric constant and permeability in farad/m and henry/m respectively. σ denotes the conductivity of the medium in $(\Omega m)^{-1}$. Non-magnetic media are considered here, therefore μ in the equation (3.1-6) can be replaced by its free space value μ_o Equations (3.1-6) and (3.1-2) thus become:

$$\underline{B} = \mu_o \underline{H} \tag{3.1-8}$$

$$\nabla x \underline{E} = - \mu_o (\partial \underline{H}/\partial t) \tag{3.1-9}$$

3.2 The Wave Equation

Operating by curl on both sides of equation (3.1-9) one gets:

$$\nabla x \nabla x \underline{E} = - \mu_o \{\partial/\partial t (\nabla x \underline{H})\} \tag{3.2-1}$$

By using the vector identity $\nabla x \nabla x \underline{E} = \nabla(\nabla . \underline{E}) - \nabla^2 \underline{E}$ one can expand the left hand side of the above equation to write the following expression:

$$\nabla(\nabla . \underline{E}) - \nabla^2 \underline{E} = - \mu_o \{\partial/\partial t (\nabla x \underline{H})\} \tag{3.2-2}$$

Substituting the value of $\nabla x \underline{H}$ from the equation (3.1-1) and making use of the relation given by equation (3.1-5) the above expression can be written as:

$$\nabla(\nabla . \underline{E}) - \nabla^2 \underline{E} = - \mu_o \partial \underline{J}/\partial t - \mu_o \varepsilon \partial^2 \underline{E}/\partial t^2 \tag{3.2-3}$$

For a source free medium $\rho = 0$, and equation (3.1-3) using the relation (3.1-5) is given by:

$$\nabla . (\varepsilon \underline{E}) \equiv \nabla \varepsilon . \underline{E} + \varepsilon \nabla . \underline{E} = 0 \tag{3.2-4}$$

or

$$\nabla . \underline{E} = - (\nabla \varepsilon / \varepsilon) . \underline{E} \tag{3.2-5}$$

For a homogeneous medium, if ε is uniform, $\nabla \varepsilon = 0$ and therefore the above equation becomes:

$$\nabla . \underline{E} = 0 \tag{3.2-6}$$

Making use of this equation and equation (3.1-7), assuming that the conductivity is independent of time, equation (3.2-3) reduces to:

$$\nabla^2 \underline{E} - \mu_o \varepsilon \partial^2 \underline{E}/\partial t^2 - \sigma \mu_o \partial \underline{E}/\partial t = 0 \tag{3.2-7}$$

This is known as a wave equation which governs the electric field vector in a homogeneous, linear medium in which the charge density is zero. This equation is applicable whether the medium is conducting or non-conducting. A similar wave equation can be derived for the magnetic field intensity $\underline{H}$. If harmonic variation of the field $\underline{E}$ is assumed, $\underline{E}$ can be written as:

$$\underline{E}(\underline{r},t) = \underline{E}(\underline{r})\exp(j\omega t) \qquad (3.2\text{-}8)$$

On substituting this expression for $\underline{E}(\underline{r},t)$ in equation (3.2-7) the following equation is obtained:

$$\exp(j\omega t)\{\nabla^2\underline{E}(\underline{r}) + \mu_o\omega^2\varepsilon\underline{E}(\underline{r}) - j\sigma\omega\mu_o\underline{E}(\underline{r})\} = 0$$

or

$$\nabla^2\underline{E}(\underline{r}) + \mu_o\omega^2\varepsilon\underline{E}(\underline{r}) - j\sigma\omega\mu_o\underline{E}(\underline{r}) = 0 \qquad (3.2\text{-}9)$$

It is pertinent at this point to discuss some solutions of the wave equation under special conditions.

3.2.1 Free space propagation

Suppose the medium in which the field is propagating is empty space so that $\sigma = 0$ and $\varepsilon = \varepsilon_o$, the equation (3.2-9) becomes:

$$\nabla^2\underline{E}(\underline{r}) + \mu_o\varepsilon_o\omega^2\underline{E}(\underline{r}) = 0 \qquad (3.2.1\text{-}1)$$

If the field is polarized in the y direction, the only non-zero component of the field is E_y. The wave equation (3.2.1-1) then gives:

$$d^2E_y/dz^2 + \mu_o\varepsilon_o\omega^2E_y = 0 \qquad (3.2.1\text{-}2)$$

where z is the direction of propagation. In this equation the expression $\mu_o\varepsilon_o$ is related to the velocity of light in vacuum by the following relation:

$$c = 1/\sqrt{\mu_o\varepsilon_o} \qquad (3.2.1\text{-}3)$$

By making use of this expression in equation (3.2.1-2) one can write equation (3.2.1-2) as below:

$$d^2E_y/dz^2 + (\omega^2/c^2)E_y = 0 \qquad (3.2.1\text{-}4)$$

The solution of this equation is of the following form:

$$E_y = A\exp(-j\beta z) \qquad (3.2.1\text{-}5)$$

where β is called the propagation constant and is defined as:

$$\beta = \omega/c \qquad (3.2.1\text{-}6)$$

The full solution of the field propagating thus becomes:

$$E_y = A\exp\{j(\omega t - \beta z)\} \qquad (3.2.1\text{-}7)$$

3.2.2 Propagation in a lossless medium

If now the field is propagating in a non-conducting dielectric medium, σ in equation (3.2-9) is still zero but now the dielectric constant is not ε_o but $\varepsilon_o\varepsilon_r = \varepsilon$. ε_r is called the relative dielectric constant of the medium. One can write equation (3.2-9) as shown below:

$$\nabla^2\underline{E}(\underline{r}) + \omega^2\mu_o\varepsilon_o\varepsilon_r\underline{E}(\underline{r}) = 0 \qquad (3.2.2\text{-}1)$$

Restricting the solution to a polarized field in the y direction it becomes:

$$d^2E_y/dz^2 + \omega^2\mu_o\varepsilon_o\varepsilon_rE_y = 0 \qquad (3.2.2\text{-}2)$$

By using the definition of the velocity of light c given in equation (3.2.1-3) the above equation reduces to:

$$d^2E_y/dz^2 + \varepsilon_r(\omega^2/c^2)E_y = 0 \qquad (3.2.2\text{-}3)$$

The solution of this equation is similar to that of equation (3.2.1-4) but β now becomes:

$$\beta = \sqrt{\varepsilon_r}(\omega/c) \qquad (3.2.2\text{-}4)$$

Defining $\sqrt{\varepsilon_r} = n$, where n is called the refractive index, one sees that the results are the same as for free space, except the velocity of propagating wave is now c/n instead of c. For a free space the value of n is unity.

3.2.3 Propagation in a conducting medium

This is a particularly important case for wave propagation in semiconductors, and it is necessary to derive relationships between the optical and electrical constants of the material. If the medium is conducting with a conductivity σ then this term must be retained in equation (3.2-9). The wave equation (3.2-9) for the y-polarized field is then given as follows:

$$d^2E_y/dz^2 + \tilde{\varepsilon}(\omega^2/c^2)E_y = 0 \qquad (3.2.3\text{-}1)$$

where $\tilde{\varepsilon}$ is a complex quantity, given below:

$$\tilde{\varepsilon} = \varepsilon_r - j(\sigma/\varepsilon_o\omega) \qquad (3.2.3\text{-}2)$$

The solution of the equation (3.2.3-1) is similar to that of (3.2.2-3) but the quantity β is complex as given below:

$$\tilde{\beta} = \sqrt{\tilde{\varepsilon}}(\omega/c) \qquad (3.2.3\text{-}3)$$

Defining $\sqrt{\tilde{\varepsilon}} = \tilde{n} \equiv (n - jK)$, where $\tilde{n}$ is called the complex refractive index with n and K as its real and imaginary parts respectively. Equation (3.2.3-3) can be written as:

$$\tilde{\beta} = (\omega/c)\{n - jK\} \qquad (3.2.3\text{-}4a)$$

$$\mathrm{Re}(\tilde{\beta}) = (\omega/c)n \qquad (3.2.3\text{-}4b)$$

$$\mathrm{Im}(\tilde{\beta}) = -(\omega/c)K \qquad (3.2.3\text{-}4c)$$

Prefixes Re and Im stand for real and imaginary parts respectively. Solution of equation (3.2.3-1) therefore is given by:

$$E_y = A \exp\{j(\omega t - \tilde{\beta} z)\}$$

or

$$E_y = A \exp\{\mathrm{Im}(\tilde{\beta})z\}\exp\{j(\omega t - \mathrm{Re}(\tilde{\beta})z)\} \qquad (3.2.3\text{-}5)$$

Further, from equation (3.2.3-2) and the definition of complex refractive index one can easily derive the following relations:

$$\mathrm{Re}(\tilde{\varepsilon}) = \varepsilon_r \equiv n^2 - K^2 \qquad (3.2.3\text{-}6a)$$

$$\mathrm{Im}(\tilde{\varepsilon}) = \sigma/\varepsilon_o\omega \equiv 2nK \qquad (3.2.3\text{-}6b)$$

It is apparent from equation (3.2.3-6b) that if $\sigma > 0$; $K > 0$ and therefore $\mathrm{Im}(\tilde{\beta})$, from the relation (3.2.3-4c), is negative. The solution to equation (3.2.3-5) then represents a decaying travelling wave. On the other hand if $\sigma < 0$ the solution to equation (3.2.3-5) represents a travelling wave which grows instead. In this case the medium in which the growing wave is travelling is called active. When the light propagates in the z direction in an absorbing medium, the decrease in intensity is governed by:

$$I = I|_{z=0}\exp(-\alpha z) \qquad (3.2.3\text{-}7)$$

where α is called the absorption coefficient. Since I is proportional to $|E_y|^2$ therefore by comparing this equation with (3.2.3-5) the following equation is obtained.

$$2\mathrm{Im}(\tilde{\beta}) = -\alpha \qquad (3.2.3\text{-}8a)$$

But $\mathrm{Im}(\tilde{\beta})$ is related to K, called the extinction coefficient, by the equation (3.2.3-4c). The above equation thus becomes:

$$K = \alpha/2k \qquad (3.2.3\text{-}8b)$$

where $k = 2\pi/\lambda$ is called the wave vector in a free space. If the absorption coefficient is negative, as in an active medium, it is called gain coefficient g.

3.3 The Three-Layer Slab Waveguide

The double heterostructure semiconductor injection laser can be treated as a three-layer dielectric waveguide in the transverse direction perpendicular to the heterojunctions (4 - 6), as shown in figure (3.3).

3.3.1 The TE mode

The dielectric waveguide shown in figure (3.3) is infinite in the y direction so that $\partial/\partial y = 0$. Only the TE modes are considered in this section. By definition therefore the only non-zero component of the electric field is E_y ($E_x = E_z = 0$) which is coupled with magnetic field components H_x and H_z ($H_y = 0$) in the x-z plane. Therefore $\underline{E}$ and $\underline{H}$ for the TE mode can be written as below:

$$\underline{E} = E_y\underline{b} \qquad (3.3.1\text{-}1a)$$

$$\underline{H} = H_x\underline{a} + H_z\underline{c} \qquad (3.3.1\text{-}1b)$$

where $\underline{a}$, $\underline{b}$ and $\underline{c}$ are unit vectors along x, y and z directions respectively. Substituting these $\underline{E}$ and $\underline{H}$ fields in the equation (3.1-9) the following expression is obtained:

$$-(\partial E_y/\partial z)\underline{a} + (\partial E_y/\partial x)\underline{c} = -\mu_o(\partial H_x/\partial t)\underline{a} - \mu_o(\partial H_z/\partial t)\underline{c} \qquad (3.3.1\text{-}2)$$

Equating the coefficients of like vectors on both sides of the above equation one gets:

$$\partial E_y/\partial z = \mu_o(\partial H_x/\partial t) \qquad (3.3.1\text{-}3a)$$

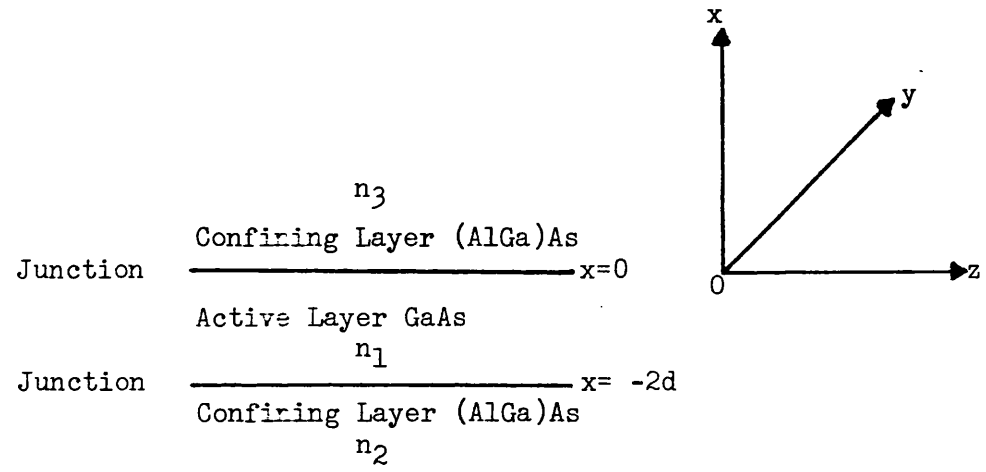

Figure 3.3 Active layer sandwiched between the confining layers with refractive indices n_2 and n_3. 2d and n_1 are the thickness and refractive index of active layer.

$$\partial E_y/\partial x = -\mu_o(\partial H_z/\partial t) \qquad (3.3.1\text{-}3b)$$

The equations above give relationships between the two magnetic field components H_x and H_z in terms of one transverse electric field component E_y. If the time variation of the field is assumed to be of the form $\exp(j\omega t)$ and is propagating in the positive z direction implying a spatial variation $\exp(-j\beta z)$ z dependence, one can substitute these variations in equations (3.3.1-3) to get:

$$H_x = -(\beta/\mu_o\omega)E_y \qquad (3.3.1\text{-}4a)$$

$$H_z = (j/\mu_o\omega)\partial E_y/\partial x \qquad (3.3.1\text{-}4b)$$

Hence once the E_y component for the TE mode is found, H_x and H_z, the magnetic field components can be calculated directly by using the above relations. Recalling section (3.2.2), the wave equation (3.2.2.1) can be written using $c = 1/\sqrt{\mu_o\varepsilon_o}$ and $\sqrt{\varepsilon_r} = n$ as follows:

$$\nabla^2\underline{E} + (\omega^2/c^2)n^2\underline{E} = 0 \qquad (3.3.1\text{-}5)$$

Dielectric media are generally assumed to be lossless. Using the definition of TE mode ($\partial/\partial y = 0$) one gets from this equation the following expression:

$$\partial^2E_y/\partial x^2 + \partial^2E_y/\partial z^2 + (\omega^2/c^2)n^2E_y = 0 \qquad (3.3.1\text{-}6)$$

It should be remembered here that the time variation of the field is assumed to be of the form $\exp(j\omega t)$ and the direction of propagation is the positive z direction. Again if the z dependence of the field is of the form $\exp(-j\beta z)$ equation (3.3.1-6) can be written as:

$$\partial^2E_y/\partial x^2 + \left(\frac{\omega^2n^2}{c^2} - \beta^2\right)E_y = 0 \qquad (3.3.1\text{-}7)$$

where the field component E_y is given below:

$$E_y(x,z,t) = E_y(x)\exp\{j(\omega t - \beta z)\} \qquad (3.3.1\text{-}8)$$

It has been shown earlier that ω/c is the propagation constant in the free space and this can be written as:

$$k = \omega/c \equiv 2\pi/\lambda \qquad (3.3.1\text{-}9)$$

where λ is the wavelength of the propagating wave in a free space. If ω/c is replaced by the wave vector in the equation (3.3.1-7) then:

$$\partial^2 E_y/\partial x^2 + (k^2n^2 - \beta^2)E_y = 0 \qquad (3.3.1\text{-}10)$$

It is possible to proceed by writing the above equation for each region shown in figure (3.3) with refractive indices n_1, n_2 and n_3:

$$\left.\begin{aligned} \partial^2 E_{y3}/\partial x^2 - (\beta^2 - n_3^2k^2)E_{y3} = 0 \qquad & x \geqslant 0 \\ \partial^2 E_{y1}/\partial x^2 + (n_1^2k^2 - \beta^2)E_{y1} = 0 \qquad & 0 \geqslant x \geqslant -2d \\ \partial^2 E_{y2}/\partial x^2 - (\beta^2 - n_2^2k^2)E_{y2} = 0 \qquad & x \leqslant -2d \end{aligned}\right\} \qquad (3.3.1\text{-}11)$$

A guided mode is one whose field energy is located in the central region and the mode being a propagating wave implies that the electromagnetic energy travels along the waveguide. The electromagnetic energy stays predominantly in the central region of figure (3.3) with the highest refractive index. In the outer passive regions on the other hand, the field must decay exponentially. For guided modes the field energy must be confined to the central region ($0 \geqslant x \geqslant -2d$) therefore this suggests that:

$$n_1^2k^2 - \beta^2 > 0 \qquad (3.3.1\text{-}12)$$

so that the solution of equation (3.3.1-11) in the central region should have an oscillatory behaviour. Furthermore, outside the central region

the solution should have an exponential dacaying field suggests that the following inequalities should hold:

$$\beta^2 - n_2^2k^2 > 0 \qquad (3.3.1\text{-}13)$$

$$\beta^2 - n_3^2k^2 > 0 \qquad (3.3.1\text{-}14)$$

If it is assumed that $n_2 > n_3$, the above conditions can be summed up as:

$$n_1 > n_2 > n_3 \qquad (3.3.1\text{-}15)$$

It should be pointed out that similar results can be obtained by using a ray model. From this type of model it is clear that the central region is an optically denser medium which is the essential requirement for total internal reflection to take place, so as to confine the light in the central or active region. Furthermore if $(n_2 = n_3)$ in figure (3.3) the structure of the waveguide is symmetrical. The solution of the set of equations (3.3.1-11) must be found in such a way that E_y and H_z components are continuous at the interfaces x = 0 and x = -2d of the 3-layer dielectric waveguide. The solution of the set of equations (3.3.1-11) can be written as follows:

$$E_y = \begin{cases} A\exp(-\delta x) & x \geq 0 \\ A\,\mathrm{Cos}\kappa x + B\,\mathrm{Sin}\kappa x & 0 \geq x \geq -2d \\ \{A\,\mathrm{Cos}(2\kappa d) - B\,\mathrm{Sin}(2\kappa d)\}\exp\{\gamma(x+2d)\} & x \leq -2d \end{cases} \qquad (3.3.1\text{-}16)$$

where

$$\left.\begin{aligned} \delta^2 &= \beta^2 - n_3^2k^2 \\ \kappa^2 &= n_1^2k^2 - \beta^2 \\ \gamma^2 &= \beta^2 - n_2^2k^2 \end{aligned}\right\} \qquad (3.3.1\text{-}17)$$

It becomes clear immediately that the solution (3.3.1-16) satisfies the continuity requirement of E_y at the junctions x = 0 and x = -2d. It should

be noticed that it is still required for the solution (3.3.1-16) to satisfy the continuity condition of H_z. Making use of the relation (3.3.1-4b) it is possible to write H_z from the solution (3.3.1-16) as:

$$H_z = j/(\mu_o\omega)\begin{cases} -\delta A \exp(-\delta x) & x \geqslant 0 \\ -\kappa(A \sin\kappa x - B \cos\kappa x) & 0 \geqslant x \geqslant -2d \\ \gamma\{A \cos(2\kappa d) - B \sin(2\kappa d)\}\exp\{\gamma(x+2d)\} & x \leqslant -2d \end{cases} \quad (3.3.1\text{-}18)$$

Unlike the solution (3.3.1-16) H_z does not satisfy the continuity requirements at the junctions x = 0 and x = -2d by itself. On applying the continuity condition, the following relations are obtained:

At x = 0; $\quad \delta A + \kappa B = 0 \quad (3.3.1\text{-}19a)$

At x = -2d; $\quad \{\kappa \sin(2\kappa d) - \gamma \cos(2\kappa d)\}A + \{\kappa \cos(2\kappa d) + \gamma \sin(2\kappa d)\}B = 0 \quad (3.3.1\text{-}19b)$

For a non-trivial solution of the above two equations, the determinant of the coefficients of A and B must vanish. On substituting the value of A in terms of B from the equation (3.3.1-19a) into the equation (3.3.1-19b) the following relation is obtained:

$$\tan(2\kappa d) = \{\kappa(\delta + \gamma)/(\kappa^2 - \delta\gamma)\} \quad (3.3.1\text{-}20)$$

This eigenvalue equation gives the allowed values of the propagation constant β which is related to κ, γ and δ by the relations (3.3.1-17). If the frequency ω is such that $(k = \omega/c)\ km_2 = \beta$, the value of γ vanishes. The field solution from the equation (3.3.1-16) thus spreads out into the region $x \leqslant -2d$. Hence this corresponds to cut-off condition i.e field is no longer confined to the central active region.

$$\text{(cut-off)} \quad \beta = km_2 \quad (3.3.1\text{-}21)$$

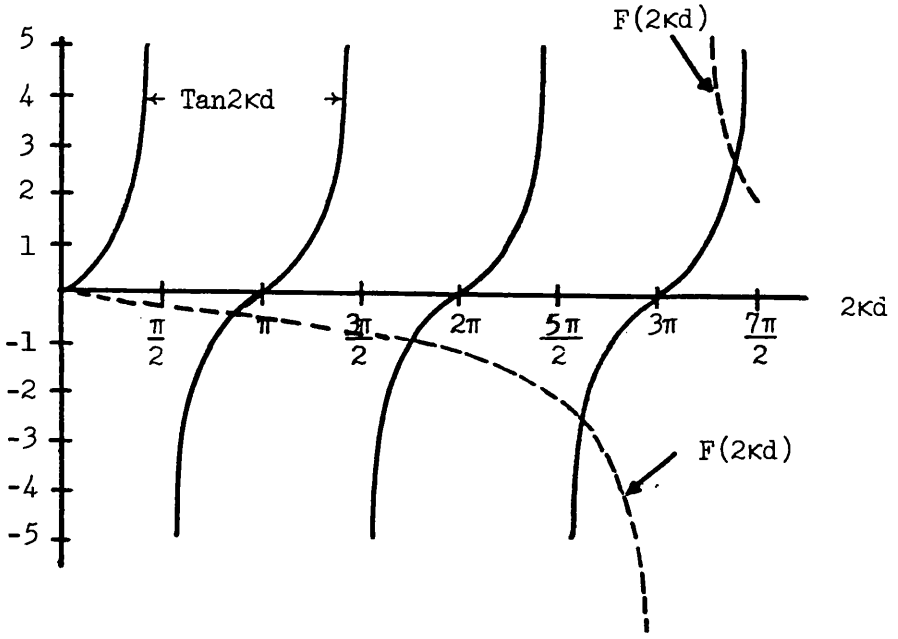

Figure 3.3.1 Graphical solution of the transcendental equation (3.3.1-20). The crossing points of the solid and dashed lines correspond to solutions. F(2Kd) can be determined from equation (3.3.1-22) (Ref. 2).

One can now immediately determine the propagation constant from the above given cut-off condition. Graphical solution of the transcendental equation (3.3.1-20) is shown in figure (3.3.1). Points of intersection of the dotted curve and the solid curve in this figure correspond to the solutions of the equation (3.3.1-20). The right hand side of this equation F(Kd) can be represented in terms of the refractive indices n_1, n_2 and n_3 by using relations (3.3.1-17) as given below:

$$F(Kd) = \frac{Kd\{\{(n_1^2 - n_2^2)(kd)^2 - (Kd)^2\}^{\frac{1}{2}} + \{(n_1^2 - n_3^2)(kd)^2 - (Kd)^2\}^{\frac{1}{2}}\}}{(Kd)^2 - \{(n_1^2 - n_2^2)(kd)^2 - (Kd)^2\}^{\frac{1}{2}}\{(n_1^2 - n_3^2)(kd)^2 - (Kd)^2\}^{\frac{1}{2}}} \qquad (3.3.1\text{-}22)$$

If v is the normalized frequency, defined as:

$$v = (n_1^2 - n_2^2)^{\frac{1}{2}}kd \qquad (3.3.1\text{-}23)$$

one sees that for $v < Kd$, one of the expression under the square root sign becomes negative, therefore F(Kd) curve ends at the point where $v = Kd$. In figure (3.3.1), there are four points of intersection which represent four excited modes. However from the equation (3.3.1-23) one sees that for a narrow active layer, low frequency or small refractive index difference, v is small and thus the condition $v = Kd$ occurs very close to the origin which means no guided mode is possible.

3.3.2 The symmetrical waveguide

As mentioned earlier $n_2 = n_3$ results in a symmetrical waveguide structure. Under this condition $\delta = \gamma$ in equation (3.3.1-20) which then reduces to the following expression:

$$\mathrm{Tan}(2Kd) = \{2K\gamma/(K^2 - \gamma^2)\} \qquad (3.3.2\text{-}1)$$

This may be written as:

$$\frac{2\mathrm{Tan}(Kd)}{1 - \mathrm{Tan}^2(Kd)} = \frac{2(\gamma/K)}{1 - (\gamma/K)^2} \qquad (3.3.2\text{-}2)$$

On simplification the following equation of degree two is obtained:

$$(\gamma/\kappa)\mathrm{Tan}^2(\kappa d) + \{1 - (\gamma/\kappa)^2\}\mathrm{Tan}(\kappa d) - \gamma/\kappa = 0 \qquad (3.3.2\text{-}3)$$

The roots of this quadratic equation are:

$$\mathrm{Tan}(\kappa d) = \gamma d/\kappa d \qquad (3.3.2\text{-}4)$$

$$\mathrm{Cot}(\kappa d) = -\gamma d/\kappa d \qquad (3.3.2\text{-}5)$$

Equations (3.3.2-4) and (3.3.2-5) give even and odd modes of the symmetrical waveguide respectively. Using the relations (3.3.1-17) one can write the following relation between γ^2 and κ^2 :

$$\kappa^2 d^2 + \gamma^2 d^2 = (n_1^2 - n_2^2)k^2 d^2 \qquad (3.3.2\text{-}6)$$

Since the field solution must satisfy this equation, in addition to (3.3.2-4), for even modes. Equation (3.3.2-6) represents a circle with its centre at the origin and radius $(n_1^2 - n_2^2)^{\frac{1}{2}}kd$. To find the graphical solution for even modes involves finding the intersection, in γd - κd plane, of the circle and the curve $\gamma d = \kappa d\mathrm{Tan}(\kappa d)$. Each intersection with $\gamma > 0$ corresponds to the confined mode. Even order mode solutions are shown in figure (3.3.2-1) for an active layer thickness $2d = 0.2\mu m$, $1.0\mu m$ and $1.5\mu m$. The values of n_1, n_2 and λ are 3.59, 3.385 and $0.9\mu m$ respectively. Similarly one can find the solution for odd modes. One of the important differences between the symmetrical and non-symmetrical waveguides is that the lowest order even mode in the symmetrical waveguide is never cut-off as shown in figure (3.3.2-1). This is valid for all active layer thicknesses. It is sometimes useful to derive the characteristic equation (3.3.2-1) in terms of normalized frequency v and normalized propagation constant b. From (3.3.1-17) u is defined below:

$$u^2 = (n_1^2 k^2 - \beta^2)d^2 \equiv \kappa^2 d^2 \qquad (3.3.2\text{-}7)$$

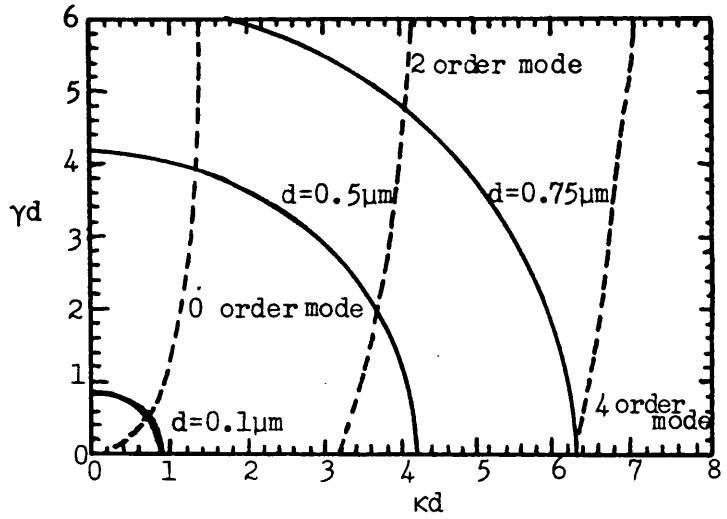

Figure 3.3.2-1 Graphical solution of the eigenvalue equation (3.3.2-4) for the even order TE modes(5).

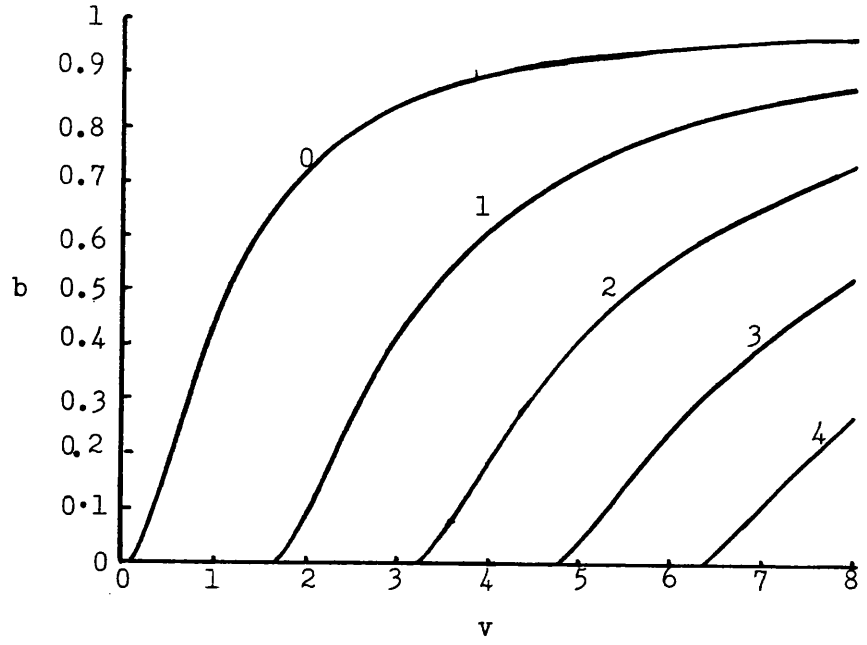

Figure 3.3.2-2 Normalized propagation constant b vs. normalized frequency v for symmetric three layer dielectric slab waveguide; labelling parameters give the value of mode number(1).

Using the normalized frequency v defined in the equation (3.3.1-23) and the equation given above, b is defined as below:

$$b = 1 - \frac{u^2}{v^2} \equiv \frac{\beta^2 - n_2^2k^2}{(n_1^2 - n_2^2)k^2} \equiv \frac{\gamma^2 d^2}{v^2} \qquad (3.3.2\text{-}8a)$$

$$b = \frac{(\beta/k)^2 - n_2^2}{(n_1^2 - n_2^2)} \qquad (3.3.2\text{-}8b)$$

On simplification the above expression can also be written as follows:

$$(\beta/k)^2 = bn_1^2 + (1 - b)n_2^2 \qquad (3.3.2\text{-}9)$$

As pointed out earlier, the cut-off condition is given by $\beta = n_2k$, and therefore b = 0. The plot of b vs. v is shown in the figure (3.3.2-2). From this figure it becomes clear that well away from cut-off (b = 0) the value of normalized propagation constant b approaches unity. Also there is no cut-off frequency v for the lowest order mode. Using the expressions (3.3.2-8a) for γ and (3.3.2-7) for κ one can write the following expression for the characteristic equation:

$$\mathrm{Tan}(2\sqrt{1 - b}\, v) = \left(\frac{2\sqrt{b}(1 - b)^{\frac{1}{2}}}{1 - 2b}\right) \qquad (3.3.2\text{-}10a)$$

or

$$2\sqrt{1 - b}\, v = \mathrm{Tan}^{-1}\left(\frac{2\sqrt{b}(1 - b)^{\frac{1}{2}}}{1 - 2b}\right) + L\pi \qquad (3.3.2\text{-}10b)$$

where L = 0,1,2,3,.... denotes the mode number. The cut-off condition b = 0 gives the cut-off frequency as below:

$$v_c = L\pi/2$$

Similar calculations can be repeated for T.M modes in which the non-zero component of magnetic field is H_y and this is coupled with E_x and E_y. The wave equation for the H_y component of magnetic field intensity is:

$$\partial^2 H_{yi}/\partial x^2 + (k^2 n_i^2 - \beta^2) H_{yi} = 0 \qquad i = 1,2,3 \qquad (3.3.2\text{-}11)$$

and solutions to this equation are obtained in a manner analogous to the electric field intensity.

3.3.3 Power flow for TE modes

The total power carried by the mode is related to the amplitude A of the propagating field. The power flow in the z direction is given by the following Poynting vector:

$$S_z = \frac{1}{2}(\underline{E} \times \underline{H}^*).\underline{c} \qquad (3.3.3\text{-}1)$$

where * denotes the complex conjugate of the field and $\underline{c}$ is the unit vector along z direction. As defined for the TE mode $\underline{E} = E_y\underline{b}$ and $\underline{H} = H_x\underline{a} + H_z\underline{c}$ one gets from the above equation S_z as below:

$$S_z = -\frac{1}{2} E_y H_x^* \qquad (3.3.3\text{-}2)$$

Substituting the value of H_x^* from equation (3.3.1-4a) and noting that the field, $E_y \propto \exp\{j(\omega t - \beta z)\}$. S_z expression reduces to:

$$S_z = \frac{\beta}{2\mu_o \omega} |E_y|^2 \qquad (3.3.3\text{-}3)$$

The time averaged power carried by the mode is given by integrating the above expression as shown below:

$$P = \frac{\beta}{2\mu_o\omega}\int_{-\infty}^{\infty} |E_y|^2 \, dx \equiv \frac{\beta}{2\mu_o\omega}\left\{\int_{-\infty}^{-2d} |E_y|^2 \, dx + \int_{-2d}^{0} |E_y|^2 \, dx + \int_{0}^{\infty} |E_y|^2 \, dx\right\} \qquad (3.3.3\text{-}4)$$

From the equation (3.3.1-16) using the appropriate field profile for each region the above integral expression can be written as shown below:

$$P_3 = \frac{\beta}{2\mu_o\omega}\int_0^{\infty}|E_y|^2dx = \left(\frac{\beta}{2\mu_o\omega}\right)\frac{A^2}{2\delta} \qquad x\geq 0$$

$$P_1 = \frac{\beta}{2\mu_o\omega}\int_{-2d}^{0}|E_y|^2dx = \left(\frac{\beta}{2\mu_o\omega}\right)\frac{A^2}{2}\left(\frac{\kappa^2+\delta^2}{\kappa^2}\right)\left(2d + \frac{\gamma}{\kappa^2+\gamma^2} + \frac{\delta}{\kappa^2+\delta^2}\right) \qquad 0\geq x\geq -2d$$

$$P_2 = \frac{\beta}{2\mu_o\omega}\int_{-\infty}^{-2d}|E_y|^2dx = \left(\frac{\beta}{2\mu_o\omega}\right)\frac{A^2}{2\gamma}\left(\frac{\kappa^2+\delta^2}{\gamma^2+\kappa^2}\right) \qquad x\leq -2d$$

(3.3.3-5)

It should be mentioned that in deriving the above expression use of relation (3.3.1-19a) has been made to eliminate B. The total power P thus becomes:

$$P = P_1 + P_2 + P_3 = \left(\frac{\beta}{2\mu_o\omega}\right)\frac{A^2}{2}\left(\frac{\kappa^2+\delta^2}{\kappa^2}\right)\left(2d + \frac{1}{\gamma} + \frac{1}{\delta}\right) \qquad (3.3.3\text{-}6)$$

The coefficient A from this expression relates to the total power P as follows:

$$A^2 \equiv \frac{\kappa^2}{\delta^2}B^2 = \frac{4\mu_o\omega P}{\beta}\left(\frac{\kappa^2}{(2d + 1/\gamma + 1/\delta)(\kappa^2+\delta^2)}\right) \qquad (3.3.3\text{-}7)$$

For a symmetrical waveguide the above expression can be further simplified by using the relation $\gamma = \delta$.

3.3.4 Confinement factor Γ

Another parameter of importance in laser devices is the confinement factor. It has been calculated in the previous section for various components of the total power in the three regions of the asymmetrical waveguide. The components P_2 and P_3 of the total power P spread out in the passive layers on either side of the active layer and therefore are not available for interaction with the population inversion in the central layer. If Γ denotes the fraction of the total power confined to the active layer, one has from the last section:

$$\Gamma = (P_1/P) = \left(\int_{-2d}^{0}|E_y|^2dx\right)\Big/\left(\int_{-\infty}^{\infty}|E_y|^2dx\right) \qquad (3.3.4\text{-}1)$$

Using expressions for P_1 and P from section (3.3.3), Γ can be written as below:

$$\Gamma = \frac{\{2d + \gamma/(\kappa^2 + \gamma^2) + \delta/(\kappa^2 + \delta^2)\}}{(2d + 1/\gamma + 1/\delta)} \qquad (3.3.4\text{-}2)$$

In a symmetrical waveguide ($\gamma = \delta$) however it becomes:

$$\Gamma = \frac{\{d + \gamma/(\kappa^2 + \gamma^2)\}}{(d + 1/\gamma)} \qquad (3.3.4\text{-}3a)$$

and

$$1 - \Gamma = \frac{\kappa^2/\{\gamma(\kappa^2 + \gamma^2)\}}{(d + 1/\gamma)} \qquad (3.3.4\text{-}3b)$$

One can easily see from the equations (3.3.3-5) and (3.3.3-6) that $(1-\Gamma)$ is nothing more than P_2/P, a fraction of the total power travelling in the passive layer for a symmetrical case. The mode travelling in the active region spreads out into the passive region and experiences loss. Thus the net gain experienced by the travelling mode is given by:

$$G = g\Gamma - \alpha_2(1 - \Gamma) \qquad (3.3.4\text{-}4)$$

where g is the gain coefficient of the active region and α_2 is the loss coefficient in the passive layer. The transverse modes in a semiconductor laser depend upon the refractive index variation perpendicular to the junction and the active layer thickness. In a real device only the fundamental transverse mode is excited a condition achieved by reducing the active layer thickness well under 1μm. It is clear from figure (1.1-2) as the refractive index step is decreased the degree of radiation confinement decreases, resulting in an increase in the threshold current density with decreasing the active layer thickness. The lowest threshold is obtained with the active layer thickness 0.1μm at $\Delta n = 0.4$ (corresponding to the composition $Al_{0.6}Ga_{0.4}As/GaAs/Al_{0.6}Ga_{0.4}As$).

3.4 Waveguiding In The Lateral Direction Of A Slab Waveguide

Unlike the transverse direction perpendicular to the heterojunctions discussed in section (3.3), there is no built-in step discontinuity in the refractive index in the lateral direction. However, because of non-uniform gain in the lateral direction of the active region a waveguide is formed (10 - 14). This non-uniform gain in the lateral direction is determined by the amount of population inversion of the carriers beneath the stripe electrodes due to current injection. The population inversion within the active region is maintained beyond the stripe edges upto a few diffusion lengths because of the diffusion of carriers and current spreading in the passive confining region. Thus a gain region under the stripe is sandwiched between the lossy regions. The injected carriers also perturb the dielectric constant of the active region as a result of the change they produce in the spectral distribution of the gain (15). This effect is governed by the Kramers-Kronig dispersion relations. From the discussion of section (3.2.3) it was learnt that if the medium has a negative absorption coefficient which is related to the extinction coefficient, the medium becomes active and the propagating field grows instead of attenuating. The complex refractive index of such a medium is given by:

$$\tilde{n} = n + jK \qquad (3.4\text{-}1)$$

Also the complex dielectric constant $\tilde{\varepsilon}_1$ for the active layer can be written as:

$$\tilde{\varepsilon}_1 = (n_1 + jK_1)^2 \qquad (3.4\text{-}2)$$

The analysis of three layer dielectric waveguide considered in section (3.3) is equally valid except that one has to retain the complex dielectric constant in the analysis. It is demonstrated here for a simple step discontinuity of the gain or loss, after Schlosser (12) as,

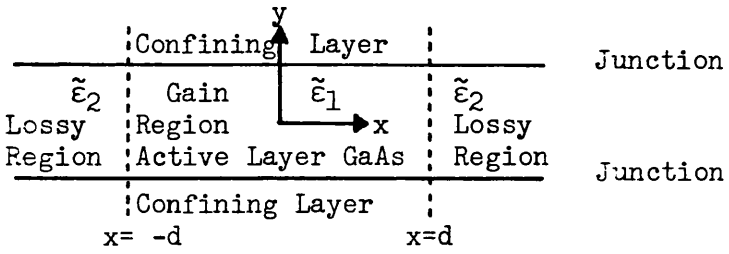

Figure (3.4-1) Gain region in the active layer of a stripe geometry injection laser surrounded by the lossy region. The lateral field is limited by the gain distribution. $\tilde{\varepsilon}_1$ and $\tilde{\varepsilon}_2$ denote the complex dielectric constants of the gain region and the lossy region of active layer.

shown in figure (3.4-1).

Using techniques analogous to the case given in section (3.3) for the TE mode, the wave equations for each region can be written. The corresponding dielectric constant for each region is used in this case. Initially the effect of junction waveguiding (perpendicular to the active region) in the y direction is ignored. For convenience a symmetrical waveguide is considered in the lateral direction x. Analogous to the set of equations (3.3.1-17) and (3.3.2-8) the following expressions can be written:

$$\left.\begin{array}{ll} \text{Normalized frequency} & v^2 = d^2k^2(\tilde{\varepsilon}_1 - \tilde{\varepsilon}_2) \\ \text{Normalized propagation constant and} & b = 1 - u^2/v^2 \equiv \gamma^2d^2/v^2 \\ & u^2 = d^2(\tilde{\varepsilon}_1k^2 - \tilde{\beta}^2) \equiv \kappa^2d^2 \\ & w^2 = \gamma^2d^2 = v\sqrt{b} \end{array}\right\} \quad (3.4\text{-}3)$$

By making use of these relations one can write equations similar to (3.3.2-4) and (3.3.2-5) given in section (3.3.2) for even and odd modes as:

Even mode $\quad u\mathrm{Tan}(u) = w \qquad (3.4\text{-}4a)$

Odd mode $\quad u\mathrm{Cot}(u) = -w \qquad (3.4\text{-}4b)$

However it should be pointed out here that u, v and w all defined by equations (3.4-3), are complex quantities. On comparing equation (3.4-4a) with (3.3.2-4) the field in the lossy regions is given by an expression of the type $\exp(-w|x|/d)$. As the field must decay to zero as $|x| \to \infty$ for the guided modes in the central region then the real part of w must be positive. Moreover the imaginary part of w must also be positive in order that phase fronts should have positive curvature in the direction

of propagation. This restricts any movement of the wavefronts from infinity towards the guiding structure and represents a wave expanding about a point (13). Hence both real and imaginary parts on the right hand side of equation (3.4-4a) are positive. Writing $u = (u_r + ju_i)$ and $w = (w_r + jw_i)$ in the equation (3.4-4a) the following expression is obtained for the left hand side of the equation:

$$uTan(u) = (u_r + ju_i)Tan(u_r + ju_i) \qquad (3.4\text{-}5a)$$

This expression must have both real and imaginary parts positive because the right hand side of the equation (3.4-4a) comprises positive real and imaginary parts. In order to split up this expression into real and imaginary parts, using the relation

$$Tan(u_r + ju_i) = \frac{Sin(u_r + ju_i)}{Cos(u_r + ju_i)} = \frac{Sin(u_r)Cosh(u_i) + jCos(u_r)Sinh(u_i)}{Cos(u_r)Cosh(u_i) - jSin(u_r)Sinh(u_i)}$$

and carrying out simplification one gets:

$$uTan(u) = \frac{Sin(2u_r) + jSinh(2u_i)}{2Cos^2(u_r)Cosh^2(u_i) + 2Sinh^2(u_i)Sin^2(u_r)}(u_r + ju_i)$$

or

$$uTan(u) = \frac{u_rSin(2u_r) - u_iSinh(2u_i)}{2Cos^2(u_r)Cosh^2(u_i) + 2Sinh^2(u_i)Sin^2(u_r)} + j\frac{u_iSin(2u_r) + u_rSinh(2u_i)}{2Cos^2(u_r)Cosh^2(u_i) + 2Sinh^2(u_i)Sin^2(u_r)}$$

(3.4-5b)

The denominator in both real as well as imaginary parts of the above expression is positive. Therefore in order that uTan(u) should have both positive real as well as imaginary parts, the following inequalities must hold.

$$u_rSin(2u_r) - u_iSinh(2u_i) > 0 \qquad (3.4\text{-}6a)$$

$$u_i \mathrm{Sin}(2u_r) + u_r \mathrm{Sinh}(2u_i) > 0 \qquad (3.4\text{-}6b)$$

After Adams (13), multiplying (3.4-6a) by u_i and (3.4-6b) by u_r and adding together gives:

$$\mathrm{Sin}(2u_r) > 0 \qquad (3.4\text{-}7)$$

Since $u_i \mathrm{Sinh}(2u_i)$ can never be negative therefore from (3.4-6a) and (3.4-7) one concludes:

$$u_r > 0 \qquad (3.4\text{-}8a)$$

The inequality (3.4-6b) can never be satisfied unless $u_i > 0$ because $\mathrm{Sin}(2u_r)$ and u_r are both positive.

$$u_i > 0 \qquad (3.4\text{-}8b)$$

From the equation (3.4-3), $w^2 = \gamma^2 d^2 \equiv (\tilde{\beta}^2 - \tilde{\varepsilon}_2 k^2) d^2$, the following expressions can be written.

$$u^2 + w^2 = v^2 \qquad (3.4\text{-}9)$$

$$\mathrm{Im}(v^2) = 2(u_r u_i + w_r w_i) \qquad (3.4\text{-}10)$$

Im denotes the imaginary part of the quantity v^2. It has been seen just above that all u_r, u_i, w_r and w_i are positive and hence $\mathrm{Im}(v^2) > 0$. After Schlosser (12) condition for guided modes can be derived as follows using the equation (3.4-3):

$$\mathrm{Im}(v^2) \equiv 2(n_1 K_1 - n_2 K_2) k^2 d^2 \qquad (3.4\text{-}11)$$

As seen above in the equation (3.4-10), $\mathrm{Im}(v^2) > 0$ this shows that the undermentioned inequality must hold.

$$(n_1 K_1 - n_2 K_2) > 0 \qquad (3.4\text{-}12)$$

From this condition various possiblities for stable conditions can occur and are given as:

(i) $K_1 = K_2$; the condition for this special case refers to standard refractive index guided waveguidance i.e $n_1 > n_2$.

(ii) $n_1 = n_2$; the inequality now gives the condition $K_1 > K_2$ (i.e the gain in the central region should be more than the outside regions which agrees well with the physical intution of the stripe geometry laser device namely that under the stripe the gain is more than outside the pumped region.)

(iii) $n_1 = n_2 + \Delta n$; where Δn is small compared with n_2 but not necessarily small compared with K_1 or K_2, the above inequality (3.4-12) becomes $(K_1 - K_2)/K_1 + \Delta n/n_2 > 0$. This gives the stability condition. Under the stripe the region of maximum gain ($K_1-K_2>0$) corresponds to the lowered refractive index ($\Delta n<0$). Therefore the gain guidance is opposed by the antiguidance due to the central region of lower refractive index. As long as the above inequality is satisfied there can be a stable mode.

3.4.1 Gain guided modes

To demonstrate this type of guiding behaviour assume that there is no change in the refractive index of the central region and the outside regions. In this case the normalized frequency v becomes from (3.4-3) ($n_1 = n_2$) as below:

$$v = dkn\left(\frac{2j(K_1 - K_2)}{n}\right)^{\frac{1}{2}} \equiv dkn\left(\frac{K_1 - K_2}{n}\right)^{\frac{1}{2}}(1 + j) \qquad (3.4.1\text{-}1)$$

This shows that the phase angle of v is always $\pi/4$ and independent of material parameters. Also from the set of equations (3.4-3) One can write for b the following equation.

$$b = \frac{(\tilde{\beta}/k)^2 - \tilde{\varepsilon}_2}{(\tilde{\varepsilon}_1 - \tilde{\varepsilon}_2)} \qquad (3.4.1\text{-}2)$$

or

$$(\tilde{\beta}/k)^2 = b\tilde{\varepsilon}_1 + (1 - b)\tilde{\varepsilon}_2 \qquad (3.4.1\text{-}3)$$

The characteristic equation (3.4-4a) can be written as:

$$\sqrt{b} = \sqrt{1 - b}\,\mathrm{Tan}(v\sqrt{1 - b}) \qquad (3.4.1\text{-}4)$$

This equation shows the dispersion of the propagation constant as a function of $|v|$ as shown in figure (3.4.1-1). From this figure it is obvious that as $|v| \to 0$, $b_r \to 0$ (i.e there is no cut-off frequency for the lowest order mode). This is identical to the real refractive index case discussed in section (3.3.2). An approximate form of equation (3.4.1-3) is:

$$(\tilde{\beta}/k) \simeq n - b_i \Delta K + j\{K_2(1 - b_r) + K_1 b_r\} \qquad (3.4.1\text{-}5)$$

where $b = b_r + jb_i$ and $\Delta K = K_1 - K_2$. Since the imaginary part of the propagation constant $\tilde{\beta}$ determines the modal gain, as $b_r \to 0$, its value becomes K_2 and the field is no longer confined to the central region. However as $b_r \to 1$, the imaginary part of $(\tilde{\beta}/k)$ approaches K_1 and the field is confined to the central region where the gain is highest.

It has already been mentioned in the beginning of section (3.4) that the refractive index is also influenced by carrier concentration and it is important to see its effect on this gain induced case. In the central region of maximum gain the refractive index is lowered by the presence of the carriers. Consider the case of an arbitrary change in refractive index Δn in the central region. Let the refractive index of the central region be $n + \Delta n$, $(\Delta n < 0)$ while that of the outside regions be n. Assuming Δn , $\Delta K \ll n$ one gets:

$$v^2 = \{(n + \Delta n + jK_1)^2 - (n + jK_2)^2\}k^2d^2 \qquad (3.4.1\text{-}6)$$

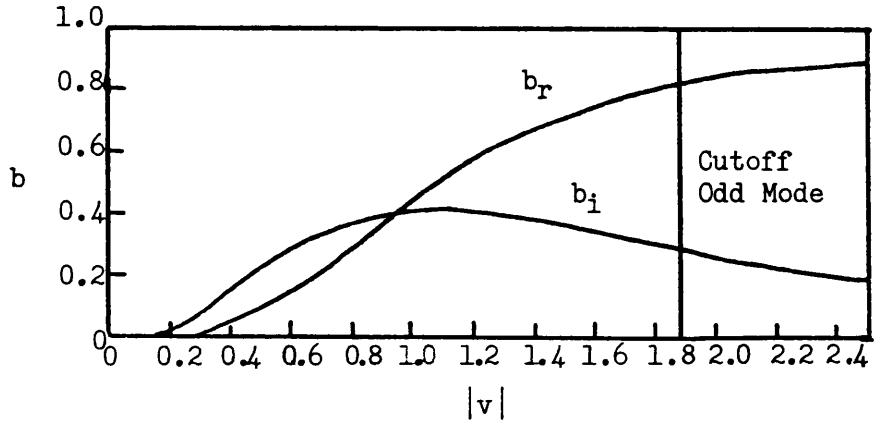

Figure 3.4.1-1 b vs. |v| for the lowest order even mode $\{n_1 = n_2\}$ after Schlosser (12).

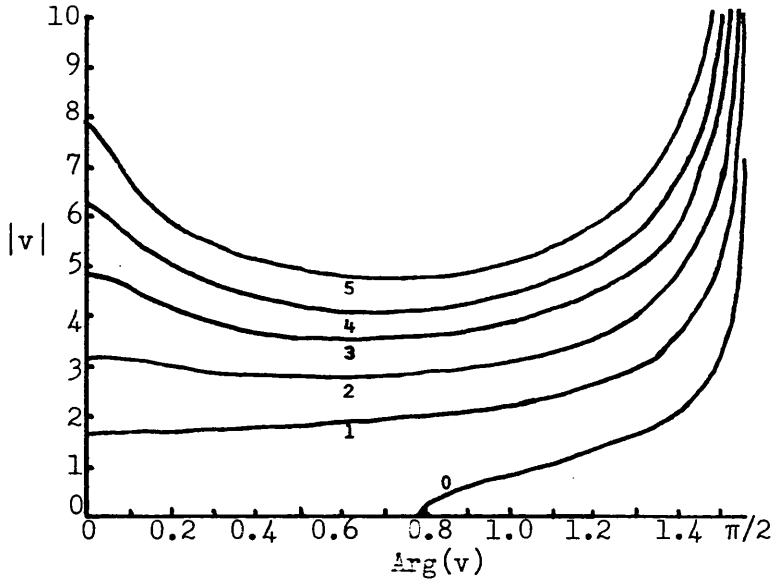

Figure 3.4.1-2 Mode cut-offs for the first six modes of symmetric slab waveguides of complex permittivity (16).

or

$$v \simeq \{2n\Delta n + 2jn(K_1 - K_2)\}^{\frac{1}{2}}dk \qquad (3.4.1\text{-}7)$$

Clearly, unlike the gain induced case the phase angle of v is no longer $\pi/4$ and independent of the material parameters. A plot of $|v|$ and Arg(v) is shown in figure (3.4.1-2). The expression (3.4.1-3) now becomes:

$$(\tilde{\beta}/k) \simeq n + \Delta n b_r - b_i \Delta K + j(K_2 + b_r \Delta K + b_i \Delta n) \qquad (3.4.1\text{-}8)$$

where $\Delta K = K_1 - K_2$ and $b = b_r + jb_i$. If $b_i \Delta n$ is positive from this equation (12) one sees that the imaginary part of $(\tilde{\beta}/k)$ gets an additional positive term $b_i \Delta n$ and therefore the guidance is improved. On the other hand in the case of a refractive index depression in the central region Δn is negative and gives rise to antiguidance to counteract the confinement provided by the gain. If the depression is sufficiently strong it completely destroys the confinement of the field to the central region. From figure (3.4.1-1) there is no cut-off frequency for the zero order mode. In figure (3.4.1-2) the line Arg(v) $=\pi/2$ is a region where no guided mode exists and may correspond to inverted structure ($n_2 > n_1$). The vertical line Arg(v) = 0 coincides with the v values for mode cut-off in case of real index guidance.

3.5 Effective Dielectric Constant Method Of Solution In Active Waveguides

It has been seen in sections (3.3) and (3.4) that the field is vertically confined due to refractive index discontinuities existing at the heterojunctions. Lateral confinement, however, is due to the variations of the complex dielectric constant along the junction in the active region. Following Marcatili's (20) analysis two types of modes supported by such a structure shown in figure (3.5-1) are E^x_{xy} and E^y_{xy}. They are TEM types i.e transverse to the direction of propagation.

The main field components of the first E^x_{xy} type are E_x and H_y while those of the second type E^y_{xy} are E_y and H_x. The suffix 'xy' with E^x_{xy} and E^y_{xy} hybrid modes are the number of zeros in the x direction and y direction field distributions. Butler et al (19) have attempted to solve the 2-dimensional wave equation for a laser device rigorously. In real laser devices, however, the active layer is very thin, (typically 0.1 to 0.3μm), the electric field is strongly polarized along the junction plane (17, 18) i.e the x direction. The E^x_{xy} mode for this rectangular structure corresponds to TM mode characteristic equation of a 3-layer dielectric slab waveguide in the x direction with infinite extent in y and z directions(17, 20). Similarly E^y_{xy} corresponds to the TE mode characteristic equation of a 3-layer dielectric waveguide in y direction with infinite extent in x and z directions. The effective dielectric constant method used by various authors (21 - 25) results in a one dimensional equation for the lateral field distribution. The effect of the cladding layers is taken into account by the use of an effective dielectric constant. Symmetrical confining layers in figure (3.5-1) sandwich the active layer and therefore the structure is symmetrical w.r.t x = 0 and y = 0 axes as shown in figure (3.5-2). Rozzi et al (25) have shown that the field is either symmetric or anti-symmetric w.r.t x and y axes. Consequently it is necessary to study only the first quadrant in the x-y plane with magnetic or electric field short circuit at x = 0 and y = 0 planes.

The section of the active layer extending between $-W/2 \leq x \leq W/2$ has a complex dielectric constant $\tilde{\varepsilon}_1$ where the imaginary part of the dielectric constant determines the gain experienced by the propagating field. The region of the active layer beyond the stripe edges ($|x| \geq W/2$) and cladding layers are assumed lossless. It should be noted that the gain region extends beyond the stripe edges due to non-uniform injection of

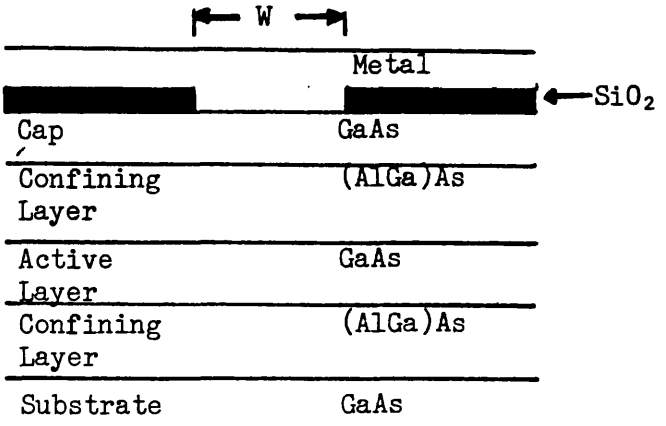

Figure 3.5-1 Cross section of contemporary stripe geometry injection laser.

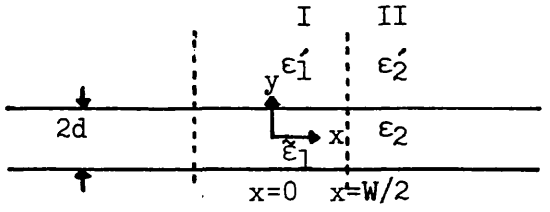

Figure 3.5-2 FIG. shows how the symmetry of the device along x and y axes allows to solve the problem for the first quadrant (25).

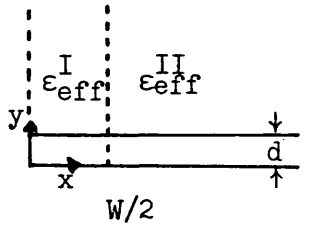

Figure 3.5-3 Equivalent reduced structure of laser following the analysis of Rozzi el al (25).

the current from the stripe electrode and out diffusion of the carriers. As mentioned earlier for this structure the E^{y}_{xy} mode is equivalent to the TE mode equation of a 3-layer slab waveguide in the y direction extending infinitely in x and z directions. From section (3.3.2) one can write the following characteristic equation for even modes in region I shown in figure (3.5-2) as below:

$$\mathrm{Tan}(\kappa_I d) = \gamma_I/\kappa_I \tag{3.5-1}$$

where

$$\tilde{\beta}^2 = \tilde{\varepsilon}_1 k^2 - \kappa_I^2 = \varepsilon_1' k^2 + \gamma_I^2 \tag{3.5-2}$$

The solution of the above equation gives κ_I. The effective dielectric constant for the region I can therefore be defined as:

$$\varepsilon^{I}_{eff} = \tilde{\varepsilon}_1 - (\kappa_I/k)^2 \tag{3.5-3}$$

Similarly, applying this analysis to region II in figure (3.5-2) the effective dielectric constant ε^{II}_{eff} can be defined as:

$$\varepsilon^{II}_{eff} = \varepsilon_2 - (\kappa_{II}/k)^2 \tag{3.5-4}$$

The problem of finding the lateral field distribution then becomes one of solving for the TM modes in a dielectric slab waveguide in x direction with dielectric constants ε^{I}_{eff} and ε^{II}_{eff} as shown in figure (3.5-3). The characteristic equation for a TM mode is given by:

$$\mathrm{Tan}(\kappa W/2) = \frac{\varepsilon^{I}_{eff}\gamma}{\varepsilon^{II}_{eff}\kappa} \tag{3.5-5}$$

where $\tilde{\beta}$ propagation constant is related to κ and γ by the following expression:

$$\tilde{\beta}^2 = \varepsilon^{I}_{eff}k^2 - \kappa^2 = \varepsilon^{II}_{eff}k^2 + \gamma^2 \tag{3.5-6}$$

In real devices $\varepsilon^{I}_{eff} \simeq \varepsilon^{II}_{eff}$ and the above equation (3.5-5) thus becomes:

$$\mathrm{Tan}(\kappa W/2) = \gamma/\kappa \qquad (3.5\text{-}7)$$

where κ, γ are complex quantities.

3.5.1 The wave equation for a stripe geometry laser

The form of the wave equation for an electric field Φ which is predominantly polarized along the x direction is (17 - 18):

$$\nabla_T^2\Phi + \{k^2\varepsilon(x,y) - \beta^2\}\Phi = 0 \qquad (3.5.1\text{-}1)$$

where

$$\nabla_T^2 = \partial^2/\partial x^2 + \partial^2/\partial y^2$$

This assumes that the propagating mode has the normal time dependence and z dependence of the form $\exp(j\omega t - j\beta z)$. Within the active layer the relative permitivity $\varepsilon(x,y)$ is constant vertically but varies along the junction in the lateral direction. After Paoli (21) a solution of the following form of the wave equation (3.5.1-1) is sought.

$$\Phi(x,y) = E(y)F(x) \qquad (3.5.1\text{-}2)$$

where E is dependent on y only and F is a function of x alone. Since the variation of the dielectric constant $\varepsilon(x,y)$ is very slow in the x direction (along the junction) when compared with the abrupt step discontinuity in the dielectric constant existing at the junctions, therefore the mode field E(y) is not appreciably affected by the confinement along x. On substituting the solution (3.5.1-2) into equation (3.5.1-1) neglecting terms dE/dx and d^2E/dx^2 (x dependence of E is very weak) one gets:

$$(1/F)d^2F/dx^2 + (1/E)d^2E/dy^2 + \{k^2\varepsilon(x,y) - \beta^2\} = 0 \qquad (3.5.1\text{-}3)$$

Clearly the term $\{(1/F)d^2F/dx^2\}$ is a function of x alone thus the above equation can be written as:

$$(1/E)d^2E/dy^2 + \{k^2\varepsilon(x,y) - \{\beta^2 - (1/F)d^2F/dx^2\}\} = 0 \qquad (3.5.1\text{-}4)$$

This wave equation can be solved at a given x for the three-layer slab waveguide in the y direction. It has been seen in section (3.3) from equation (3.3.1-16) that the solution in the active layer for guided modes is of the type Sinκy or Cosκy. κ is related to the propagation constant and the dielectric constant $\varepsilon(x,y)$ at x, $\varepsilon_a(x)$ of the active layer by:

$$\{\beta^2 - (1/F)d^2F/dx^2\} = k^2\{\varepsilon_a(x) - \kappa^2/k^2\} \qquad (3.5.1\text{-}5)$$

Also, from section (3.5) it has been seen that the right hand side of the above equation is the definition of the effective dielectric constant and hence the following equation for the lateral field profile is obtained.

$$(1/k^2)\{\beta^2 - (1/F)d^2F/dx^2\} = \varepsilon_{eff}(x)$$

or

$$d^2F/dx^2 + \{k^2\varepsilon_{eff}(x) - \beta^2\}F = 0 \qquad (3.5.1\text{-}6)$$

Various authors have assumed different pre-known approximations for the effective dielectric constant, $\varepsilon_{eff}(x)$, to get the solution of the wave equation in a closed form. Authors (21 - 24) used a parabolic profile for the complex effective dielectric constant, $\tilde{\varepsilon}_{eff}(x)$, which gives a Hermite-Gaussian solution for the field profile. This is not a bad approximation for a broad area stripe geometry laser (26) with stripe widths greater than 10μm. Asbeck et al (27) have reported a non-Gaussian field profile in a laser with a stripe width less than 10μm. However this led them to assume a Cosh^{-2} type of dielectric constant variation. After Buus (28) if one supposes that ε_1 and ε_2 are the dielectric constants of the active and passive layers respectively one can write the expression for the normalized propagation constant b similar to the equation (3.3.2-8a) as:

$$b = \frac{\{\beta^2 - (1/F)d^2F/dx^2\}/k^2 - \varepsilon_2(x)}{\varepsilon_1(x) - \varepsilon_2(x)} \qquad (3.5.1\text{-}7)$$

Since $\{\beta^2 - (1/F)d^2F/dx^2\} = \varepsilon_{eff}(x)$, therefore the above relation becomes:

$$b = \{\varepsilon_{eff}(x) - \varepsilon_2(x)\}/\{\varepsilon_1(x) - \varepsilon_2(x)\}$$

or

$$\varepsilon_{eff}(x) = b\varepsilon_1(x) + (1 - b)\varepsilon_2(x) \qquad (3.5.1\text{-}8)$$

Far away from the cut-off condition the field is confined to the active layer and from figure (3.3.2-2) if ε_1 and ε_2 are real quantities b approaches unity whereas $\varepsilon_{eff}(x) = b\varepsilon_1(x)$. Also from the relation between b and Γ which is given as below one gets (28):

$$\Gamma = b + \frac{(1 - b)v\sqrt{b}}{1 + v\sqrt{b}} \simeq b \qquad \text{as } b \to 1$$

where v is the normalized frequency defined by the equation (3.3.1-23). The effective dielectric constant from the expression (3.5.1-8) under this approximation thus becomes:

$$\varepsilon_{eff}(x) = \Gamma\varepsilon_1(x) \qquad (3.5.1\text{-}9)$$

An analogous expression, derived by Thompson (29), shows that the variation of the effective dielectric constant along the junction follows the variation of the active layer dielectric constant but reduced by the confinement factor Γ. A similar expression for the complex dielectric constant has been derived by Adams (30). In this case both real as well as imaginary parts of the effective dielectric constant follow the variation of the central layer reduced by the confinement factor Γ.

3.5.2 Effective refractive index

So far, it has been stated that the solution of the wave equation (3.5.1-6) can be written in a closed formed assuming the variation of the effective dielectric constant to be a parabolic form or $Cosh^{-2}$ form. It is not the aim of this project to pre-assume the functional variation of the effective dielectric constant. It is therefore intended to solve

the wave equation with the variation of complex dielectric constant determined by the carrier distribution in the active layer. In order to do this a linear variation of the complex dielectric constant is assumed in line with other authors (31 - 33). It has been shown in section (3.2.3) that the imaginary part of the dielectric constant is related to the gain coefficient of the propagating field and is proportional to the inversion population in the active region. After Asbeck et al (31), the linear variation of the dielectric constant is given by:

$$\Delta\varepsilon(x) = (-R + j)C_2N(x) \qquad (3.5.2\text{-}1)$$

where R is a coupling parameter between the refractive index guidance and gain guidance, N(x) is the carrier concentration, C_2 is a constant.

The value of $R \simeq 3.5 - 4.5$ (31). $(-RC_2)$ corresponds to a depression in the refractive index due to injected carriers. As mentioned earlier in section (3.4) the gain and the refractive index are related by the Kramers-Kronig relations and thus the presence of gain can change the refractive index. Furthermore, for the case of an injection laser, the injected carriers change the refractive index due to the plasma resonance (28). Therefore an increase in the gain means an increase in the population inversion and decrease in the refractive index. The variation is given by the change in real part of refractive index $(n_o - n)$ and the extinction coefficient K as:

$$R = (n_o - n)/K \qquad (3.5.2\text{-}2)$$

where n_o is the background effective refractive index which is related to the real part of refractive index of the cladding layer and the active layer by the equation given below:

$$n_o^2 \simeq \Gamma n_1^2 + (1 - \Gamma)n_2^2 \qquad (3.5.2\text{-}3)$$

where n_1 and n_2 are the real parts of the refractive indices of the active layer and the passive layer respectively. The dielectric constant variation of the active layer is found using equation (3.5.2-1) and is given as:

$$\tilde{\varepsilon}_{eff}(x) = n_o^2 + (-R + j)C_2N(x) \qquad (3.5.2\text{-}4a)$$

or

$$\tilde{\varepsilon}_{eff}(x) \simeq \{n_o + (-R + j)(C_2N(x)/2n_o)\}^2 \qquad (3.5.2\text{-}4b)$$

Furthermore $\tilde{\varepsilon}_{eff}(x)$ is the square of the complex effective refractive index $\tilde{n}_{eff}(x) = \{n(x) + jK(x)\}$ and $K(x) = g(x)/2k$ so one gets the following expression for $\tilde{\varepsilon}_{eff}(x)$:

$$\tilde{\varepsilon}_{eff}(x) \equiv \left[n(x) + j\frac{g(x)}{2k}\right]^2 = \tilde{n}_{eff}^2(x) \qquad (3.5.2\text{-}4c)$$

Equating the equations (3.5.2-4b) and (3.5.2-4c) the following expressions are obtained:

$$n(x) = n_o - R\{C_2N(x)/2n_o\} \qquad (3.5.2\text{-}5a)$$

$$g(x)/2k = \{C_2N(x)/2n_o\} \qquad (3.5.2\text{-}5b)$$

Substituting the value of $C_2N(x)$ from the equation (3.5.2-5b) in the equation (3.5.2-5a) one gets:

$$n(x) = n_o - R\{g(x)/2k\} \qquad (3.5.2\text{-}5c)$$

The effective complex refractive index $\tilde{n}_{eff}(x) = n(x) + j\frac{g(x)}{2k}$ therefore reduces to:

$$\tilde{n}_{eff}(x) = n_o + \{(-R + j)g(x)/2k\} \qquad (3.5.2\text{-}6)$$

Hence the wave equation for the lateral field profile (3.5.1-6) can be written as:

$$d^2F/dx^2 + \{k^2\tilde{n}_{eff}^2(x) - \tilde{\beta}^2\}F = 0 \qquad (3.5.2\text{-}7)$$

The local gain ,g(x), given in equation (3.5.2-6), is related to the local carrier density N(x) by the following linear relation (34, 35):

$$g(x) = a'N(x) - b' \qquad (3.5.2\text{-}8)$$

where a' and b' are constants whose values are given by Asbeck et al (31) as 300×10^{-18} cm^2 and 450 cm^{-1}. A more general discussion of this relation and its validity is given by Thompson (36).

To calculate the optical intensity of the laser let S_o be the number of photons per unit active volume of the cavity of the laser. The intensity is defined as:

$$\int_{-\infty}^{\infty}|F|^2dx = S_o\int_{-\infty}^{\infty}|\psi(x)|^2dx \qquad (3.5.2\text{-}9)$$

The wave equation (3.5.2-7) can therefore be written as below:

$$d^2\psi/dx^2 + \{k^2\tilde{n}_{eff}^2(x) - \tilde{\beta}^2\}\psi = 0 \qquad (3.5.2\text{-}10)$$

The normalized field distribution can be defined as:

$$\Psi(x) = \frac{W|\psi(x)|^2}{\int_{-\infty}^{\infty}|\psi(x)|^2dx} \qquad (3.5.2\text{-}11)$$

where W is called scaling factor which can be chosen as the stripe width of the laser. From the equation (3.5.2-10) the following expression can be written by multiplying the equation by ψ^* and carrying out integration:

$$\tilde{\beta}^2 = \frac{\int_{-\infty}^{\infty}\psi^*(d^2\psi/dx^2)dx + k^2\int_{-\infty}^{\infty}\tilde{n}_{eff}^2(x)|\psi|^2dx}{\int_{-\infty}^{\infty}|\psi|^2dx} \qquad (3.5.2\text{-}12)$$

On substituting the value of $\tilde{n}_{eff}$ from the equation (3.5.2-6) the following expression is obtained:

$$\tilde{\beta}^2 = \frac{\int_{-\infty}^{\infty}\psi^*(d^2\psi/dx^2)dx + n_o^2k^2\int_{-\infty}^{\infty}|\psi|^2dx + (-R + j)n_ok\int_{-\infty}^{\infty}g(x)|\psi|^2dx}{\int_{-\infty}^{\infty}|\psi|^2dx}$$

The contribution from the integral containing $d^2\psi/dx^2$ in its integrand is negligible when compared with the integral having multiplication factor $n_o^2k^2$ therefore one can write the above expression as:

$$\tilde{\beta}^2 \simeq \frac{\left[n_o^2k^2\int_{-\infty}^{\infty}|\psi|^2dx - Rn_ok\int_{-\infty}^{\infty}g(x)|\psi|^2dx\right] + jn_ok\int_{-\infty}^{\infty}g(x)|\psi|^2dx}{\int_{-\infty}^{\infty}|\psi|^2dx} \qquad (3.5.2\text{-}13)$$

$\tilde{\beta}^2$ is the square of the propagation constant, which is complex and can be approximated by the expression:

$$\tilde{\beta}^2 \simeq \{Re(\tilde{\beta})\}^2 + 2jRe(\tilde{\beta})Im(\tilde{\beta}) \qquad (3.5.2\text{-}14)$$

Equating real and imaginary parts from equations (3.5.2-13) and (3.5.2-14) one gets:

$$\{Re(\tilde{\beta})\}^2 = \frac{n_o^2k^2\int_{-\infty}^{\infty}|\psi|^2dx - Rn_ok\int_{-\infty}^{\infty}g(x)|\psi|^2dx}{\int_{-\infty}^{\infty}|\psi|^2dx}$$

Again under the approximation $n_o^2k^2\int_{-\infty}^{\infty}|\psi|^2dx >> Rn_ok\int_{-\infty}^{\infty}g(x)|\psi|^2dx$ the above expression becomes:

$$Re(\tilde{\beta}) \simeq n_ok \qquad (3.5.2\text{-}15)$$

Similarly

$$2\mathrm{Im}(\tilde{\beta}) \simeq \frac{n_o k\int_{-\infty}^{\infty} g(x)|\psi|^2 dx}{\mathrm{Re}(\tilde{\beta})\int_{-\infty}^{\infty}|\psi|^2 dx} = \frac{\int_{-\infty}^{\infty} g(x)|\psi|^2 dx}{\int_{-\infty}^{\infty}|\psi|^2 dx} \qquad (3.5.2\text{-}16)$$

It has been shown already that twice the imaginary part of the complex propagating constant $\tilde{\beta}$ is the modal gain, thus the above equation gives the modal gain (37). The modal gain must make up for the various losses in the cavity discussed in chapter II in order for the mode to be sustained.

3.6 Conclusions

In this chapter the basic theory of three-layer slab waveguides and its application to the waveguiding mechanism in double heterostructure lasers have been presented. The relations between the optical and electrical constants were also given. The confinement factor, which is a fraction of the propagating mode within the active layer, was introduced. The waveguiding mechanism in the lateral direction of a stripe geometry laser which is extremely important for the stability of the device was also discussed. The idea of effective dielectric constant was introduced which reduced the 2-dimensional wave equation (perpendicular and parallel to the junctions) to one dimensional wave equation for the calculation of the field profile in the lateral direction. The relations given in section (3.5.2) will be used frequently in the later part of this thesis.

References

1. M.J. Adams: "Introduction to Optical Waveguides", John Wiley, New York, 1981.

2. D. Marcuse: "Theory of Dielectric Optical Waveguides", Academic Press, New York, 1974.

3. T. Tamir(Ed.): "Integrated Optics: Topics in Applied Physics", Vol.7, Springer Verlag, Berlin, 1975.

4. H.J. Kressel and J.K. Butler: "Semiconductor Lasers and Heterojunction LEDS", Academic Press, New York, 1977.

5. H.C. Casey, Jr. and M.B. Panish: "Heterostructure Lasers, Part A: Fundamental Principles", Academic Press, New York, 1978.

6. G.H.B. Thompson: "Physics of Semiconductor Laser Devices", Wiley, New York, 1980.

7. D. Marcuse: "Light Transmission Optics", Van Nostrand-Rienhold, Princeton New Jersey, 1972.

8. N.S. Kapany and J.J. Burke: "Optical Waveguides", Academic Press, New York, 1972.

9. H.C. Casey, Jr. and M.B. Panish: "Heterostructure Lasers, Part B: Materials and Operating Characteristics", Academic Press, New York, 1978.

10. W. Streifer, R.D. Burnham and D.R. Scifres: "An analytic study of (GaAl)As gain guided lasers at threshold", IEEE J. Quantum Electron., Vol. QE-18, pp.857-863, 1982.

11. F.R. Nash: "Mode guidance parallel to the junction plane of double heterostructure GaAs lasers", J. Appl. Phys., Vol.44, pp.4696-4706, 1973.

12. W.O. Schlosser: "Gain-induced modes in planar structures", Bell Syst. Tech. J., Vol.52(6), pp.887-905, 1973.

13. M.J. Adams: "An Introduction to Optical Waveguides", pp.50-58, Wiley, New York, 1981.

14. W. Streifer, D.R. Scifres and R.D. Burnham: "Analysis of gain induced waveguiding in stripe geometry diode lasers", IEEE J. Quantum Electron., Vol. QE-14, pp.418-427, 1978.

15. G.H.B. Thompson: "Physics of Semiconductor Laser Devices", pp.535-537, Wiley, New York, 1980.

16. J. Buus: "The theory of the dielectric slab waveguide with complex refractive index applied to GaAs lasers", Proc. Seventh European Microwave Conference, Copenhagen, Microwave Exhibitions and Publishers Ltd., Sevenoaks, pp.29-33

17. J.B. Delaney and J.K. Butler: "The effect of device geometry on lateral mode content of stripe geometry lasers", IEEE J. Quantum Electron.,pp.750-755, 1979.

18. H.S. Sommers, Jr.: "Experimental properties of injection lasers , V.strong polarization", J. Appl. Phys.,Vol.45, pp.237-242, 1974.

19. J.K. Butler and J.B. Delaney: "A rigorous boundary value solution for the lateral modes of stripe geometry injection lasers", IEEE J. Quantum Electron., Vol. QE-14, pp.507-513, 1978.

20. E.A.J. Marcatili: "Dielectric rectangular waveguide and directional coupler for the integrated optics", Bell Syst. Tech. J., Vol.48, pp2071-2102, 1969.

21. T.L. Paoli: "Waveguiding in a stripe geometry injection laser" IEEE J. Quantum Electron., Vol. QE-13, pp.662-668, 1977.

22. J.K. Butler and J.B. Delaney: "Field solutions for the lateral modes of stripe geometry injection lasers", IEEE J. Quantum Electron., Vol. QE-16, pp.1326-1328, 1980.

23. J. Buus: "The effective index method and its application to semiconductor lasers", IEEE J. Quantum Electron., pp.1083-1089 1982.

24. G.H.B. Thompson, D.F. Lovelace and S.E.H. Turley: "Kinks in the light/current characteristics and near-field shifts in (GaAl)As-heterostructure stripe lasers and their explanation by the effect of self focusing on a built-in optical waveguide", Solid State Electron Devices, pp.12-30, 1977.

25. T.E. Rozzi, T. Itoh and L. Grun: "Two-dimensional analysis of the GaAs double heterostructure stripe-geometry laser", Radio Science, Vol.12, pp.543-549, 1977.

26. D.D. Cook and F.R. Nash: "Gain induced guiding and astigmatic output of GaAs laser", J. Appl. Phys., Vol.46, pp.1661-1672, 1975.

27. P.M. Asbeck, D.A. Cammack and J.J. Daniele: "Non-Gaussian fundamental mode patterns in a narrow stripe geometry lasers", Appl. Phys. Lett., Vol.33, pp.504-506, 1978.

28. J. Buus: "Detailed field model for DH stripe lasers", Opt. Quantum Electron., Vol.10, pp.459-474, 1978.

29. G.H.B. Thompson: "Physics of Semiconductor Laser Devices", pp.528-530, Wiley, New York, 1980.

30. M.J. Adams: "An Introduction to Optical Waveguides", pp.208-213, Wiley, New York, 1981.

31. P.M. Asbeck, D.A. Cammack, J.J. Daniele and V. Klebanoff: "Lateral mode behaviour in narrow stripe lasers", IEEE J. Quantum Electron., Vol. QE-15, pp.727-733, 1979.

32. R. Lang: "Lateral transverse mode instability and its stabilization in stripe geometry injection lasers", IEEE J. Quantum Electron., Vol. QE-15, pp.718-726, 1979.

33. C. Guo and K. Wang: "Intrinsic pulsation in stripe-geometry DH semiconductor lasers", IEEE J. Quantum Electron., Vol. QE-18, pp.1728-1737, 1982.

34. F. Stern: "Calculated spectral dependence of gain in excited GaAs", J. Appl. Phys., Vol.47, pp.5382-5386, 1976.

35. B.W. Hakki and T.L Paoli: "Gain spectra in GaAs DH injection lasers", J. Appl. Phys., Vol.46, pp.1299-1306, 1975.

36. G.H.B. Thompson: "Physics of Semiconductor Laser Devices", pp.82-92, Wiley, New York, 1980.

37. R. Lang: "Mode deformation effects on modal gain of stripe geometry injection lasers", The Trans. IECE Japan, Vol. E62, pp.299-304, 1979.

CHAPTER IV

MULTIPLE-STRIPE LASERS

This chapter is devoted to a brief review of the work carried out by the various authors in the field of multiple-stripe lasers.

4.1 Introduction

In the past few years there has been a lot of interest in optical communications, integrated optics, optical signal processing and optical logics. Many types of passive device have been developed for use in these applications based on lithium niobate or GaAs substrate and a variety of light guiding techniques. These passive devices tend to be fairly lossy and require quite large optical powers from the source. Active devices, however, have inherent gain when appropriately biased and have immense potential in integrated optics circuits. More importantly perhaps the active device may have externally controllable regions of optical gain and loss which may be utilized in optical logics and integrated optics. In particular regions of loss, or a saturable absorbing region in an active device can give rise to a wide variety of optical and temporal instabilities such as bistability, beam steering and optical modulation which are useful in the above areas (1 - 4).

The idea of a bistable laser diode was initially proposed by Lasher (5) for homojunction GaAs devices. The important feature of this device was the division of its broad contact into two electrically isolated sections, as shown in figure (4.1-1), the channel separating the two contacts parallel to the cleaved facets to form a tandem or split stripe laser. This device is different from the parallel twin stripe laser discussed in this thesis, nevertheless both types of laser show bistability. The current through the two contacts can be independently monitored. When one of the contacts is biased below threshold while the other is just above threshold, the two regions act as emitter and saturable absorber respectively (6). The device is said to be in "off" state. However, if

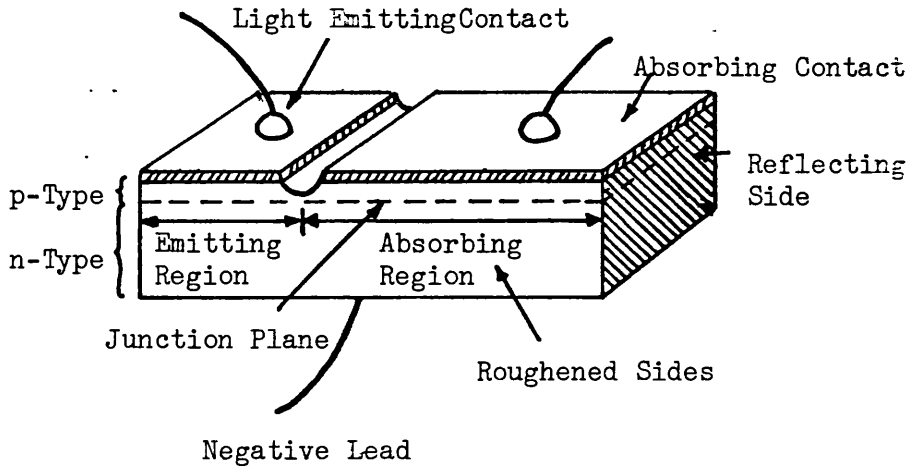

Figure 4.1-1 Idealised bistable homojunction laser. The light emitting contact is biased to cause the injection of electrons into the p-layer directly beneath it and acts as a light emitting section. The other has a somewhat smaller voltage so that negligible injection current is present in that portion and acts as the light absorbing section. If a sufficient number of conduction band electrons are formed in the absorbing region due to photon absorption, the light from the emitting region will not be strongly absorbed and some will be reflected back by the reflecting side. The lasing threshold will then be reduced and the absorbing region becomes transparent (5).

the emitter contact is pumped harder the absorbing region becomes transparent and the device radiates coherently and the light output may increase by as much as 30 times. On reducing the current slightly the passive region remains optically pumped. This type of device was predicted to show hysteresis in its light/current characteristics. Nathan et al(7) demonstrated experimentally the bistable operation in this device shortly after the predicted behaviour had been published. Since the threshold current density of a homojunction laser diode at room temperature is very high, it was necessary to cool the device to liquid nitrogen temperature for its operation. However, since the development of the practical GaAs/$Al_xGa_{1-x}As$ heterostructure lasers, with much reduced threshold current densities at room temperature, the potential of laser diodes for various applications has been realized.

4.2 Survey Of Previous Work

In the early days considerable efforts went into to producing a coherent high power laser beam by the expedient of placing two or more stripes close to each other (8 - 10). The reason for this is that a broad area single stripe laser produces a light/current characteristic with kinks as shown in figure (4.2-1). The kink in the light/current characteristic corresponds to the occurrence of the hole burning underneath the stripe due to high rate of stimulated recombination. This leads to a higher order lateral mode excitation and results in the instabilities of modal behaviour of the device and filamentation of the optical output. The current level at which the kink in the light/current characteristic appears can be raised by reducing the stripe width (11 - 13) as shown in figure (4.2-1). Although semiconductor lasers with wide stripe contacts are capable of generating high power optical pulses by virtue of their large emitting area, they operate in higher order lateral modes or in several independent filaments. In order to overcome this problem a multiple

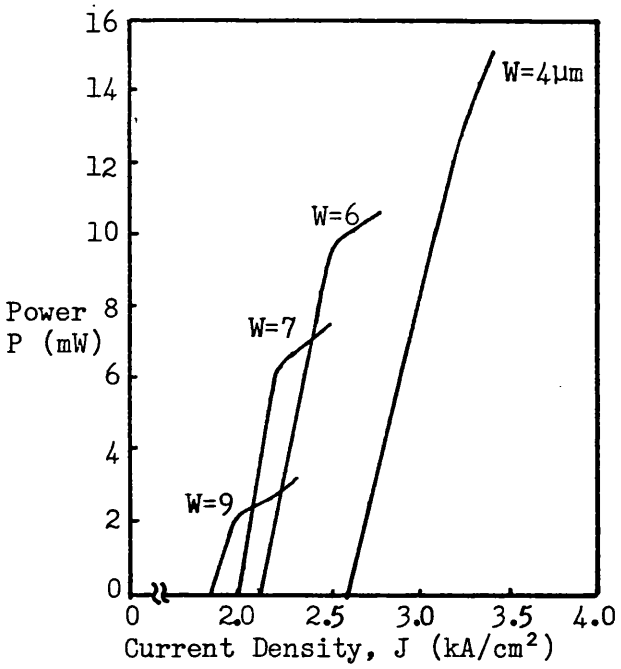

Figure 4.2-1 Power output vs. injection current density for different stripe widths, W labelled in diagram in the case of a single stripe laser. The analytic expression approximating the current spreading in the confining layer of the laser is used (11).

stripe laser in a phase locked state is used which produces a high power as shown by Scifres et al (14 - 15). At 300°K, a threshold current density of 1 KA/cm^2 for a device with five parallel stripes each with a stripe width of 3.5 μm and separated by 8 μm from centre-to-centre is reported in the reference (14). It is further reported that the emitted power through one facet is 0.9 watt at 5 times the threshold current.

Katz et al (16) reported that by tailoring the distribution of the currents through multiple contacts of the laser array a narrow single lobe far-field pattern can be obtained which can be of a great value in optical communications and optical recording where in addition to increased power level, stable radiation distributions are required. Recently, Carlin et al (17) have successfully demonstrated high data rate multi-channel optical recording using an array of individually addressible diode laser structure as the source.

White et al (18) experimentally demonstrated the bistability behaviour in a twin stripe laser with stripe widths of 3 μm and a separation between the stripes of 3 μm. They have reported two forms of bistability. One effect is the waveguiding mechanisms from gain guiding to self focusing. The second mechanism exhibits a large shift in the near-field distribution from one side of the laser to the other. In the reference (19) White et al have shown experimentally that the bistable mechanism in a symmetrically pumped twin stripe laser occurs from the central self focused mode to a diagonal gain guided mode through the application of short (10 ns) electrical pulses. By adjusting the current into the two stripes of a twin stripe laser with a sufficient separation between the two stripes, a dip in the carrier density can be produced. The dip in the carrier density corresponds to a bump locally in the refractive index and results in a self focusing of the mode. The near-field and the carrier density

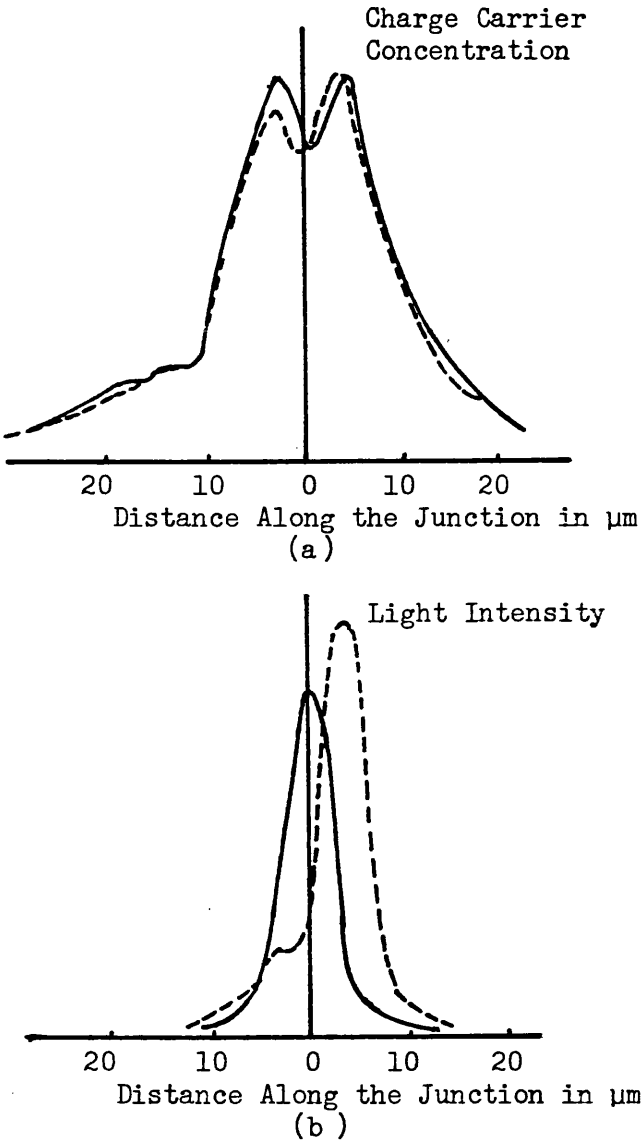

Figure 4.2-2 Charge carrier concentration (a) and near field (b) distributions measured with the twin stripe laser in two separate bistable states: (—) self-focused mode and (---) gain-guided mode (Ref. 18).

distributions, after reference (18), are shown in the figure (4.2-2). Optically switched bistability actions in a twin stripe laser are analysed theoretically by Shore (20).

Ultrashort pulses are of considerable importance for future pulse modulated high speed optical communication systems (22). Twin stripe lasers can be used to generate picosecond pulses as short as 20 ps (18). Also the dependence of the pulse width on the waveguiding structure which can be altered by adjusting the ratio of the current through the two stripes is reported (21).

Scifres et al (23) demonstrated experimentally beam scanning in a twin stripe laser with the two stripes each of width 2 μm having a centre-to-centre separation 8 μm. They have shown laser beam-steering via the modification of the dielectric constant. The peak of the radiation pattern was deflected ± 14^{o} with respect to the normal to the laser facets as shown in figure (4.2-3). Since the graded index is induced by the injected carriers, scanning is obtained by monitoring the pumping currents through the two stripes. The symmetrically pumped case gives the lowest threshold current, which is confirmed by Kumar et al (24). It has been shown in the reference (23) that in a symmetrically pumped case the light spreads over 10 μm, whereas in asymmetrically pumped case the light is confined to the region under the more strongly pumped contact. The effect of optical injection under one of the stripes in a twin stripe laser is computed by Shore (25). In his analysis he has pointed out that although the field rotation by varying the currents through the two stripes is larger than by optical means, the modulation of the injection currents takes time to be conveyed to the optical field. Optical steering should bring potential gains in speed as well as integrability within an all optical system.

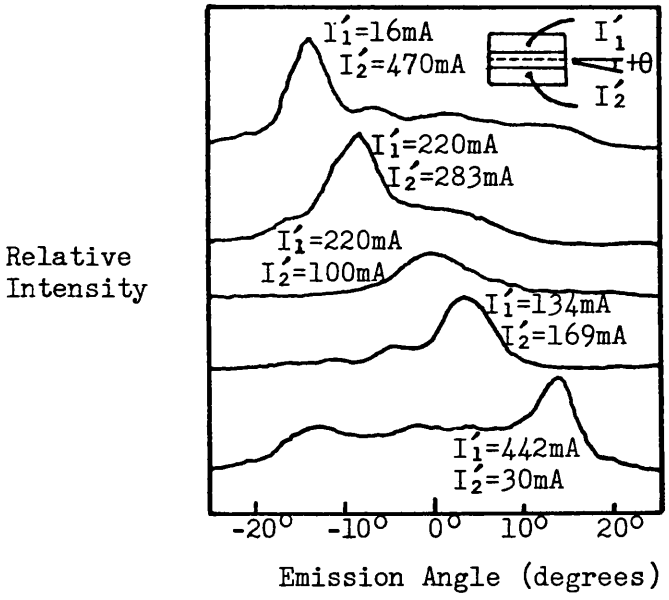

Figure 4.2-3 Far-field radiation pattern of twin stripe laser under five different pumping conditions (22).

Katz (26) works out theoretically the perturbation of the dielectric constant required to produce a prescribed beam steering. In his analysis he pointed out that asymmetrical modification of the dielectric constant is an essential requirement if the beam deflection is to be obtained. Further he suggested the major contribution to beam steering is due to the modification in the imaginary part of the dielectric constant. Since the imaginary part of the dielectric constant is related to the gain in the laser medium and the gain is determined by the carrier density distribution. It can be easily perturbed by monitoring the current through the two stripes of a twin stripe laser. The results of reference (23) show that the amount of beam deflection depends upon both the current ratio and magnitude, a more refined model of the laser is required to describe the operation of the device.

4.3 Model Outlines

It is noticed in the previous section that there are numerous research activities currently involving a double heterostructure lasers with two or more closely coupled stripes. Recently Katz et al (27) derived theoretically a coupling coefficient in a gain guided twin stripe laser as a function of interstripe separation and pointed out that the coupling coefficient which is a complex number has a quadratic exponential decay as a function of the separation between the stripes. Their derivation is based upon the assumption of a parabolic variation of the effective dielectric constant in the active region. However, it has been seen from the literature (28) on a single stripe laser that the parabolic variation of the effective dielectric constant along the length of the active layer is not valid for a narrow stripe geometry laser. It should be quite helpful, therefore, to understand the device behaviour if a more refined model is examined. For example, Shore and Rozzi (29) have solved the multiple stripe model shown in the figure (4.3-1). In their model they

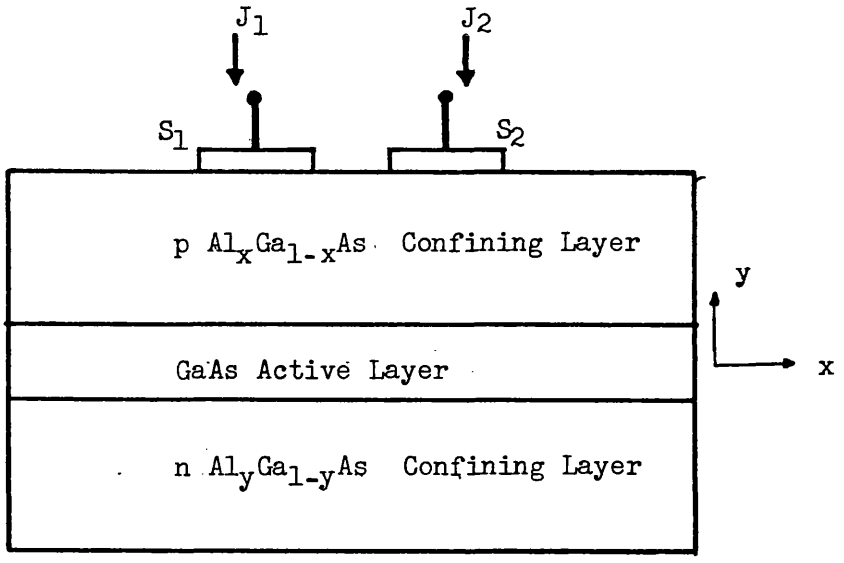

Figure 4.3-1 Schematic diagram of the twin-stripe-geometry laser (29).

use a closed form of injected current distribution after Hakki (30). The current spreading occurring in the top $Al_xGa_{1-x}As$ layer is derived in the reference (30) using an ideal diode equation which ignores the diffusion of carriers in the active layer along the x direction in figure (4.3-1). Thus the model does not take into account the effect of the lateral diffusion of the carriers on the current spreading in the top layer. Furthermore, Paoli et al (31) reported the saturation of the junction voltage of a stripe geometry laser at the onset of lasing. This implies that the quasi-Fermi levels are pinned above threshold as a result of the high stimulated recombination rate. Both these effects were incorporated by Wilt and Yariv (32) in their self-consistent single stripe laser model which assumed the continuity of quasi-Fermi levels across the active layer.

The purpose of this project is to extend the model of Wilt and Yariv for the case of a twin stripe laser. It is believed that no such model exists to date. The detailed analysis of this model will be discussed in chapters to follow.

4.4 Conclusions

A brief discussion of the research efforts put into the multiple stripe geometry lasers by various research workers has been presented in this chapter. Clearly, the twin stripe laser forms an important component of integrated optics and therefore it will be a useful attempt to study the detailed behaviour of the device.

References

1. J. Kuhl and E.O. Gobel: "Synchronous mode locking of a GaAs/GaAlAs laser diode by a picosecond and optoelectronic switch", J. Opt. Soc. Am. B, Vol.1(3), p.452, 1984.

2. K. Okumura and Y. Ogawa: "Optical bistability and monolithic logic functions based on bistable bistable-laser light-emitting diodes", J. Opt. Soc. Am. B, Vol.1(3), p.465, 1984.

3. Y. Ogawa, H. Ito and H. Inaba: "New bistable optical device using a semiconductor laser diode", Jap. J. Appl. Phys., Vol.20(9), pp.L646-L648, 1981.

4. A. Szoke, V. Daneu, J. Goldhar and N.A. Kurnit: "Bistable optical element and its applications", Appl. Phys. Lett., Vol.15, pp.376-379, 1969.

5. G.J. Lasher: "Analysis of a proposed bistable injection laser", Solid State Electron., pp.707-716, 1964.

6. N.G. Basov: "0-1-Dynamic of injection lasers", IEEE J. Quantum Electron., Vol. QE-4, pp.855-864, 1968.

7. M.I. Nathan, J.C. Marinace, R.F. Rutz, A.E. Michel and G.J. Lasher: "GaAs injection laser with novel mode control and switching properties", J. Appl. Phys., Vol.36, pp.473-480, 1965.

8. J.E. Ripper and T.L. Paoli: "Optical coupling of adjacent stripe geometry junction lasers", Appl. Phys. Lett., Vol.17, pp.371-373, 1970.

9. W.T. Tsang, R.A. Logan and R.P. Salathe: "A densely packed monolithic linear array of GaAs-$Al_xGa_{1-x}As$ stripe buried heterostructure laser", Appl. Phys. Lett., Vol.34(2), pp.162-165, 1979.

10. D.E. Ackley and R.W.H. Engelmann: "Twin-stripe laser with leaky mode coupling", ibid, 37, pp.866-868, 1980.

11. N. Chinone: "Non-linearity in power output-current characteristics of stripe geometry injection lasers", J. Appl. Phys., Vol.48, pp.3237-3243, 1977.

12. R. Lang: "Lateral transverse mode instability and its stabilisation in stripe geometry injection lasers", IEEE J. Quantum Electron., Vol. QE-15, pp.718-726, 1979.

13. K.A. Shore and T.E. Rozzi: "Stability analysis of transverse modes in stripe-geometry injection lasers", IEE Proc. Part I, Vol.128, pp.154-159, 1981.

14. D.R. Scifres, W. Streifer, and R.D. Burnham: "High-power coupled-multiple-stripe phase-locked injection laser", Appl. Phys. Lett., Vol.34(4), pp.259-261, 1979.

15. D.R. Scifres, R.D. Burnham and W. Streifer: "Continuous wave high-power, high-temperature semiconductor laser phase-locked arrays", Appl. Phys. Lett., Vol.41(11), pp.1030-1032, 1982.

16. J. Katz, C. Lindsey, S. Margalit and A. Yariv: "Far-field distributions of semiconductor phase-locked arrays with multiple contacts", Electron. Lett., Vol.19(17), pp.660-662, 1983.

17. D.B. Carlin, J.P. Bednarz, C.J. Kaiser, J.C. Connolly, and M.G. Harvey: "Multichannel optical recording using monolithic arrays of diode lasers", Appl. Opt., Vol.23(22), pp.3994-4000, 1984.

18. I.H. White, J.E. Carroll and R.G. Plumb: "Closely coupled twin-stripe lasers", IEE Proc. Part I, Vol.129, pp.291-296, 1982.

19. I.H. White and J.E. Carroll: "New mechanism for bistable operation of closely coupled twin stripe lasers", Electron. Lett., Vol.19(9) pp.337-339, 1983.

20. K.A. Shore: "Optically induced spatial instability in twin stripe geometry lasers", Opt. & Quantum Electron., Vol.14, pp.171-181, 1982.

21. I.H. White, G. Aspin and J.E. Carroll: "Picosecond pulse generation by lateral mode switching of (GaAl)As heterostructure stripe lasers", Electron. Lett., Vol.17(15), pp.541-543, 1981.

22. A.B. Miller and D.J. Eilenberger: "Passive mode-locking of semiconductor laser diode", J. Opt. Soc. Am. B, Vol.1(3), pp.452-453, 1984.

23. D.R. Scifres, W. Streifer and R.D. Burnham: "Beam scanning with twin-stripe injection lasers", Appl. Phys. Lett., Vol.38, pp.702-704, 1978.

24. T. Kumar, R.F. Ormondroyd and T.E. Rozzi: "Interstripe coupling and current spreading in a sub-threshold double heterostructure twin-stripe laser", IEEE J. Quantum Electron.,Vol. QE-20,pp.364-373, 1984.

25. K.A. Shore: "Radiation patterns for optically steered semiconductor laser-beam scanner", Appl. Opt., Vol.23(9), pp.1386-1390, 1984.

26. J. Katz: "Electronic beam steering of semiconductor injection lasers: a theoretical analysis", Appl. Opt., Vol.22, p.313, 1983.

27. J. Katz, E. Kapon, C. Lindsey, S. Margalit and A. Yariv: "Coupling coefficient of gain guided lasers", Appl. Opt., Vol.23(14), pp.2231-2233, 1984.

28. P.M. Asbeck, D.A. Commack and J.J. Daniele: "Non-Gaussian fundamental mode patterns in narrow-stripe-geometry lasers", Appl. Phys. Lett., Vol.33, p.504, 1978.

29. K.A. Shore and T.E. Rozzi: "Near-field control in multi-stripe geometry lasers", IEEE J. Quantum Electron., Vol. QE-17, pp.718-722, 1981.

30. B.W. Hakki: "GaAs double-heterostructure lasing action along the junction plane", J. Appl. Phys., Vol.46, pp.292-302, 1975.

31. T.L. Paoli and P.A. Barnes: "Saturation of the junction voltage in stripe-geometry (AlGa)As double heterostructure junction lasers", Appl. Phys. Lett., Vol.28(12), pp.714-716, 1976.

32. D. Wilt and A. Yariv: "A self-consistent static model of the double heterostructure laser", IEEE J. Quantum Electron., Vol. QE-17, pp.1941-1949, 1981.

CHAPTER V

CURRENT SPREADING AND INTERSTRIPE COUPLING IN A TWIN STRIPE LASER

5.1 Introduction

The performance of a stripe geometry laser is influenced by the current spreading taking place in the region between the stripe contact and the junction. Various authors (1 - 4) have used simple approximations to get an analytic expression for current spreading which they then used in their device analysis. Dumke (5), in his analysis, assumed that beyond the stripe edge equipotential lines are normal to the junction and therefore the resistance of the layer in the normal direction in a real device is very small when compared with its resistance in the lateral direction i.e along the junction in figure (5.1-1). Dumke then invokes the current continuity equation to relate the two components of the current density J_x and J_y along the x-axis and y-axis respectively. Various other authors make use of a similar approach to approximate the current spreading in their device analysis.

However Lengyel et al (6), in a recent paper, have pointed out that such a sheet resistance model is not a true representation of the device. They further suggested that as long as the stripe width to the resistive layer thickness ratios are relatively large i.e greater than 1.5 such approximations are permissible. In recent years, however, it has been seen that the instability of the device corresponding to the kink in the light/current characteristics shown in figure (4.2-1) can be improved by making the width of the stripe less than 6μm (3, 9). The reduction in the stripe width to improve stability of the device breaks down the sheet resistance model and therefore one must give attention to a 2-dimensional current spreading problem in the resistive layer. Several authors, (6 - 8), have attempted to solve the 2-dimensional Laplace equation in the resistive layer subject to a diode boundary condition for a single stripe geometry double heterostructure laser. In this chapter a similar boundary problem is extended to a twin stripe laser

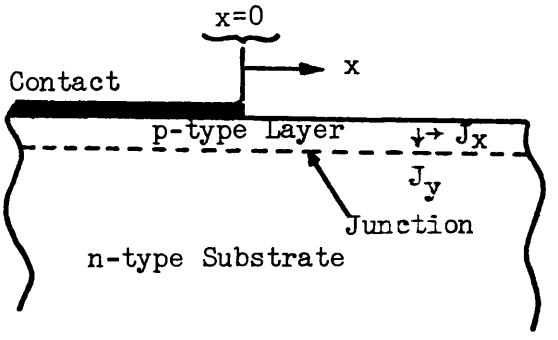

Figure 5.1-1 Geometry of stripe contact laser with an edge of top contact at x = 0. Only one edge of the contact is shown (After Dumke (5)).

so that the current spreading and interstripe coupling of the injected currents may be considered. While the problem of current spreading is well studied in a single stripe laser (1 - 12), very little is known about it in a twin stripe laser. Many novel optical properties have been predicted for the twin stripe laser (See chapter IV). These include beam steering, ultrashort pulse generation and optical bistability and since these predictions were made, many of these predictions have been observed in real twin stripe laser devices (13 - 15).

The lateral distribution of the optical output of the device is determined by the lateral variation in the carrier density profile and the complex dielectric constant, which themselves are coupled. Pumping each stripe independently modifies both the carrier density and the refractive index profiles. Further because the two stripes are coupled together via p-type resistive layer as shown in figure (4.3-1) the conductivity and thickness of the p-type layer have a significant effect on the current density distribution actually injected into the active layer and this has a controlling influence on the gain profile. Scifres et al (13) have reported earlier that beam scanning in a twin stripe laser can be accompalished by adjusting the current levels between the two stripe contacts. Asymmetrical injection leads to an asymmetrical variation in the carrier density profile (and hence gain) and the complex dielectric constant. This must,therefore, affect the lateral position of the optical field.

A self-consistent solution of the problem is required to determine the true behaviour of the device. The coupling of the stripes via both the p-type passive and lateral diffusion of carriers in the active region interacting with the optical field makes this a more complex task than for a single stripe laser. In the present chapter the self-consistent model is not discussed but it is attempted to get some information

regarding the terminal behaviour of the device as a function of the injected currents in each stripe. In particular, the effects of electrode widths, electrode spacing, thickness of p-passive layer and its conductivity on the current density distributions are examined for the twin stripe laser.

5.2 The Model

The model used in this analysis does not take into account the top heavily doped GaAs layer shown in figure (1.1-3c) used to make a good ohmic contact. Lengyel et al (6) have also reported that it is possible to make a good ohmic contact without using the heavily doped top layer. Moreover, in order to achieve interstripe isolation from the neighbouring electrodes, the top layer (heavily doped) has to be etched away. Further the substrate and n-type passive layer in figure (1.1-3) are replaced by an equipotential contact at the active/n-type passive interface which is assumed to be at zero potential. This is a valid approximation because the substrate is heavily doped and has a broad area contact which implies the current in the n-type passive layer is not constrained to flow parallel to the active layer. In this analysis therefore current spreading in the p-type passive region is considered.

In the model described in this chapter the active layer is represented by spatially separated diodes, one per unit length in the lateral direction, as shown in figure (5.2-1). The effect of lateral diffusion of the carriers is not considered here. Lengyel et al have shown that for larger values of the resistivity ($\rho > 0.3\Omega.cm$) of the p-type passive layer, the diffusion problem can be decoupled from the current spreading problem. However the larger value of resistivity can result in excessive heat generation in the passive layer due to ohmic voltage drop. In figure (5.2-1) $\underline{a}$ and $\underline{b}$ denote the unit vectors along x and y axes

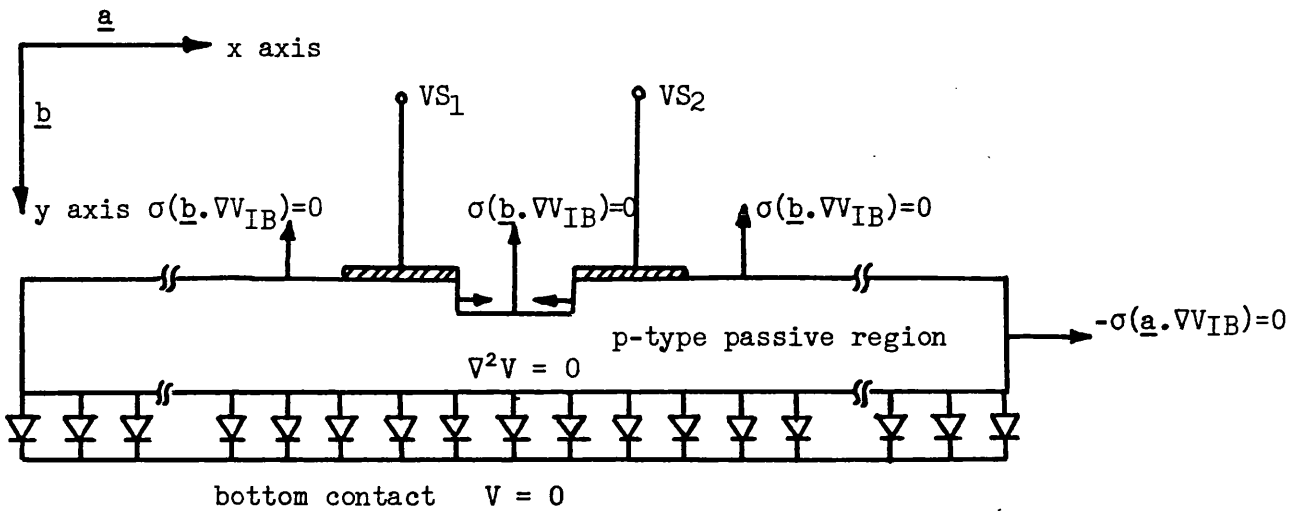

Figure 5.2-1 The twin stripe model assumed for the current and potential distributions. $\underline{a}$ and $\underline{b}$ denote the unit vectors along the x and y axes respectively.

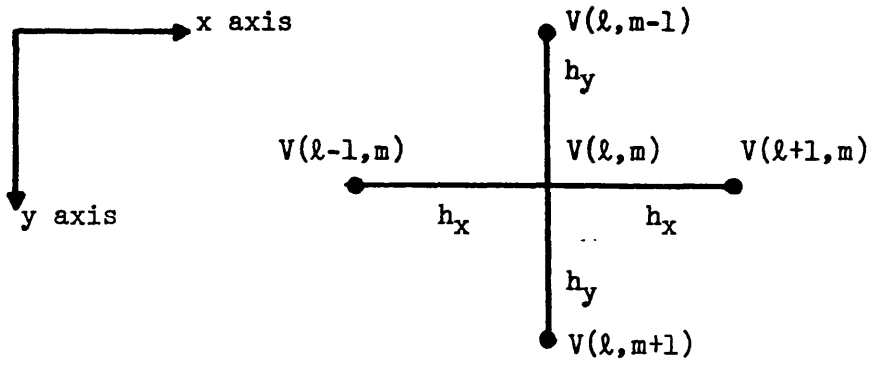

Figure 5.2-2 Finite difference model for an interior node (ℓ,m) in the passive region.

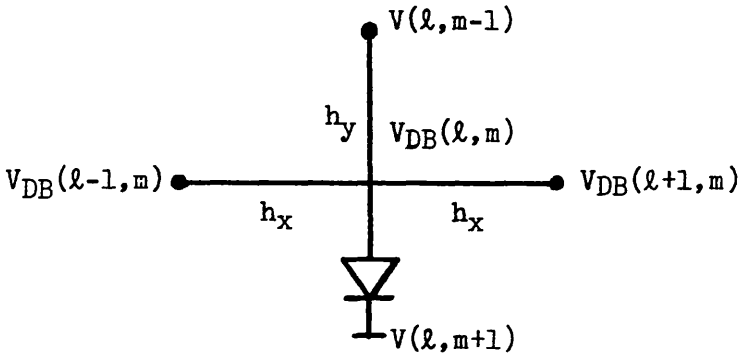

Figure 5.2-3 Finite difference representation for the node (ℓ,m) lying on the diode boundary.

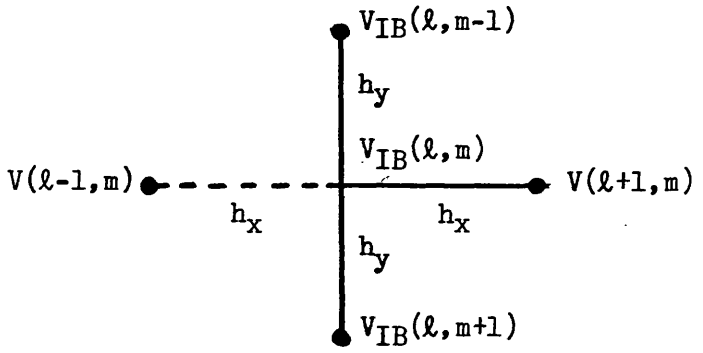

Figure 5.2-4 Finite difference model for the node lying on the insulator boundary.

respectively. As the bottom contact is assumed to be grounded, the voltage appearing across the equivalent diode is the same as the voltage appearing at the p-type passive/active interface. The problem reduces to solving the 2-dimensional Laplace's equation in the p-type resistive region given below:

$$\nabla^2 V = 0 \qquad (5.2\text{-}1)$$

subject to the non-linear boundary condition at the p-type passive/active interface. The current density flowing through equivalent diode shown in figure (5.2-1) is given by the following expression (1, 5, 7):

$$J(\ell) = J_o\{\exp\{eV_{DB}(\ell,m)/\eta k_B T\} - 1\} \qquad (5.2\text{-}2)$$

where J_o is the dark current density of the equivalent GaAs diode, $V_{DB}(\ell,m)$ is the voltage across the ℓ^{th} diode, η takes the value 2 after Hakki (1) and $J(\ell)$ is numerically equal to the current density through the active layer at the ℓ^{th} point on the interface. The potential distribution in the p-type passive layer gives the current density going into the active region as below:

$$J(\ell) = -\sigma\{\nabla V_{DB}(\ell,m)\}.\underline{b} \qquad (5.2\text{-}3)$$

where the suffix 'DB' denotes the diode boundary at the p-type passive/active interface. Also $J(\ell)$ is the current density through the diode given by equation (5.2-2), therefore from equation (5.2-3) one gets:

$$-\sigma\{\nabla V_{DB}(\ell,m)\}.\underline{b} = J_o\{\exp\{eV_{DB}(\ell,m)/\eta k_B T\} - 1\} \qquad (5.2\text{-}4)$$

This represents the non-linear boundary condition corresponding to the p-type passive/acive interface. The rest of the boundary conditions are insulated types of boundary conditions, as shown in figure (5.2-1), and correspond to zero normal components of the current density. As one would expect, there is a lot of current crowding near the edges of the

stripe contacts, and it is not valid to assume that a uniform current density is injected into each stripe. To solve Laplace's equation the p-type resistive region in figure (5.2-1) is discretized into a rectangular mesh and for each interior node, as shown in figure (5.2-2), one can write Laplace's equation (5.2-1) into a finite difference form, as given below:

$$\frac{V(\ell-1,m) - 2V(\ell,m) + V(\ell+1,m)}{h_x^2} + \frac{V(\ell,m-1) + 2V(\ell,m) + V(\ell,m+1)}{h_y^2} = 0 \qquad (5.2\text{-}5)$$

If the node lies on the p-type passive/active interface then the diode equation (5.2-2) must be satisfied. Let (ℓ,m) be the node lying on this boundary. Consider an imaginary node $(\ell,m+1)$ below the $(\ell,m)^{th}$ node, as shown in figure (5.2-3). Since the node $(\ell,m+1)$ lies outside the domain of the p-type region, it must be eliminated from the finite difference form of Laplace's equation similar to equation (5.2-5), by using the boundary condition (5.2-4). Writing Laplace's equation similar to equation (5.2-5) for the boundary node (ℓ,m) one obtains:

$$\frac{V_{DB}(\ell-1,m) - 2V_{DB}(\ell,m) + V_{DB}(\ell+1,m)}{h_x^2} + \frac{V(\ell,m-1) - 2V_{DB}(\ell,m) + V(\ell,m+1)}{h_y^2} = 0 \qquad (5.2\text{-}6)$$

Clearly, $V_{DB}(\ell,m)$ is also the voltage across the diode, therefore it must satisfy the diode equation (5.2-2). Equation (5.2-3) representing current injected into the active layer at node (ℓ,m) can be written as:

$$-\sigma\{\underline{b}.\nabla V_{DB}(\ell,m)\} \equiv -\sigma\{dV_{DB}(\ell,m)/dy\} = -\sigma\left\{\frac{V(\ell,m+1) - V(\ell,m-1)}{2h_y}\right\} \qquad (5.2\text{-}7)$$

From this equation substituting the value of $-\sigma\{\underline{b}.\nabla V_{DB}(\ell,m)\}$ in

equation (5.2-4) one gets:

$$V(\ell,m+1) = V(\ell,m-1) - (2J_o h_y/\sigma)\{\exp\{eV_{DB}(\ell,m)/\eta k_B T\} - 1\} \qquad (5.2\text{-}8)$$

On substituting the value of $V(\ell,m+1)$ in equation (5.2-6) the following expression is obtained:

$$\frac{V_{DB}(\ell+1,m) - 2V_{DB}(\ell,m) + V_{DB}(\ell-1,m)}{h_x^2} + \frac{2V(\ell,m-1) - 2V_{DB}(\ell,m)}{h_y^2} - \frac{2J_o}{\sigma h_y}\left[\exp\{eV_{DB}(\ell,m)/\eta k_B T\} - 1\right] = 0 \qquad (5.2\text{-}9)$$

For the nodes lying on the insulator boundary the finite difference form of Laplace's equation is written and the boundary condition is employed. Let (ℓ,m) represents a node lying on the left insulated boundary, as in figure (5.2-1). Considering an imaginary node $(\ell-1,m)$ outside the p-type region and writing the finite difference form of Laplace's equation for the boundary node, as shown in figure (5.2-4) the following expression is obtained:

$$\frac{V(\ell-1,m) - 2V_{IB}(\ell,m) + V(\ell+1,m)}{h_x^2} + \frac{V_{IB}(\ell,m-1) - 2V_{IB}(\ell,m) + V_{IB}(\ell,m+1)}{h_y^2} = 0 \qquad (5.2\text{-}10)$$

where 'IB' suffix stands for the node lying on the insulated boundary. In equation (5.2-10) the potential $V(\ell-1,m)$ corresponds to the node $(\ell-1,m)$ lying outside the domain of the p-type region and therefore it must be eliminated using the boundary condition $\sigma\{\underline{a}.\nabla V_{IB}(\ell,m)\} = 0$. Thus:

$$\sigma\{\underline{a}.\nabla V_{IB}(\ell,m)\} \equiv \sigma\{dV_{IB}(\ell,m)/dx\} = (\sigma/2h_x)\{V(\ell+1,m) - V(\ell-1,m)\} = 0$$

or

$$V(\ell+1,m) = V(\ell-1,m) \qquad (5.2\text{-}11)$$

Substituting the value of $V(\ell-1,m)$ from the above relation in equation

(5.2-10) the following equation is obtained:

$$\frac{2V(\ell+1,m) - 2V_{IB}(\ell,m)}{h_x^2} + \frac{V_{IB}(\ell,m-1) - 2V_{IB}(\ell,m) + V_{IB}(\ell,m+1)}{h_y^2} = 0 \qquad (5.2\text{-}12)$$

Similarly, the algebric equations for nodes lying on the other insulated boundaries shown in figure (5.2-1) can be derived. The current density going into the active layer may be evaluated either directly from the diode equation (5.2-2) by using the potential along the p-type passive/ active interface or from the following expression:

$$J(\ell) = -\sigma\{\underline{b}.\nabla V_{DB}(\ell,m)\} \equiv -\sigma\{dV_{DB}(\ell,m)/dy\} \qquad (5.2\text{-}13)$$

Similarly, the current density beneath the stripe contacts are calculated by making use of the relation given below:

$$J(0) = -\sigma\{\underline{b}.\nabla V(\ell,0)\} \equiv -\sigma\ \{dV(\ell,0)/dy\} \qquad (5.2\text{-}14)$$

The total current per unit length of the device injected into or out of each electrode was computed from:

$$I_S = h_x \sum J(\ell,0) \qquad \text{for all values of nodes, } \ell \text{ over each electrode}$$

I_S flowing into the electrodes is represented with positive sign while that flowing out of the electrode is represented by negative sign.

5.3 Solution Technique

An iterative scheme was implemented to solve the system of linear and non-linear algebric equations obtained in section (5.2) at the various nodes of the p-type passive region. It will have been noticed in the previous section that all equations, except those corresponding to the nodes lying on the p-type passive/active interface, are linear. For this system of linear equations the successive-over-relaxation (S.O.R) technique is used. Initially, the estimation of potential values over the whole

domain and then new potentials at each node is calculated using the appropriate finite difference form of Laplace's equation, discussed earlier. The new corrected value of potential $V(\ell,m)$ at the $(\ell,m)^{th}$ internal node becomes:

$$V(\ell,m)\big|_{new} = V(\ell,m) + \theta\left[\left(\frac{V(\ell+1,m) + V(\ell-1,m)}{h_x^2} + \frac{V(\ell,m+1) + V(\ell,m-1)}{h_y^2}\right)\Big/\left(\frac{2}{h_x^2} + \frac{2}{h_y^2}\right) - V(\ell,m)\right] \tag{5.3-1}$$

The correction value for $(\ell,m)^{th}$ node is given by:

$$\Delta_{\ell m} = V(\ell,m)\big|_{new} - V(\ell,m) \tag{5.3-2}$$

In equation (5.3-1) θ is over-relaxation parameter whose value can be optimized between 1 and 2 to obtain the least number of iterations required to solve the problem within a given accuracy. Equation (5.3-1) can be modified accordingly for the nodes lying on the insulated boundary. However, attention must be drawn to the non-linear algebric equations corresponding to the nodes lying on the p-type passive/active interface. Here the Newton-Raphson technique has been used to handle this set of equations. In this technique the values of functions f and f′ are first calculated and these are then used to get the correction term for the boundary potential $V_{DB}(\ell,m)$.

$$f = \frac{V_{DB}(\ell-1,m) + V_{DB}(\ell+1,m)}{h_x^2} + \frac{2V(\ell,m-1)}{h_y^2} - \left(\frac{2}{h_x^2} + \frac{2}{h_y^2}\right)V_{DB}(\ell,m) - (2J_o/h_y\sigma)\exp\{eV_{DB}(\ell,m)/\eta k_B T\} \tag{5.3-4}$$

The function f′ is calculated by differentiating w.r.t $V_{DB}(\ell,m)$

as given below:

$$f' = -\left[\frac{2J_o e}{\eta k_B T h_y \sigma}\right] \exp\{eV_{DB}(\ell,m)/\eta k_B T\} - \left[\frac{2}{h_x^2} + \frac{2}{h_y^2}\right] \qquad (5.3\text{-}5)$$

Using the Newton-Raphson method the correction $\Delta_{\ell m}$ term to the potential $V_{DB}(\ell,m)$ becomes:

$$\Delta_{\ell m} = -(f/f') \qquad (5.3\text{-}6)$$

The corrected value $V_{DB}(\ell,m)$ is therefore given as:

$$V_{DB}(\ell,m)\big|_{new} = V_{DB}(\ell,m) + \Delta_{\ell m} \qquad (5.3\text{-}7)$$

For the two end nodes along the p-type passive/active interface expression (5.3-4) can be modified to incorporate the insulated boundary condition as well. The convergence criterion used in the simulation is the sum of absolute values of the global error must be less than a set tolerance value 'TOL'.

$$\sum_{\ell,m} |\Delta_{\ell m}| \leq TOL \qquad (5.3\text{-}8)$$

where the summation is taken over all the nodes along the x and y axes. 'TOL' is the specified accuracy, which in this case is 1×10^{-4}. Convergence is not a problem with this technique. However, because exponential terms containing the k_BT/e (1/40 volts) term in their argument appear in equation (5.3-4) and (5.3-5) there is a problem of exponential overflow during the iterations. This difficulty was successfully overcome by using a damping factor which prevents the argument of exponential terms having a large value. There are several damping factor techniques which may be used but the one used in this work is as follows:

$$\left.\begin{aligned} &\ell n|V_{DB}(\ell,m)| && \text{-for } V_{DB}(\ell,m) \geq 4.0 \\ &-\ell n|V_{DB}(\ell,m)| && \text{-for } V_{DB}(\ell,m) \leq -4.0 \end{aligned}\right\} \qquad (5.3\text{-}9)$$

These tests are built-in within the program and successfully remove the possibility of exponential overflow. The check is imposed on the values of potential $V_{DB}(\ell,m)$ at the p-type passive/active interface as the iteration progresses. If the value of $V_{DB}(\ell,m)$ is numerically greater than or equal to 4.0 volts, the natural logarithm of its asolute value is taken to get a smaller number as shown in equation (5.3-9). Various mesh sizes have been tried in solving the problem in order to check the accuracy of the solution and to optimize the mesh size as discussed in the following section.

5.4 Results Obtained For The Twin Stripe Laser

The various parameters used in the calculations to follow are shown in table (5.4-1). As the current density distributions under the stripe contacts are non-uniform, the only valid assumption made in this model is that of an equipotential contact. In all the results given here the use of constant potentials applied to the stripe contacts is made. However, the current density immediately underneath the each stripe contact is calculated from the fundamental definition viz $\underline{J} = -\sigma\nabla V$, and the injected electrode current is thus:

$$I_S = \sum_{\text{stripe}} J_y h_x$$

where h_x is the step length of the mesh size along the stripe and J_y is the component of current density normal to the stripe contact.

5.4.1 Optimizing the mesh size

In order to minimize unnecessary computation the mesh size was optimized in the problem to achieve adequate accuracy without using unnecessarily small mesh sizes. Different mesh sizes were tried for the case of a symmetrically pumped twin stripe laser and the results are given in table (5.4.1-1). In these tabular results the current density going

$J_o = 6 \times 10^{-5}$ Am^{-2} (1)
p-type (AlGa)As resistivity, $\rho = 1/\sigma = 2.0 \times 10^{-3}$ ohm m (6)
Stripe width S_1 = 3.0 μm
Stripe width S_2 = 3.0 μm
Spacing between stripe electrodes = 3.0 μm
(AlGa)As thickness = 2.0 μm
Width of the device along p-n junction = 69.0 μm
VS_1 = 1.55V
VS_2 = 1.55V

Table 5.4-1 Parameters used in the simulation of the twin stripe laser.

Mesh Size, h_x x h_y (μm)	0.5 x 1.0	0.6 x 0.2	0.3 x 0.2	0.2 x 0.2	0.3 x 0.1	0.3 x 0.2
Current density along the p-n junction at centre of stripe 1: x $10^6 Am^{-2}$	76.57	41.48	40.91	40.75	40.82	40.91
Current density along the p-n junction at mid point between stripes: x $10^6 Am^{-2}$	33.11	33.20	32.16	31.95	32.03	32.16
Current density along the p-n junction at centre of stripe 2: x $10^6 Am^{-2}$	76.57	41.48	40.91	40.95	40.82	40.91
Net difference between total input current/ unit length, and total injected current across p-n junction/unit length: Am^{-2}	754.590 - 718.620 = 35.97	498.888 - 499.086 = -0.198	487.456 - 487.292 = 0.164	483.919 - 483.750 = 0.169	485.919 - 485.631 = 0.288	487.400 - 487.236 = 0.164

Table 5.4.1-1 Values of reference current densities of the trial problem as a function of the mesh size.

into the points on the p-type passive/active interface lying on the lines through the midpoints of each electrode and the line through the midpoint of interelectrodes gap are compared. The current per unit length going into the device and across the active layer is also compared. It must be pointed out here that the error in the current density calculated immediately underneath stripes is attributable to the current crowding near the stripe edges even though the higher order central difference formula is used to calculate the first order derivative. Clearly, for the rectangular fine mesh the change in values of current density are less than 1%. In this chapter the optimized mesh size is with step lengths h_x = 0.3μm and h_y = 0.2μm in the horizontal and vertical directions respectively. This mesh size provides adequate accuracy without putting an unnecessary burden on the storage requirements of the computer. The value of over-relaxation parameter (S.O.R) θ in the iteration process is found to be in the range 1.85~1.99 for the least number of iterations. Despite the fact that the model is a crude one, the results of the potential and the injected current density distributions provide very useful information for the terminal behaviour of the device.

5.4.2 Variation of applied potential

Figure (5.4.2-1) shows the current density distributions going into the p-type passive/active interface when one of the electrodes is kept at a fixed potential VS_1 = 1.55 volts while the potential VS_2 on the other electrode is varied. It is clear from this figure that the effect of VS_2 on the injected current density is minimal until the two electrode potentials are within 150mV. The tabulation of injected currents shows that the current flowing into the electrodes is reduced quite considerably as the potential on the second electrode approaches that of the first electrode. This is due to the lowering of interstripe leakage current. Figure (5.4.2-2) shows the current density distribution just beneath

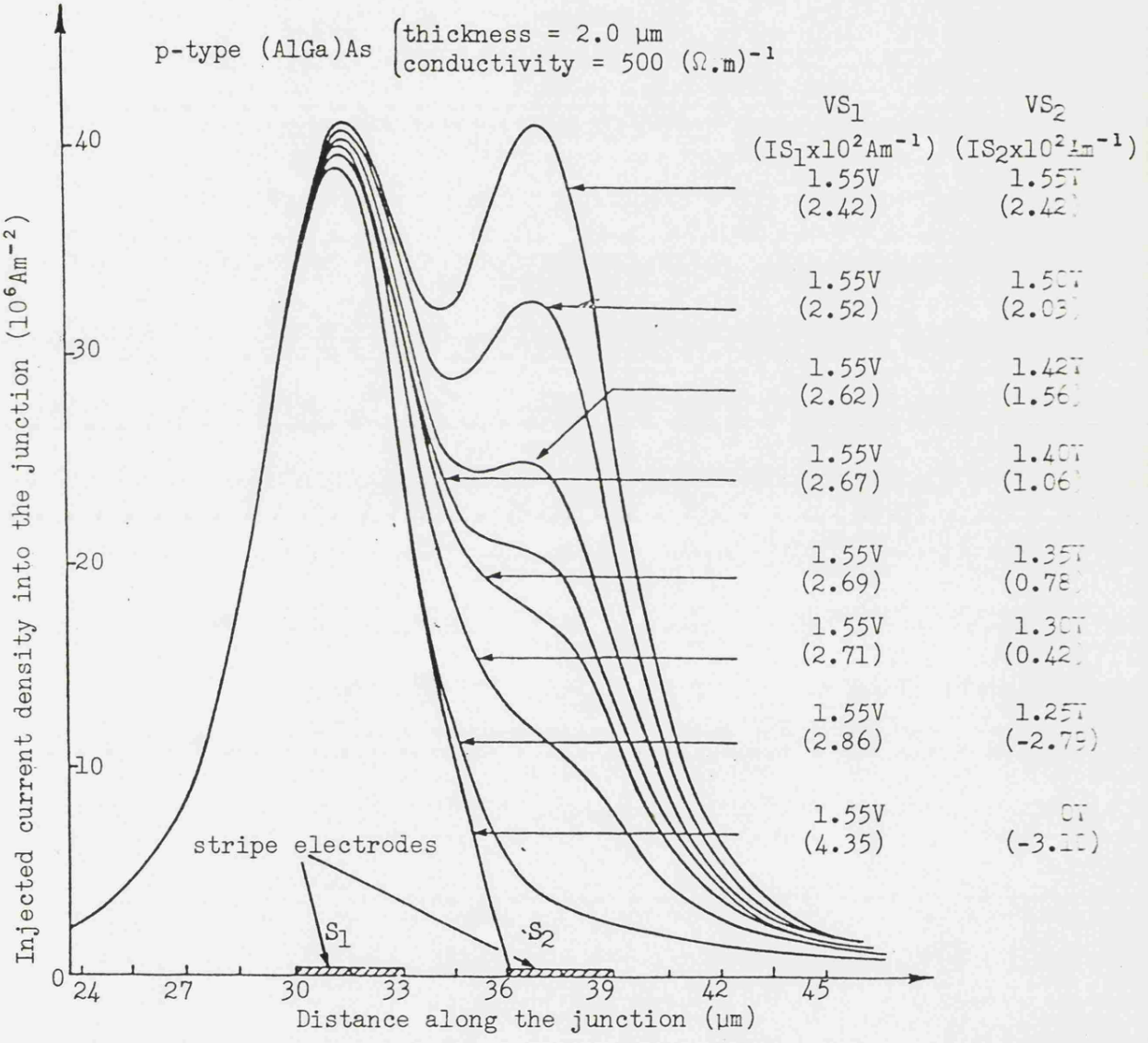

Figure 5.4.2-1 Current density distribution at the GaAs/(AlGa)As hetero-junction as a function of the stripe potentials. The currents injected into each stripe are also given. The thickness and the conductivity of the (AlGa)As layer are labelled in diagram.

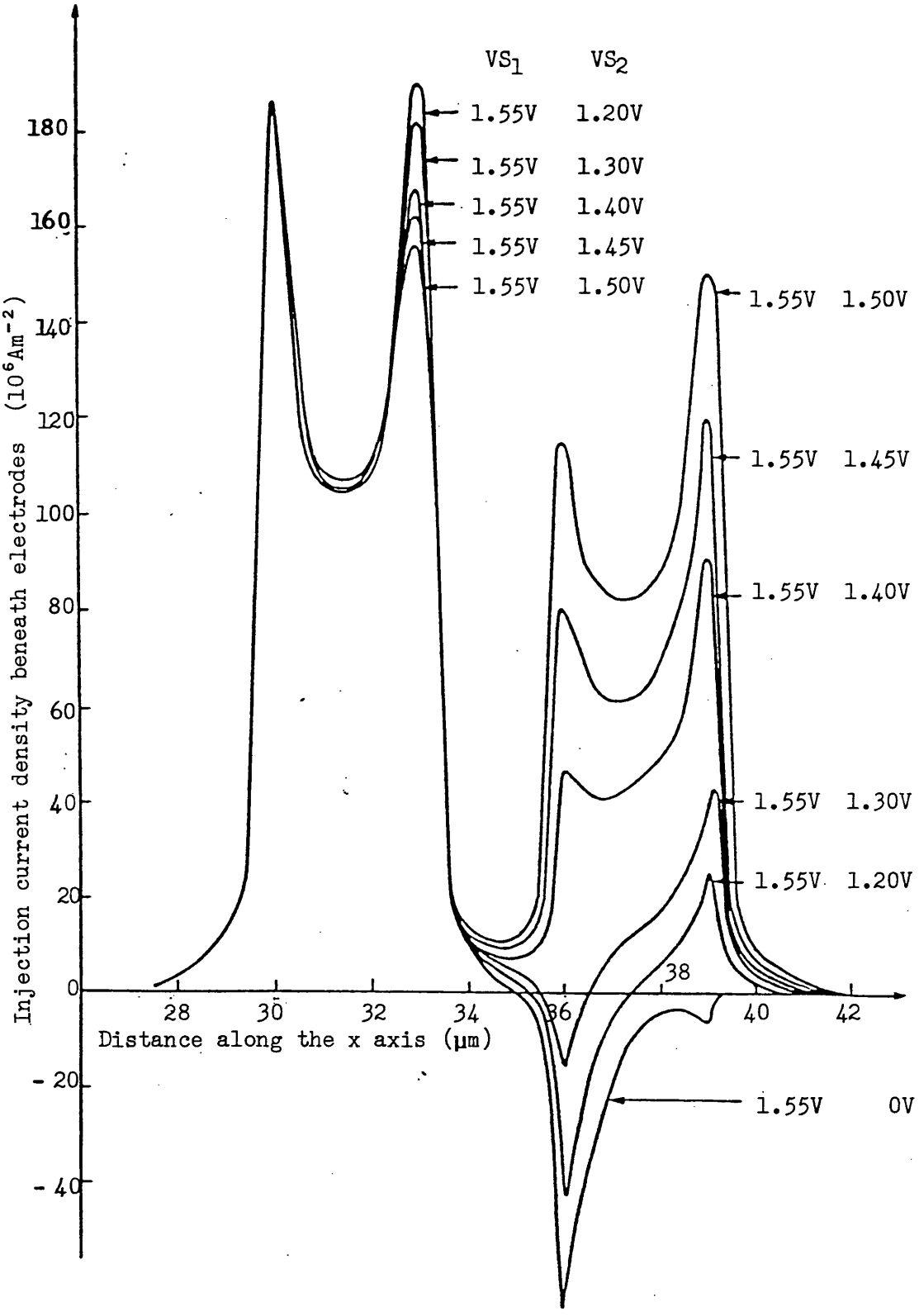

Figure 5.4.2-2 Current density distribution of the y component of the injected electrode currents calculated at a depth of 0.1 μm beneath the electrodes for a range of labelled voltages.

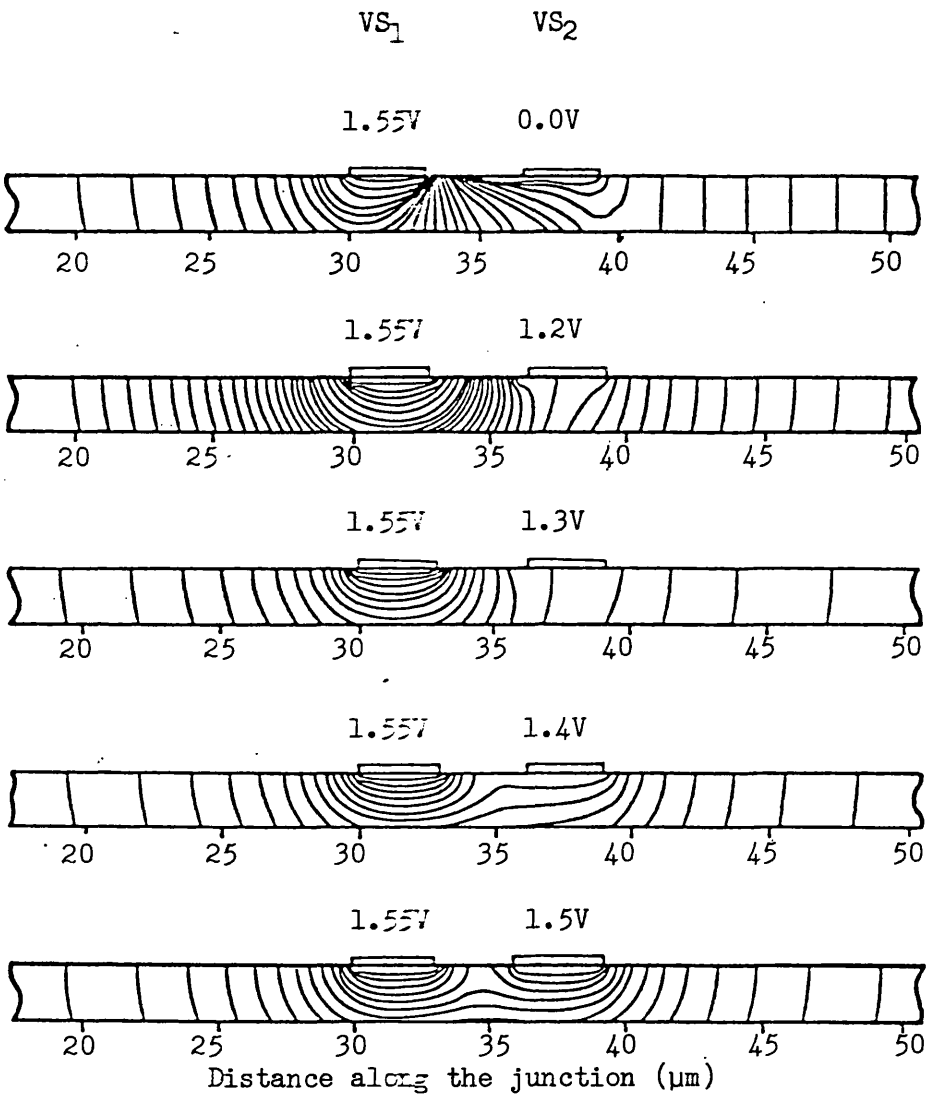

Figure 5.4.2-3 Equipotential plot of the twin stripe laser as a function of the stripe voltage for the case of a 2 μm thick (AlGa)As layer with σ = 500 $(\Omega m)^{-1}$

the each electrode for various potential values. Clearly from this figure there is a lot of current leakage taking place from the electrode S_1, at the higher potential VS_1 = 1.55 volts, to the neighbouring electrode S_2 at the lower potential VS_2 = 1.3 volts or less. Therefore the electrode S_1 draws a lot of current, of which much leaks directly through the low biased neighbouring electrode, this results in an increase in the threshold current density of the device. However, when the two electrodes are at nearly the same potentials, interstripe leakage is reduced and the current spreading from the two electrodes contribute to the current density injected into the p-type passive/active interface, thus reducing the thershold current density of the device. This is in accordance with the experimental results (13 - 15). Consequently if the stripe S_1 is being pumped just below threshold (S_2 open circuit determines the threshold current density for S_1), pumping the stripe S_2 below the threshold value, due to current spreading from S_2, may bring the injection level of S_1 above threshold and as a result the most significant change in the optical output occurs beneath the electrode S_1. This feature has also been observed experimentally (13 - 15). Figure (5.4.2-3) shows the equipotential plot for different sets of voltage applied on the two electrodes. The current density, which is directed normal to the equipotential lines, leaks into the low biased electrode in the case when the two potentials are quite different. From the above discussion it becomes apparent that even neglecting the effect of lateral diffusion of the carriers in the active region there is a significant interaction of the injected currents between the electrodes. This is entirely due to the p-type resistive region. Further, the effect of the p-type region on the interaction is studied by varying its thickness and conductivity.

5.4.3 Variation of the thickness of the cladding layer

As shown in figure (5.4.3-1), reducing the thickness of the p-type region

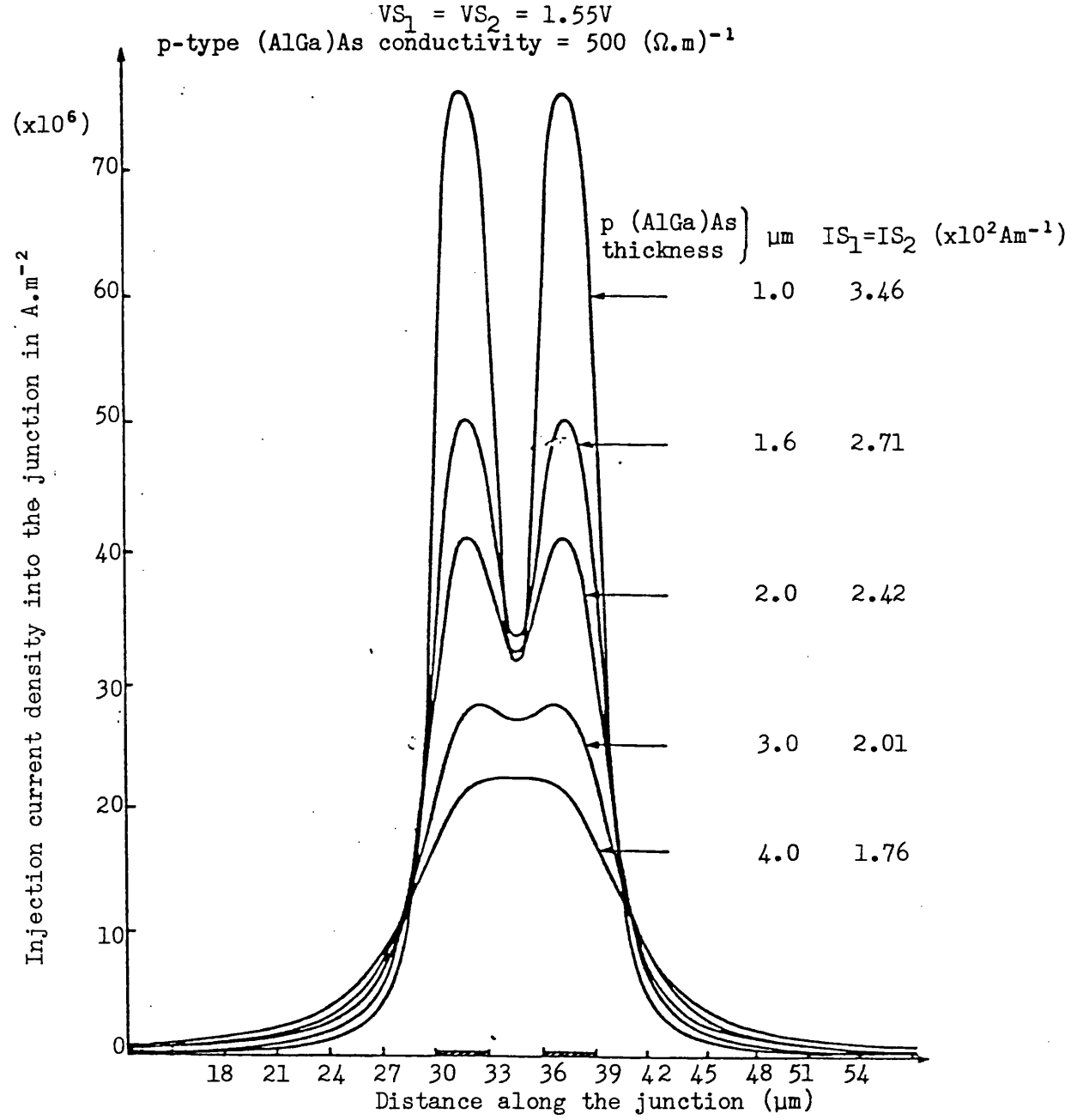

Figure 5.4.3-1 Current density distribution at the GaAs/(AlGa)As heterojunction as a function of (AlGa)As thickness for the case where $VS_1 = VS_2 = 1.55V$ and $\sigma = 500\ (\Omega.m)^{-1}$

reduces the overall device resistance, thereby increasing both the current injected into the electrodes and the level of injection current density into the p-type passive/active interface. The absolute minimum value of the valley current density between the electrodes in the symmetrically pumped case is seen to change very little as the thickness is reduced, but because of the greater level of injection the parameter of importance which indicates the reduction in interstripe coupling is an increase in the maximum to minimum current injection beneath the stripes. Table (5.4.3-1) shows these ratios for different values of thickness of the p-type region. The ratio increases from 1.27 to 2.42 as the thickness of the p-type region is reduced from 2μm to 1μm. However, for a thickness of the resistive layer of 3μm, or more, coupling between the stripes becomes so strong that separate injection beneath each electrode is hardly discernible. This is an important design parameter for a practical twin stripe laser device.

5.4.4 Variation of the resistivity of the cladding layer

Figure (5.4.4-1) shows the current density distribution injected into the p-type passive/active interface for varying resistivity values of the p-type region, while its thickness is kept fixed at 2μm and is symmetrically pumped. The case of a high resistivity value (2Ωcm) is included which Lengyel et al (6) have shown is more reasonable to decouple the problem of lateral diffusion of carriers in the active region from the current spreading problem in the p-type passive region. The main feature of the graph is that the injected current is reduced but there is little effect on the current spreading. The ratio of the peak to valley current density in table (5.4.4-1) shows a slight increase as the resistivity is increased, indicating that the non-linear boundary does not have a significant role to play, particularly when the most of the potential is dropped across the p-type region. If the level of injection

$VS_1 = VS_2 = 1.55V$

Conductivity of p-type (AlGa)As = 500 $(ohm\ m)^{-1}$

thickness	peak/trough current ratio
1 μm	2.42
1.6 μm	1.51
2 μm	1.27
3 μm	1.04
4 μm	0.93

Table 5.4.3-1 Ratio of the peak current to the trough of the current between the electrodes for varying thickness of the p -type (AlGa)As layer.

$VS_1 = VS_2 = 1.55V$

p-type (AlGa)As thickness = 2 μm

(AlGa)As conductivity	peak/trough current ratio
500 $(ohm\ m)^{-1}$	1.27
200 $(ohm\ m)^{-1}$	1.29
100 $(ohm\ m)^{-1}$	1.30
50 $(ohm\ m)^{-1}$	1.31
$VS_1 = VS_2 = 2.5V$ 100 $(ohm\ m)^{-1}$	1.47

Table 5.4.4-1 Ratio of the peak current to the trough of the current between the electrodes for varying conductivity of the p-type (AlGa)As layer.

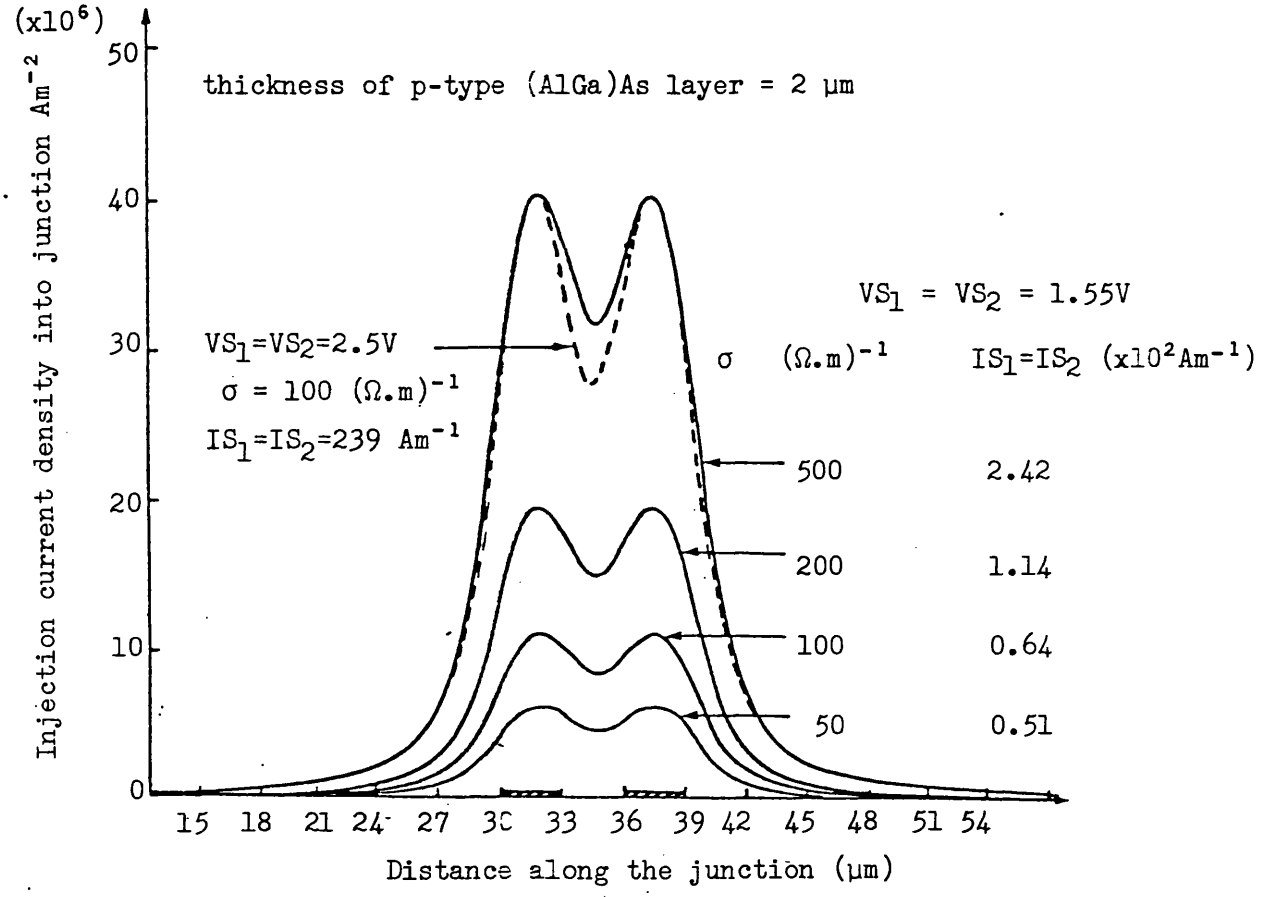

Figure 5.4.4-1 Current density distribution at the GaAs/(AlGa)As interface as a function of the conductivity of the p-type (AlGa)As layer with thickness 2 μm.

for the 1Ωcm resistivity layer is raised to $VS_1 = VS_2 = 2.5$ volts, in order to restore the level of injection current into the active layer, it is seen that there is a reduction in the current spreading and an increase in the peak to valley ratio. Joyce (16) has shown that the conductivity of the p-type layer has an important role to play in a single stripe laser as far as stability of the device is concerned. Thus a primary requirement for a twin stripe device in the first instance is a relatively thin low resistivity p-type (GaAl)As layer. The current density injected into the p-type passive/active interface is the source of carrier density generation in the active region which in turn produces the optical output. The distribution of the carrier density, and hence the current density, is important for analysing the device behaviour. Because of lateral diffusion the carriers in the active region will not follow the current density distribution precisely. However, symmetric and asymmetric injected current density distribution features will be reflected in the carrier density distribution, which means that changes in the complex dielectric constant and hence optical field are expected to be observed. These facts have been confirmed experimentally by Scifres (13).

5.4.5 Variation of the interelectrode spacing

Figure (5.4.5-1) shows the effect of interelectrode spacing on the current density distributions. As would be expected, increasing the stripe spacing significantly decreases the stripe coupling due to the resistive or passive layer. Moreover, for close spacing of the electrodes typically 1.8μm or less the coupling via the passive region is very strong which would give rise to strong interstripe leakage current. To avoid this leakage of current an extremely thin cladding layer should be used. However, vertical confinement of the optical field may be seriously affected. One method of reducing interstripe leakage without using an extremely thin p-type layer is to isolate the two stripes by proton

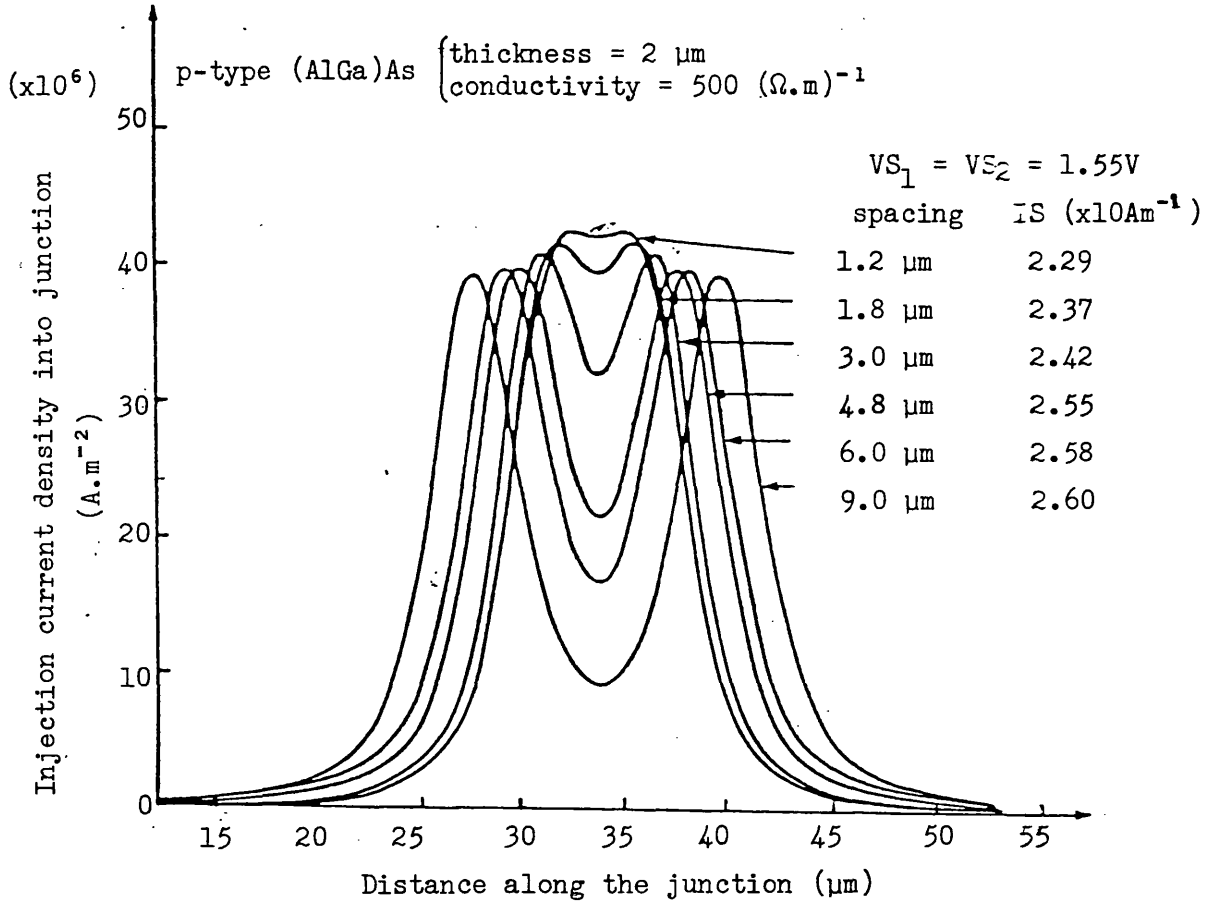

Figure 5.4.5-1 Current density distribution at the GaAs/(AlGa)As heterojunction as a function of the spacing of the 3 μm wide electrodes. The (AlGa)As layer thickness and conductivity are labelled in diagram.

bombardment or etching through the part of the p-type layer in between the two stripes. The effect of etching through the confining layer can also be modelled. Figure (5.4.5-2) shows that as the depth of the notch is increased, the current confinement under the stripe improves, as expected. The maximum notch depth considered in a 2μm thick resistive layer was 1.2μm. Such a notch should not have a significant effect on the waveguiding properties in the direction perpendicular to the passive/active interface. This technique would be required for stripe spacings less than 2μm, with electrode widths of 2μm or 3μm if a high injection efficiency and isolation of the stripes are to be achieved. The interstripe resistance can be calculated approximately by assuming a slab representing the material between the two stripes. Although the non-linear boundary at the passive/active interface will have some effect on the interstripe resistance, a linear dependence with the interstripe spacing is expected. Suppose L_c is the length of the laser cavity and d' is the thickness of the p-type region. If S_1S_2 is the distance between the centres of the two stripes, one can write down the interstripe resistance approximately as given below:

$$R_{IS} = \rho\{S_1S_2/(L_c d')\} \qquad (5.4.5\text{-}1)$$

where ρ is the resistivity of the p-type region. Alternatively, when one of the electrodes S_2 is kept at zero potential while the other stripe S_1 is maintained at a potential VS_1, the current density directly leaks through the electrode at zero potential. One can work out IS_2, the current leaking through the electrode S_2 and therefore $R_{IS} = VS_1/IS_2$. R_{IS} is plotted in figure (5.4.5-3) for different electrode spacings. As has already been seen in figure (5.4.2-2) there is a lot of current crowding near the edges of the electrodes and therefore it is unreasonable to assume a uniform current density injected into the electrodes. Figure (5.4.5-4) shows the percentage of the total current injected into the

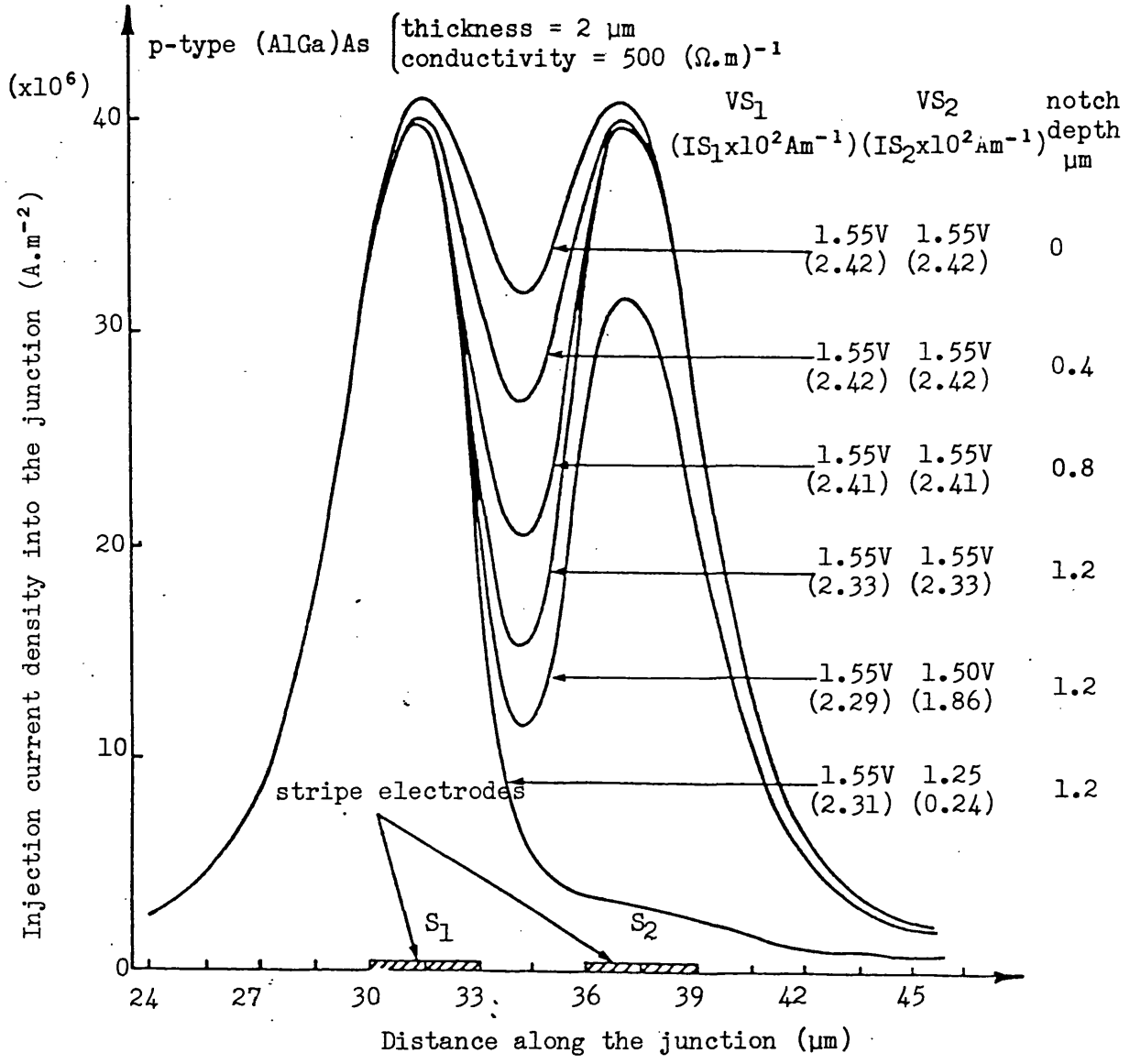

Figure 5.4.5-2 Current density distributions of the current injected into the active region as a function of the notch depth between the two stripes, for the case of VS_1 = 1.55V.

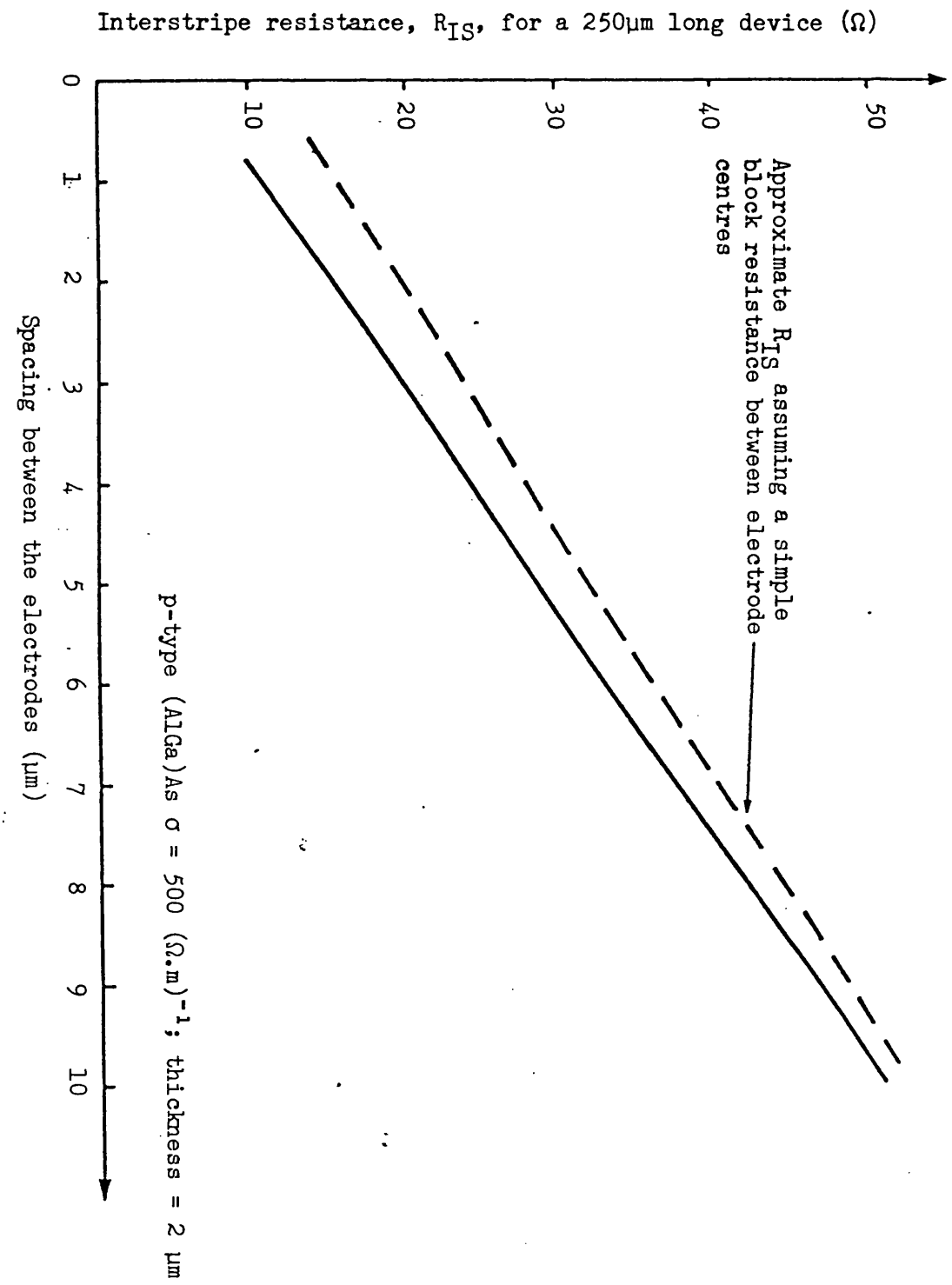

Figure 5.4.5-3 Variation of R_{IS} with interstripe spacing for the case of 3 μm wide electrodes and a 2μm thick (AlGa)As layer of conductivity 500 $(\Omega.m)^{-1}$.

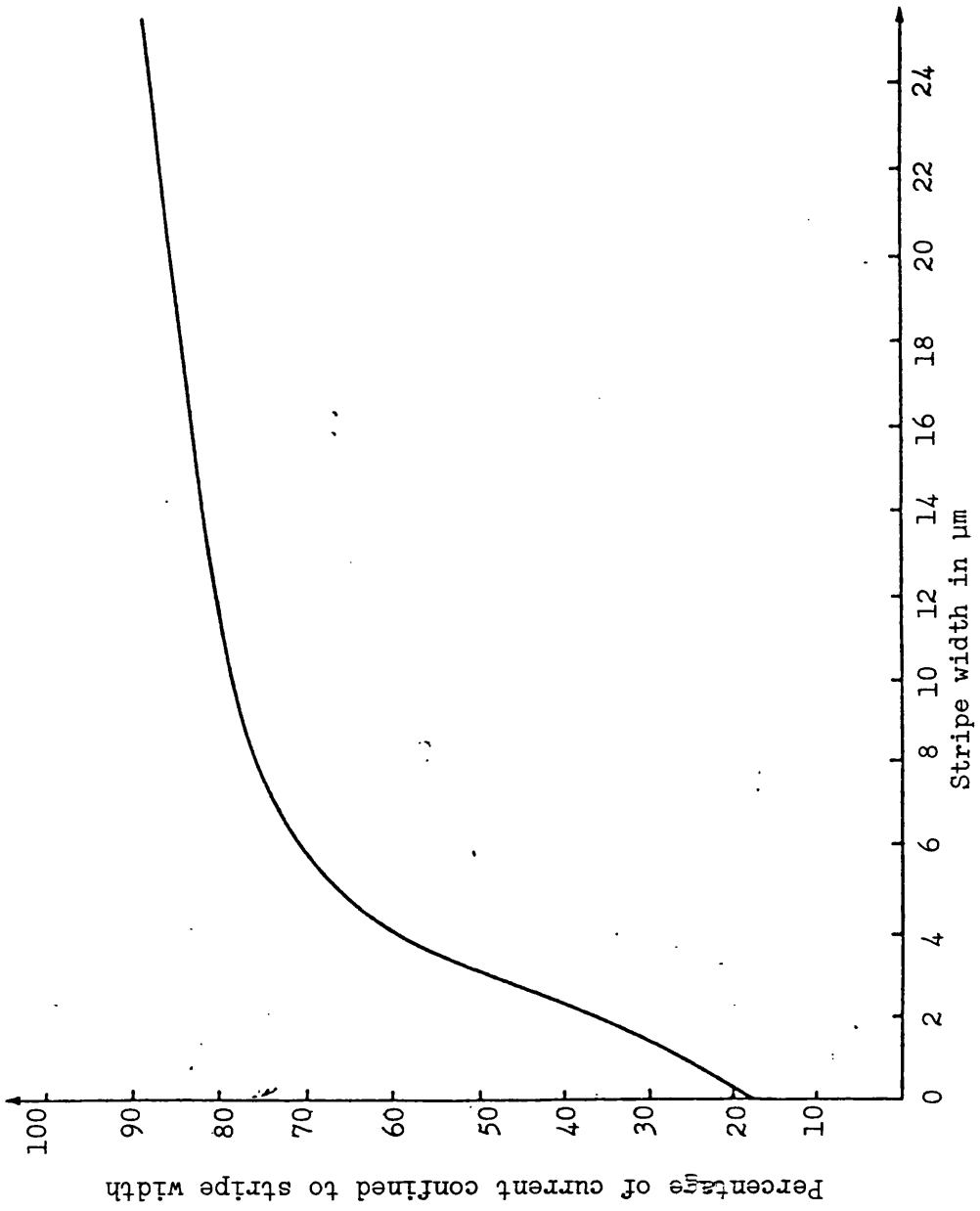

Figure 5.4.5-4 Percentage of the total current injected into the active layer which remains confined to the electrode width as a function of the electrode width, showing how the threshold current increases as the electrode width is reduced to a filament.

junction which remains confined to the electrode width as a function of the width of the stripe for a single stripe case pumped at VS_1 = 1.55 volts with remaining parameters kept the same as in table (5.4-1). For electrode widths above 20μm the assumption of uniform current density is reasonably valid as 83% of the current is confined within the electrode width, however for the 3μm stripe width case it is only 49%. This compares with 71% current confinement for the 6μm wide electrode. It has been seen in a single stripe laser (3, 9) that small electrode widths are important to get the stable behaviour of the device upto a large range of injected current thus the uniform current injection assumption gets violated. Further it may be of practical value to have electrode widths less than 3μm so that centre-to-centre spacing between the two stripes can be minimized in order to improve coupling. Hence the thickness of the resistive layer, its resistivity and stripe spacing are important parameters determining the behaviour of twin stripe lasers and therefore must be carefully tailored.

5.5 Discussion

The chapter has highlighted the problem of interstripe coupling in a twin stripe laser via the resistive layer. The effect of interstripe coupling is to increase the threshold current density of an individual laser when the other is grounded, yet to reduce the the threshold for the comparitively higher pumped stripe when both stripes are pumped. The results show that the current density distribution both into the p-type passive/active interface and the electrodes cannot be considered uniform for the case of narrow stripe ($\leq$ 3μm) electrodes. Resistive coupling of the two stripes provides a significant level of injection between the stripes. The results also suggest that an aspect ratio of stripe width to (GaAl)As thickness of 1.5 represents a limit as far as efficient current injection is concerned (even then only 49% of the

injected current is confined to the stripe width). Isolation techniques, however, can significantly improve this and would be considered vital for electrode spacing 2μm or less with equally narrow stripe electrodes.

References

1. B.W. Hakki: "GaAs double-heterostructure lasing behaviour along the junction plane", J. Appl. Phys., Vol.46, pp.292-302, 1975.

2. B.S. Poh and T.E. Rozzi: "Intrinsic instabilities in narrow stripe geometry lasers caused by lateral current spreading", IEEE J. Quantum Electron., Vol. QE-17, pp.723-731, 1981.

3. N. Chinone: "Non-linearity in power output-current characteristics of stripe geometry laser", J. Appl. Phys., Vol.48, pp.3237-3243, 1977.

4. W.T. Tsang: "The effects of lateral current spreading, carrier out-diffusion and optical mode losses on the threshold current density of GaAs-$Al_xGa_{1-x}As$ stripe geometry D.H. lasers", J. Appl. Phys., Vol.49, pp.1031-1044, 1978.

5. W.P. Dumke: "Current thresholds in stripe injection lasers", Solid State Electron., Vol.16, pp.1279-1281, 1973.

6. G. Lengyel, D. Meissner, E. Patzak and K.H. Zschauer: "An analytic solution of the lateral current spreading and diffusion problem in a narrow oxide stripe (GaAl)As/GaAs DH lasers", IEEE J. Quantum Electron., Vol. QE-18, pp.618-625, 1982.

7. J.E.A. Whiteaway: "Theoretical analysis of current spreading in stripe geometry injection lasers", IEE Proc., Part I, Vol.129, pp.89-95, 1982.

8. S.J. Chua, M.S. Leong and D.S.H. Chan: "Lateral current spreading in stripe contact semiconductor lasers", IEE Proc., Part I, pp.302-303, 1983.

9. P.M. Asbeck, D.A. Cammack, J.J. Daniele and V. Klebanoff: "Lateral mode behaviour in narrow stripe lasers", IEEE J. Quantum Electron., Vol. QE-15, pp.727-733, 1979.

10. I. Ladany: "The influence of stripe width on the threshold current of double heterojunction lasers", J. Appl. Phys., Vol.48, pp.1935-1940, 1977.

11. W.B. Joyce: "Current-crowded carrier confinement in double heterojunction lasers", J. Appl. Phys., Vol.51, pp.2394-2401, 1980.

12. T.L. Paoli: "Non-linearity in the emission characteristics of stripe-geometry (AlGa)As double heterojunction lasers", IEEE J. Quantum Electron., Vol. QE-12, pp.770-776, 1976.

13. D.R. Scifres, W. Streifer and R.D. Burnham: "Beam scanning with twin-stripe injection lasers" Appl. Phys. Lett., Vol.33(8), pp.702-704, 1978.

14. I.H. White, J.E. Carroll and R.G. Plumb: "Closely coupled twin-stripe lasers", IEE Proc., Part I, Vol.129, pp.291-296, 1982.

15. T. Kumar, R.F. Ormondroyd and T.E. Rozzi: "Interstripe coupling and current spreading in a subthreshold double heterostructure twin stripe laser", IEEE J. Quantum Electron., Vol. QE-20, pp.364-373, 1984.

16. W.B. Joyce: "Role of conductivity of the confining layers in DH laser spatial hole burning effects", IEEE J. Quantum Electron., Vol. QE-18, pp.2005-2009, 1982.

CHAPTER VI

SELF-CONSISTENT SOLUTION OF CURRENT SPREADING AND LATERAL CARRIER DIFFUSION IN BELOW THRESHOLD TWIN STRIPE LASERS

6.1 Introduction

In the previous chapter the effect of current spreading was considered in a twin stripe laser device using a simple distributed diode model to represent the heterojunction. Whilst the model gives a good indication of the current spreading and coupling via the confining layer, it does not give any information concerning the lateral diffusion of the carriers which affects the current spreading and is responsible for the waveguiding mechanism in the lateral direction. Also it has been pointed out by Wilt and Yariv (1) that the approximation of a junction diode does not take into account the saturation of the diode voltage above lasing threshold and the effect of lateral diffusion of carriers in the active region. In this chapter a more realistic approach to the heterojunctions is considered. The model includes the effect of spontaneous radiative recombination (a non-linear process) but the effect of stimulated recombination is not considered at this stage. Consequently the analysis is valid upto the point at which the stimulated recombination becomes dominant. It has been shown in references (2, 3) that electrode widths of order of 3μm are necessary to raise the level of light output at which the kink (responsible for the instability of the device) in the light/current characteristic appears. Because of the aspect ratio of the stripe width to the resistive layer thickness is of the order of 1.5 as mentioned in the previous chapter, it is necessary to use a 2-dimensional model of Laplace's equation in the resistive layer (4) and therefore simple sheet resistance models (5, 6) are not valid to estimate the current spreading problem.

This chapter attempts to solve the lateral carrier diffusion problem and the current spreading problem in the p-type resistive layer shown in figure (6.2-1) simultaneously. The solution technique adopted will then act as a building block for the fully consistent model above threshold

which will be discussed in the next chapter. In a real double heterostructure laser device, the thickness of the active layer (0.1-0.3μm) is very much smaller than the diffusion length (4 ∿ 9μm) of the carriers injected into the active layer. Because of this it is usual to assume that the quasi-Fermi levels are constant across the active layer in a direction perpendicular to the junctions (1). As the position of the quasi-Fermi levels within the energy band diagram dictates the carrier concentration, this too may be assumed constant across the active layer. However, because of both lateral diffusion of carriers and the current spreading in the confining layers, the separation of the quasi-Fermi levels determining the voltage across the junction will vary laterally along the active layer. It is further assumed that the laser diode has a broad area contact with a moderately doped n-type (GaAl)As confining layer so that the current in the substrate is not constrained to flow parallel to the active layer. Joyce (7) has described the type of carrier transport in such a device with one kind of carriers diffusing laterally while the other type of carriers are stationary. In the model considered in this chapter, electrons are stationary while the holes are diffusing laterally. This leads to a model in which only one double heterojunction is considered as shown in figure (6.2-1) the other being an equipotential contact. The charge neutrality condition of the lightly doped active layer is also assumed in this model. To preserve neutrality, electrons are supplied by the equipotential contact locally while the holes are diffusing laterally. Furthermore, it is assumed that the only significant injection of carriers will be into the active layer from the large band gap passive layers.

6.2 Theoretical Analysis

The model used in this numerical analysis is given in figure (6.2-1) together with the boundary conditions used. In this figure a and b are

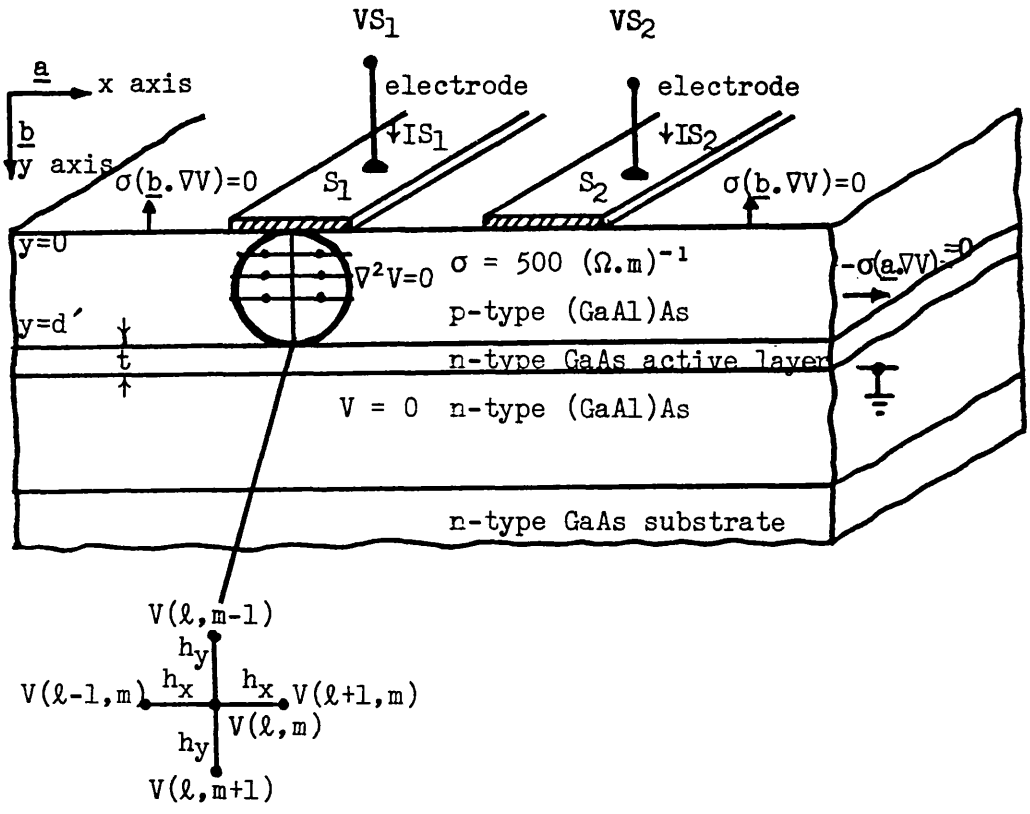

Figure 6.2-1 The 2-dimensional twin stripe model assumed for the numerical computation.

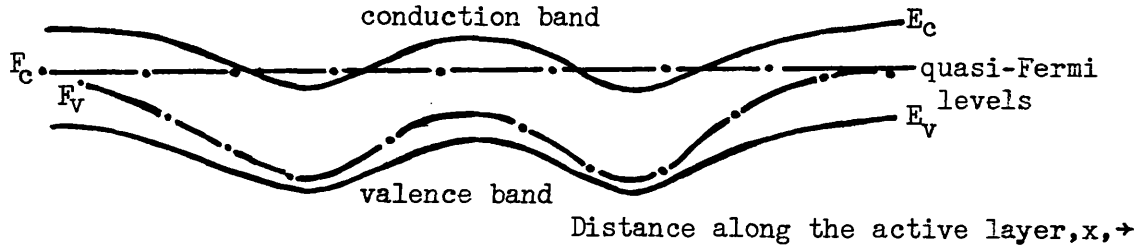

Figure 6.2-2 Lateral variation of the quasi-Fermi levels in the active layer for two arbitrary stripe potentials near threshold.

unit vectors in the x and y directions respectively. The heterojunction under consideration exists at $y = d'$ and the active layer has a thickness t.

In common with other authors (4, 7, 8) the effect of the p-type GaAs layer which is normally grown to facilitate contacting has not been considered. The reason for this is that this layer is relatively highly doped. In order to achieve any form of interstripe isolation as pointed out in the previous chapter, it is necessary to either, (i) etch away the GaAs from around the stripes, or (ii) use semi-insulating GaAs with localized stripe regions of heavily doped Zn diffusions, as shown in figure (1.1-3). In all cases the p-type GaAs under the stripes should have negligible resistance in the transverse direction, compared with the (GaAl)As regions beyond the stripes, and will not contribute to the lateral current spreading.

In reference (9) it was shown that the current density injected into 3μm wide electrodes was not uniform due to current spreading, and that the only valid boundary condition on the electrodes should be a constant potential. In this chapter the same boundary condition is adopted. However, it is appreciated that it is the terminal current which is the most useful parameter in describing laser behaviour, particularly so in the case of the twin stripe structure. The electrode currents are thus calculated from the final solution to Laplace's equation and are quoted together with the electrode potential. In this way it is possible to establish exactly how the working point of one stripe is modified by a change in the operating conditions of the other stripe, or by a change in geometry.

Considering first the confining layer; because the region is assumed to be passive and homogeneous, the potential distribution may be found

by a solution to the 2-dimensional Laplace's equation:

$$\nabla^2 V = 0 \tag{6.2-1}$$

under the boundary conditions shown in figure (6.2-1). Solving equation (6.2-1) subject to these boundary conditions then enables the current density to be calculated using:

$$\underline{J}(x,y) = -\sigma \nabla V(x,y) \tag{6.2-2}$$

where σ is the conductivity of the p-type (GaAl)As region and $V(x,y)$ is the potential distribution calculated from equation (6.2-1). It is particularly important to calculate the current injected into the heterojunction at $y = d'$. This couples the diffusion equation for the carriers in the active layer to Laplace's equation for the resistive region. Using equation (6.2-2) the y component of current density becomes:

$$J(x)\big|_{y=d'} = -\sigma(\nabla V)_y \tag{6.2-3}$$

where suffix y denotes the y component of (∇V). The total current injected into the (GaAl)As region from the stripe electrodes may now be obtained from:

$$I_{stripe} = \int_{stripe} J(x)\big|_{y=0}\, dx \tag{6.2-4}$$

In the model of the heterojunction it is assumed that the GaAs active layer is very thin (very much less than the diffusion length of injected holes and electrons). It may therefore be assumed, in keeping with other authors (1, 4) a constant carrier density across the active layer, which may be determined from the one dimensional diffusion equation:

$$D_{amb} \frac{d^2N}{dx^2} - BN^2 = - \frac{J(x)\big|_{y=d'}}{et} \tag{6.2-5}$$

where D_{amb} is the ambipolar diffusion coefficient, BN^2 is the bimolecular

(radiative) recombination term, t is the active layer thickness and e is the electronic charge. Joyce (7) has shown that for the geometry of the DH structure considered here the effective diffusion coefficient is the same as the ambiploar diffusion coefficient, D_{amb}. This reduces the problem to that of solving one diffusion equation only. The potential difference appearing across the active layer will vary laterally because of current spreading and carrier diffusion. This potential difference, at any point, x, along the junction can be related to the Fermi levels, as shown in figure (6.2-2), which in turn dictates the carrier density at that point, such that the electron and hole densities are respectively:

$$N(x) = N_c F_{\frac{1}{2}}\left(\frac{F_c(x) - E_c(x)}{k_B T}\right) \qquad (6.2\text{-}6)$$

$$N(x) = N_v F_{\frac{1}{2}}\left(\frac{E_v(x) - F_v(x)}{k_B T}\right) \qquad (6.2\text{-}7)$$

(Both electron and hole concentrations are the same under charge neutrality assumption of the active region)

$$\text{where} \quad F_{\frac{1}{2}}(\zeta) = \frac{2}{\sqrt{\pi}} \int_0^\infty \frac{\sqrt{\zeta}\, d\zeta}{1 + \exp(\zeta - \zeta')} \qquad (6.2\text{-}8)$$

is the Fermi integral. F_c, F_v, E_c and E_v are defined in figure (6.2-2). F_c and F_v are the quasi-Fermi levels of electrons and holes respectively, E_c and E_v are the conduction and valence band edges of the active layer and N_c and N_v are the conduction and valence band density of states in the active layer. The potential drop across the active layer at x is just equal to $F_c(x) - F_v(x)$ eV. For the purpose of numerical analysis Joyce (10) has suggested an approximate solution of the Fermi integrals of the form:

$$\psi_e = \left(\frac{F_c - E_c}{k_B T}\right) = \ln(N/N_c) + K_1(N/N_c) + K_2(N/N_c)^2 + K_3(N/N_c)^3 + K_4(N/N_c)^4 + \ldots$$

(6.2-9)

Similarly, assuming charge neutrality of the active region ψ_h may be expressed as:

$$\psi_h = \left(\frac{E_v - F_v}{k_B T}\right) = \ell n(N/N_v) + K_1(N/N_v) + K_2(N/N_v)^2 + K_3(N/N_v)^3 + K_4(N/N_v)^4 + \ldots \quad (6.2\text{-}10)$$

where $K_1 = 3.53553\times10^{-1}$, $K_2 = -4.95009\times10^{-3}$

$K_3 = 1.48386\times10^{-4}$, $K_4 = -4.42563\times10^{-6}$

and $E_g = E_c - E_v$ is the energy gap of the active region in eV. From equations (6.2-9) and (6.2-10) one can write the potential difference across the active region in the form:

$$\{F_c - F_v(x)\} = k_B T\left(\frac{F_c - E_c(x)}{k_B T} + \frac{E_v(x) - F_v(x)}{k_B T} + \frac{E_g}{k_B T}\right)$$

or

$$\{F_c - F_v(x)\} = k_B T\{\psi_e(x) + \psi_h(x) + E_g/k_B T\} \quad (6.2\text{-}11)$$

Finally the potential difference across the active layer in volts is given by:

$$V(x)\big|_{y=d'} - V\big|_{y=d'+t} = V(x)\big|_{y=d'} - 0 = (k_B T/e)\{\psi_e(x) + \psi_h(x) + E_g/(k_B T)\} \quad (6.2\text{-}12)$$

The problem thus reduces to solving equation (6.2-1) subject to the boundary conditions shown in figure (6.2-1) consistent with equation (6.2-5) using equations (6.2-3) and (6.2-12). The technique may be readily applied to the case where the n-type confining layer and substrate have finite resistance, but the computational requirements increase significantly for little improvement in accuracy.

6.3 Solution Technique

The finite difference method is used to solve both Laplace's equation

and the diffusion equation self consistently. The solution may be broken into two main steps.

Step 1 - The resistive region

The resistive p-type (GaAl)As region is discretized into a rectangular mesh. At each internal node of the mesh the 2-dimensional Laplace's equation:

$$\partial^2 V/\partial x^2 + \partial^2 V/\partial y^2 = 0 \qquad (6.3\text{-}1)$$

can be written in finite difference form:

$$\frac{V(\ell-1,m) - 2V(\ell,m) + V(\ell+1,m)}{h_x^2} + \frac{V(\ell,m-1) - 2V(\ell,m) + V(\ell,m+1)}{h_y^2} = 0 \qquad (6.3\text{-}2)$$

according to figure (6.2-1). At the boundary nodes, equation (6.3-2) can be modified to include the boundary condition as in ref. (9). In this way, equation (6.3-1) reduces to a set of linear algebric equations corresponding to the nodes in the resistive region, which may be solved using a successive-over-relaxation technique (S.O.R) optimized to the problem. Initially, an estimate of the potential distribution along the heterojunction ($y = d'$) is made, $V(\ell)_{est}$, and Laplace's equation solved using S.O.R technique. $J(x)|_{y=d'}$, is solved numerically using the appropriate difference form of equation (6.2-3). These calculated values of $J(x)|_{y=d'}$, are used in the second step to determine the carrier concentration.

Step 2 - The heterojunction

The distribution of nodes along the heterojunction $y = d'$ in the previous step becomes the desired discretization for solving the diffusion equation. The diffusion equation (6.2-5) appropriate to this region can be written in finite difference form:

$$D_{amb}\left[\frac{N(\ell-1) - 2N(\ell) + N(\ell+1)}{h_x^2}\right] - BN^2(\ell) = -\frac{J(\ell)}{et} \qquad (6.3\text{-}3)$$

where $J(\ell) = J(x)\big|_{y=d}$, at the node ℓ on the junction. The carrier concentration is generally a large quantity and can cause instability in the simulation through truncation errors and "exponential overload". To avoid this problem the carrier density is normalized by the factor N_i (the intrinsic carrier density) so that the normalized diffusion equation becomes:

$$D_{amb}\left[\frac{N(\ell-1)/N_i - 2N(\ell)/N_i + N(\ell+1)/N_i}{h_x^2}\right] - BN_i\left[\frac{N(\ell)}{N_i}\right]^2 = -\frac{J(\ell)}{etN_i} \qquad (6.3\text{-}4)$$

This equation is valid for all the nodes along the heterojunction except the end nodes. As it is not feasible to model an infinitely wide device, approximations must be made at the two end nodes. In the simulation the device is truncated 36μm from the outer edge of each stripe electrode. At such a distance (approximately six times the diffusion lengths of injected carriers) one can make several assumptions regarding the carrier density distribution. The validity of these boundary conditions are considered in section (6.4).

A set of non-linear algebric equations is thus obtained which can be solved by the Newton-Raphson over-relaxation method which is described in the appendix (A).

6.4 Boundary Conditions at the End Nodes

The following alternative boundary conditions were considered:

i) $N(L) = 0$, $N(0) = 0$, $(dN/dx)\big|_{x=0} \neq (dN/dx)\big|_{x=L} \neq 0$

Asbeck et al (11) have suggested that this is not such a good approximation since the carrier density can be significant well away from the stripe.

ii) $N(L) \neq 0$, $N(0) \neq 0$, $(dN/dx)|_{x=0} = (dN/dx)|_{x=L} = 0$

This may be put into an appropriate finite difference form also. Because of the shape of the diffusion tail well beyond the stripe, this is generally considered as a reasonable approximation. This is the boundary condition which is used for all the results presented in this chapter.

iii) An alternative to the boundary condition at x = L may be obtained by means of an analytic extrapolation of N(x) from x = L to $x \to \infty$. It is reasonable to assume that the current density is approximately zero at 36μm, and beyond, from the stripe edge:

$$J(0) = J(L) \simeq 0 \tag{6.4-1}$$

However, it does not follow that the carrier density is also zero at the end nodes. The two boundary conditions are:

$$N(-\infty) = N(\infty) = 0 \text{ and } (dN/dx)|_{x=-\infty} = (dN/dx)|_{x=\infty} = 0 \tag{6.4-2}$$

Using equation (6.4-1), equation (6.2-5) may be written as:

$$d^2N/dx^2 = (B/D_{amb})N^2 \qquad \text{for } -\infty < x < 0 \text{ and } L < x < \infty \tag{6.4-3}$$

Considering the region $L < x < \infty$ for convenience, equation (6.4-3) may be integrated to give:

$$\int_L^{\infty} \frac{d}{dx}\left[\frac{dN}{dx}\right]^2 dx = \frac{2B}{D_{amb}} \int_L^{\infty} N^2 \frac{dN}{dx}\, dx \tag{6.4-4}$$

Applying the boundary conditions of (6.4-2) yields a solution:

$$-\frac{dN(L)}{dx} = N^{\frac{3}{2}}(L)\left[\frac{2B}{3D_{amb}}\right]^{\frac{1}{2}} \tag{6.4-5}$$

Similarly for region $-\infty < x < 0$ the solution is:

$$\frac{dN(0)}{dx} = N^{\frac{3}{2}}(0)\left[\frac{2B}{3D_{amb}}\right]^{\frac{1}{2}} \tag{6.4-6}$$

These may be put into finite difference form to yield the boundary condition for the end nodes N(L) and N(0), in terms of the imaginary nodes N(L + 1) and N(0 - 1), such as:

$$N(L+1) = N(L) - N^{\frac{3}{2}}(L)h_x\left(\frac{2B}{3D_{amb}}\right)^{\frac{1}{2}}$$
$$N(0-1) = N(0) - N^{\frac{3}{2}}(0)h_x\left(\frac{2B}{3D_{amb}}\right)^{\frac{1}{2}} \qquad (6.4\text{-}7)$$

where h_x is the step length along the junction. If $\left(\frac{2B}{3D_{amb}}\right)^{\frac{1}{2}} N^{\frac{3}{2}}(L)h_x \ll N(L)$ the boundary condition reduces to $N(L+1) \simeq N(L)$ i.e $\{dN(L)/dx\} = 0$. Similarly for $x = 0$. The above boundary conditions may be normalized by dividing throughout by N_i as appropriate.

To test the validity of boundary conditions (ii) and (iii), a trial twin stripe problem was set up using the different boundary conditions. Details of the problem are outlined in the next section. The results are shown in figures (6.4-1a) and (6.4-1b). It is clear that the boundary conditions plotted give consistent results for J(x) and N(x) under the stripe, although there is considerable difference at the boundaries, as might be expected.

6.5 Single Stripe Solution

A single stripe laser just below threshold was initially considered, primarily for comparison with other, existing, solution techniques and to determine the required mesh size for the analysis. The parameters used for the simulation are shown in table (6.5). To reduce computational effort the device is modelled using a line of symmetry about the centre of the stripe electrode.

p-type (GaAl)As resistivity, $\rho = 2.0 \times 10^{-3}$ ohm.m
ambipolar diffusion coefficient of carriers in active layer D_{amb} $= 40\ cm^2/s$
thickness of p-type (GaAl)As layer = 2.0 μm
thickness of active layer, t = 0.1 μm
stripe width of electrode S_1 = 3.0 μm
stripe width of electrode S_2 = 3.0 μm
spacing between electrodes = 3.0 μm
$VS_1 = VS_2 = 1.60V$
band gap of active region material GaAs = 1.43 eV
density of states of conduction band of active layer material, N_c $= 4.7 \times 10^{17}\ cm^{-3}$
density of states of valence band of active layer material, N_v $= 7.0 \times 10^{18}\ cm^{-3}$
bimolecular recombination coefficient, $B = 9.7 \times 10^{-11} cm^3/s$

Table 6.5 Parameters used in the simulation of the twin stripe and single stripe laser, unless otherwise stated.

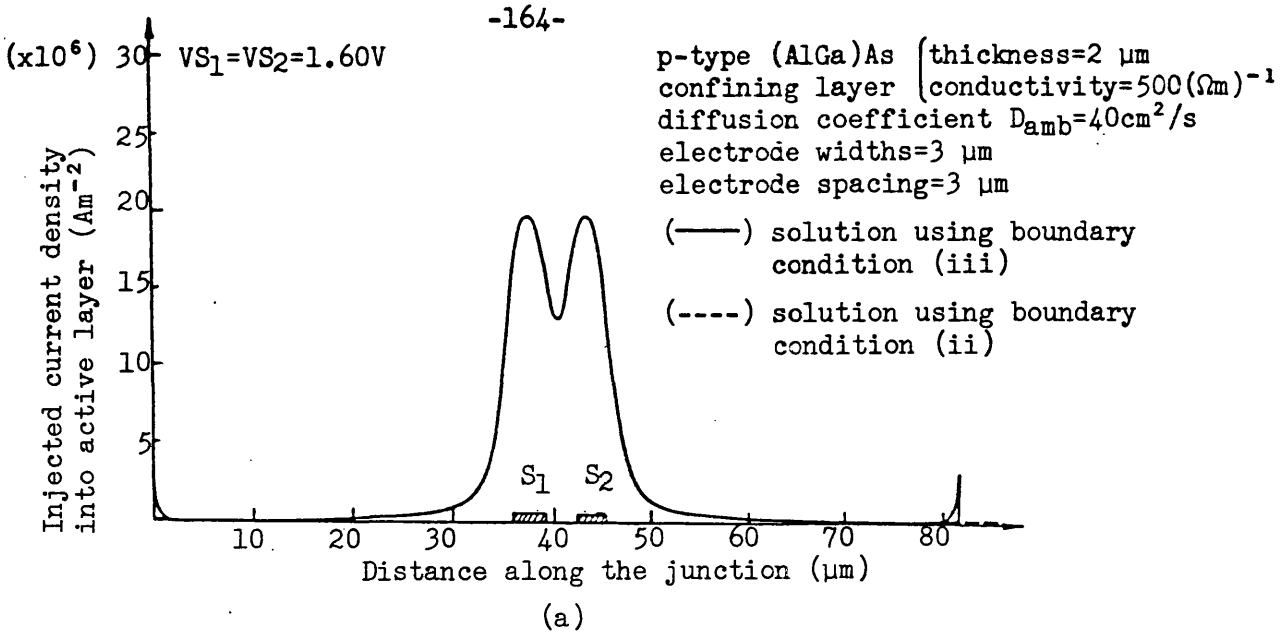

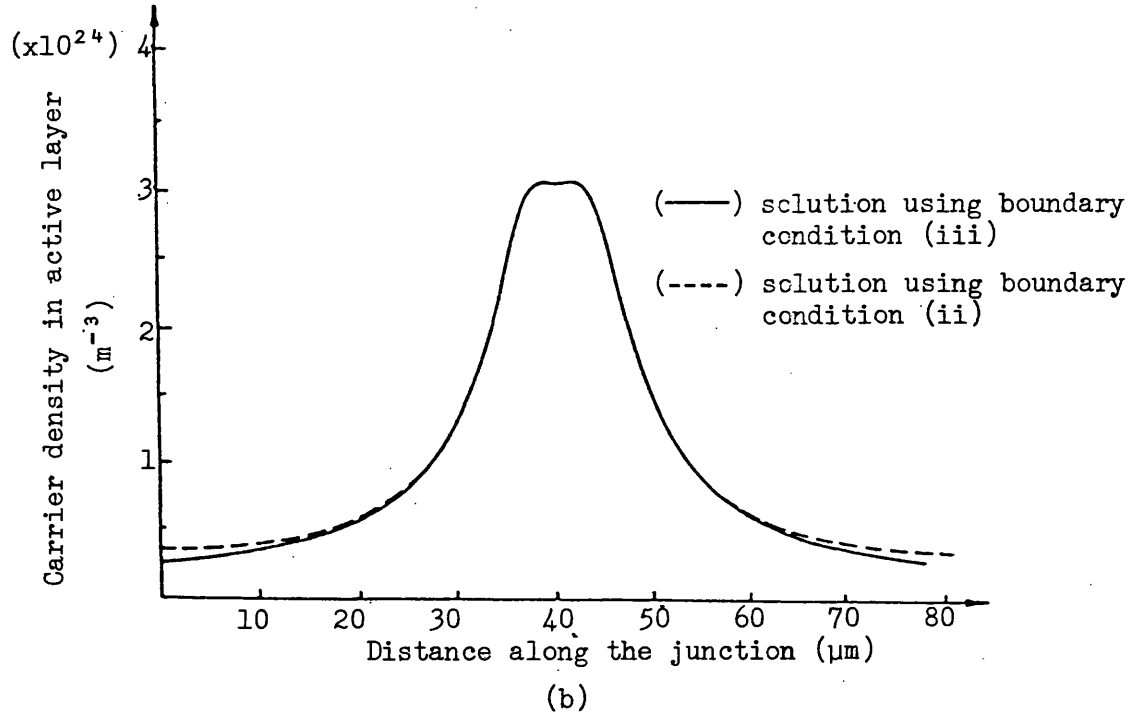

Figure 6.4-1 Trial solution of the (a) current density distribution and (b) carrier density distribution in a twin stripe laser subject tc che boundary conditions

(——) $J(0)=J(L)\simeq 0$, $N(-\infty)=N(\infty)=0$ and $dN/dx\big|_{x=\infty} = dN/dx\big|_{x=-\infty}=0$

(---) $dN/dx\big|_{x=0} = dN/dx\big|_{x=L}=0$, $N(L) = N(0) = 0$

6.5.1 Effect of stripe width and diffusion coefficient on the single stripe solution

Figures (6.5.1-1a) and (6.5.1-1b) show the distributions of J(x) and N(x) along the active layer junction for several electrode widths. The voltage applied to the stripe was constant at 1.60 V, which gives a value of peak current density and carrier density which is just below that required to give significant population inversion. A striking feature of figure (6.5.1-1a) is the dip in the current density distribution about the centre of devices with relatively wide electrodes (stripe width > 6 μm) which is absent from narrow stripe devices. These current density distributions confirm the results of Lengyel et al (4) who were the first to point out the dip in current density distributions, but using a completely different method of solution. However, it should be pointed out here that these dips in current density are not accompanied by a corresponding dip in the carrier density distribution shown in figure (6.5.1-1b) a fact which, it is believed, has not been presented before. Before discussing these results further it is useful to examine the effect of the ambipolar diffusion coefficient on the injected current density distribution and the carrier density distribution in the active layer. Figure (6.5.1-2a) shows the current density distribution at the active layer interface for VS = 1.60 V as a function of the diffusion coefficient D_{amb} in the range 20-60 cm^2/s for a 9 μm wide electrode. The immediate effect of increasing the diffusion coefficient is to increase the peak value of current density beneath the stripe electrode, by a small amount, and to increase the dip in the current density distribution. The effect of the diffusion coefficient on the injected current from the supply into the device is small. Figure (6.5.1-2b) shows that increasing D_{amb} causes a small reduction in carrier density beneath the electrode, as might be expected.

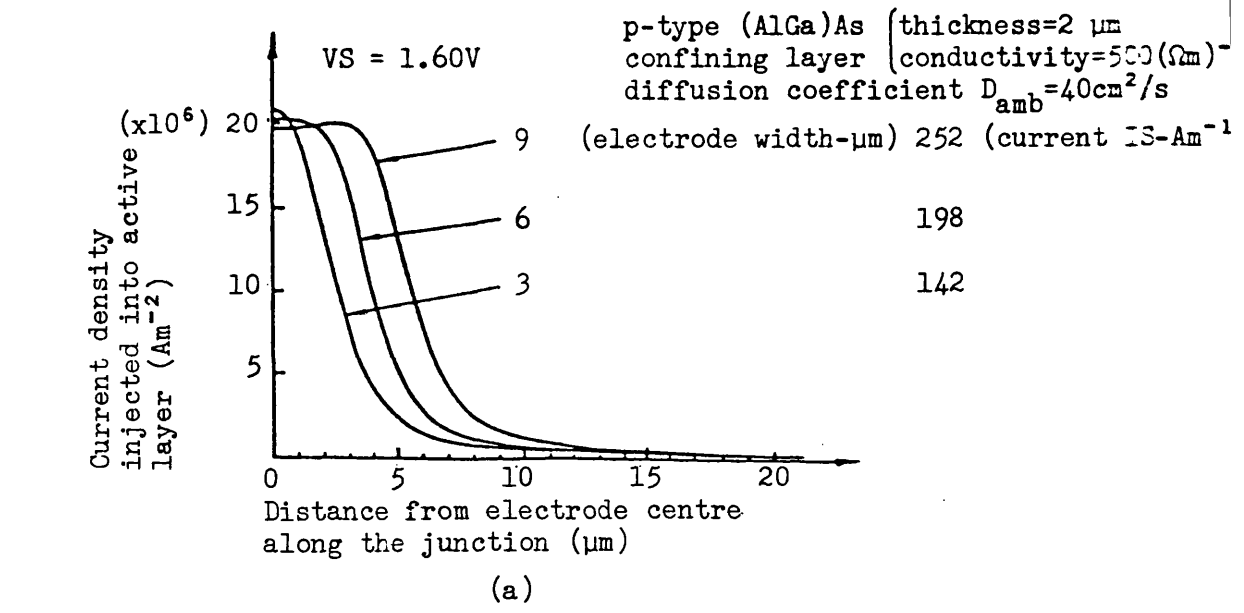

(a)

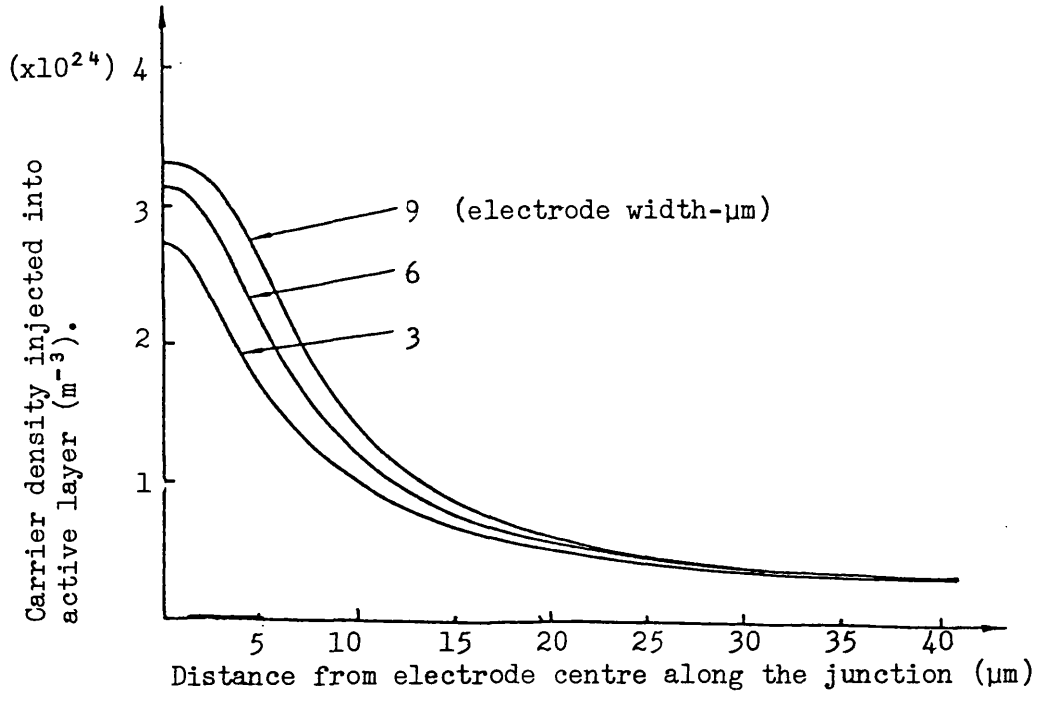

(b)

Figure 6.5.1-1 The effect of the electrode width on (a)the injected current density and (b) the carrier density distribution of a single stripe laser. Injection currents into the electrode are also labelled.

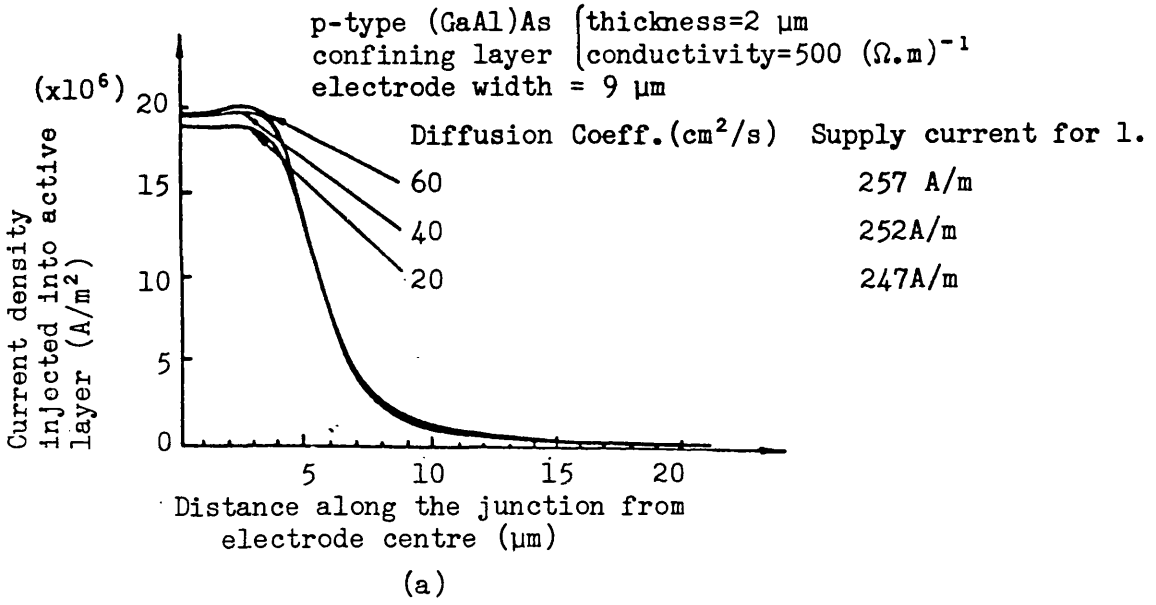

(a)

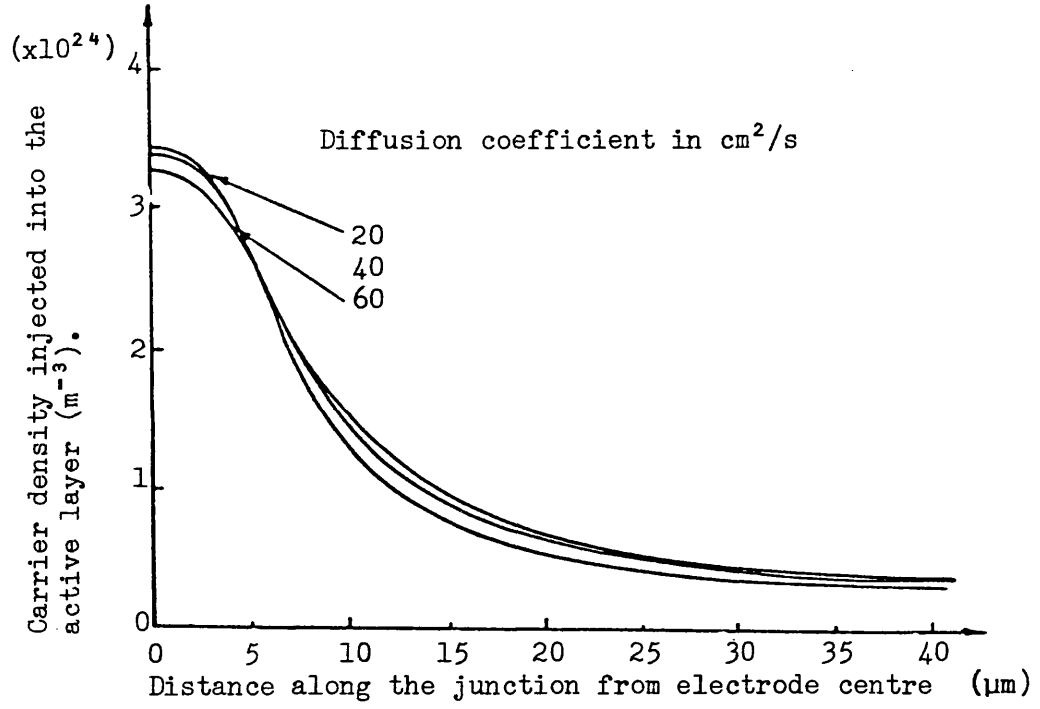

(a)

Figure 6.5.1-2 The effect of diffusion coefficient D_{amb} on (a) the injected current density and (b) the carrier density distributions of a single stripe laser with stripe width 9 μm

Lengyel et al (4) have reported that the mechanism of the dip in the current density distribution is due to the non-linear boundary at the confining layer/active layer interface. Almost certainly this has an effect, however the results of figures (6.5.1-2a) and (6.5.1-2b) show that diffusion plays an equally important role in determining the current density and carrier density distributions since the dip in the current density distribution almost disappears as $D_{amb} \rightarrow 0$. It is clear from figure (6.5.1-2b) that as the diffusion coefficient is reduced the curvature on the carrier density distribution near the electrode centre is reduced. As $D_{amb} \rightarrow 0$ the carrier density distribution and the current density distribution tend to the same general distribution, as would be expected. The carrier density distribution in the active layer cannot be considered uniform. Further, it is shown in figure (6.5.1-1b) that increasing the stripe width does NOT result in a proportionate broadening of the carrier density distribution. Conversely for the case of narrow electrodes (not shown) the distribution is also little altered. The thickness and resistivity of the p-type (GaAl)As layer play an important role in determining the exact carrier density and current density distributions but it will be seen that electrode widths of 5-6 μm represent an "optimum" from the point of achieving maximum confinement of the carrier density beneath the electrode with maximum injection efficiency. Figure (6.5.1-2b) shows that there is also a small degree of broadening of the carrier density distribution, as D_{amb} increases, analogous to increasing the stripe electrode width. This can cause a destabilising effect on the solution to the optical field (12 - 14). It is clear from these results that the importance of diffusion is likely to be greater for narrow electrode devices, where (dN/dx) is largest.

6.6 Twin Stripe Solution

One of the principal geometric factors of the twin stripe laser is the spacing between the stripe centres. This, in turn, places some constraint on the width of each electrode. It has been suggested (15) that a twin stripe structure displaying beam steering characteristics should consist of 2-3 μm wide electrodes separated by approximately 3-5 μm, and this has been used as a starting point in the presented model. In this section the effect of electrode width, spacing between electrodes and the applied electrode potential on the current density and carrier density distributions are considered. The general parameters used are given in table (6.5).

6.6.1 Variation of the stripe potentials

Figures (6.6.1-1a) and (6.6.1-1b) show the current density and carrier density distributions of a twin stripe laser as a function of the electrode potentials. In this section the potential applied to electrode 1, VS_1 was kept constant at 1.70 volts and potential VS_2 varied over a range from 1.50 volts to 1.70 volts. Figure (6.6.1-1a) shows the effect of the relatively low resistivity of the p-type (GaAl)As confining layer and lateral diffusion on the current density distribution at the junction. It is clear that the second stripe has little effect on the current density distribution until > 1.6 volts, which corresponds to the beginning of the region where beam steering has been observed experimentally (16). For the case of $VS_1 = VS_2$ the current density distribution is symmetrical. The effect of current spreading in the (GaAl)As confining layer and lateral diffusion of carriers in the active layer cause a significant level of current to be injected into the active region between the pumped stripe electrodes. However, figure (6.6.1-1b) shows that the carrier distribution is very unlike that of the current distribution. Despite a large dip in current density between the electrodes strong lateral diffusion of the carriers ensures that no such dip exists in the carrier

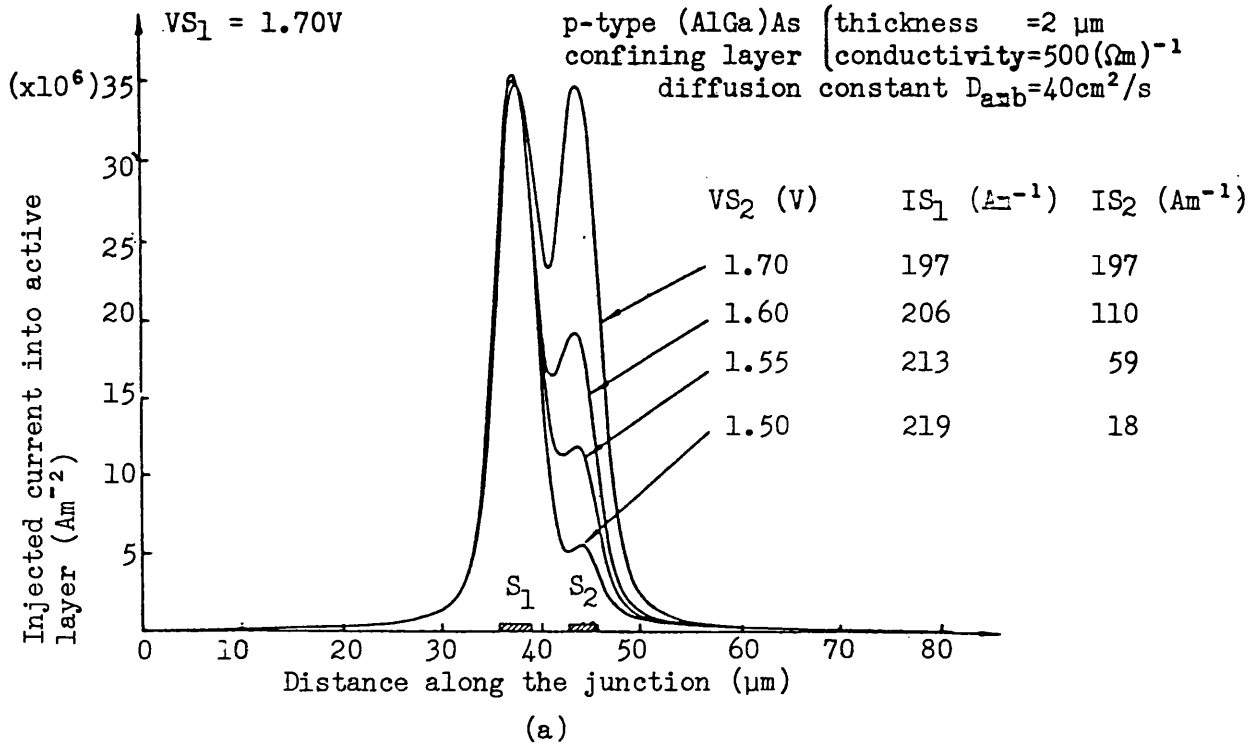

Figure 6.6.1-1 The effect of electrode voltage VS_2 on (a) the injected current density distribution and (b) the carrier density distribution of a twin stripe laser with electrode spacing 3 μm and electrode width 3 μm.

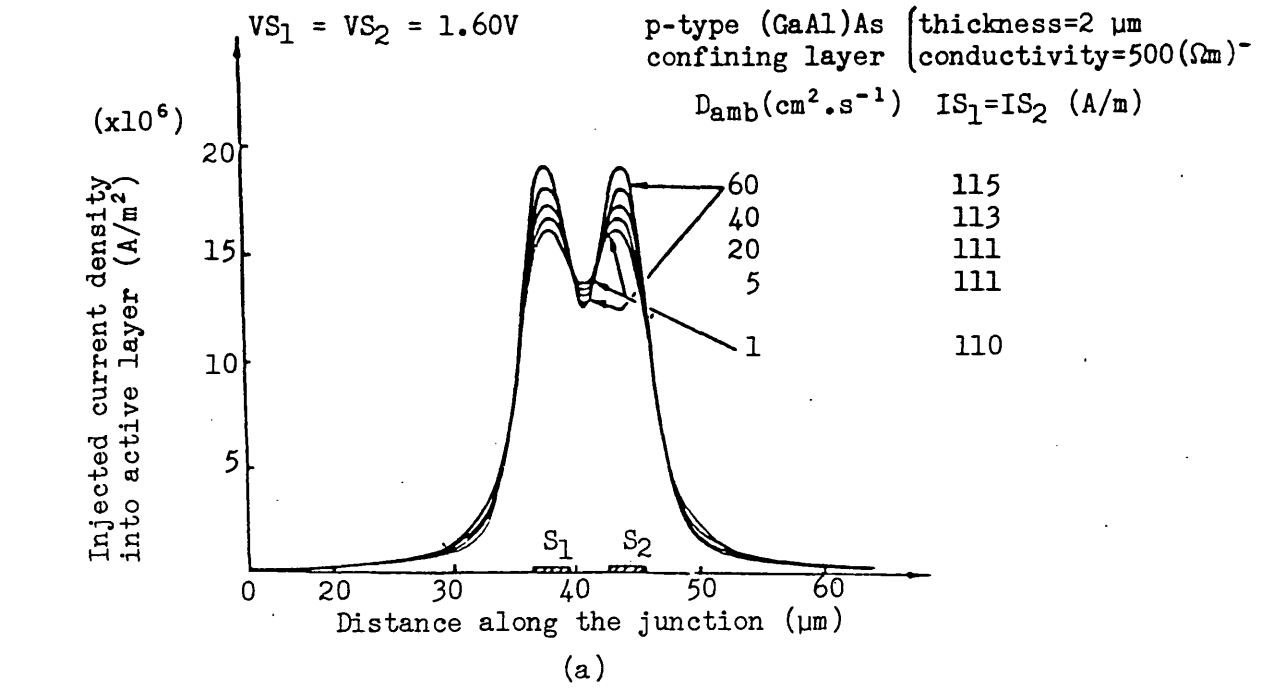

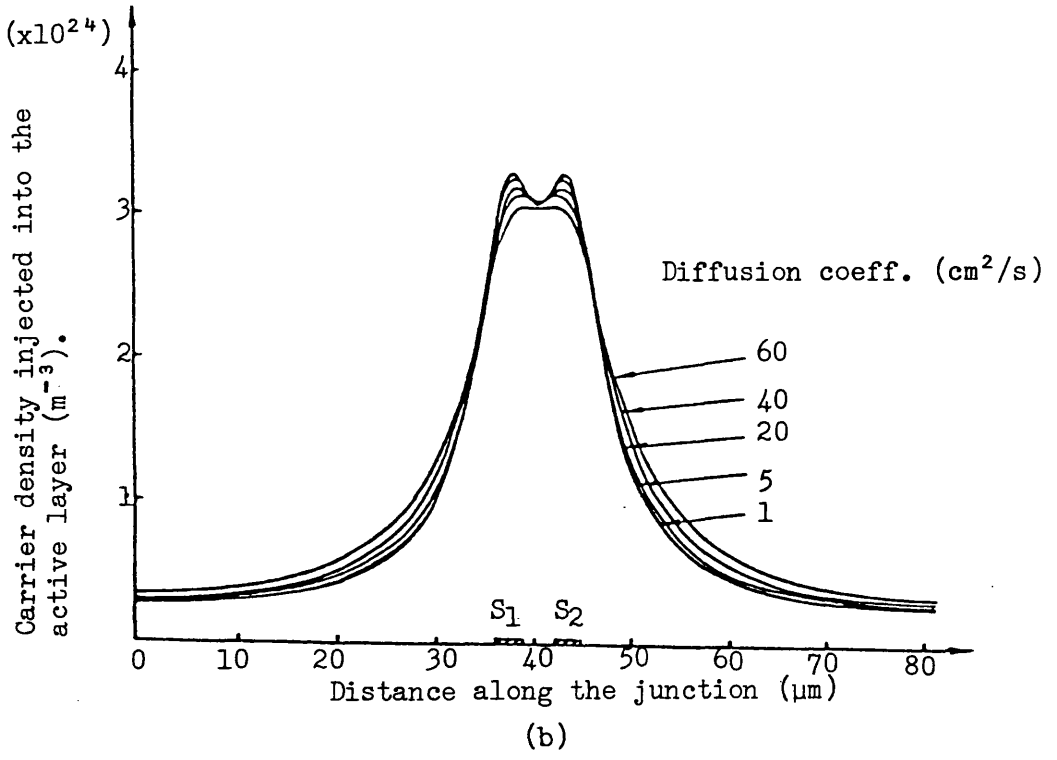

Figure 6.6.1-2 The effect of the diffusion coefficient D_{amb} on (a) the current density injected into the active layer and (b) the carrier density distribution in the active layer.

density for relatively narrow stripe spacings (here 3 μm).

In fact, the effect of diffusion on the carrier concentration is extremely important where the stripe spacing is less than the carrier diffusion length. This is illustrated in figures (6.6.1-2a) and (6.6.1-2b) for the case where $VS_1 = VS_2 = 1.60$ volts. Figure (6.6.1-2a) shows the effect of diffusion coefficient, D_{amb}, on the current density distribution and figure (6.6.1-2b) shows the corresponding carrier concentrations. It is clear from figure a that increasing the diffusion coefficient significantly deepens the dip in the current density profile between the stripes yet at the same time causes a dramatic reduction in the dip in carrier concentration (shown in figure 6.6.1-2b). This case might be viewed as an extreme case of the broad stripe laser (stripe width > 6μm) with the dip in current density enhanced due to the unpumped region between the stripes. The results of figure (6.6.1-2a) reinforce statements made in an earlier paper (9) regarding the accuracy of the terminal behaviour of the device model when diffusion is neglected. It is clear that diffusion has a large effect on the carrier concentration in the unpumped region between the electrodes and this has a strong influence on the optical behaviour of the device. However, the peak current densities in the pumped regions are not significantly altered and this results in a change in the total current injected into each stripe of less than 5% for a change in D_{amb} from 1 to 60 cm^2/s.

6.6.2 Variation of electrode spacing

Figures (6.6.2-1a) and (6.6.2-1b) show that the effect of electrode spacing on the current density and carrier density distributions respectively, for the condition $VS_1 = VS_2 = 1.60$ volts. For very close spacings, current spreading and lateral carrier diffusion conspire to eliminate the dip in carrier density, as figure (6.6.2-1b) shows, and

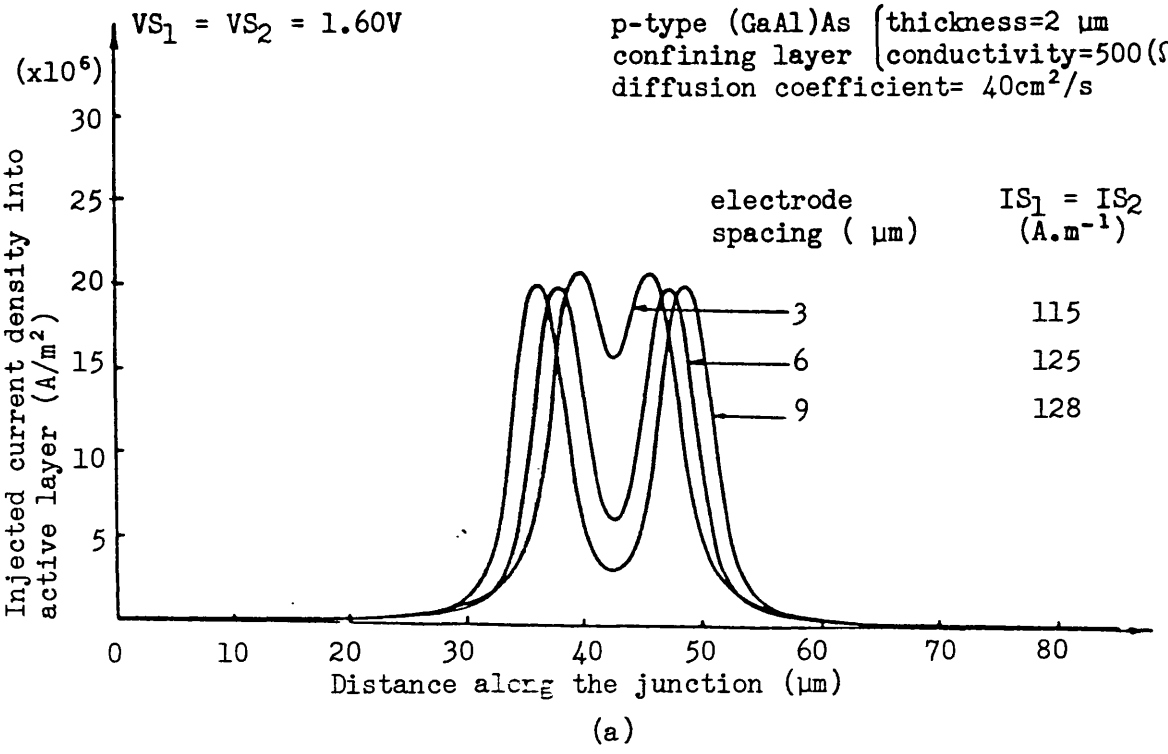

(a)

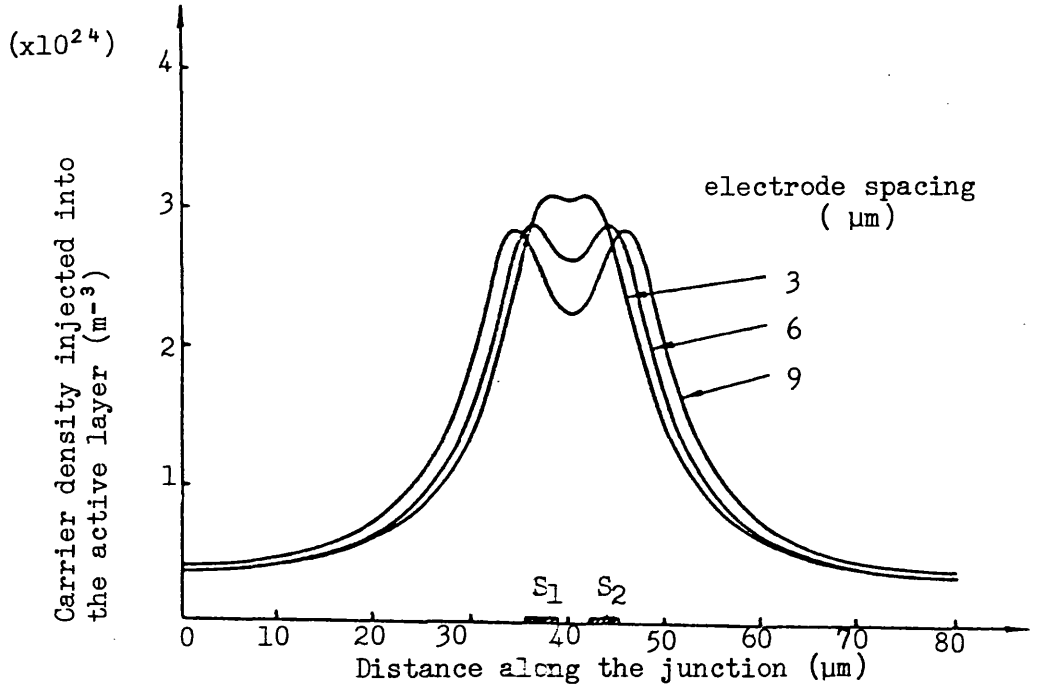

(b)

Figure 6.6.2-1 The effect of electrode spacing on (a) the current density injected into active layer and (b) the carrier distribution in the active layer. The electrode widths are each 3 μm.

and the dip in the carrier density between the stripes is small. Obviously the relative stripe potentials will have some effect on the exact position of the carrier maximum. As pointed out in (9) the penalty of using very narrow electrode spacings to maximize stripe coupling is the very low value of interstripe resistance. This results in an increase in the threshold current of the individual laser devices. One method of attempting to increase the interstripe resistance is to reduce the current spreading component either by reducing the thickness of the p-type (GaAl)As layer or by increasing the resistivity of the p-type (GaAl)As layer, however this enhances hole burning effects above threshold (17). The important criterion is to maximize the interstripe carrier coupling via diffusion, yet at the same time minimize injection current leakage. In the following sections the effect of varying these parameters according to this criterion will be considered. For the case of closely coupled, e.g. (3 μm - 4 μm separation) symmetrically pumped twin stripe laser, the slight dip in carrier density in the centre, between the two stripes results in a local maximum in the refractive index and a local minimum in the gain; a situation not dissimilar to that of broad area device. Varying the stripe potential slightly would change the distribution, and hence the optical field. With reference to an earlier statement, one might expect the region of stability on the current/light characteristics to be small.

For narrow stripe spacings (< 3 μm), symmetrically pumped, the dip in carrier density disappears and the result is a carrier density profile similar to a single stripe laser.

As the interstripe spacing is increased it is clear from the carrier density distribution of figure (6.6.2-1b) that the two electrodes become increasingly decoupled. For the case of a 9 μm spacing (between electrode

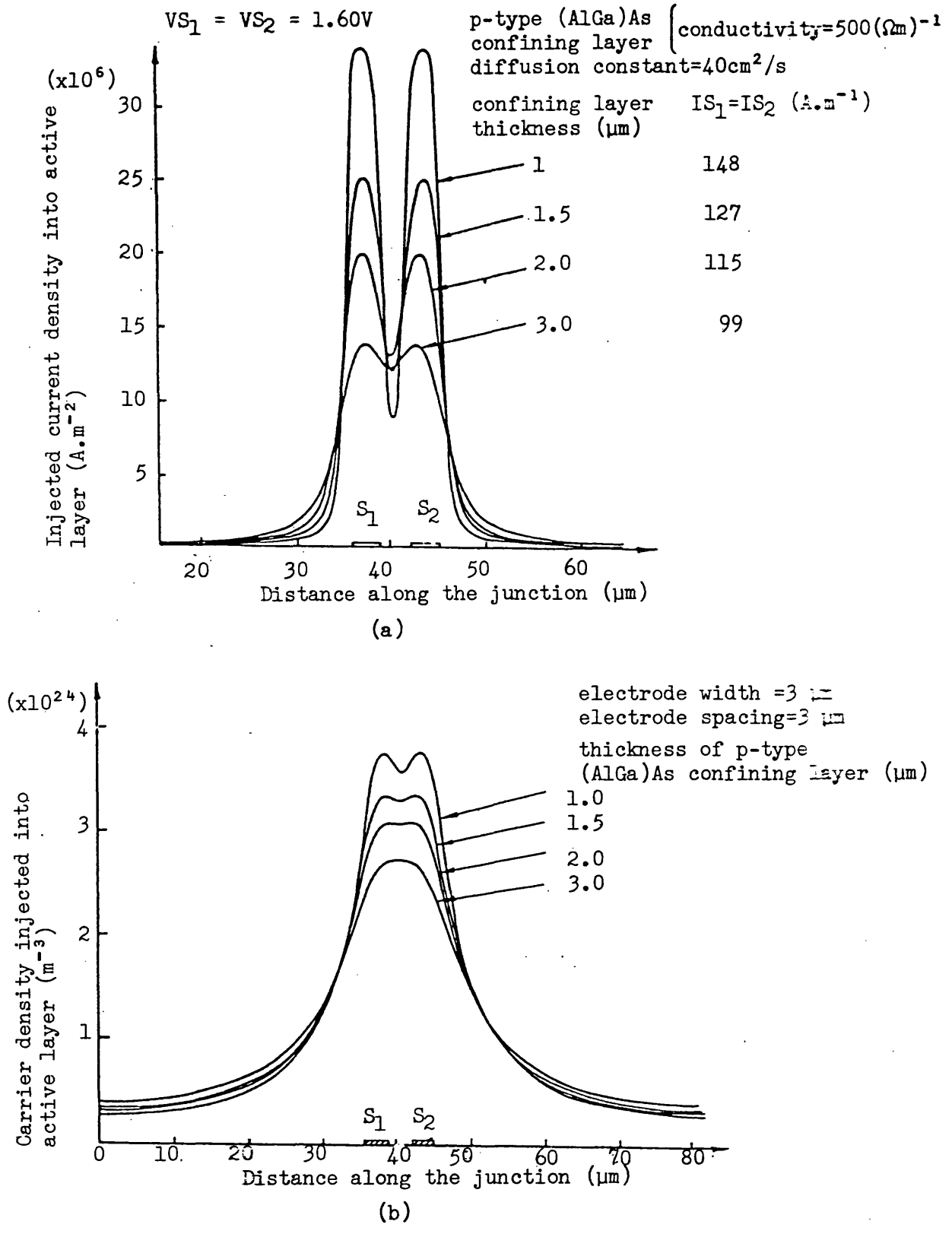

Figure 6.6.3-1 The effect of the thickness of the p-type (AlGa)As confining layer on (a) the current density distribution and (b) the carrier density distribution.

edges) the carrier density between stripes is only 15% of the peak value. This should be compared with 76% of the peak value when the electrodes have a 3 μm spacing between them. This result shows clearly the large fall in gain to be expected in the region between the electrodes as the spacing is increased. Although the refractive index is highest between the electrodes for the wide spaced structure, the low value of gain in this region would make self focusing of the beam in this central region difficult.

6.6.3 Variation of the thickness of the p-type (GaAl)As confining layer

Figures (6.6.3-1a) and (6.6.3-1b) show the effect of the thickness of the p-type (GaAl)As confining layer on the injected current density distribution and carrier density distribution respectively. Because the p-type confining layer effectively controls the terminal resistance of the device when the heterojunction is conducting, modifying the thickness is expected to have a significant effect on the current injected into each electrode. This is certainly seen to be true. However, the graph of carrier density in the active region shows how increased spreading resistance in the thicker confining layers has the effect of removing the dip in carrier density, which would be expected to affect the stability of the laser output. This result is analogous to that obtained for hole burning in a single stripe laser examined by Joyce (17). It is also worth noting that although the injected current density has over 200% fluctuation because of a modification of the confining layer thickness by 300%, the variation in peak carrier density is only 27%.

6.6.4 Variation of the conductivity of the p-type (GaAl)As confining layer

This is effectively a dual of the effect of the confining layer thickness. Again it is clear from figures (6.6.4-1a) and (6.6.4-1b) that a low confining layer conductivity causes coupling of the carriers between

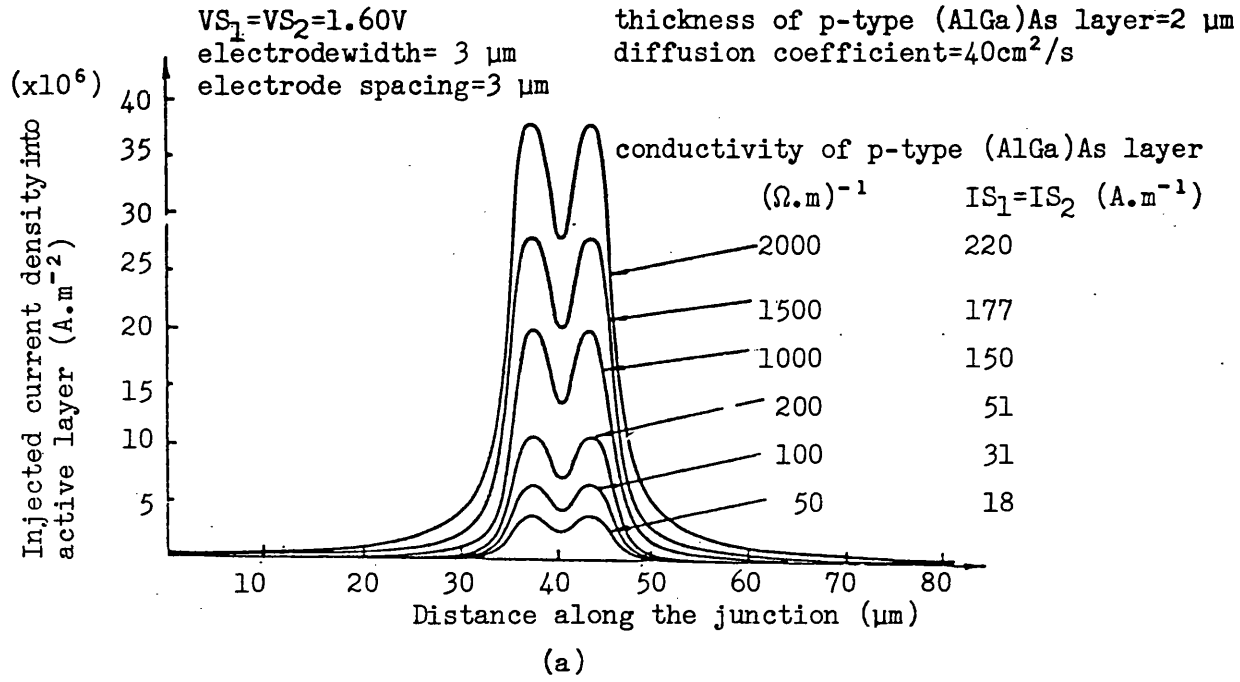

Figure 6.6.4-1 The effect of the conductivity of the p-type (AlGa)As confining layer on (a) the current density distribution and (b) the carrier density distribution in the active layer.

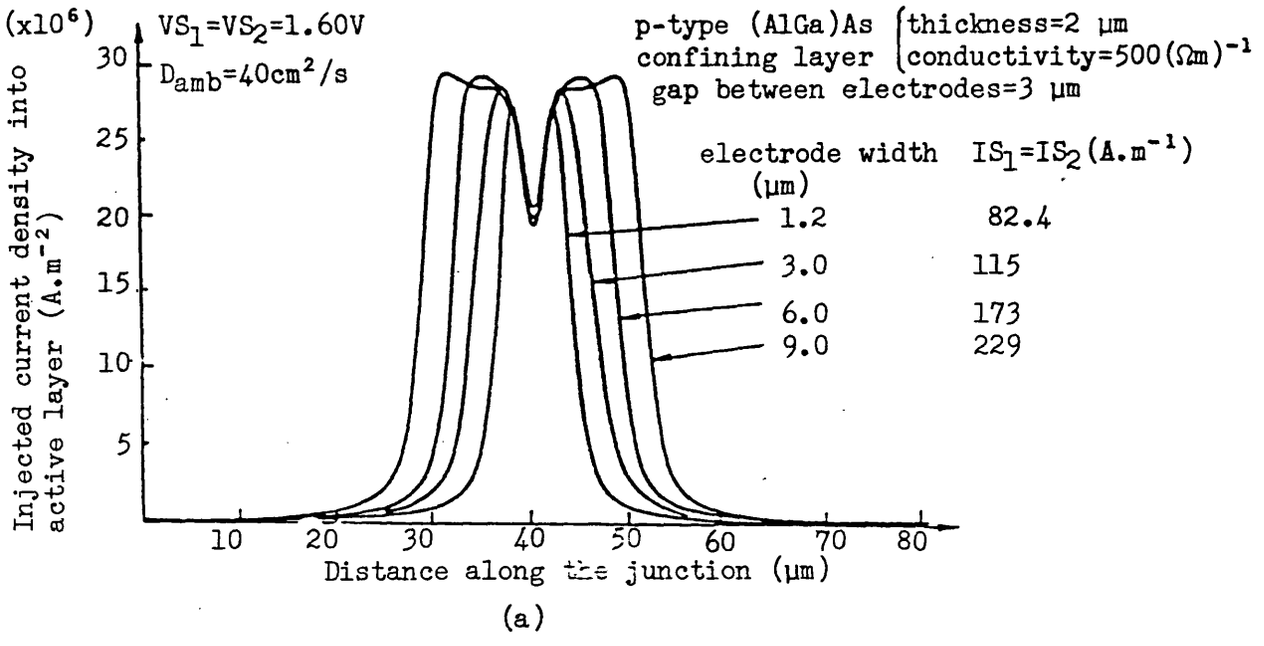

Figure 6.6.5-1 The effect of electrode width when the spacing between them is kept fixed on (a) the current density distribution and (b) the carrier density distribution.

the electrodes via an ohmic conduction process rather than by diffusion in the active layer. Clearly a low confining layer conductivity is an advantage, however this has the disadvantage that it increases the effect of hole burning above threshold (17).

6.6.5 Variation of the electrode width

The effect of electrode width on the injected carrier density distribution is shown in figure (6.6.5-1b). It is clear that increasing electrode width, for the case of a fixed 3 μm spacing causes a weakening of the coupling between the stripes. The peak carrier density is also increased by a relatively small amount, corresponding to a lower threshold current density for each stripe when calculated on the basis of an equivalent electrode area. It is clear from this graph perhaps more than any other, that because of the effect of diffusion and current spreading it is the distance between electrode centres rather than the gap between the electrode, which is the controlling factor of a twin stripe laser. Further, it is clearly not correct to simply assume a 5 region model for the device in which uniform current injection occurs beneath each electrode as is sometimes the case. At best an equivalent width narrower than the original may be used. It is interesting to note that a dip in the current density distribution shown in figure (6.6.5-1a) occurs beneath each electrode, as well as in the region between the stripes, and this can give rise to a complicated profile for the refractive index.

6.7 Conclusions

In this chapter a numerical solution of the non-linear problem of lateral carrier diffusion in the active layer consistent with current spreading in the (GaAl)As layer was presented. By appropriate choice of under and over-relaxation factors a stable solution was always found. However, the choice of the boundary condition $(dN/dx) = 0$ for the end nodes

significantly simplified the problem without a large sacrifice in accuracy or computational speed, unlike the analytic boundary condition which required careful tailoring of the under-relaxation parameter for stability of the numerical solution.

The solution to the single stripe laser problem was in close agreement with solutions from other authors using different techniques, and illustrated the importance of carrier diffusion in wide stripe lasers. It was further shown that dips in the current density are not matched by dips in the carrier density distribution. Diffusion in the active layer, as well as the non-linear boundary are seen as the main reasons for the dip in the injected current density distribution.

The main thrust of the chapter, however, was to show the effect of current spreading and carrier diffusion in the twin stripe laser. In particular it was found that the p-type (GaAl)As layer coupled the carrier densities beneath the stripes, and that a low confining layer resistivity or a thick confining layer produced much the same effect on the carrier density distribution. Three classes of twin stripe lasers are identified.

i) Very closely coupled lasers in which no local minimum is observed in the carrier density distribution

ii) Closely coupled lasers (gap $\simeq$ 3-4 μm) in which a local minimum is observed between the stripes

iii) Weakly coupled, where a large local minimum is observed between the electrodes, which effectively decouples the electrodes.

Stripe potential also has an effect on the carrier density distribution.

References

1. D.P. Wilt and A. Yariv: "A self-consistent static model of the double heterostructure laser", IEEE J. Quantum Electron., Vol. QE-17, pp.1941-1949, 1981.

2. N. Chinone: "Non-linearity in power output-current characteristics of stripe geometry injection lasers", J. Appl. Phys., Vol.48, pp.3237-3243, 1977.

3. T.L. Paoli: "Non-linearity in the emission characteristics of stripe geometry (AlGa)As double heterostructure junction lasers", IEEE J. Quantum Electron., Vol. QE-12, pp.770-776, 1976.

4. G. Lengyel, P. Meissner, E. Patzak and K.H. Zschauer: "An analytical solution of the lateral current spreading and diffusion problem in a narrow oxide stripe (GaAl)As/GaAs DH laser", IEEE J. Quantum Electron., Vol. QE-18, pp.618-625, 1982.

5. W.T. Tsang: "The effects of lateral current spreading, carrier out diffusion and optical mode losses on the threshold current density of GaAs/$Al_xGa_{1-x}As$ stripe geometry DH lasers", J. Appl. Phys., Vol.49, pp.1031-1044, 1978.

6. B.S. Poh and T.E. Rozzi: "Intrinsic instabilities in narrow stripe geometry lasers caused by lateral current spreading", IEEE J. Quantum Electron., Vol. QE-17, pp.723-731, 1981.

7. W.B. Joyce: "Carrier transport in double heterostructure active layer", J. Appl. Phys., Vol.53, pp.7235-7239, 1982.

8. W.B. Joyce: "Current-crowded carrier confinement in double heterojunction lasers", J. Appl. Phys., Vol.51, pp.2394-2401, 1980.

9. T. Kumar, R.F. Ormondroyd and T.E. Rozzi: "Interstripe coupling and current spreading in a sub-threshold double heterostructure twin stripe laser", IEEE J. Quantum Electron., Vol. QE-20, pp.364-373, 1984.

10. W.B. Joyce: "Analytic approximations for the Fermi energy of an ideal Fermi gas", Appl. Phys. Lett., Vol.31(5), pp.354-356, 1977.

11. P.M. Asbeck, D.A. Camack, J.J. Daniele and V. Klebanoff: "Lateral mode behaviour in narrow stripe lasers", IEEE J. Quantum Electron., Vol. QE-15, pp.727-733, 1979.

12. G.H.B. Thompson, D.F. Lovelace and S.E.H. Turley: "Kinks in the light/current characteristics and near field shifts in (GaAl)As heterostructure stripe lasers and their explanation by the effect self-focusing on a built-in optical waveguide", IEE J. of Solid State and Electron. Devices, Vol.2(1), pp.12-30, 1978.

13. R. Lang: "Lateral transverse mode instability and a stabilisation interstripe geometry injection lasers", IEEE J. Quantum Electron., Vol. QE-15, pp.718-736, 1979.

14. K.A. Shore and T.E. Rozzi: "Stability analysis of transverse modes in stripe-geometry injection lasers", IEE Proc. Part I, vol.128, pp.154-159, 1981.

15. D.R. Scifres, W. Streifer and R.D. Burnham: "Beam scanning with twin stripe injection lasers", Appl. Phys. Lett., Vol.38(8), pp.702-704, 1978.

16. R.F. Ormondroyd, T.E. Rozzi, J. Singh and P.A. Morton: "Negative dL/dI and beam steering in GaAlAs DH twin stripe lasers", submitted to IEE Proc. Part J

17. W.B. Joyce: "Role of conductivity of the continuing layer in DH laser spatial hole burning effects", IEEE J. Quantum Electron., Vol. QE-18, pp.2005-2009, 1982.

CHAPTER VII

SELF-CONSISTENT SOLUTION OF CURRENT SPREADING, CARRIER DIFFUSION AND LATERAL FIELD DISTRIBUTION IN ABOVE THRESHOLD TWIN STRIPE LASERS

7.1 Introduction

In the last chapter the carrier distribution in the active layer and the current distribution in the active layer and passive layer of a twin stripe laser were found using a consistent procedure for currents below threshold. In order to study the operation of a device above threshold it is essential to study the optical field and its influence on the carrier distribution in the active layer, which in turn affects the current distribution in the passive layer of the device shown in figure (6.2-1). This inter-coupling of the various effects therefore demands a self-consistent solution of the Laplace's equation in the passive layer with the diffusion equation in the active layer and the wave equation. The technique used to achieve this will be described in this chapter.

It is believed that a solution of this kind has not been developed for a twin stripe laser. The only current model of a twin stripe laser, reported by Shore and Rozzi (11), does not solve for current spreading consistently with the diffusion of carriers in the presence of the interacting optical field. It was learnt in the chapter on optical waveguides that there is a confinement of both carriers as well as optical field in the direction perpendicular to junction. This occurs because at the heterojunctions potential barriers exist which prevent flow of carriers from the active region to the passive region of large energy gaps. Moreover, the heterojunctions represent the interfaces of the materials of different dielectric constants forming a slab waveguide which has been discussed at length in chapter (III). In the lateral direction, however, there is no such well defined guiding structure and weak waveguiding is provided by the lateral variation of the complex refractive index due to the spatial variation of the carrier density which influences the dielectric constant of the active layer. Maximum

gain in the laser corresponds to the region of highest pumping, i.e. beneath the electrodes, but the lateral variation of the complex dielectric constant dictates whether guiding is predominantly gain-guiding or index-guiding. Thus, by controlling the injected currents into the two stripes the carrier density distribution and hence the lateral waveguiding may be affected.

For the single stripe laser it has been seen that the lateral waveguiding is a very important mechanism deciding the stability of the device (1 - 10). Single mode operation and a kink free light/current characteristic upto relatively a large light output without affecting the stability demands a good waveguidance in the lateral direction. On the other hand a large light output is quite damaging for the reflecting mirrors which can be avoided if the lateral modes are allowed to spread out rather than very narrowly confined. Thus a compromise must be achieved between the lateral mode guidance and the light output. It has been shown in the last chapter that in a small single stripe laser the gradient of gain near the edge of the stripe is very steep and therefore it produces strong gain guidance. As the intensity maximum exists underneath the stripe, there appears a dip in the carrier concentration under the stripe. This effect is due to strong stimulated recombination caused by optical interaction with the carriers and is often called hole burning. The local exhaustion of carriers thus results in a local increase in the refractive index near the centre of the electrode and therefore causes self focusing of the mode, which reinforces the gain guiding action.

Prior to the work reported in this thesis there were only two full self-consistent models (9, 10) of a single stripe laser which take into consideration current spreading in the passive layer and the diffusion of carriers interacting with the optical field in the active layer.

It was pointed out by Wilt and Yariv (10) that the representation of p-n junction by an ordinary diode equation is incorrect. The use of this relationship does not show the saturation of the carrier populations associated with the lasing threshold (10). Since the active layer is very narrow and is sandwiched between the passive layers of large energy gaps, it is reasonable to assume that the carrier density is constant across the active layer. This assumption leads to the argument that the quasi-Fermi levels are continuous across the active layer. It has been discussed in the last chapter how this assumption can be incorporated in the model of the laser. The solution technique of the previous chapter forms a building block of the solution technique which is discussed here.

7.2 Theoretical Analysis

In the fully self-consistent model of the laser it is necessary to include the interaction of the optical field with the carriers in the active layer via the stimulated recombination coefficient in the continuity equation for the carriers. The optical field can be found by solving the one dimesional scalar wave equation along the active layer using the effective dielectric constant method which takes into account the field confinement in the transverse direction (perpendicular to the heterojunctions). However, in the lateral direction the one-dimensional wave equation must be solved simultaneously with Laplace's equation, defining current spreading in the passive layers, and the continuity equation describing the density of carriers in the active layer.

The DH structure of lasers allows several approximations to be made:

i) The active layer is generally very thin (0.2-0.3 μm) and very

much less than the diffusion length of the carriers. It is reasonable to assume that the transverse variation of the carriers is uniform across the active layer. This assumption leads to the argument that the quasi-Fermi levels are continuous across the active layer (10).

ii) Under the strong pumping requirements of the semiconductor laser, drift conduction in the active layer, which is lightly doped, is negligible as compared with diffusion. (However, Joyce (12) has shown that the drift term may be lumped together with the diffusion term if greater accuracy is required).

iii) The highly doped n-type substrate and the n-type confining layer do not contribute significantly to current spreading or excess resistance due to their effective broad contact areas.

iv) The highly doped p^+ GaAs capping layer does not contribute to current spreading because of electrode isolation techniques such as:

a) proton isolation, b) mesa etching or c) stripe contact isolation of p^+ doped GaAs electrodes in semi-insulating GaAs (13).

7.2.1 The current spreading and carrier density problem

This aspect of the problem has been considered in detail in the previous chapters and references (13, 14). The 2-dimesional potential distribution in the p-type (AlGa)As confining layer may be found by a solution to the 2-dimensional Laplace's equation:

$$\nabla^2 V = 0 \qquad (7.2.1\text{-}1)$$

subject to the boundary conditions shown in figure (6.2-1). From this potential distribution thus obtained the current density at a point (x,y) within the passive layer may be calculated as:

$$\underline{J}(x,y) = -\sigma\nabla V(x,y) \qquad (7.2.1\text{-}2)$$

where σ is the conductivity of the p-type (AlGa)As passive layer and $V(x,y)$ is the potential at (x,y) calculated from equation (7.2.1-1). The current density injected into the active layer may be found from equation (7.2.1-2) by setting $y = d'$ as:

$$J(x)|_{y=d'} = -\sigma\{\nabla V(x)\}|_{y=d'} \qquad (7.2.1\text{-}3)$$

The current injected into the (AlGa)As region from the stripe electrodes may be obtained from:

$$I_{stripe} = \int_{\substack{\text{stripe}\\\text{width}}} J(x)|_{y=0}\, dx \qquad (7.2.1\text{-}4)$$

The current injected into the active layer acts as the source of injected carriers and it may be equated with the carriers in the active layer, $N(x)$, via 1-dimensional continuity equation given by:

$$D_{amb}\{d^2N(x)/dx^2\} - BN^2(x) - (c/n_o)g(x)S_o\Psi(x) = -\{J(x)|_{y=d'}/et\} \qquad (7.2.1\text{-}5)$$

where D_{amb} is the ambipolar diffusion coefficient which is equivalent to the effective diffusion coefficient for the considered structure as shown by Joyce (12). BN^2 is the bimolecular recombination term, c is the velocity of light in vacuum, n_o is the refractive index of the active layer, $g(x)$ is the local optical gain in the lateral direction of the device, S_o represents the number of stimulated photons per unit cavity volume, $\Psi(x)$ is the normalised optical intensity distribution and t is the thickness of active layer.

The carrier density along the active layer, $N(x)$, is also related to the potential difference appearing across the p-n junction by the

quasi-Fermi level separation ($F_c - F_v$) such that the potential difference at any position, x, along the active layer is given by:

$$V(x) = \frac{k_B T}{e}\left[\psi_e(x) + \psi_h(x) + \frac{E_g}{k_B T}\right] \qquad (7.2.1\text{-}6)$$

where E_g is the energy gap of the GaAs active layer and

$$\psi_e = \left[\frac{F_c - E_c}{k_B T}\right] = \ell n\left[\frac{N}{N_c}\right] + K_1\left[\frac{N}{N_c}\right] + K_2\left[\frac{N}{N_c}\right]^2 + K_3\left[\frac{N}{N_c}\right]^3 + \ldots. \qquad (7.2.1\text{-}7)$$

and

$$\psi_h = \left[\frac{E_v - F_v}{k_B T}\right] = \ell n\left[\frac{N}{N_v}\right] + K_1\left[\frac{N}{N_v}\right] + K_2\left[\frac{N}{N_v}\right]^2 + K_3\left[\frac{N}{N_v}\right]^3 + \ldots. \qquad (7.2.1\text{-}8)$$

assuming the quasi-neutrality of the active layer as defined in the previous chapter after Joyce (15). N_c and N_v denote the density of states of the conduction and valence bands respectively.

Simultaneous solution of these equations has been detailed in chapter (VI) for the condition where $S_o = 0$ and $\Psi(x) = 0$ to yield the current density distribution $J(x)|_{y=d}$, and the carrier density distribution, N(x). The purpose of this chapter is to consider the case where $\Psi(x) \neq 0$. The local optical gain g(x), is related to the carrier concentration by:

$$g(x) = a'N(x) - b' \qquad (7.2.1\text{-}9)$$

where a′ and b′ are constants. The continuity equation in the active layer (7.2.1-5) thus becomes:

$$D_{amb}\frac{d^2N(x)}{dx^2} - BN^2(x) - \frac{c}{n_o}S_o\Psi(x)a'N(x) + \frac{c}{n_o}S_o\Psi(x)b' = -\frac{J(x)|_{y=d}}{et}$$

(7.2.1-10)

7.2.2 The lateral optical field problem

In order to calculate the normalised optical intensity $\Psi(x)$ it is necessary to solve the one dimensional scalar wave equation given below:

$$d^2\psi/dx^2 + \{k^2\tilde{\varepsilon}_{eff}(x) - \tilde{\beta}^2\}\psi = 0 \qquad (7.2.2\text{-}1)$$

where k is the free space wave vector, $\tilde{\varepsilon}_{eff}$ is the complex effective dielectric constant of the active layer and $\tilde{\beta}$ is the complex propagation constant. $\tilde{\varepsilon}_{eff}(x)$ may be expressed by the following expression as described in chapter (III):

$$\tilde{\varepsilon}_{eff}(x) = n_o^2 + (-R + j)\frac{n_o g(x)}{k} \qquad (7.2.2\text{-}2)$$

where R denotes the ratio of the change in the real and imaginary parts of the complex dielectric constant due to the carrier concentration. Thus the term:

$$\Delta\varepsilon = (-R + j)\frac{n_o g(x)}{k} \qquad (7.2.2\text{-}3)$$

gives the variation in the complex dielectric constant due to the carrier concentration. R is often taken to be constant, with a value ranging from 4 to 6.

Thus, once an estimate of N(x) is known (assuming $\Psi(x)=0$) it is possible to estimate the local gain profile, g(x) and hence the effective complex dielectric constant, $\tilde{\varepsilon}_{eff}(x)$, using equation (7.2.2-2). The wave equation may then be solved to calculate the field profile and the propagation constant. The normalised optical intensity may be obtained from the field profile $\psi(x)$ using:

$$\Psi(x) = \frac{W|\psi(x)|^2}{\int_{-\infty}^{\infty}|\psi(x)|^2 dx} \qquad (7.2.2\text{-}4)$$

where W is a scaling factor.

Clearly, for an excited mode in the laser cavity to be sustained it is necessary for the modal gain to compensate for the various cavity losses. The modal gain is related to the imaginary part of $\tilde{\beta}$, and this leads to the condition:

$$2\mathrm{Im}(\tilde{\beta}) = \alpha_{mode} + \frac{1}{L_c} \ell n\left(\frac{1}{R_1 R_2}\right) \qquad (7.2.2\text{-}5)$$

where α_{mode} is the internal mode loss, L_c is the cavity length and R_1 and R_2 are the reflectances of the cavity mirrors for the mode under consideration. It is assumed that spontaneous emissions into the mode are negligible. The modal gain is related to the local gain profile and the field intensity by the following approximate expression:

$$2\mathrm{Im}(\tilde{\beta}) \simeq \frac{\int_{-\infty}^{\infty} g(x)|\psi(x)|^2 \, dx}{\int_{-\infty}^{\infty} |\psi(x)|^2 \, dx} \qquad (7.2.2\text{-}6)$$

and so there are two means of calculating modal gain offered by solutions to equation (7.2.2-1) and (7.2.2-6). Equations (7.2.2.1) to (7.2.2-6) summarise the relavent equations for the solution of the optical field once N(x) is known. However, as $\Psi(x)$ is necessary to calculate N(x), the carrier density profile above threshold, then the current spreading and the optical field profile must be solved simultaneously. The solution techniques adopted are outlined in the next section.

7.3 Solution Technique

A numerical solution technique has been used for the simultaneous solution of the above differential equations using the finite difference method. This technique has been detailed for the special case where $\Psi(x) = 0$ in previous chapter (VI) and will not be reiterated. For the case where

$\Psi(x) \neq 0$ the continuity equation (7.2.1-10) for the active layer becomes:

$$D_{amb}\left[\frac{N(\ell-1)}{N_i} - \frac{2N(\ell)}{N_i} + \frac{N(\ell+1)}{N_i}\right] - Bh_x^2 N_i \left[\frac{N(\ell)}{N_i}\right]^2 - \frac{c}{n_o} h_x^2 S_o a' \frac{N(\ell)}{N_i} \Psi(\ell)$$

$$+ \frac{c}{n_o} h_x^2 \frac{S_o}{N_i} \Psi(\ell) b' = - \frac{J(\ell) h_x^2}{etN_i} \qquad (7.3\text{-}1)$$

where N_i is the intrinsic carrier density in the active layer, and is used for normalisation, h_x is the horizontal step length and ℓ represents the node number along the junction. A similar equation may be written for each node along the junction. At a distance of 5 - 6 diffusion lengths from the outer edge of each electrode the boundary condition $(dN/dx) = 0$ is imposed (14). A set of non-linear equations is thus obtained which are solved by the Newton-Raphson successive-over-relaxation technique.

The solution procedure can be described in the following steps.

Step 1

Potentials VS_1 and VS_2 are applied to the stripe electrodes S_1 and S_2 as known boundary conditions. Initially it is assumed that there is no field interaction i.e. $\Psi(x) = 0$ which means no stimulated recombination term is included in equation (7.3-1). This equation is then no different to the one solved simultaneously with the Laplace's equation in the previous chapter. It has been shown in chapter (VI) how the consistent solution of the carrier density distribution along the junction in the active layer and the current distribution in passive layer can be obtained. Solutions to these equations provide an estimate of the carrier density, $N(x)$, in the active layer consistent with the current density profile, $J(x)$, injected into the active layer. Estimates of the currents injected into each electrode can also be calculated at this stage.

Step 2

In order to evaluate the lateral field profile $\psi(x)$ and the propagation constant, $\tilde{\beta}$, $\tilde{\varepsilon}_{eff}(x)$ must be calculated using the estimate of carrier density $N(x)$ found in step 1. This is achieved by calculating the local gain, $g(x)$ using equation (7.2.1-9), which is substituted into equation (7.2.2-3). Although many techniques are available, the wave equation (7.2.2-1) was also solved using a finite difference technique, however, in the first instance the mesh used is very coarse (typically 1 μm). The finite difference form of the 1-dimensional wave equation may be written as:

$$\frac{\psi(\ell-1) - 2\psi(\ell) + \psi(\ell+1)}{h_x'^2} + k^2\tilde{\varepsilon}_{eff}(\ell)\psi(\ell) = \tilde{\beta}^2\psi(\ell) \qquad (7.3\text{-}2)$$

where h_x' is the coarse mesh step length. An equation of this form may be written for each node. For the optical solution it is expected that the field will die away at a distance of one or two times the diffusion length from the electrode edges where the boundary condition $d\psi/dx = 0$ is applicable, however, symmetry of $\psi(x)$ is <u>not</u> assumed. The system of equations, thus formed, results in an algebric eigenvalue problem. This problem can be solved by an L-R decomposition technique (16 - 18) for all values of $\tilde{\beta}^2$ satisfying equation (7.3-2). The value of $\tilde{\beta}^2$ with the largest positive imaginary value of $\tilde{\beta}$ corresponds to the dominant lateral mode. At this stage the value of $\tilde{\beta}^2$ and the corresponding field distribution ψ of the dominant lateral mode can be obtained in a refined form using a much finer mesh, by applying an efficient shooting method, described in Appendix B.

Step 3

Once $\tilde{\beta}^2$ has been calculated the modal gain can be found. This is defined as being twice the value of the imaginary part of $\tilde{\beta}$. If the modal gain

of the dominant lateral mode is less than the set cavity loss given by equation (7.2.2-5) the device is operating below threshold and the calculations are repeated with increased applied potentials on the electrodes from step 1. The value of cavity loss is clearly an important parameter which in practical terms depend on carrier absorption, facet reflectance and cavity length. In this work a typical value of cavity loss of 60 cm^{-1} has been used. If the modal gain is greater than the cavity loss the calculations are continued further using the accurate, but as yet, first estimate of the field profile $\psi(x)$ calculated in step 2.

Step 4

The normalised optical intensity $\Psi(x)$ is calculated from $\psi(x)$ using equation (7.2.2-4) and simple numerical integration of:

$$\int_{-\infty}^{\infty} |\psi(x)|^2 \, dx \quad ,$$

but over limits confined to the assumed extent of the optical field of 1 - 2 diffusion lengths.

Step 5

Assuming a value for the photon density, S_o, appropriate to the cavity volume, together with the normalised optical intensity distribution, $\Psi(x)$, the stimulated recombination term in the continuity equation can be calculated. It is now possible to re-solve the continuity equation under the condition of stimulated recombination, which gives a new estimate of $N(x)$. The quasi-Fermi levels are not recalculated for this new value of $N(x)$ however and Laplace's equation is not re-solved at this stage either. With this new estimate of $N(x)$, $g(x)$ may be recalculated, and from this the modal gain may be re-estimated using the approximate expression

(7.2.2-6) rather than from a solution to equation (7.3-2). The use of equation (7.3-2) to estimate $\tilde{\beta}$ is necessary in the first iteration to "cold start" the problem and achieve the initial estimate of the field profile $\psi(x)$.

This value of modal gain obtained from equation (7.2.2-6) is compared with the cavity loss. If the modal gain is not equal to the cavity loss within a tolerance error then the value of S_o is adjusted, as explained in Appendix C, and all the calculations in step 5 are repeated with this new value of S_o until the lasing condition (equation 7.2.2-5) is satisfied.

Step 6

Step 5 ignores the effect that the new estimate of $N(x)$ has on the complex dielectric constant, $\tilde{\varepsilon}_{eff}(x)$. The new estimate of $N(x)$ is used to calculate a new set of values of $\tilde{\varepsilon}_{eff}(x)$ which then allows to evaluate $\psi'(x)$ and hence $\Psi'(x)$ from equations (7.3-2) and (7.2.2-4) respectively. The calculations are thus repeated from step 2 missing step 3 completely. If $\Psi'(x)$ evaluated in step 4 is not within a tolerable error of $\Psi(x)$ then step 5 is repeated successively. If, however, consistent solutions of the carrier density and the field profiles are obtained then the new value of carrier density profile is used in equations (7.2.1-6, 7.2.1-7 and 7.2.1-8) and Laplace's equation re-solved to take into account the change in quasi-Fermi levels and carrier density due to stimulated recombination because of the optical field interaction.

Step 7

Laplace's equation, the quasi-Fermi level separation and the continuity equation, together with $\Psi(x)$ and S_o found on successful completion of the above steps, are then re-solved self consistently according to step 1 which further modifies the carrier density distribution $N(x)$. All

the steps of calculation from step 2 to step 7 are then repeated, skipping step 3, to recalculate a stable optical field, $\psi(x)$, for this new value of $N(x)$. Step 3 is not necessary after the first pass because $\tilde{\beta}$ is re-estimated in step 6.

An iterative scheme is thus developed in which the optical field modifies the carrier profile directly. This perturbs the heterojunction voltage and current spreading which enhances this change in carrier density profile. The optical modes to this new condition are recalculated and the stimulated output is recomputed. The process is continued until convergence is achieved, i.e. when $V(x,y)$, $N(x)$, and the optical intensity profile, $\Psi(x)$, are all within a tolerable global error of the previous iteration values.

This complex iteration scheme may not always achieve convergence however due to several competing reasons.

i) Above threshold the stimulated recombination effect may perturb the carrier distribution so that the original lateral mode can no longer be supported. It is thus vital to keep constant track of the modes which can be supported at each stage of the iteration, and to select only the mode with the largest modal gain above the condition given by equation (7.2.2-5).

ii) Well above threshold it is possible that several modes compete for the same gain such that having recalculated the propagation constant and modal gain at each step of the iterative process oscillation between two dominant modes occurs every alternate iterative cycle.

conductivity of p-type (AlGa)As confining layer = 500 $(ohm.m)^{-1}$
thickness of p-type (AlGa)As confining layer = 2.0 μm
width of electrode S_1 = 3.0 μm
width of electrode S_2 = 3.0 μm
spacing between the electrodes = 3.0 μm
ambipolar diffusion coefficient of carriers in active layer = 68 cm^2/s
thickness of active layer = 0.3 μm
bimolecular recombination coefficient 'B' = 9.7×10^{-11} cm^3/s
energy gap of the active layer material GaAs = 1.43 eV
density of states of conduction band 'N_c' = 4.7×10^{17} cm^{-3}
density of states of valence band 'N_v' = 7.0×10^{18} cm^{-3}
background refractive index of active layer 'n_o' = 3.5
parameter a' in gain relation = $300 \times 10^{-18} cm^2$
parameter b' in gain relation = 450 cm^{-1}
cavity loss C_{loss} = 60 cm^{-1}
anti-guidance and gain-guidance coupling parameter R = 4

Table 7.4 Material parameters listed above are used in the computer simulation unless otherwise specified in figures.

Using the above procedure a computer program was developed which provided self-consistent solutions for $N(x)$, $J(x)$ and $\Psi(x)$ within a very fine tolerance level over a wide range of electrical and geometrical conditions.

Table(7.4) lists the main parameters used in the computer simulation results unless otherwise stated. At every stage of the solution extensive checks were made to ensure that the mesh size was sufficiently small to provide adequate accuracy, but not so small that excessive demands were placed on the storage requirements of the computer. In the case of the solution to the optical waveguide problem the mesh size was made adaptive, controlled by the allowable global error for $\Psi(x)$ and the tolerance error for $\tilde{\beta}$.

7.4 Numerical Results of a Single Stripe Laser

In the first instance the device with electrode width 12μm is examined, which although relatively wide and sufficient to allow modal instability, is used in practical (AlGa)As laser, and is useful in illustrating the various effects. An important difference between experimental conditions and those which have been imposed by the electrode boundary conditions for the theoretical model must be stressed. In practice, it is common to drive lasers from constant current sources, corresponding to the case of a constant generation rate of carriers. However, the only valid boundary condition which may be imposed in the theoretical model is that of constant electrode voltage. Stimulated recombination reduces the carrier density in the active layer and the heterojunction potential varies as a consequence. With a fixed electrode potential this means that generation rate which is dependent on the current drawn by the electrode, can vary. In the results which follow the electrode current is calculated from the solution to Laplace's equation and equation

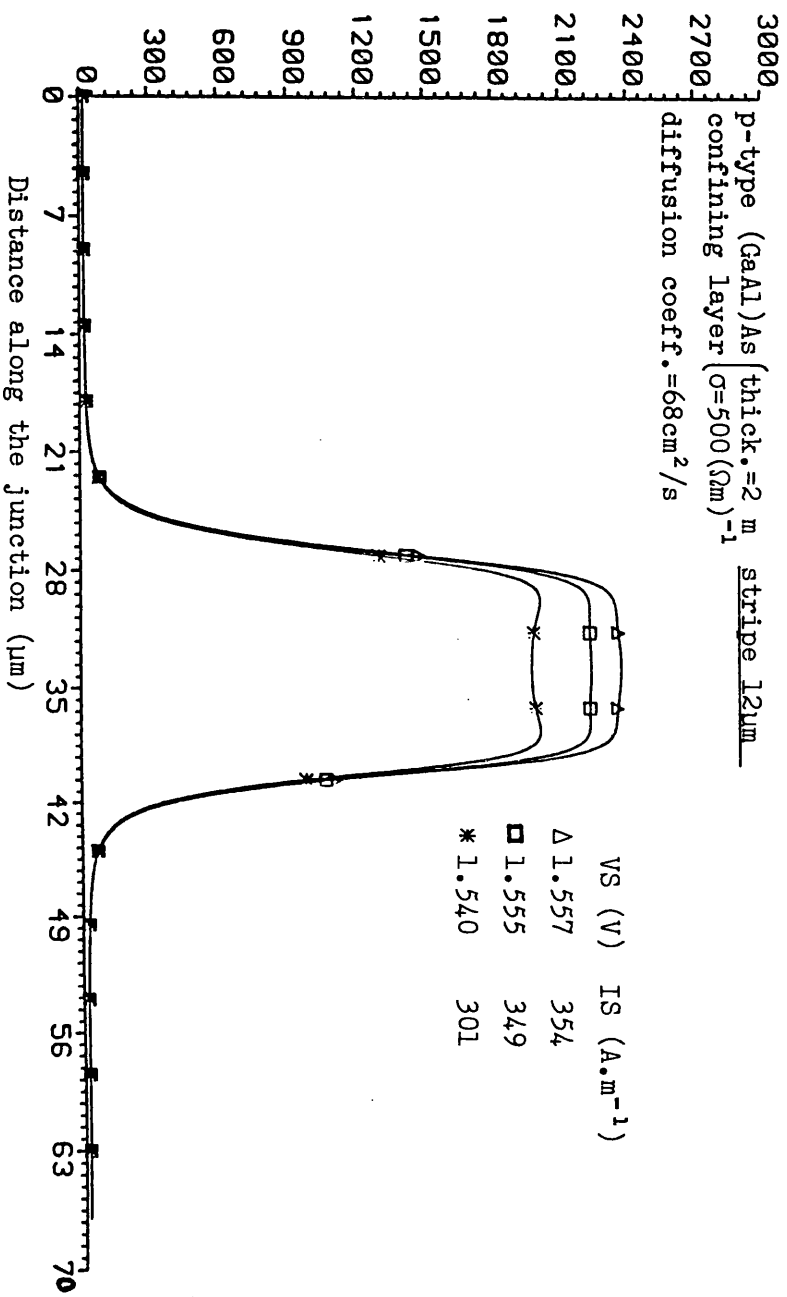

Fig. 7.4-1a Effect of electrode current on the injection current density into active layer of a 12µm single stripe laser above threshold when current spreading, carrier diffusion and stimulated recombination are all taken into account.

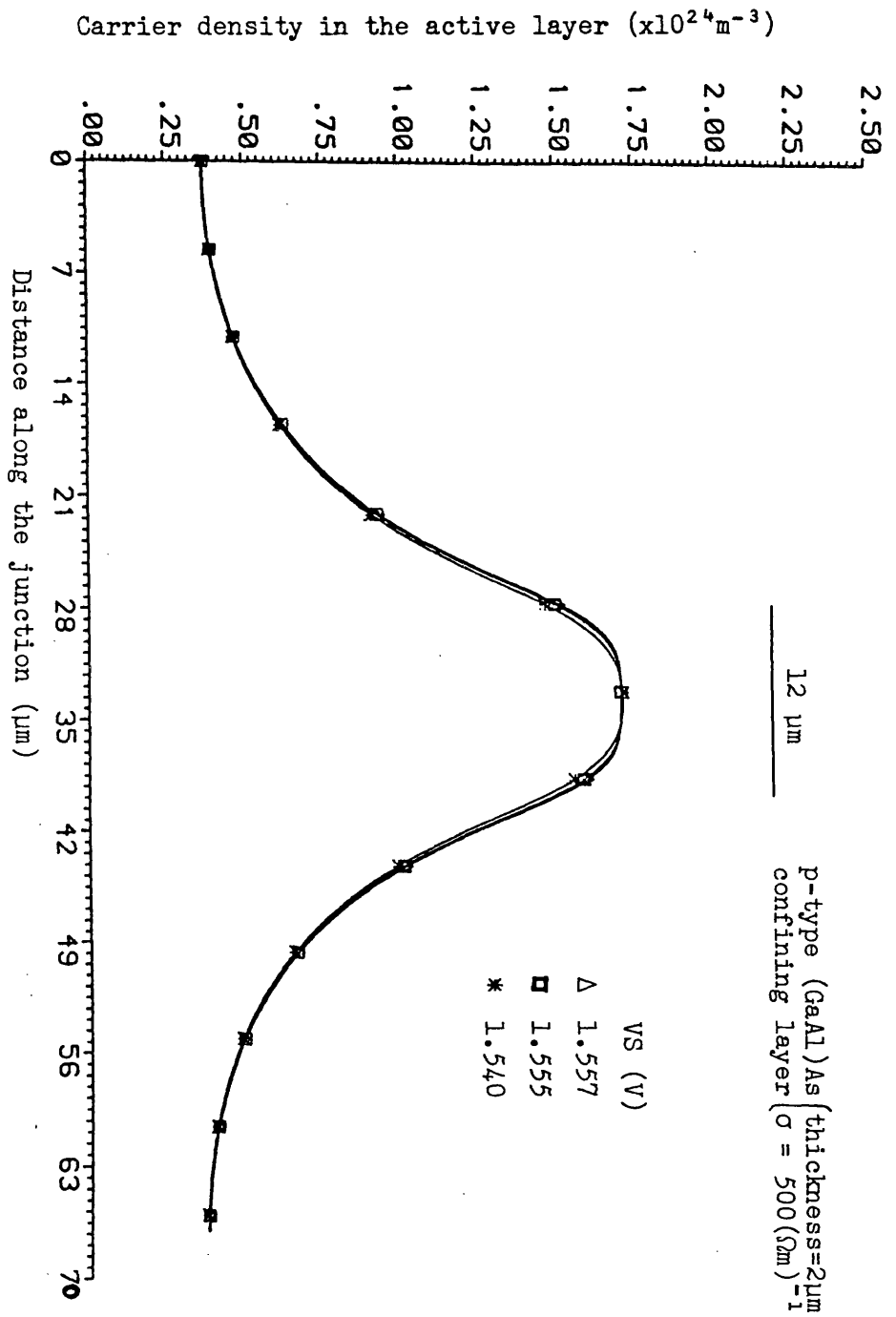

Figure 7.4-1b Carrier density distribution of a 12μm single stripe laser corresponding to the injected current density distribution shown in Fig. 7.4-1a.

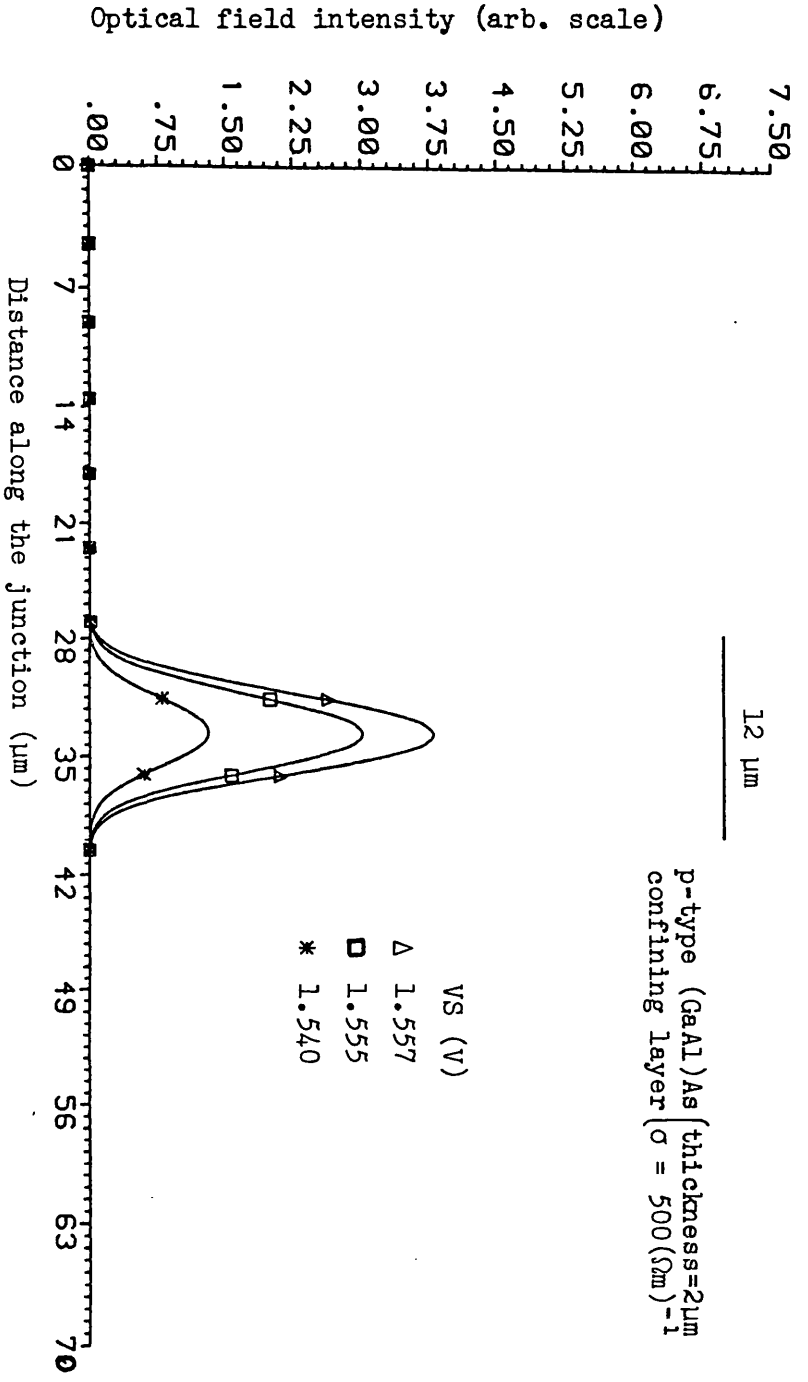

Figure 7.4-1c Intensity distribution of a 12μm single stripe laser corresponding to the current density and the carrier density distributions shown in figures 7.4-1a and 7.4-1b respectively.

(7.2.1-4) to show the movement of the working point as the various device parameters are modified.

Figures (7.4-1a), (7.4-1b) and (7.4-1c) show the current density distribution injected into the active layer, the carrier density distribution in the active layer and the optical intensity distribution for the laser with the above characteristics at three different values of stripe current. In each case the dominant lateral mode was the fundamental mode whose distributions are shown in figure (7.4-1c). The injection current density distribution into the active layer, shown in figure (7.4-1a), illustrates the effect of stimulated recombination and lateral carrier diffusion. At low current, just above threshold, the current density injected into the active layer shows a pronounced dip underneath the stripe. This is due to the non-linear boundary provided by the heterojunction and lateral carrier diffusion, as detailed in reference (14) and initially presented by Lengyel et al (19). This effect is most marked for relatively wide electrodes. As the level of pumping is increased the local minimum in current density is replaced by a shallow hump, and an associated dip in the carrier density. Similar results have been reported by Shore (20). The reason for this effect is stimulated recombination. The increased recombination rate due to stimulated recombination locally depletes the carriers beneath the electrode, as shown in figure (7.4-1b). This is known as hole burning effect and gives rise to the modal instabilities of the device. Moreover, because of the constant potential boundary condition the current must increase to establish a new steady state as the increased recombination of carriers occur due to stimulated recombination. This corresponds to the excess stimulated recombination current. Figure (7.4-1b) also shows that the carrier density distribution, and hence the quasi-Fermi levels, become pinned above threshold. This does not happen if a simple

diode of the heterojunction is used, and considerable distortion of the carrier and intensity distributions result. Although the symmetrical boundary condition was not assumed, the method of solution adopted here prevents certain types of solutions such as near field shift (1) from being observed. However, as the pumping current is increased the peaks of the radiation intensity and the carrier density get displaced. The carriers tend to accumulate more to the region where the laser radiation is less while the beam has a tendency to move to the region of accumulated carriers with a large gain producing there a depletion of carriers. In this way oscillations set in and no stable solution was obtained.

Similar set of results of a 3μm wide stripe geometry laser with all other parameters as above are shown in figures (7.4-2a), (7.4-2b) and (7.4-2c). The applied voltage to the electrode has to be increased as compared with the above case due to increased spreading resistance of the device. The dip in current density is now absent,and carrier diffusion and current spreading become dominant features of the characteristics, and this increases the threshold current density which becomes clear on comparing the peak values of current density in figures (7.4-2a) and (7.4-1a). The carrier and, hence gain saturation above threshold is evident in figure (7.4-2b). Also the gradient of carrier distribution underneath the stripe is very steep which leads to an improved gain guidance in the lateral direction. On comparing figure (7.4-3) with (7.4.1-2) shown in the next section, it appears that this device can be pumped upto a higher value of light output without any problem of modal instability. On the other hand the I-L characteristics shown in figure (7.4.1-2) are not perfectly linear but kink very slightly at a relatively lower light output , as one might expect in practice for a 12μm wide electrode.

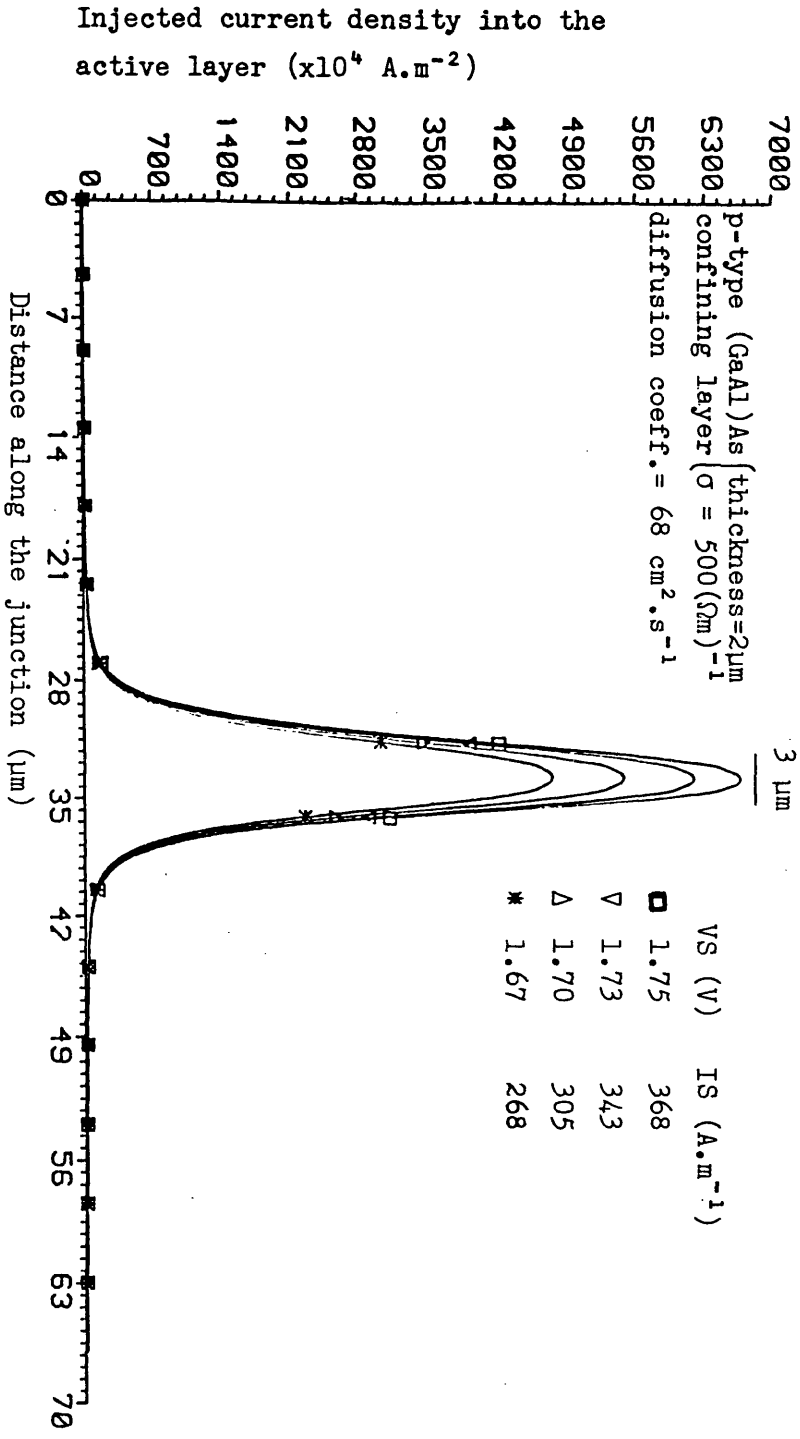

Figure 7.4-2a Injected current density distribution in a 3μm single stripe laser under four different values of pumping current labelled in figure.

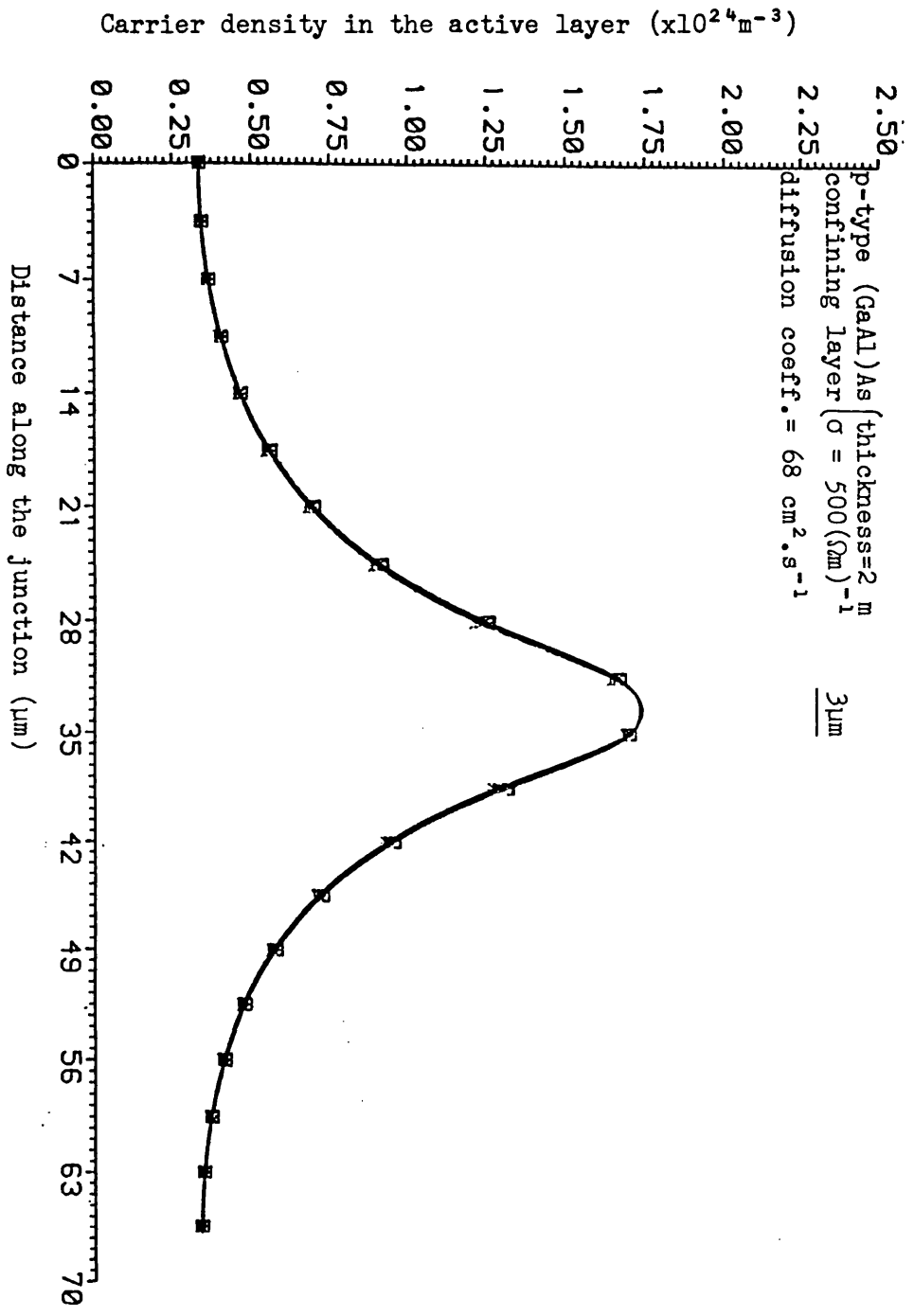

Figure 7.4-2b The carrier density distribution in the active layer of a 3μm single stripe laser found consistent with the current density distribution shown in figure 7.4-2a.

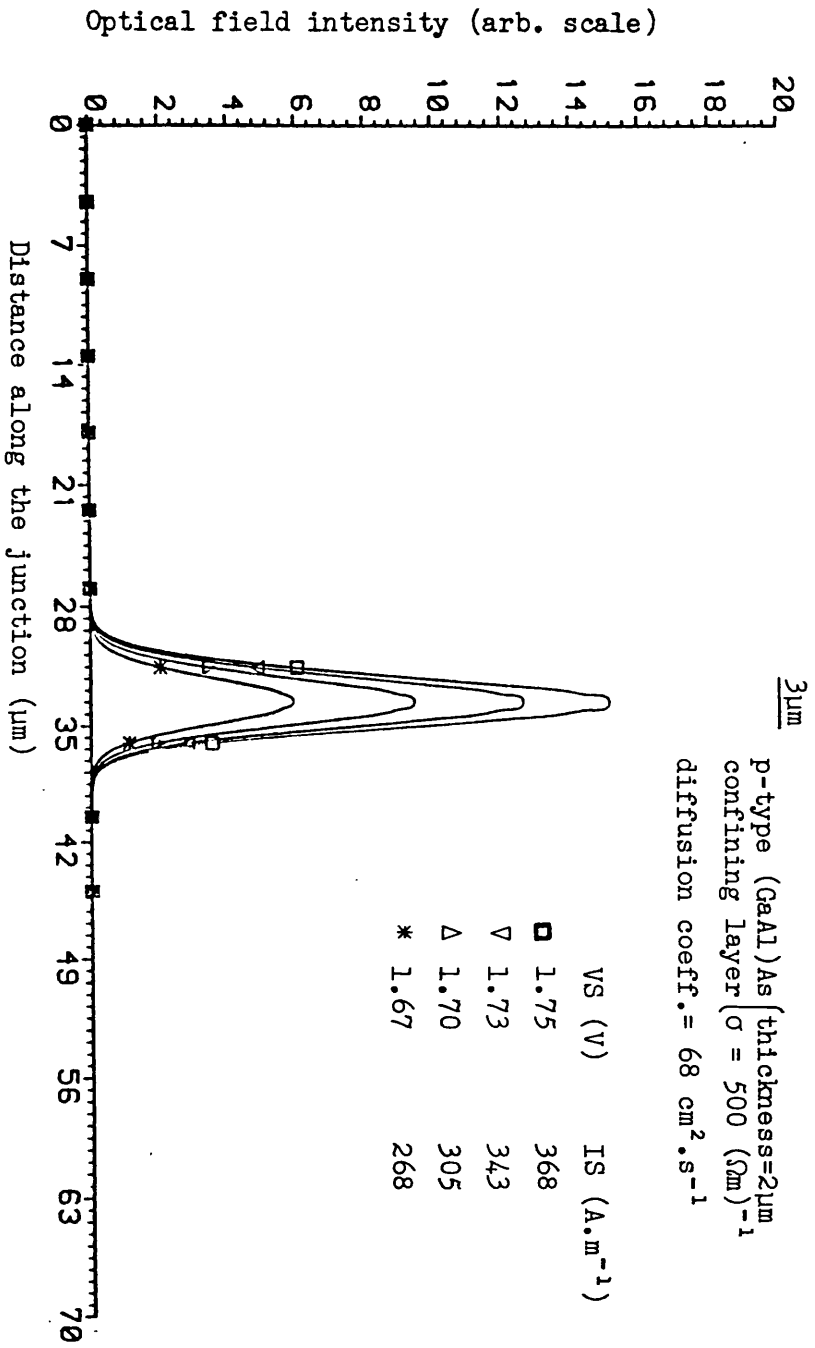

Figure 7.4-2c The lateral field intensity distribution of a 3μm single stripe laser corresponding to the current and carrier density distributions shown in figures 7.4-2a and 7.4-2b respectively.

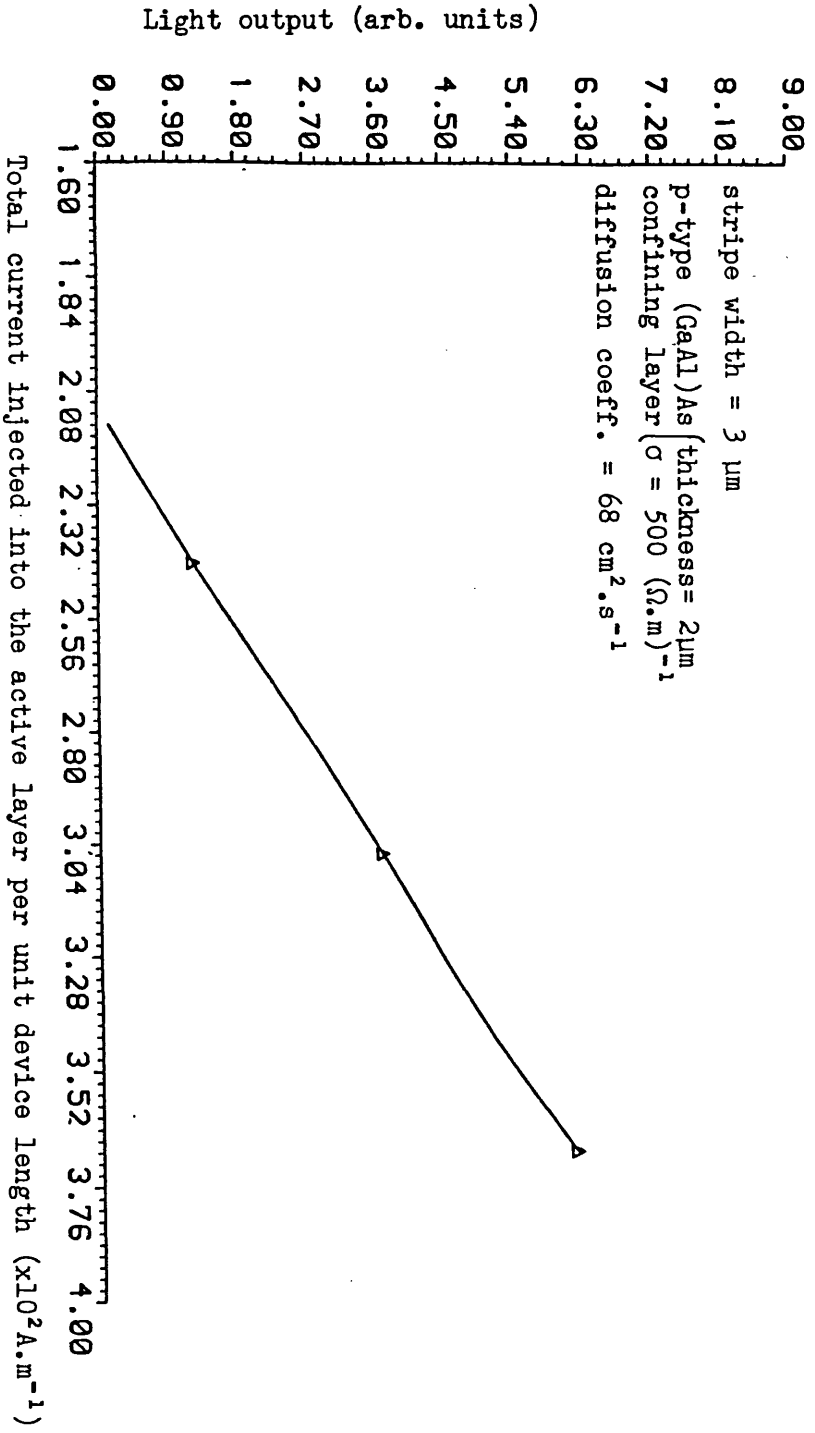

Figure 7.4-3 Light/Current chracteristic of a 3μm single stripe laser. The total current per unit device length injected into active layer is labelled in figure 7.4-2a corresponding to each pumping condition.

7.4.1 Effect of the resistivity of the p-type confining layer on the device behaviour

The effect of the resistive confining layer is important because it controls the current spreading effect and acts as a series resistance to the voltage source driving the laser. A similar result may be obtained by maintaining the resistivity and increasing the thickness of the confining layer, however in this case current spreading is also worsened.

The results of the device with the resistivity of the p-type confining layer increased from 0.2 ohm.cm (σ = 500 $(ohm.m)^{-1}$) to 1 ohm.cm (σ = 100 $(ohm.m)^{-1}$) and thickness reduced from 2μm to 1.2μm are computed. On comparing the current distributions of the two devices (i.e Figures 7.4-1a and 7.4.1-1a) current spreading beyond the electrode edge of the stripe is significantly reduced. However, the increased resistivity of the layer has raised the threshold voltage from approximately 1.54V to 1.70V due to excessive ohmic drop in the resistive layer. There is also a pronounced dip in the current distributions just above threshold which changes to a slight hump well above threshold, as in the previous case. However, it is also seen from figure (7.4.1-1b) that the gradient of the carrier density beneath the stripe just above laser threshold is steeper than that in figure (7.4-1b). It is also clear that hole burning effects are more apparent in the carrier distribution of (7.4.1-1b) than (7.4-1b) for the case of much higher light levels which is analogous to the predictions made by Joyce (21). Optical confinement of this device is also good. Consequently, thin relatively high resistivity confining layers can raise the level of light output shown in figure (7.4.1-2) at which hole burning effects appear and are more apparent. Therefore the stability of the device is improved but at the cost of excessive heat dissipation due to ohmic loss in the resistive layer. The optical intensity distributions of the device for three current values are shown in figure (7.4.1-1c)

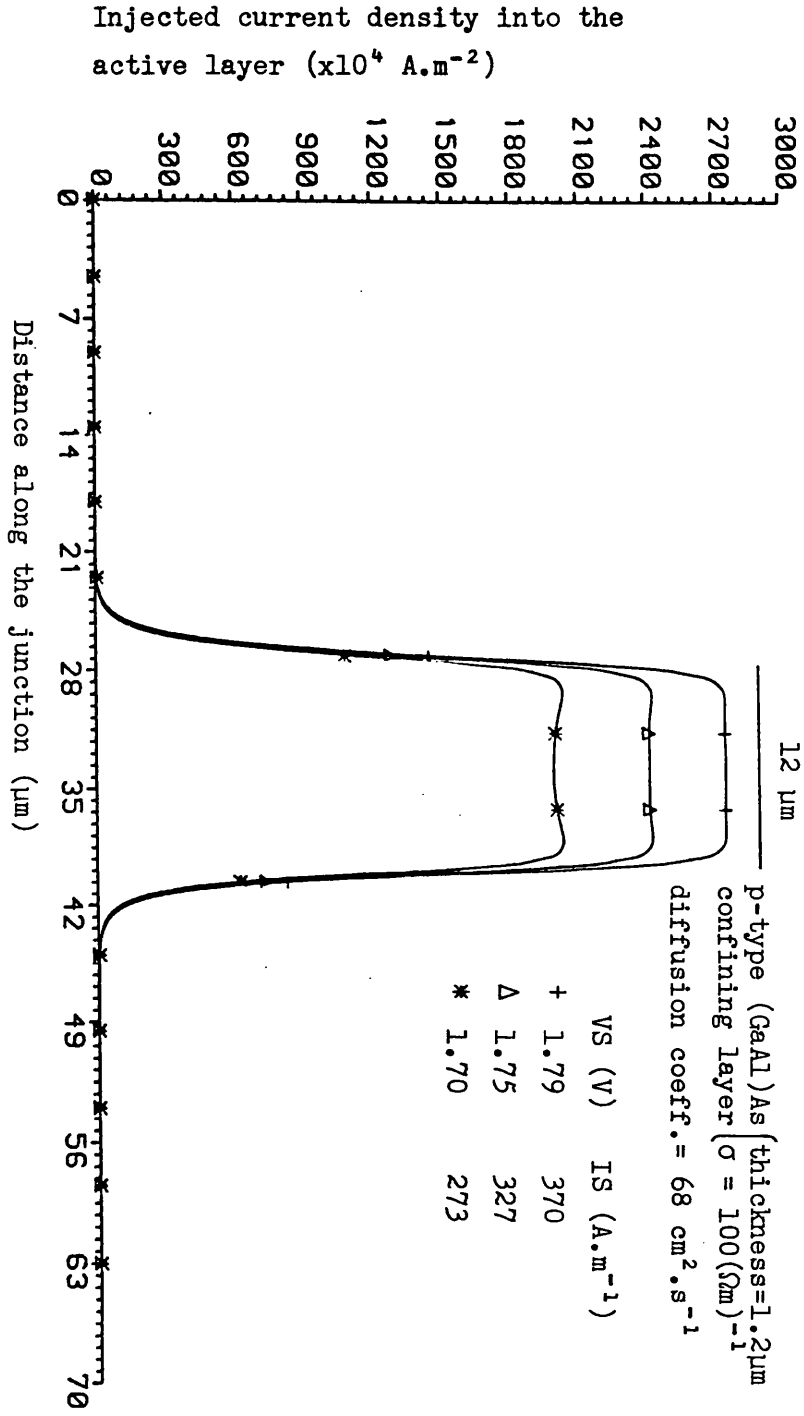

Figure 7.4.1-1a Current density distribution injected into the active layer of a 12µm single stripe laser with conductivity 100 $(ohm.m)^{-1}$ of the confining layer, 1.2µm thick. The corresponding carrier density and intensity distributions are shown in figures 7.4.1-1b and 7.4.1-1c respectively.

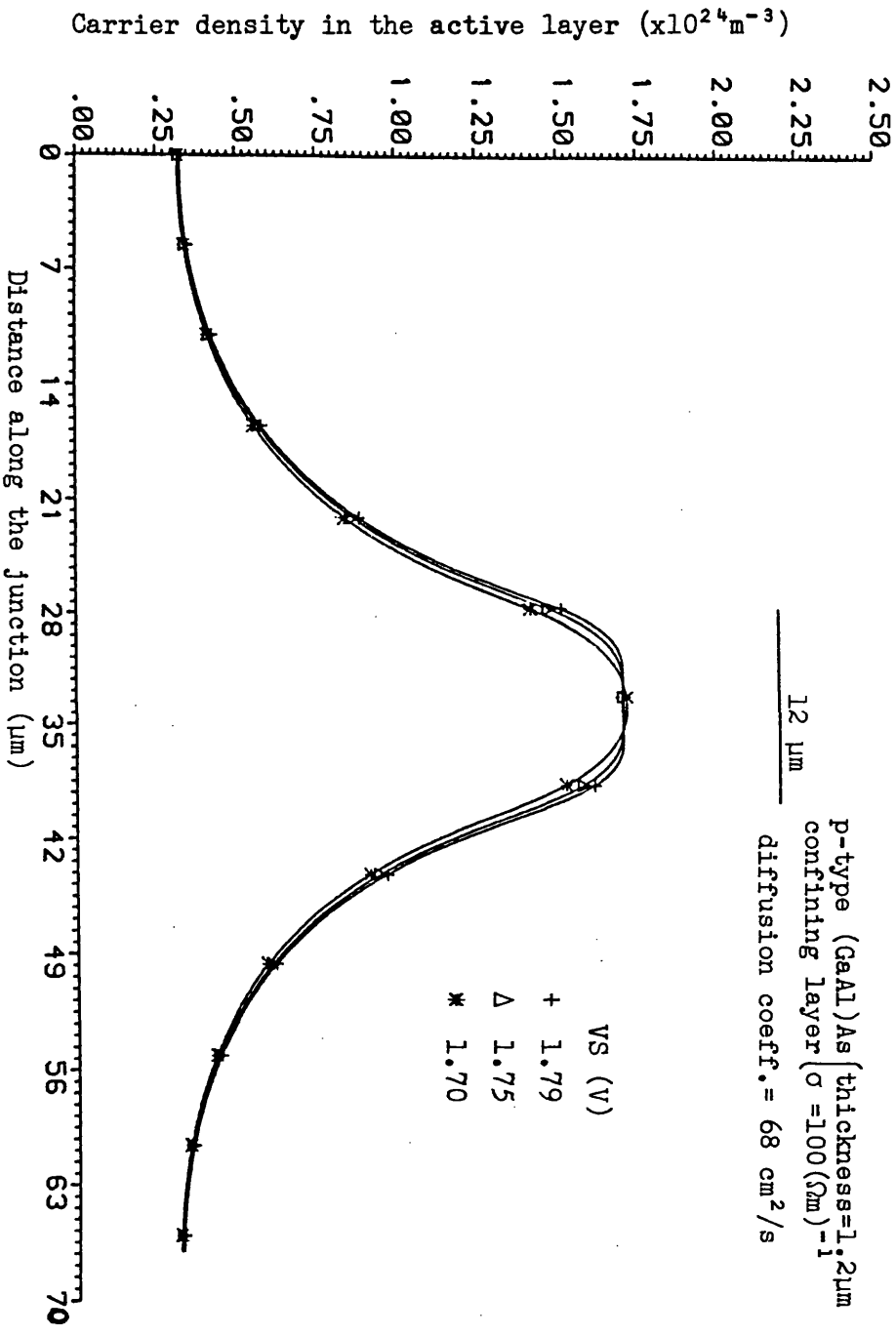

Figure 7.4.1-1b Carrier density distribution in the active layer of a 12μm single stripe laser with 100 (ohm.m)$^{-1}$ conductivity of the confining layer, 1.2μm thick.

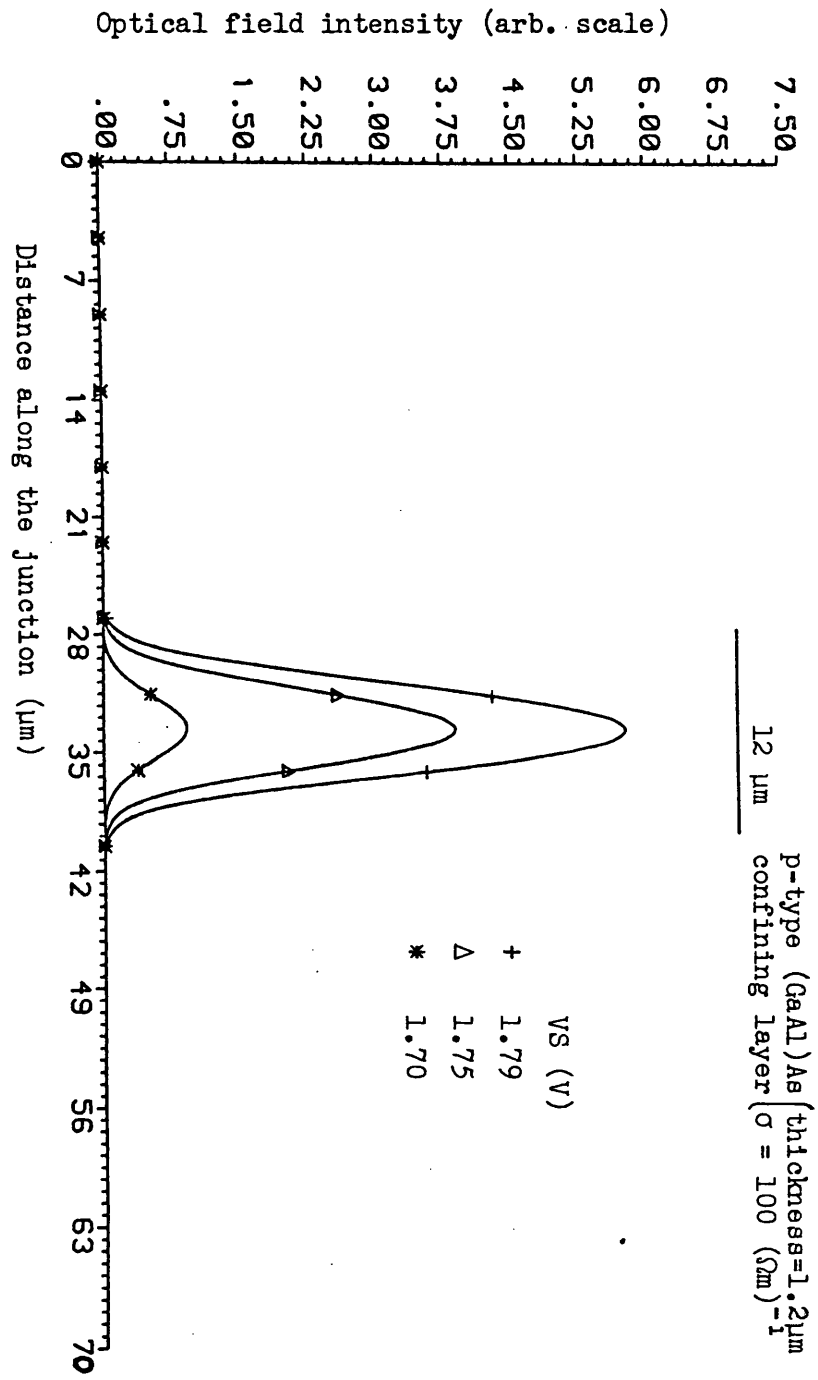

Figure 7.4.1-1c The lateral field intensity distribution of a 12μm single stripe laser with 100 $(ohm.m)^{-1}$ conductivity of the confining layer, 1.2μm thick.

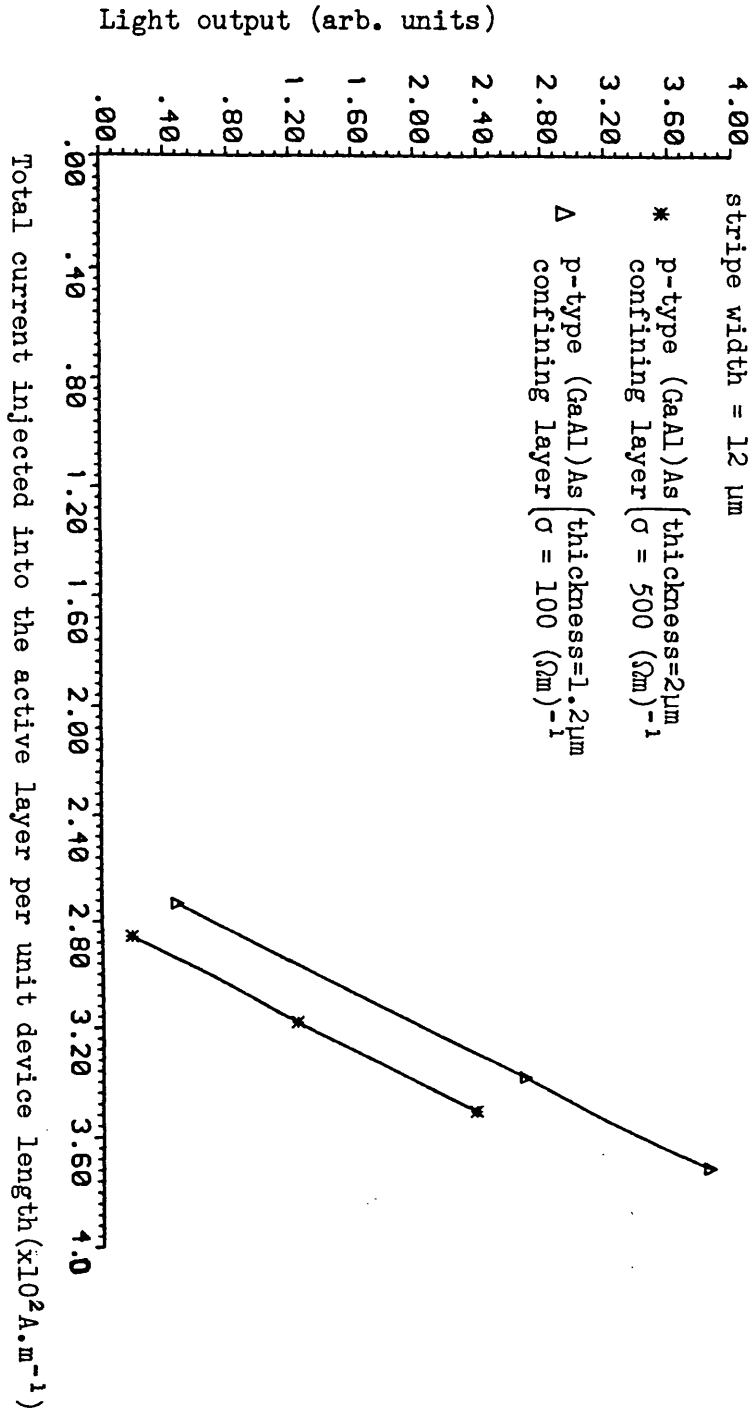

Figure 7.4.1-2 Comparison of I-L characteristics of a 12μm single stripe laser with the respective conductivity and thickness of the confining layer as:

(*) 500 $(ohm.m)^{-1}$ and 2.0 μm

(Δ) 100 $(ohm.m)^{-1}$ and 1.2 μm

7.4.2 The effect of stimulated recombination on current spreading

If the calculations are terminated at step 6 without solving Laplace's equation in section (7.3) the current density distribution J(x) is NOT consistent with the carrier density and the optical intensity distributions. The effective generation rate determined by J(x) distributions is fixed and is unaffected by the stimulated recombination of carriers. Therefore the generation rate term given by the right hand side of equation (7.2.1-10) is fixed. By including the stimulated recombination term this implies less contribution from the diffusion term, or the effective diffusion length of carriers becomes less and the dips in the carrier density becomes more noticeable. An increase in recombination of the carriers results in an increase in the injected current density J(x) if it is found consistently with the rest of the solution and will therefore compensate to some extent the local depletion of carriers underneath the stripe (due to strong stimulated recombination) by increasing the generation rate.

Figures (7.4.2-1a) and (7.4.2-1b) show the increase in current density in a 12μm stripe laser when the optical interaction occurs. The graphs are drawn for two different pumping currents above threshold. The dip in current density when stimulated recombination is ignored (14) is largely removed by the increased carrier generation needed to overcome the stimulated recombination. The excess current in this latter case represents the conversion of carriers to photons via stimulated recombination and is called stimulated recombination current. As the current level is increased, strong stimulated recombination removes the dip in the current density profile beneath the stripe entirely, and replaces it by a small hump in the current density.

In this section the results of the computer simulation in the case

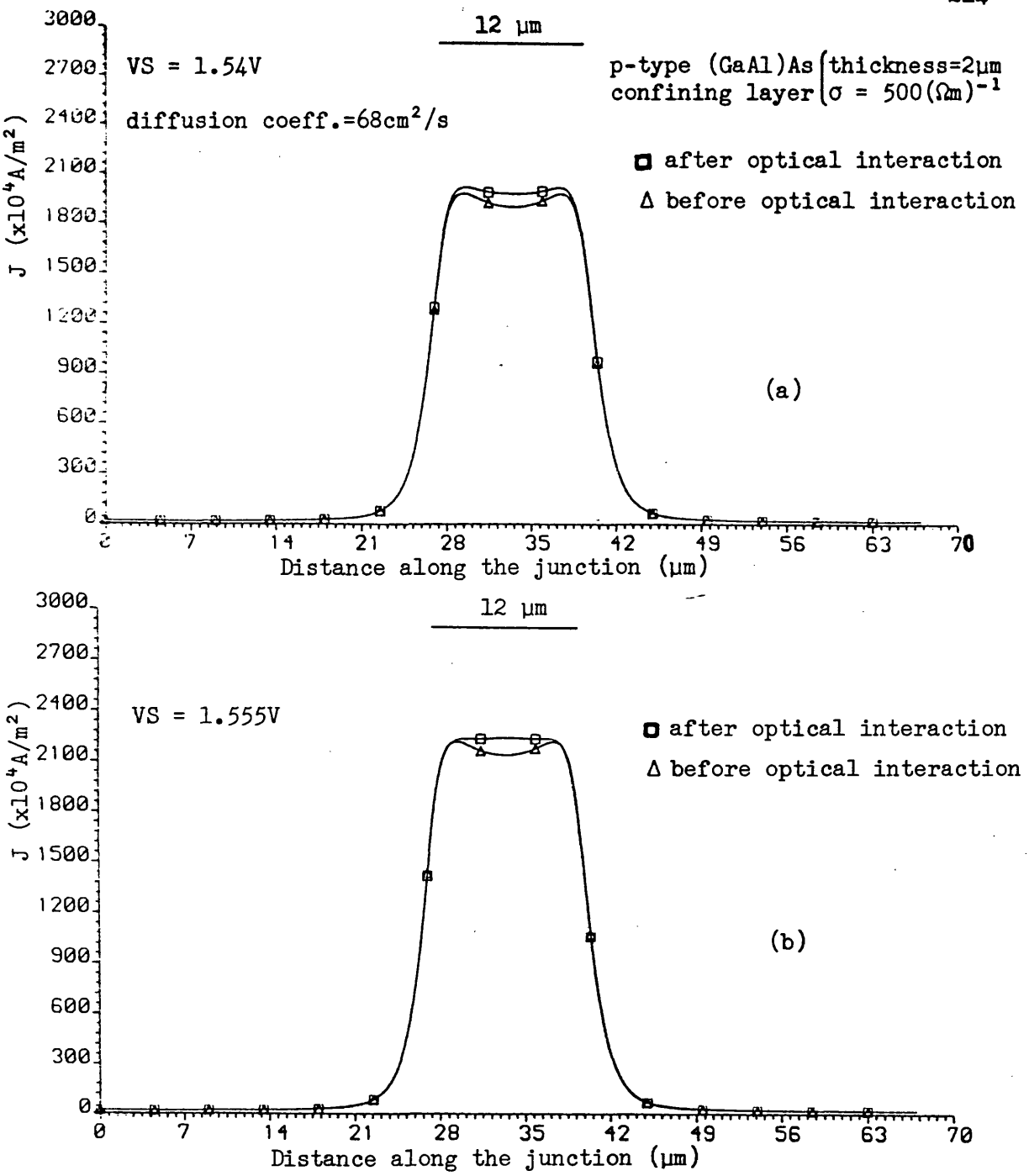

Figure 7.4.2-1 The effect of the interaction of stimulated recombination on the current density distribution of a 12μm single stripe laser with pumping current per unit device length

(a) 301 $A.m^{-1}$

(b) 349 $A.m^{-1}$

of single stripe laser were presented. Although this problem has been solved in a self-consistent manner by Asbeck et al (9) and Wilt and Yariv (10) the results presented here have highlighted important aspects which have not been presented before using a self-consistent model. These include the effect of stimulated recombination on the current spreading within the device and the effect of confining layer parameters on the optical output and modal stability.

7.5 Results of Computer Simulation of a Twin Stripe Laser

In the work by Scifres et al (22) near field beam steering was observed in twin stripe lasers with a stripe electrode width of 2μm and a stripe spacing between electrode centres of 6μm. Other, more recent work (23) has used devices with 3μm wide electrodes and 6μm spacing between centres and this geometry has been used as a starting point for the simulated results. As in the previous case the electrode potential is used as a known boundary condition from which the electrode current is calculated. The following results are representative of results obtained with the computer model. To show the effect of changing parameters, the electrode currents are calculated using equation (7.2.1-4) and tabulated in the respective diagrams.

7.5.1 Effect of electrode potential on the lateral field distribution

In this section the consistent solution of the current density, carrier density and field distribution is presented when the applied potentials on the electrodes S_1 and S_2 are varied.

Figures (7.5.1-1a), (7.5.1-1b) and (7.5.1-1c) show the distributions of injected current density, the carrier density in the active layer and the lateral optical field intensity distribution for different sets of electrode potentials VS_1 and VS_2. Although the injected current density

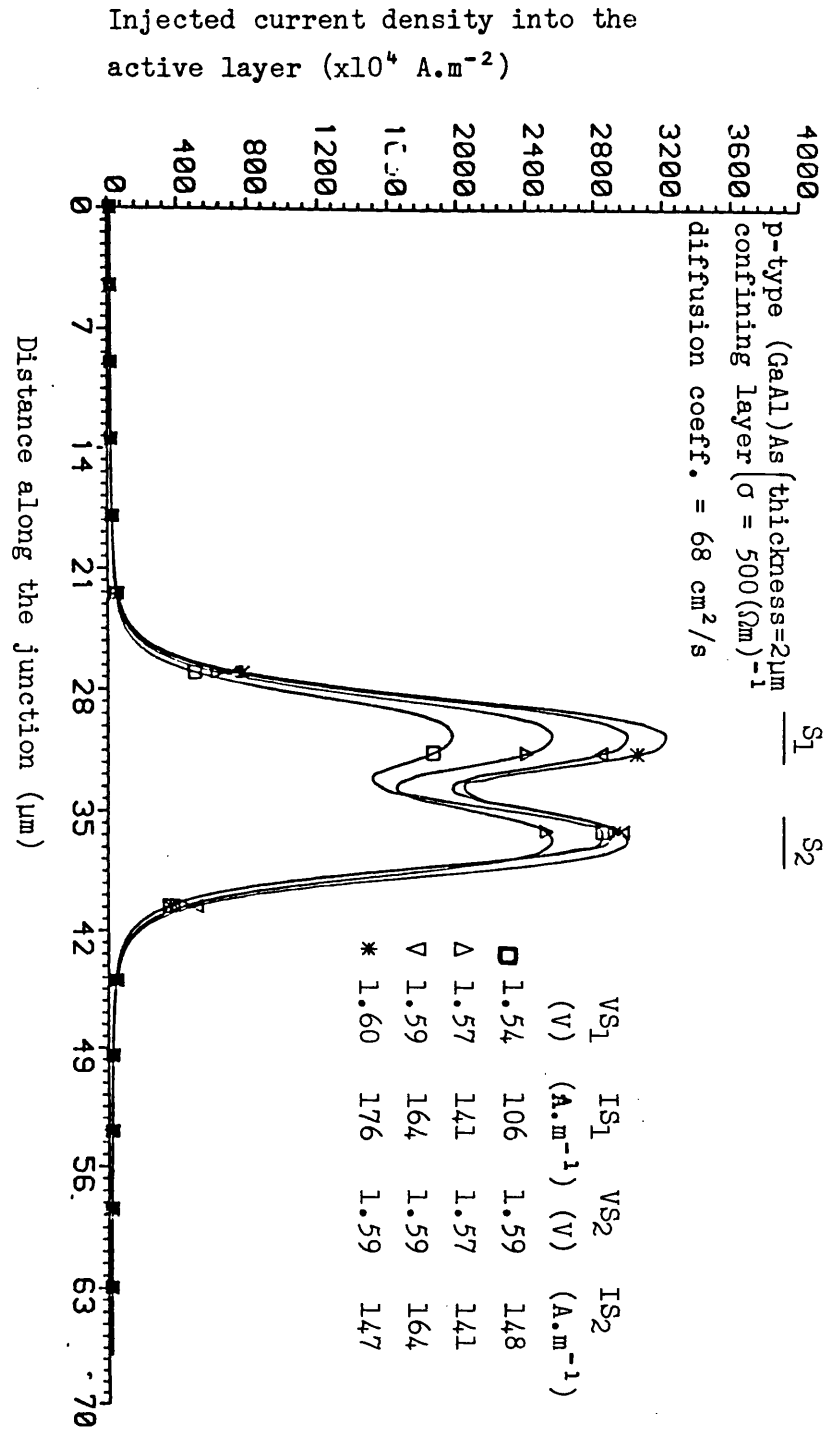

Figure 7.5.1-1a Current density distribution injected into the active layer of a twin stripe laser as the electrode potentials VS_1 and VS_2 are varied. The stripe currents IS_1 and IS_2 per unit device length are listed in figure. Each stripe width is 3μm with a spacing 3μm in between them. The corresponding carrier density and intensity distributions are shown in figures 7.5.1-1b and 7.5.1-1c respectively.

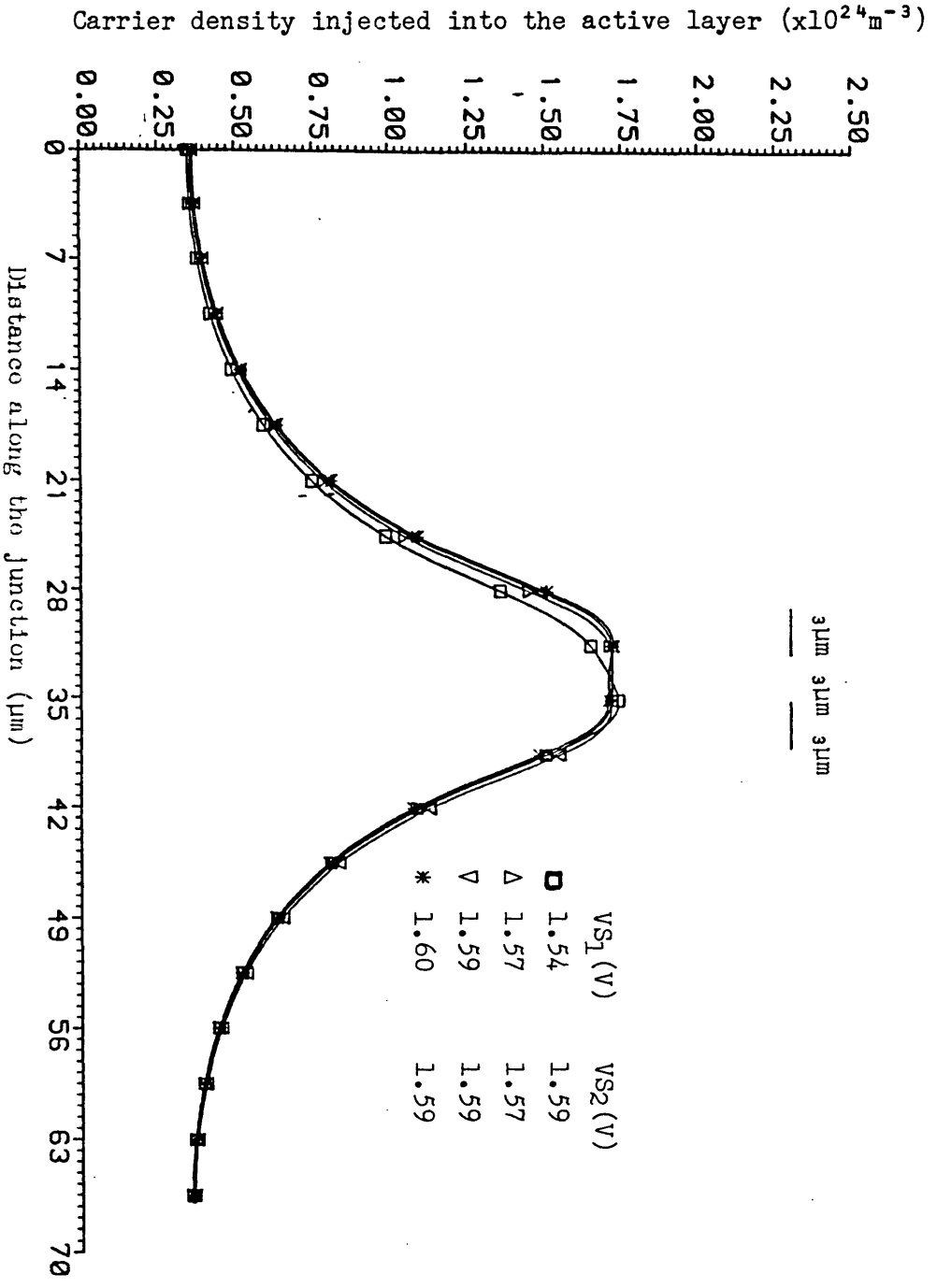

Figure 7.5.1-1b Carrier density distribution in the active layer of a twin stripe laser as the electrode potentials VS_1 and VS_2 are varied.

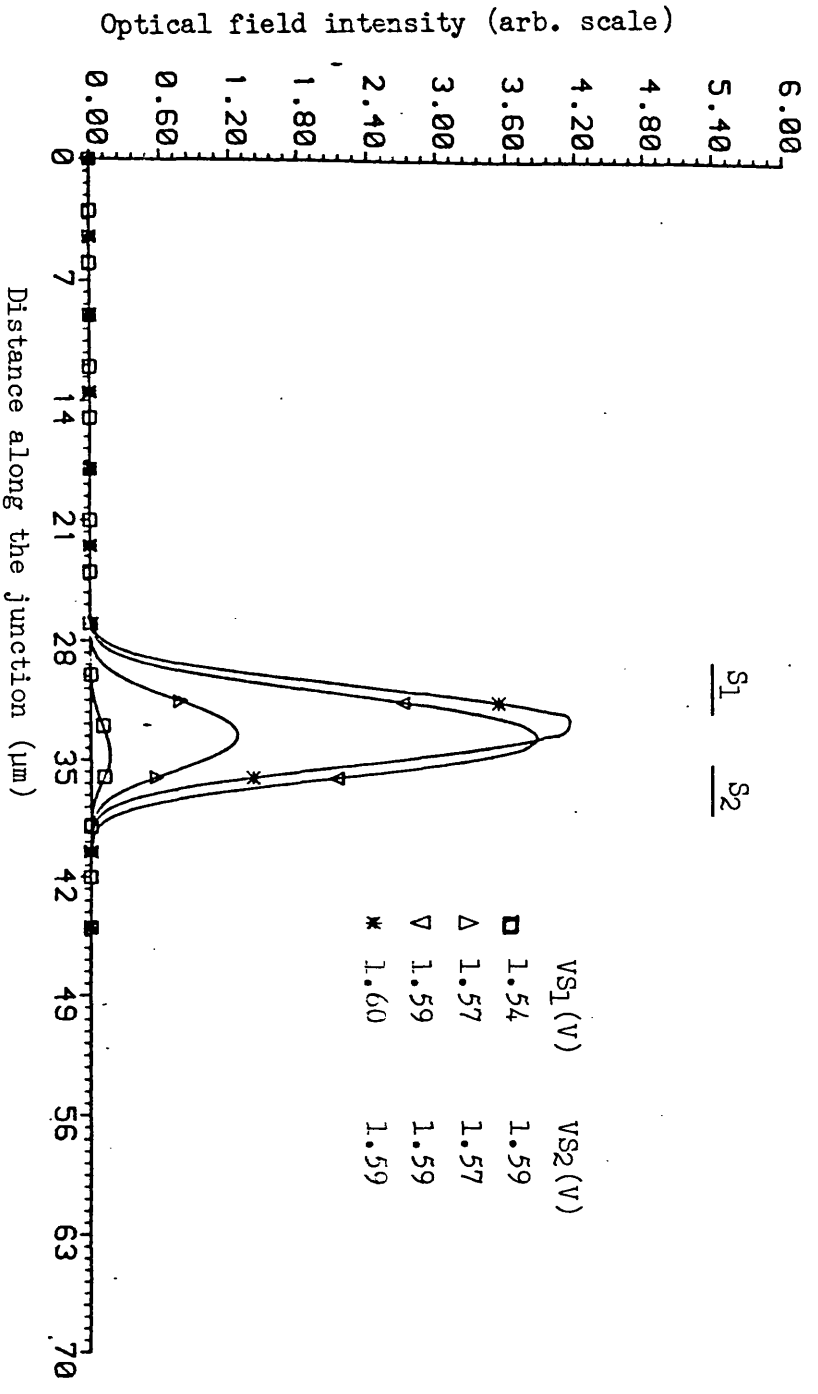

Figure 7.5.1-1c Lateral field intensity distribution corresponding to current density distribution shown in figure 7.5.1-1a of a twin stripe laser predicting beam movement.

is highly asymmetric except for the symmetrical pumped case $VS_1 = VS_2$ (1.57V and 1.59V), strong carrier diffusion in the active layer results in a much lower asymmetry for the carriers. Nevertheless, the asymmetry is sufficient to perturb the complex dielectric constant. It is seen that the field profile, under a wide range of pumping conditions remains as the fundamental lateral mode and is symmetrical in the main lobe and only slightly asymmetric in the tails. It is also seen that the beam position moves as VS_1 is increased. Initially the field is located closer to the stripe S_2 at $VS_2 = 1.59V$ for $VS_1 = 1.54V$ because contribution to the carrier density from VS_1 is negligible and the device behaviour approaches that of a single stripe laser. As VS_1 and IS_1 increase the net number of carriers increase, however it is clear from figure (7.5.1-1b) that the carrier density in the active region remains largely constant i.e the gain, $g(x)$, has saturated, and so the total flux increases to maintain carrier-flux conservation. There is no tendency for higher lateral modes to be supported. However, the beam does shift from S_2 to S_1 as VS_1 becomes greater than VS_2. At these injection levels there was no tendency for bistability. Under symmetrical pumping the beam is fundamental mode and is confined to the region between the electrodes. In the case of a large diffusion coefficient and relatively narrow spacing between the electrodes, there is no observable dip in carrier concentration in the region between the electrodes and thus no local maxima in the real part of the refractive index. Under the conditions of narrow stripe spacing and diffusion, as above, it is clear from figure (7.5.1-1c) that the intensity does not decrease when beam movement occurs. This is due to the very broad gain distribution, $g(x)$, relative to the intensity distribution, $\Psi(x)$, which ensures that adequate gain is available, given that the injected current has been forced to increase in order to move the beam position in the first place.

Figures (7.5.1-2a), (7.5.1-2b) and (7.5.1-2c) show the current density, carrier density and intensity distributions of the same device, but VS_2 is now fixed at 1.55V while VS_1 is varied from 1.58V to 1.65V. The total current per unit device length injected into the active layer is also tabulated in figure (7.5.1-2a) and is used to plot I/L characteristics in figure (7.5.1-3). From these results it is seen that the field is nearer to the more heavily pumped electrode. As the potential VS_1 is reduced beam movement occurs towards the gap between the electrodes. However under symmetrical conditions ($VS_1 = VS_2$) it was not found possible to stabilise the solution upto a high value of pumping current. Under symmetrical conditions as the applied potential ($VS_1 = VS_2$) is increased it is likely that the significant dip in the carrier distribution between the electrodes and stimulated recombination tend to favour higher order modes. The case is very similar to the strongly pumped broad-area single stripe laser. The kink in the I/L characteristics has been observed experimentally by White et al (23) at a relatively low light output for the symmetrically pumped case.

Figure (7.5.1-3) shows the I/L characteristics of the stimulated light vs. total current per unit device length injected into the active layer both for the symmetrical and the asymmetrical pumping conditions. It is clear from these graphs that although the two characteristics are close to each other in the beginning they move apart as the injected current increases. This is due to the fact that in the beginning $VS_1 = 1.58V$ is not far too different from $VS_2 = 1.55V$ and the device behaviour is not very different from the symmetrical case. However, if the pumping current is increased by increasing VS_1 to 1.65V the asymmetry becomes strong resulting in a significant departure from the symmetrical case and the device approaches in its behaviour to that of a narrow single stripe laser. Thus it is possible to achieve relatively more light output in

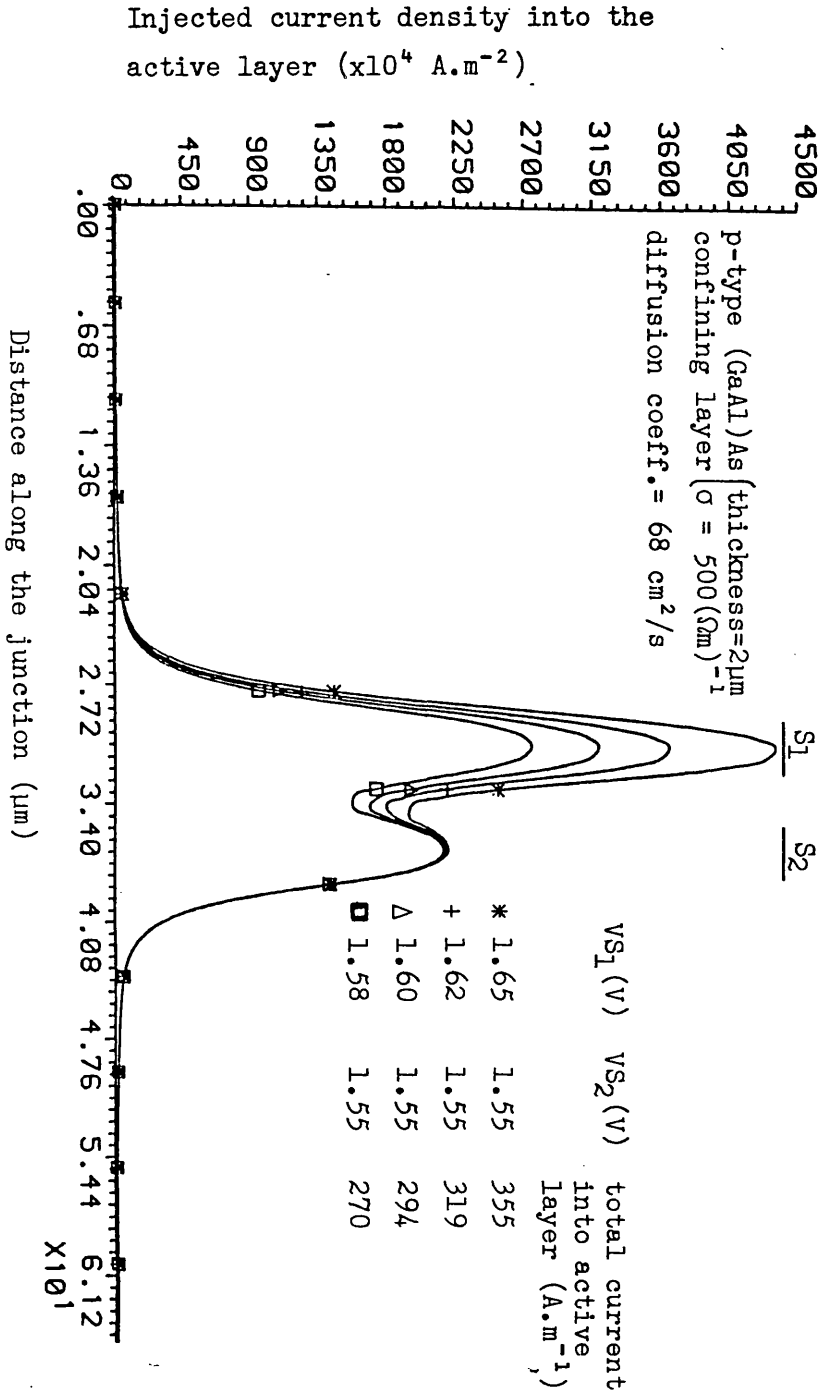

Figure 7.5.1-2a Current density distribution injected into active layer when the applied potential on electrode S_2 of a twin stripe laser is fixed at VS_2=1.55V while VS_1 is varied. The total current per unit device length due to both electrodes injected into the active layer is also listed in figure.

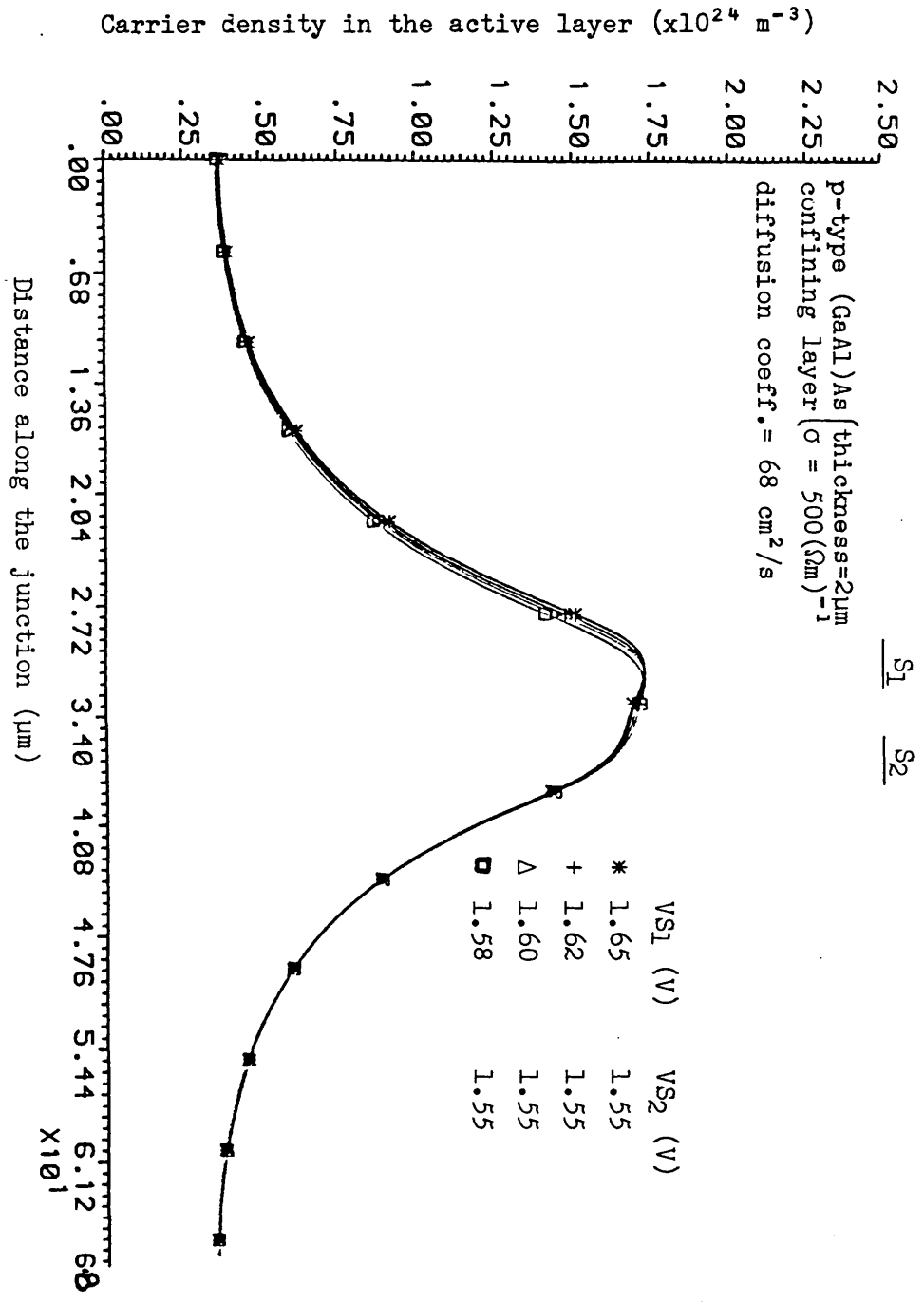

Figure 7.5.1-2b Carrier density distributions in the active layer of a twin stripe laser when the electrode S_2 is kept at a fixed potential VS_2 = 1.55V while VS_1 is varied.

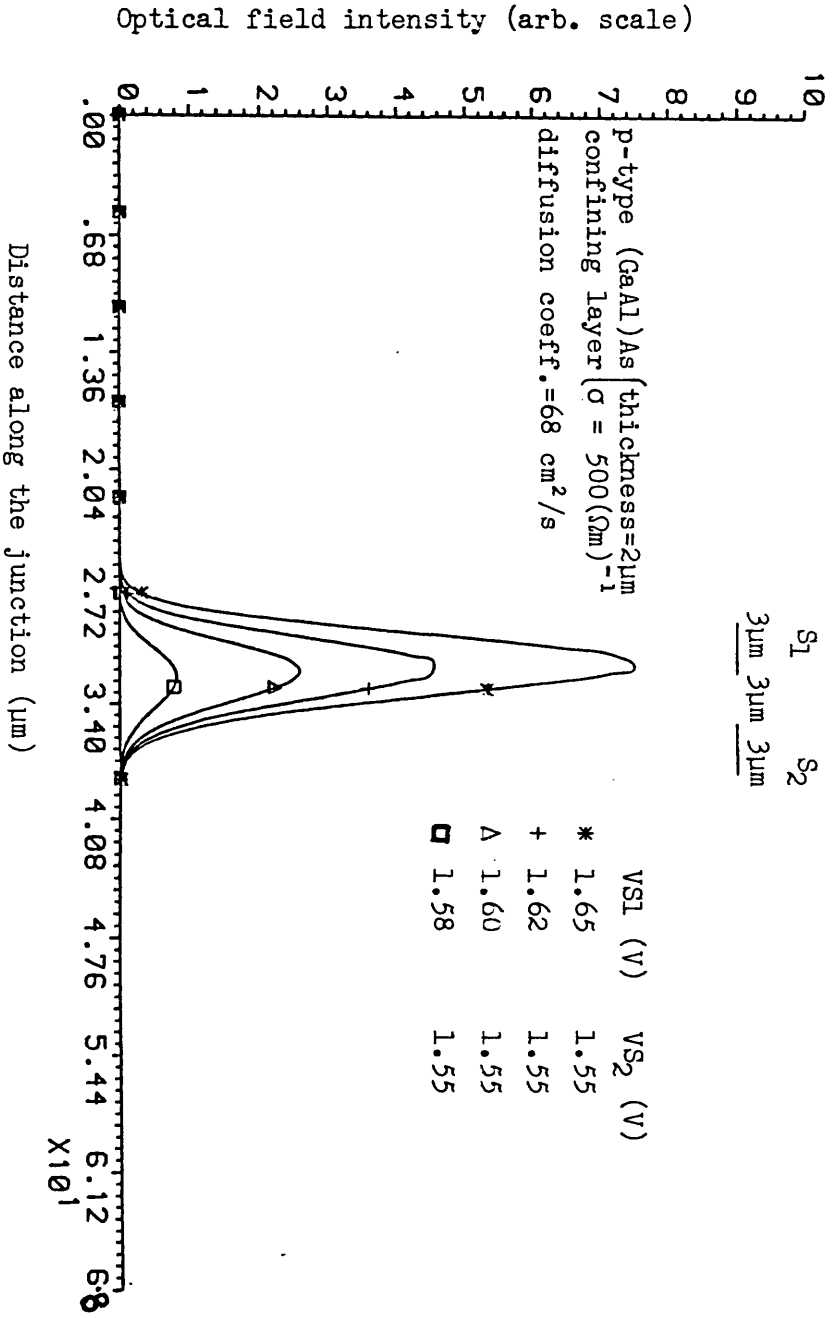

Figure 7.5.1-2c Lateral field intensity distribution of a twin stripe laser when the potential on S_2 is fixed at VS_2 = 1.55V while the potential VS_1 is varied. The beam movement is evident from this figure.

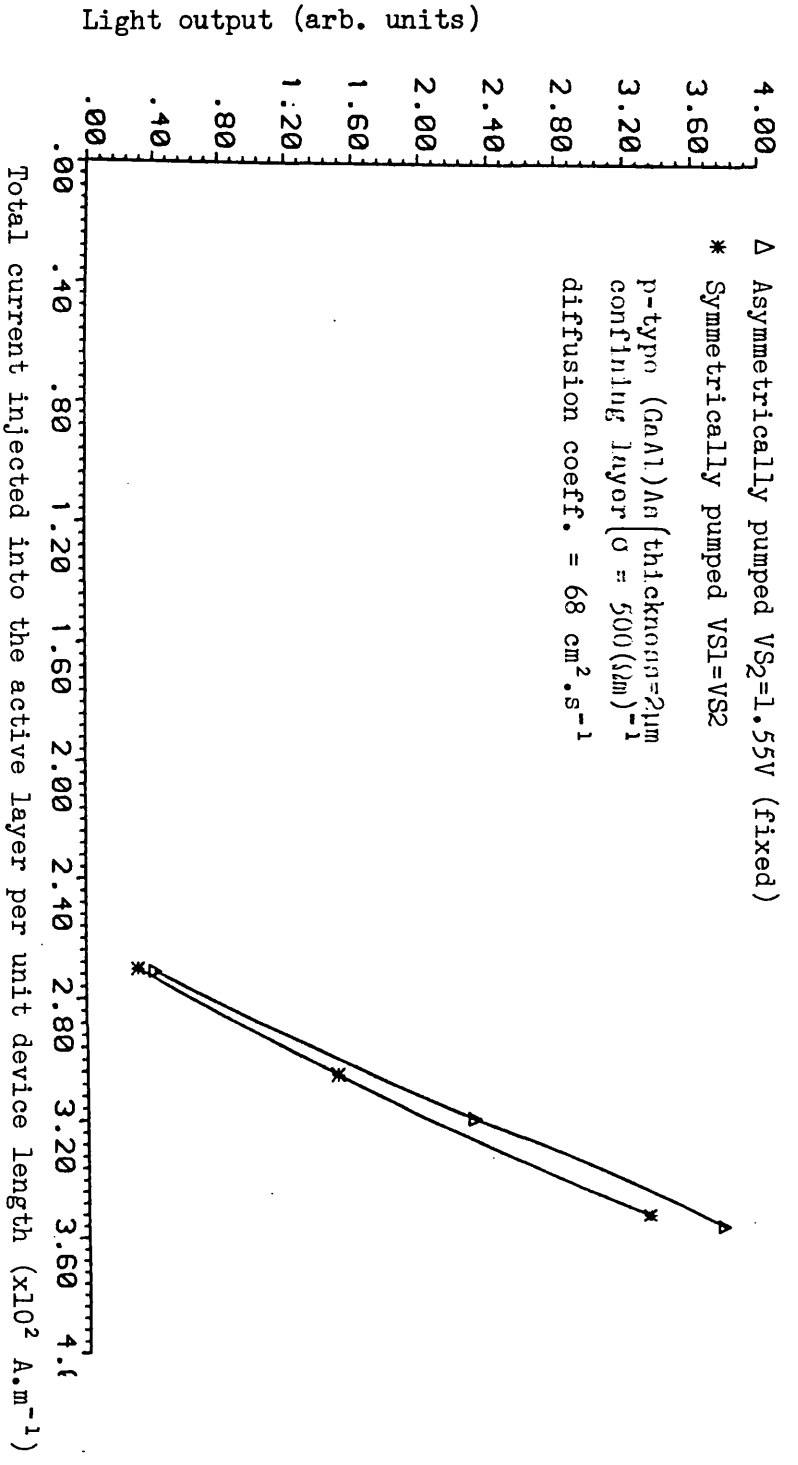

Figure 7.5.1-3 Comparison of I/L characteristics (Δ) asymmetrically pumped with current density distribution shown in figure 7.5.1-2a (*) symmetrically pumped corresponding to the injected current density distribution shown in figure 7.5.3-1a.

in the asymmetrical case as compared with the symmetrical one without facing any modal instability problem.

7.5.2 Effect of electrode spacing

Electrode spacing is clearly an important parameter as it controls the electrical interaction between the two stripes. To illustrate the effect of stripe spacing asymmetric pumping was employed such that VS_1 = 1.65V and VS_2 = 1.55V. Figures (7.5.2-1a), (7.5.2-1b) and (7.5.2-1c) show the injection current density, carrier density and field intensity distributions as a function of electrode spacing in the range 4μm - 9μm (between electrode centres). It is clear that as the spacing is increased and the electrodes become increasingly decoupled and the dip in current and carrier density distributions increases. The peak value of flux is closer to the strongly pumped electrode. The peak value of intensity is lower for wide electrode spacing due to increased losses (or lower gain) between the electrodes. This results in a lower stimulated recombination term in the continuity equation and the peak value of carrier density is higher as result. There is a small reduction in peak current density to match the reduced photon flux. Figure (7.5.2-2) shows the excess current in the case of 6μm electrode spacing (between electrode centres) representing the conversion of carriers to photons via stimulated recombination. It is seen from these graphs that strong coupling in the narrow electrode spacing effectively centres the peak intensity between the electrodes even with asymmetric pumping, but as the electrodes become decoupled the field prefers to remain gain guided close to the more heavily pumped stripe, albeit with a reduced flux. There is a greater tendency for modal instability with wider electrode spacing because the two spatially separate regions of high gain will favour the support of higher order modes such as the 1st order mode and both the zero order mode and first order mode will compete for the same gain. It will be

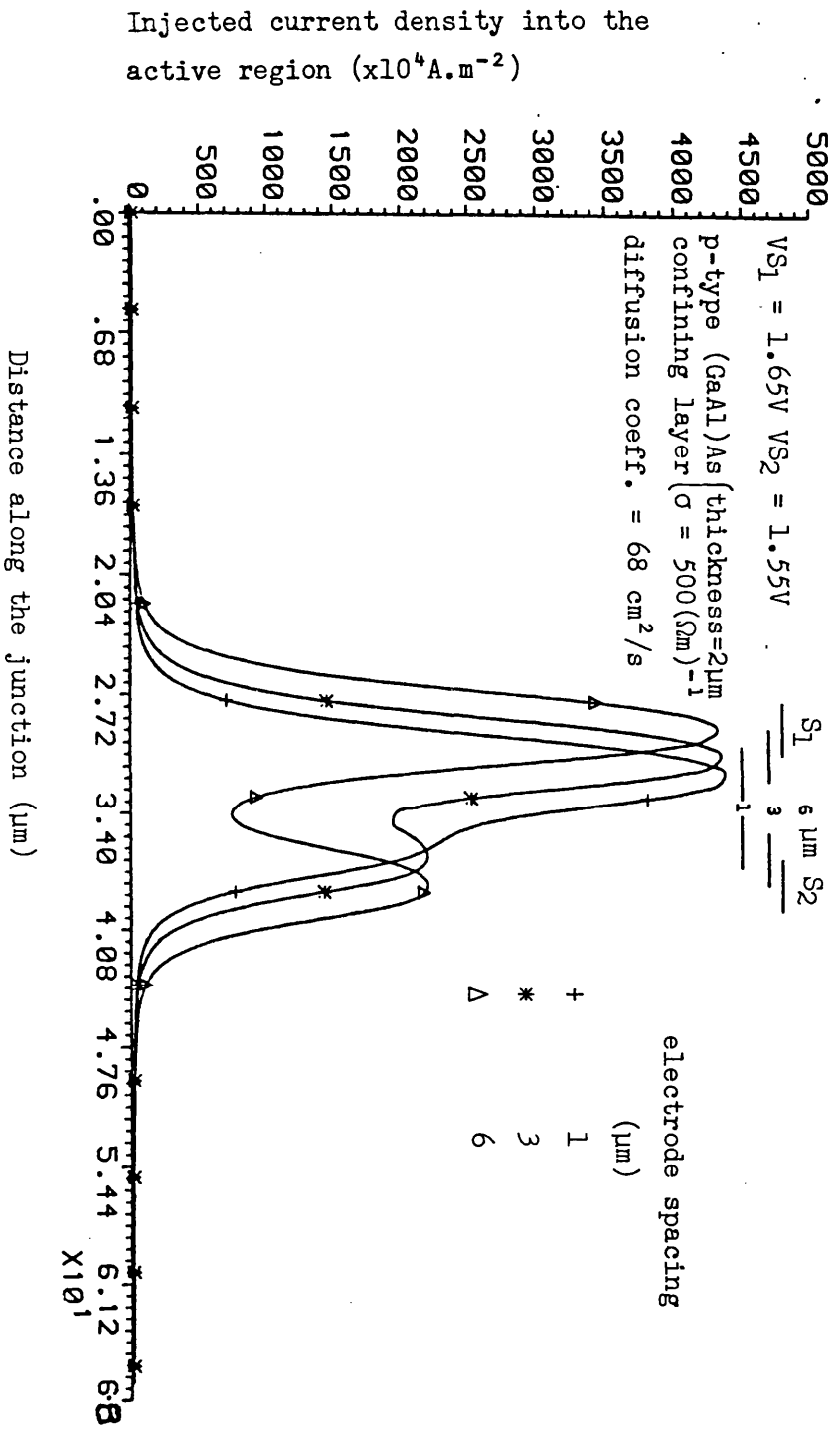

Figure 7.5.2-1a The effect of electrode spacing on current density injected into the active layer of an asymmetrically pumped twin stripe laser.

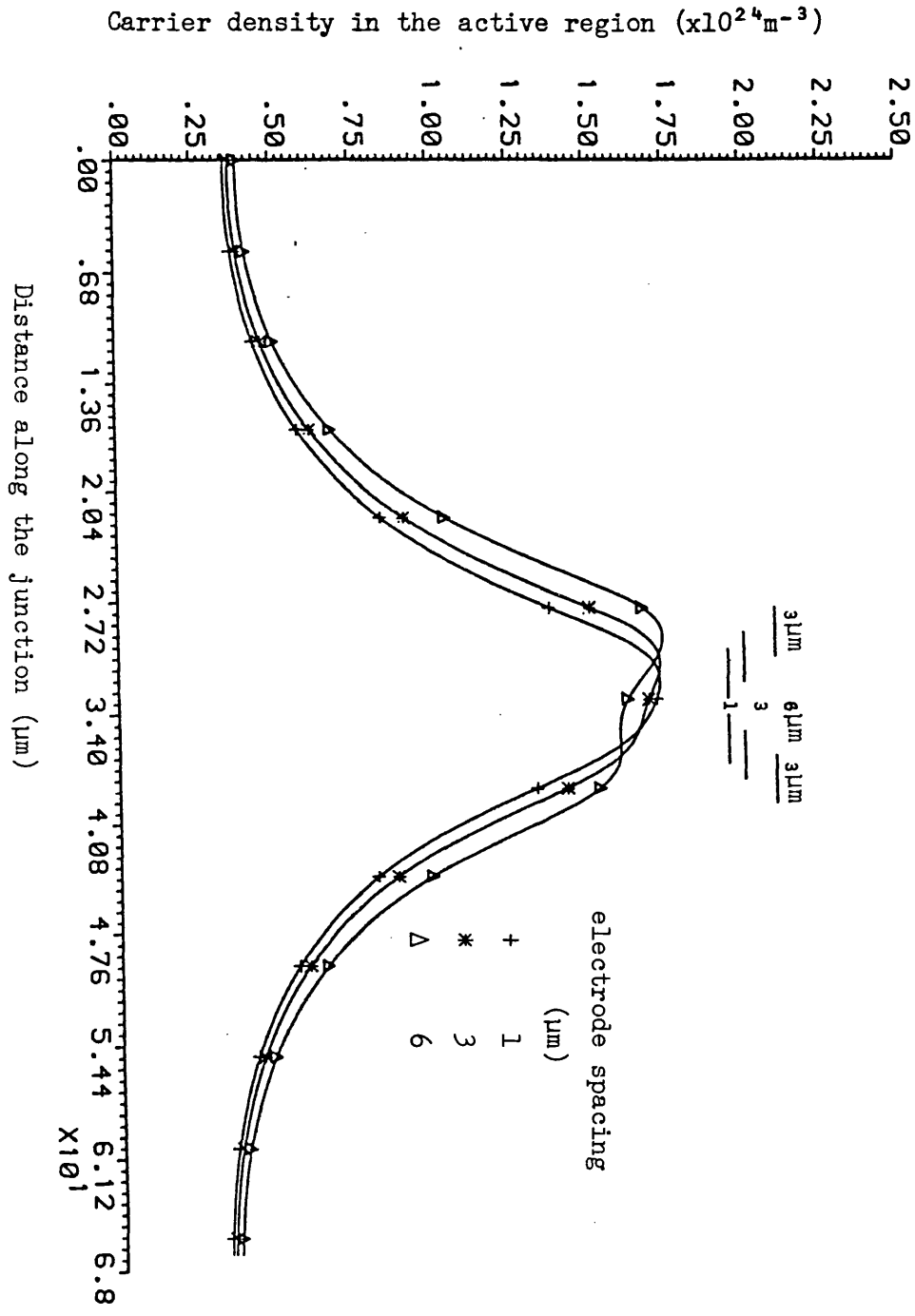

Figure 7.5.2-1b Effect of electrode spacing on carrier density distribution of an asymmetrically pumped twin stripe laser.

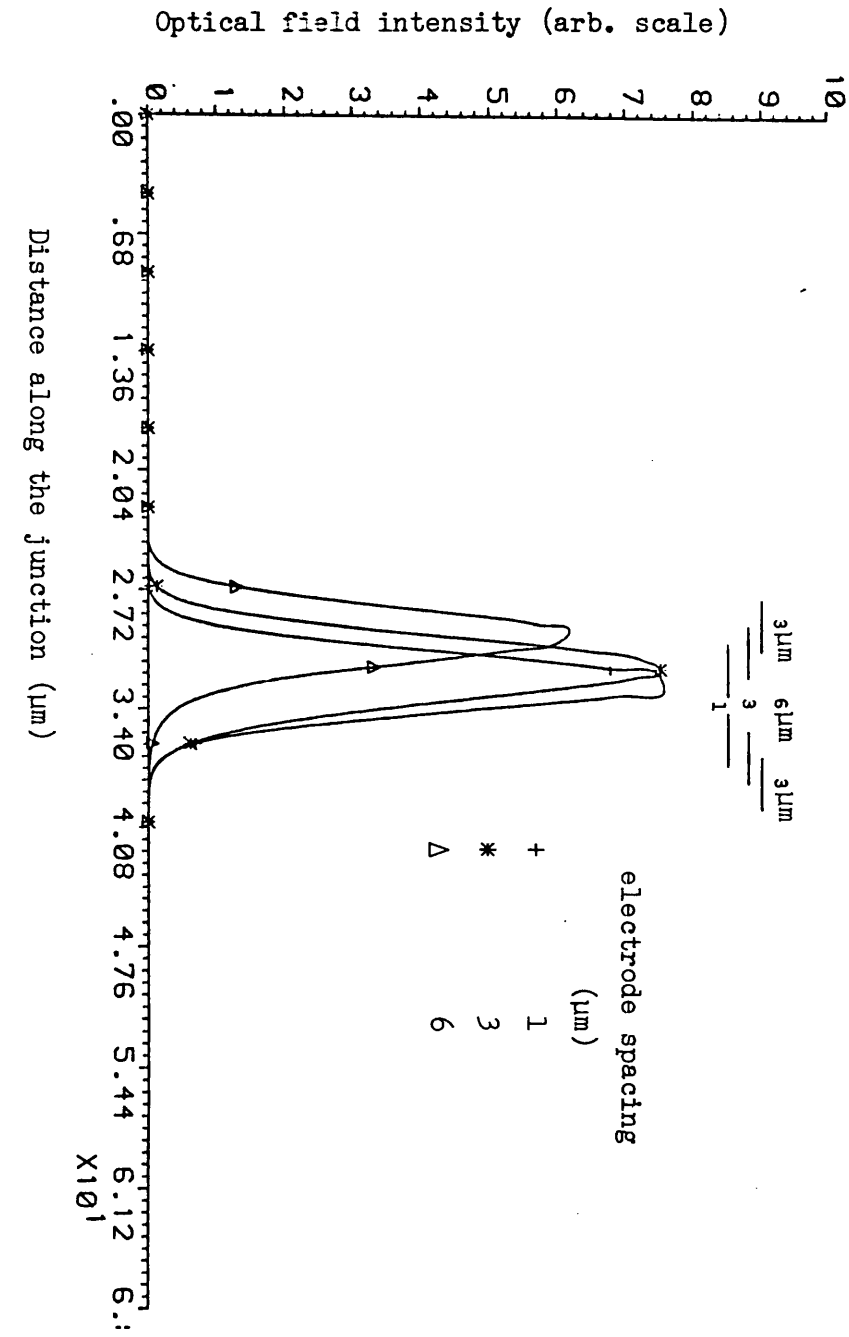

Figure 7.5.2-1c The effect of electrode spacing on field distribution of a twin stripe laser corresponding to the injected current density distribution shown in figure 7.5.2-1a.

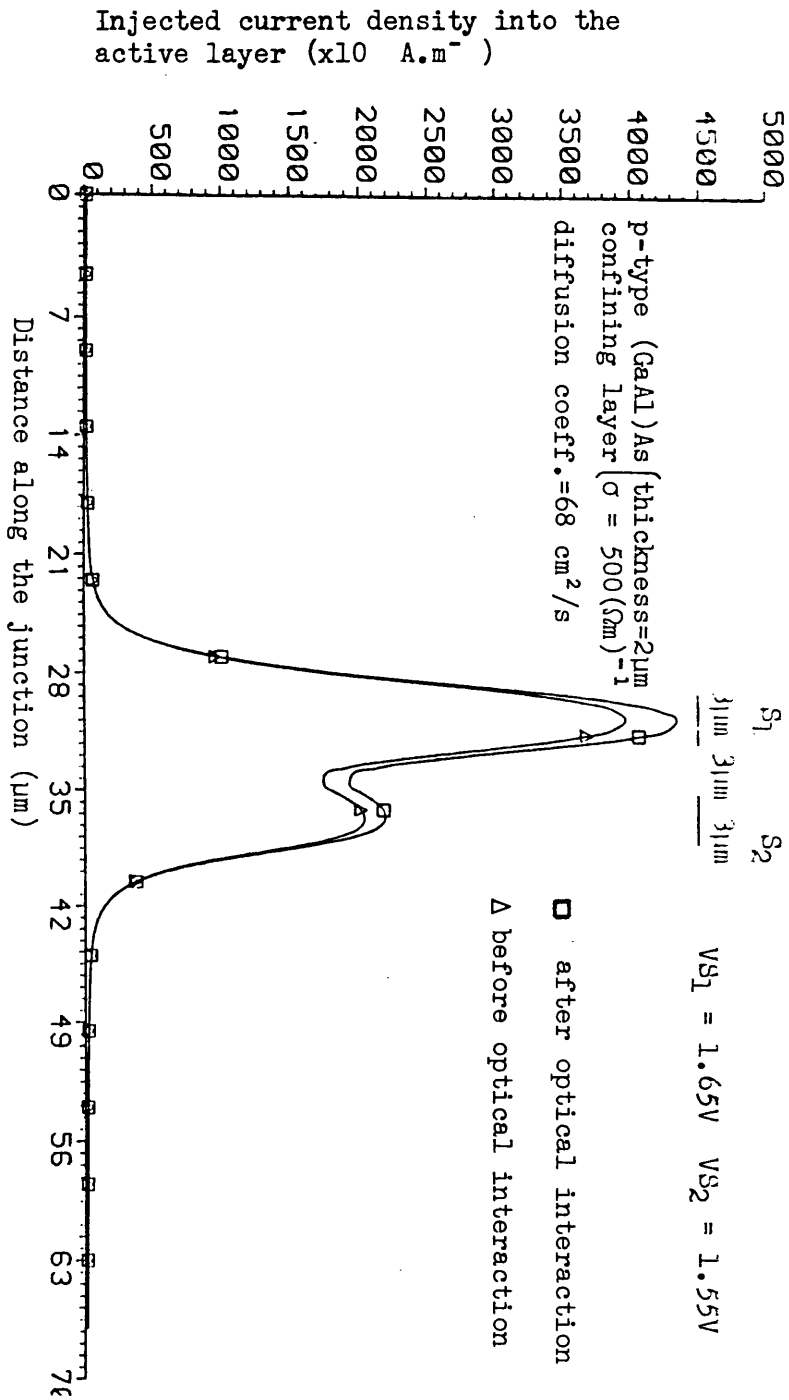

Figure 7.5.2-2 The effect of optical interaction on the injected current density distribution of a twin stripe laser under asymmetric pumping condition.

further worsened if the device is symmetrically pumped.

7.5.3 Effect of the carrier diffusion coefficient

Figures (7.5.3-1a), (7.5.3-1b) and (7.5.3-1c) show the current density, carrier density and lateral field intensity distributions for the symmetrically pumped twin stripe laser with the standard value of diffusion cofficient, D_{amb} = 68 cm^2/s, used throughout this section. Similar set of results are shown in figures (7.5.3-2a), (7.5.3-2b) and (7.5.3-2c) when the diffusion coefficient is reduced to 20 cm^2/s. Figure (7.5.3-3) compares the light output vs. total injected current per unit device length characteristics for the two values of diffusion coefficient, D_{amb} = 68 cm^2/s and D_{amb} = 20 cm^2/s. It is immediately seen from this figure that the lower value of diffusion coefficient produces a lower value of threshold current. However, the region of the I/L characteristic over which the stable solutions are obtained is much smaller for the lower value of diffusion coefficient. The pumping conditions are indicated in figures (7.5.3-1a) and (7.5.3-2a). Instability in program occurs when the gain for the higher order mode approaches that of the fundamental mode. The reason for this is as follows. At low values of diffusion coefficient carrier spreading laterally in the active layer is low, and this also has an effect on current spreading. The net result is that the local gain g(x) is increased for the same value of stripe voltage as a device with a high diffusion coefficient, and therefore threshold occurs at a lower current. However, the increased gain ensures that modal instability will also occur at a lower current. It is seen that D_{amb} acts as a stabilising influence. The reason for this is that a large value of D_{amb} allows carriers to be replenished in a local region of exhaustion to a greater extent than with a small D_{amb}, as shown in figures (7.5.3-1b) and (7.5.3-2b). In other words, the carrier density dip in between the electrodes is less for high value of D_{amb}, and this

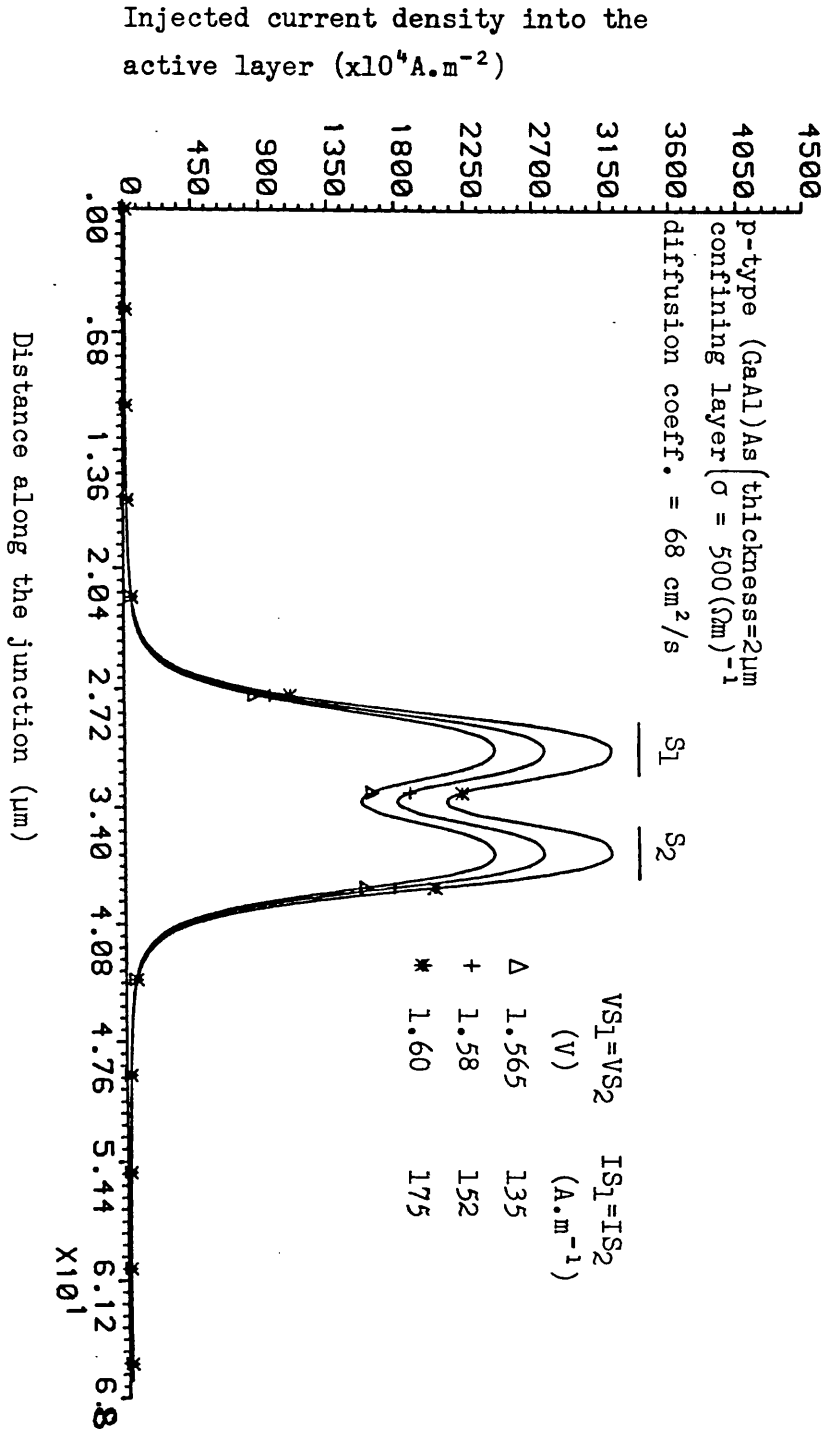

Figure 7.5.3-1a Effect of diffusion coefficient of a symmetrically pumped twin stripe laser on the injected current density into the active layer. The diffusion coefficient of the device is 68 cm^2/s. The corresponding carrier density and optical intensity distributions are shown in figures 7.5.3-1b and 7.5.3-1c respectively.

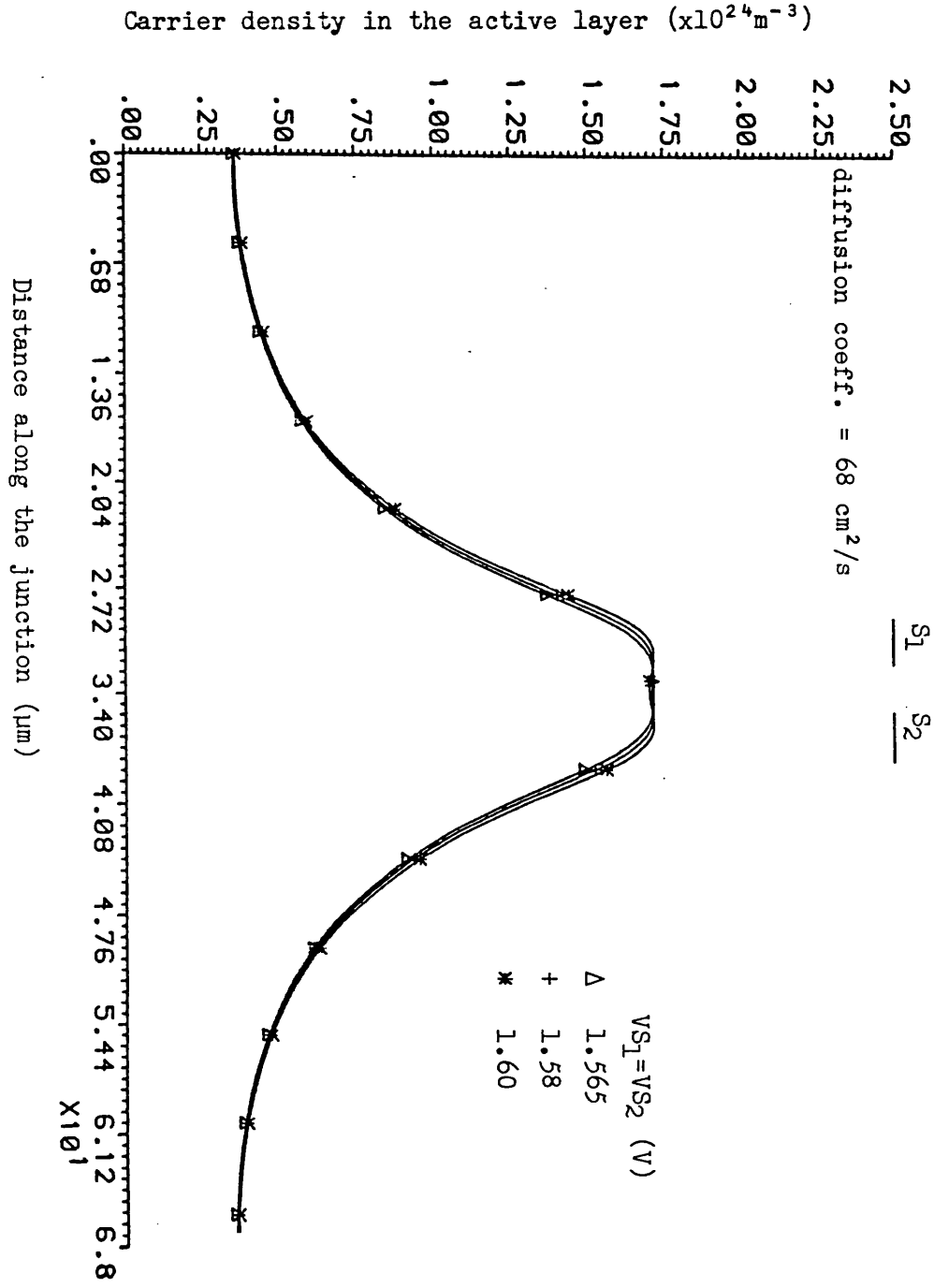

Figure 7.5.3-1b Carrier density distribution in the active layer of a symmetrically pumped twin stripe laser with diffusion coefficient D_{amb} = 68 cm^2/s.

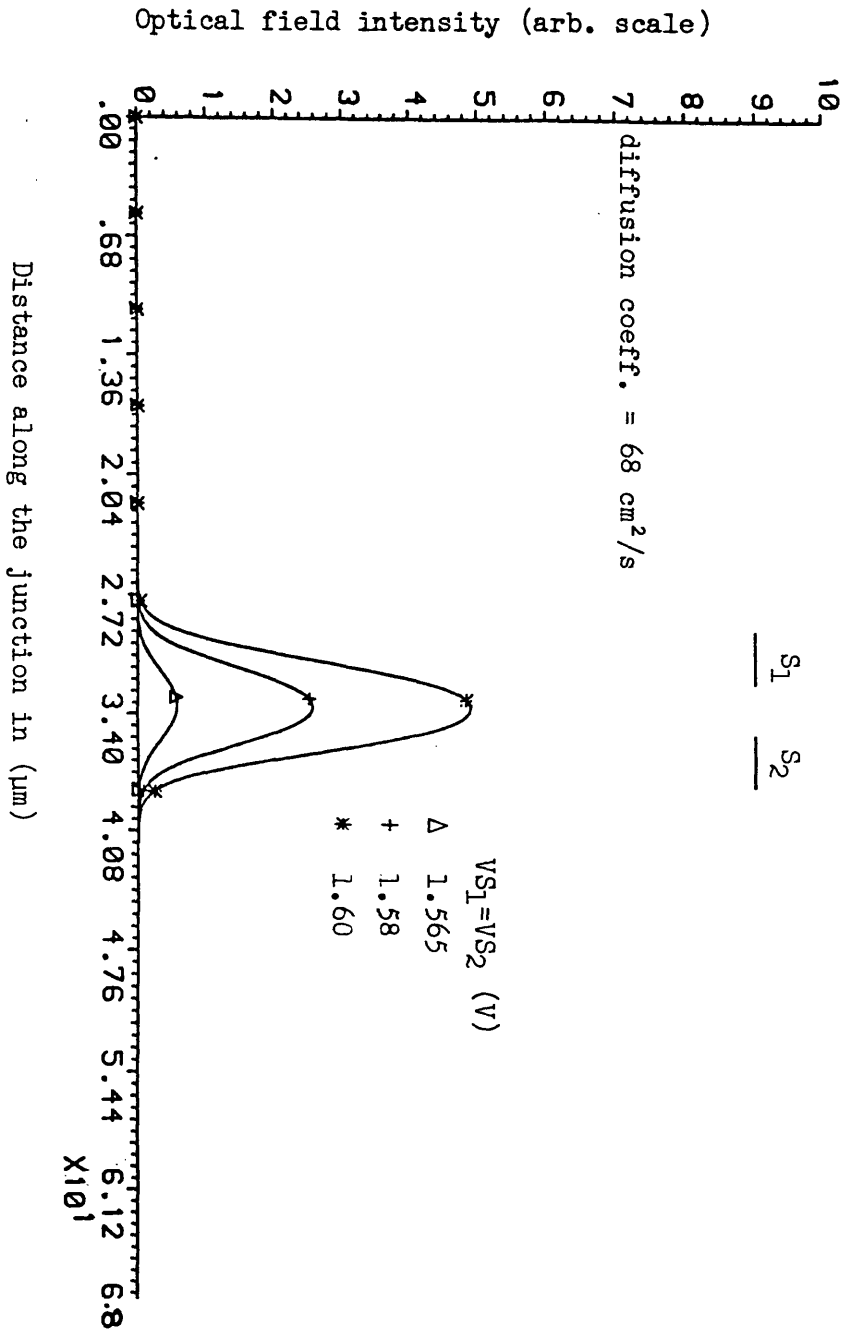

Figure 7.5.3-1c Lateral field intensity of a symmetrically pumped twin stripe laser when its diffusion constant is 68 cm^2/s.

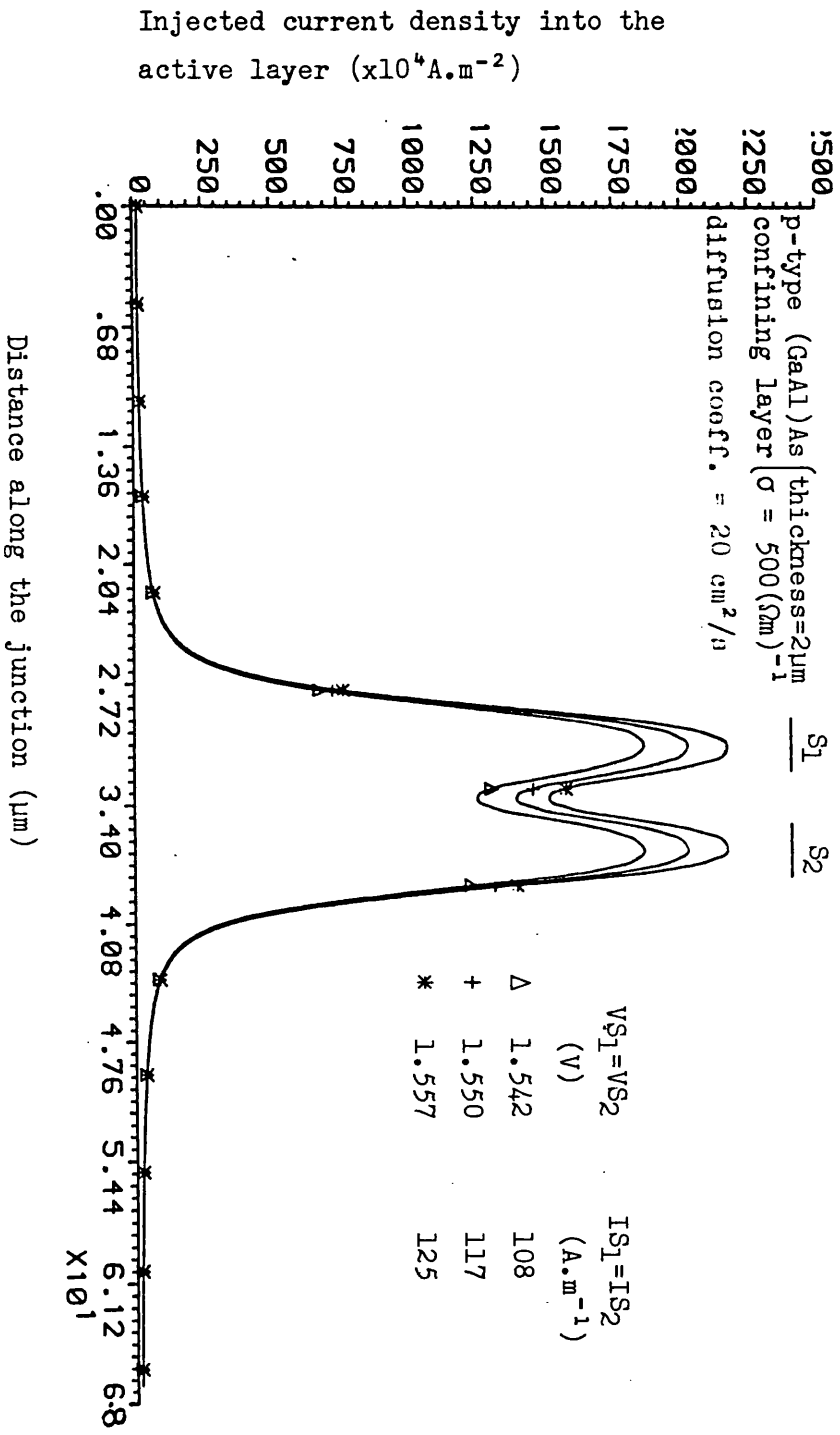

Figure 7.5.3-2a Injected current density distribution of a symmetrically pumped twin stripe laser when its diffusion constant is 20 cm²/s. The corresponding carrier density and intensity distributions are shown in figures 7.5.3-2b and 7.5.3-2c respectively.

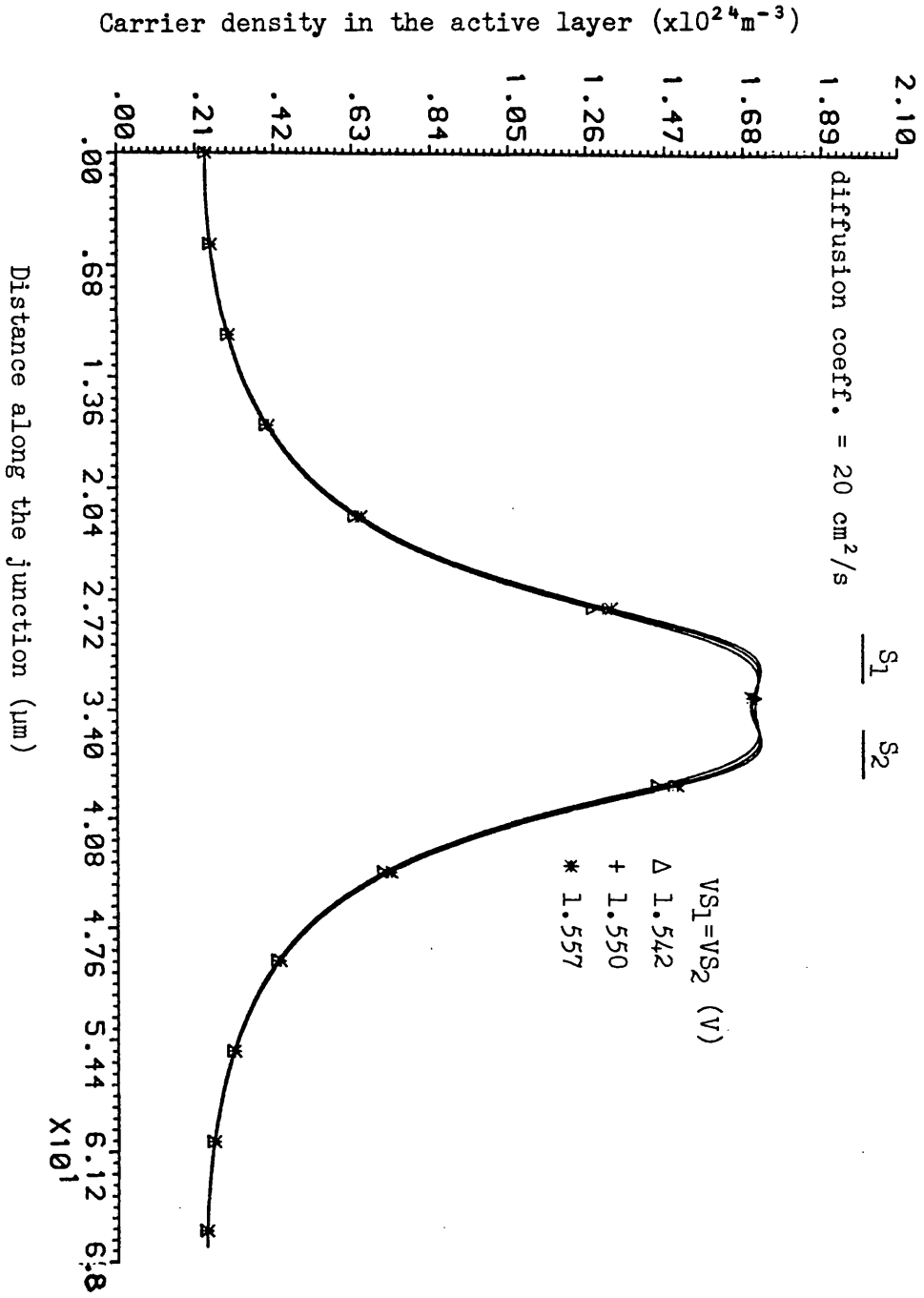

Figure 7.5.3-2b Carrier density distribution found consistent with the injected current density distribution shown in figure 7.5.3-2a of a twin stripe laser under symmetric pumping condition.

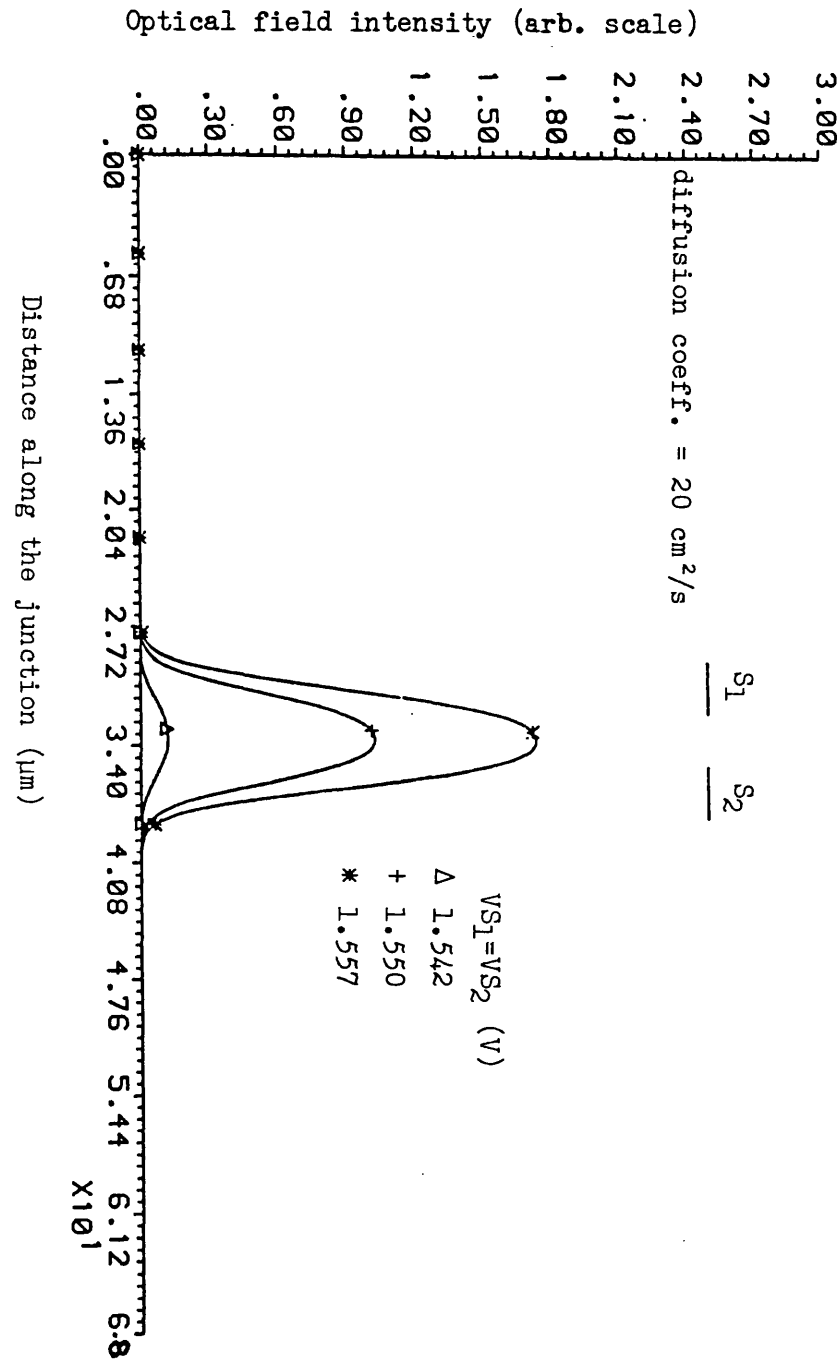

Figure 7.5.3-2c Optical field intensity of a symmetrically pumped twin stripe laser with diffusion coefficient D_{amb} = 20 cm^2/s.

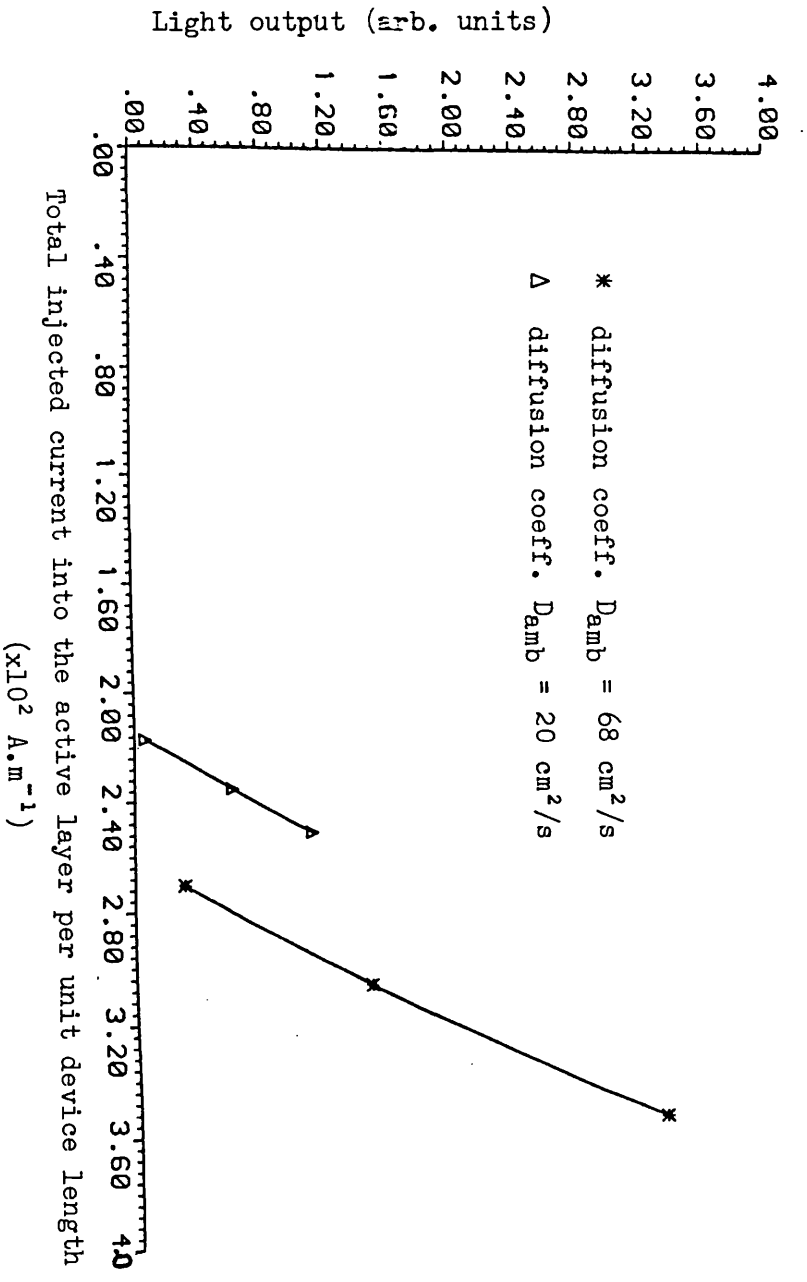

Figure 7.5.3-3 Comparison of I-L characteristics of a twin stripe laser under symmetric pumping conditions and with diffusion coefficient:

(*) 68 cm^2/s

(Δ) 20 cm^2/s

helps to prevent higher order modes from being generated due to the favourable carrier density distribution.

7.5.4 Effect of R

R has been defined in section (7.2.2) as the ratio of the change in the real part of the refractive index to the change in imaginary part of the refractive index. The solution $\psi(x)$ is very sensitive to the value of R (2,24,25) and largely determines the stability of a laser device because it sets the point at which gain guidance is dominated by index anti-guidance. R is commonly taken as a constant quantity varying from 0 (pure gain guidance) to 6. R can vary with carrier density and wavelength, but in a somewhat complex manner (24). Figures (7.5.4-1b) and (7.5.4-1c) show the effect of R on the carrier density distribution and intensity distribution for R = 2 and R = 6 under symmetrical pumping resulting in a symmetrical injected current distribution shown in figure (7.5.4-1a). When R = 6 the negative dependence of the real part of the refractive index on the carrier density is higher and therefore the dip in the carrier concentration gives rise to a larger peak in the real part of the refractive index relative to R = 2. This gives rise to a stronger self-focussing for the case when R = 6 and this is clearly seen by the field narrowing in figure (7.5.4-1c). This strong self-focussing leads to trapped radiation which produces strong hole burning at high flux values as shown in the carrier density distribution of figure (7.5.4-1b) and this destabilises the problem. It was found that the larger value of R resulted in the solution becoming unstable at a much lower value of current than for R = 2.

7.5.5 Effect of passive layer resistivity

Figures 7.5.5-1a,b,c show the injected current density distribution, the carrier density distribution and the field intensity distribution

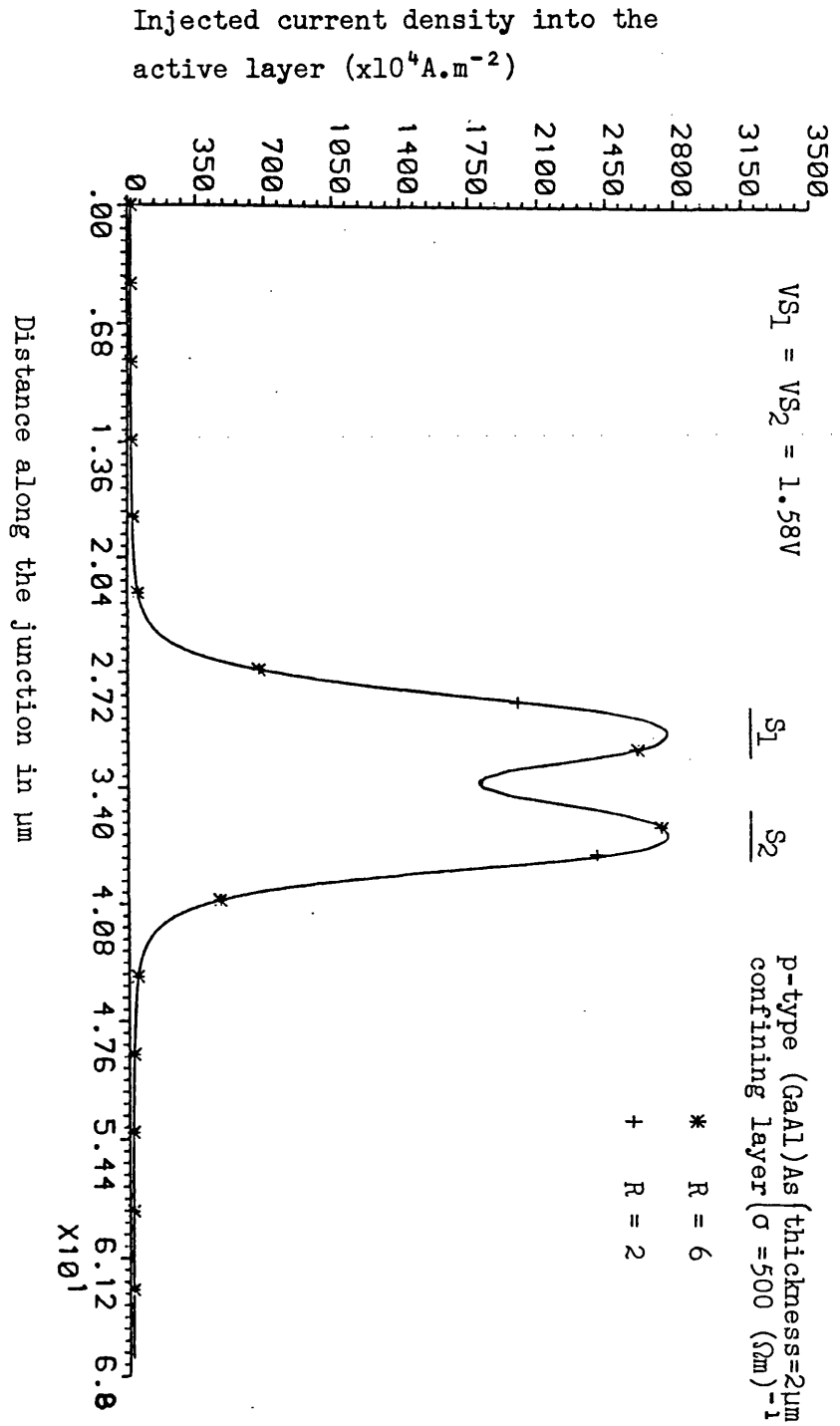

Figure 7.5.4-1a Effect of the coupling parameter R between index-guidance and gain-guidance, on the injected current density distribution under symmetrical pumping of a twin stripe laser.

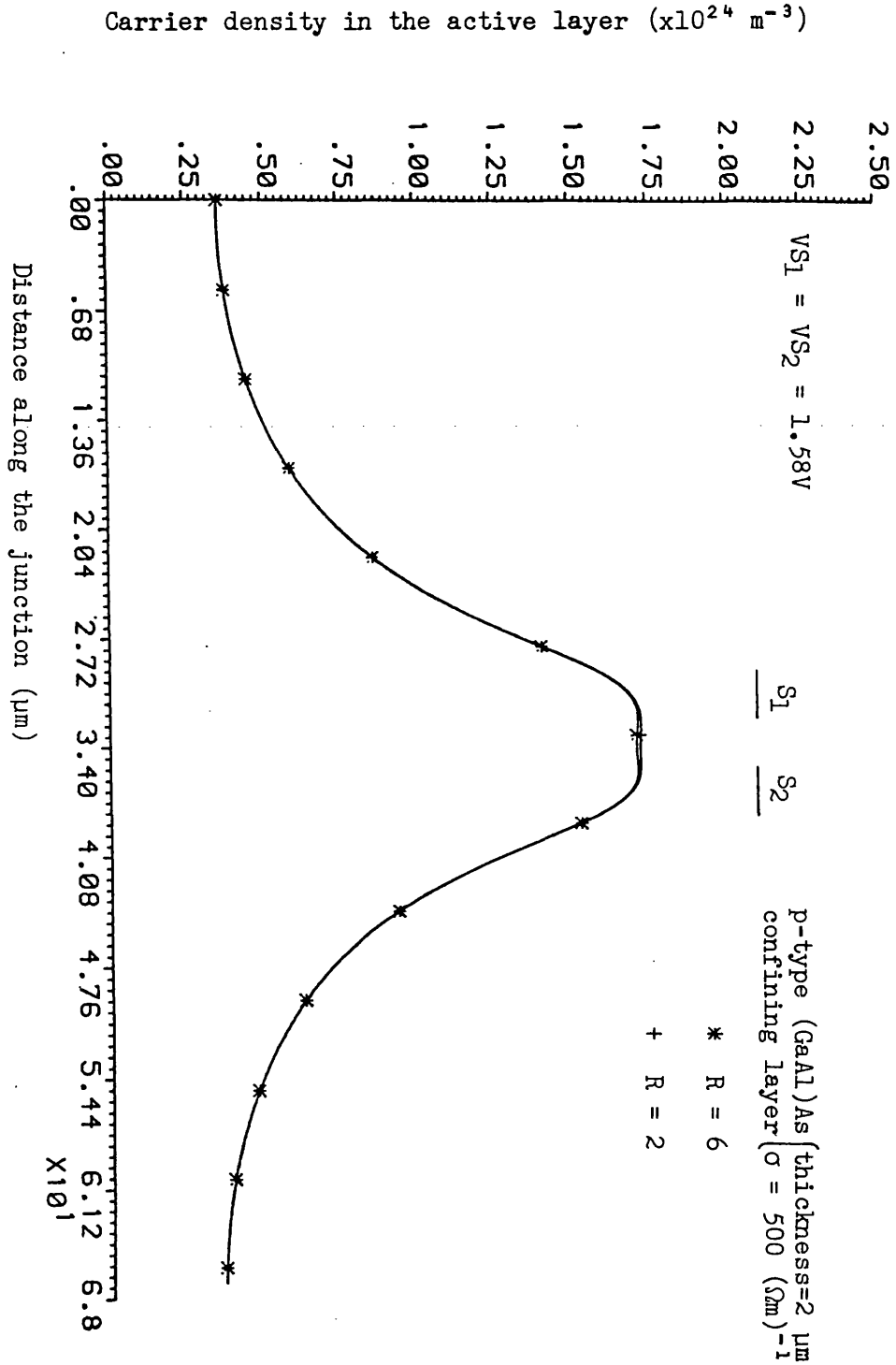

Figure 7.5.4-1b Effect of R on the carrier density distribution of a symmetrically pumped twin stripe laser.

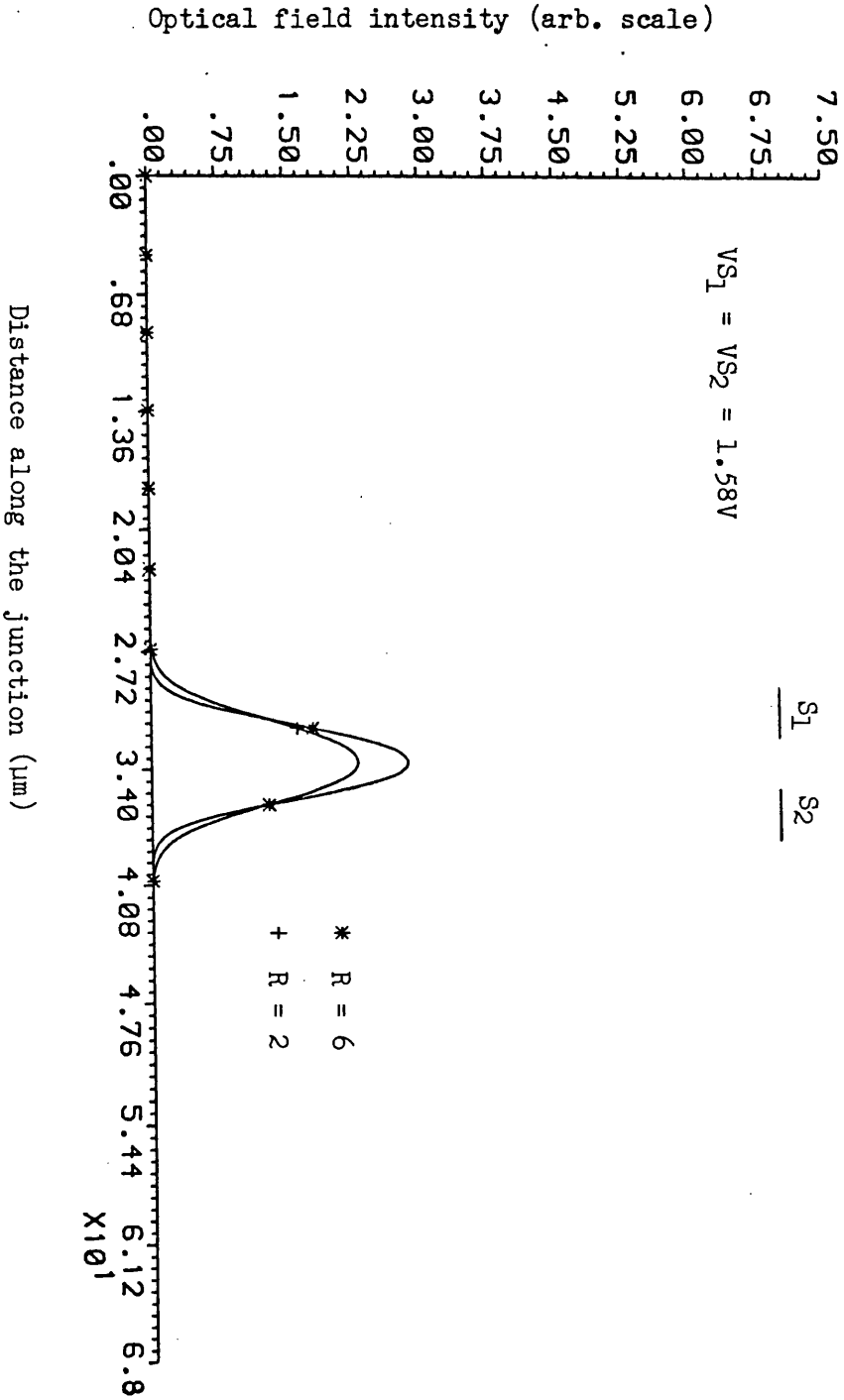

Figure 7.5.4-1c Effect of the coupling parameter R on the lateral field intensity of a symmetrically pumped twin stripe laser demonstrating self-focussing effect as R increases.

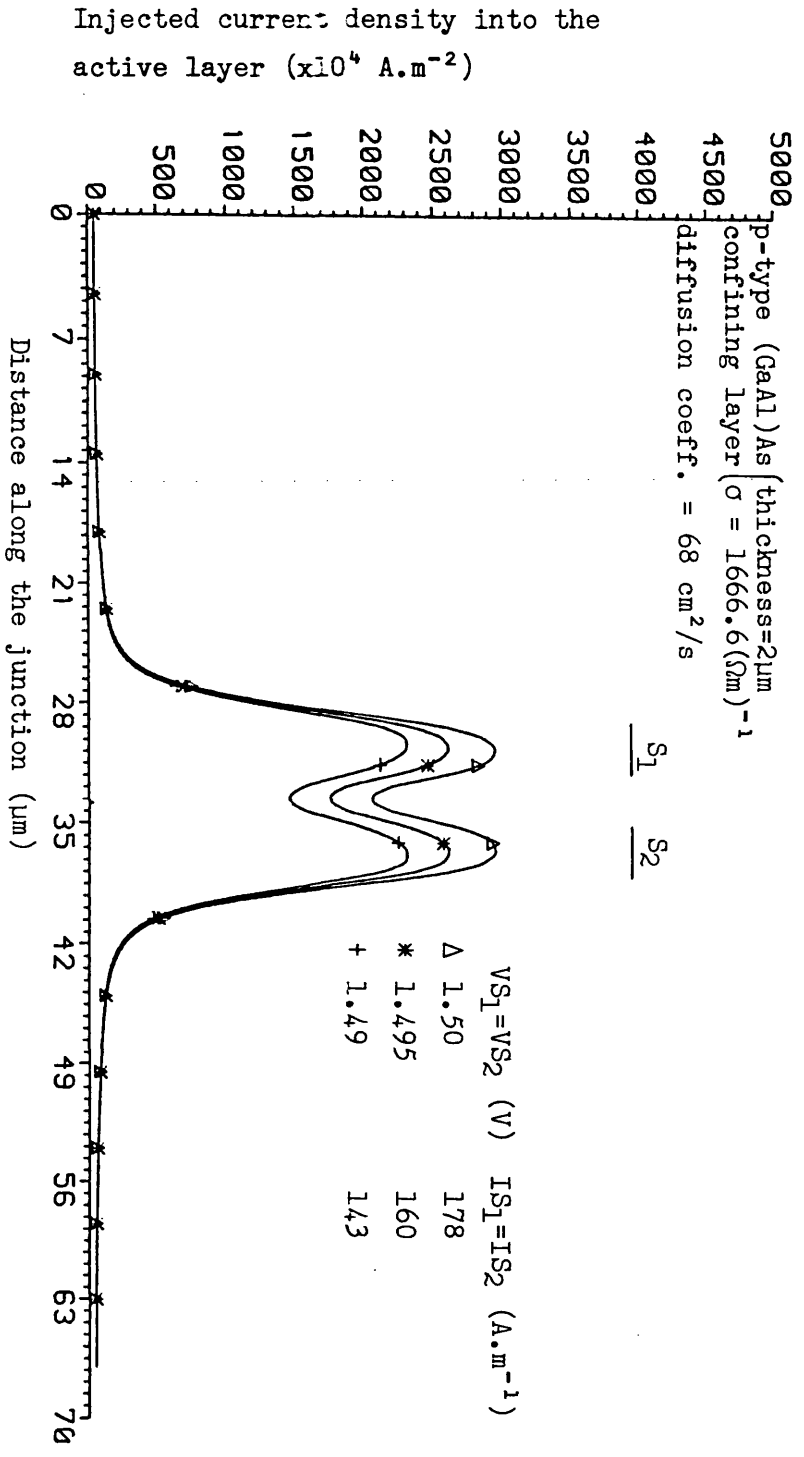

Figure 7.5.5-1a Injected current density distribution into the active layer of a twin stripe laser with conductivity of the confining layer 1666.6 $(ohm.m)^{-1}$, 2.0μm thick under symmetric pumping conditions.

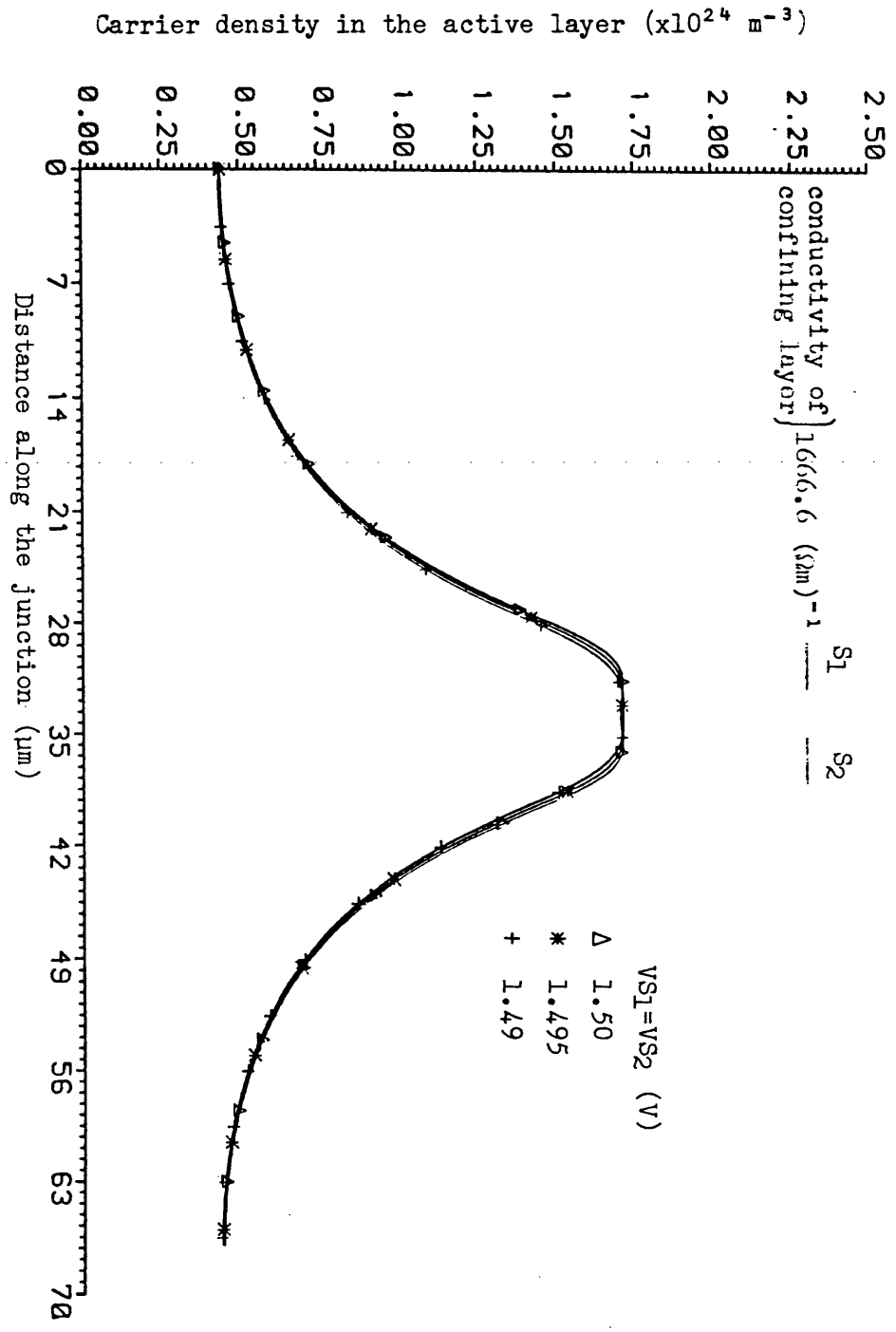

Figure 7.5.5-1b Carrier density distribution in the active layer of a twin stripe laser whose confining layer is 2.0μm thick with conductivity 1666.6 $(ohm.m)^{-1}$ under symmetric pumping conditions.

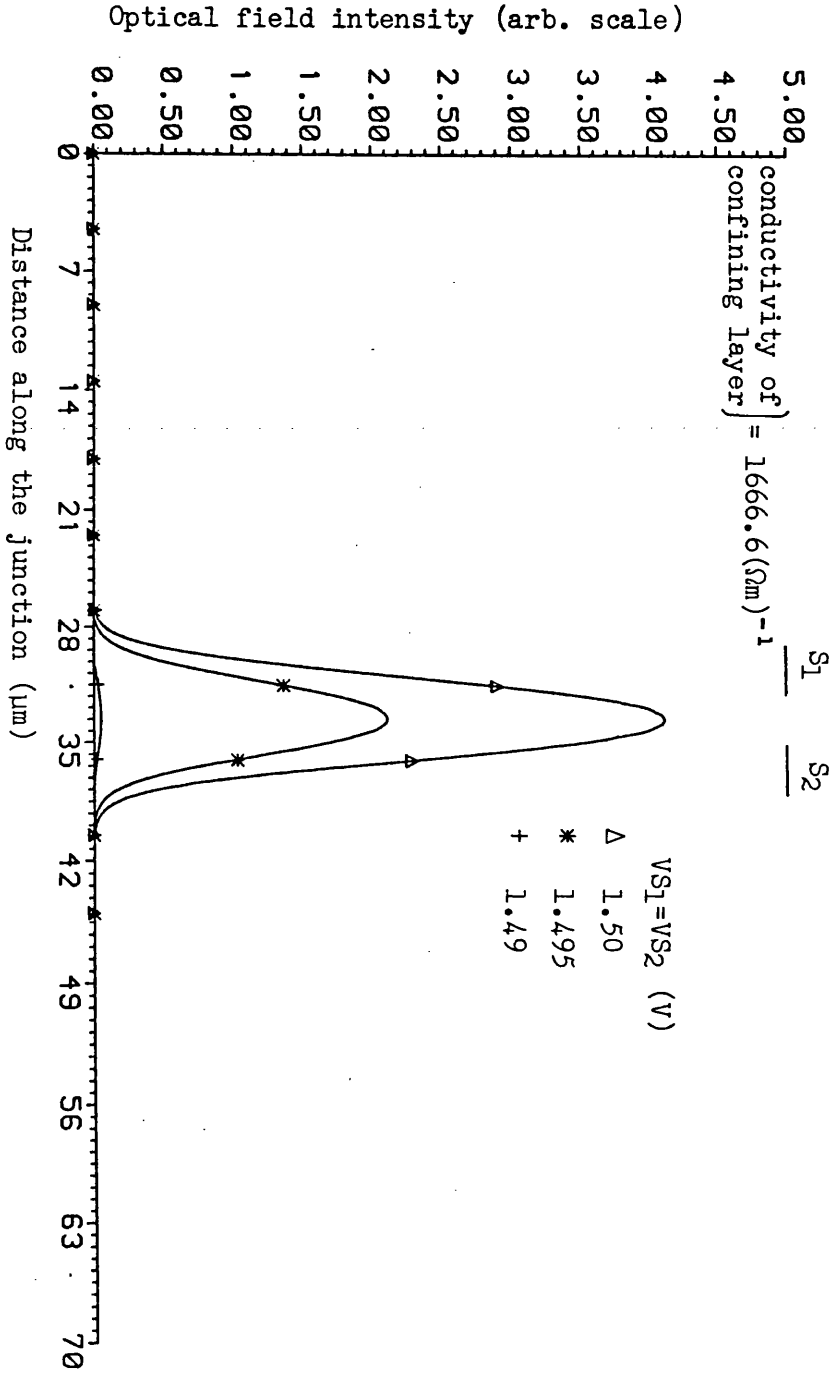

Figure 7.5.5-1c Optical field intensity of a twin stripe laser whose confining layer conductivity is 1666.6 $(ohm.m)^{-1}$ and is symmetrically pumped.

for the symmetrically pumped twin stripe laser with the (AlGa)As confining layer resistivity as 0.6 ohm.cm (or σ = 1666.6 $ohm^{-1}.m^{-1}$) for three different values of pumping current. Similar set of graphs are shown in figures 7.5.5-2a,b,c when the resistivity of the confining layer is increased to 0.6 ohm.cm (σ = 166.6 $ohm^{-1}.m^{-1}$). Analogous to the single stripe case discussed in section (7.4.1), the threshold voltage increases from $VS_1=VS_2=1.49V$ to $VS_1=VS_2=1.79V$ as the resistivity is increased due to excessive ohmic voltage drop in the confining layer. It becomes clear from figure (7.5.5-3a) that the current spreading beyond the stripe edges is reduced when the resistivity of the confining layer is increased. As seen in section (7.4.1) of the single stripe laser, the gradient of carrier concentration near the stripe edges is relatively steep when the resistivity of the confining layer is high as shown in figure (7.5.5-3b), and thus the lateral field guidance is improved. Consequently, although one gains in stability of the device by increasing the resistivity of the confining layer it happens at the cost of excessive heat generation in the resistive layer due to ohmic loss.

7.6 Conclusions

The chapter has outlined a numerical technique for the self-consistent modelling of single and twin stripe laser devices. The results have shown that beam-steering of the optical near field results when the electrodes are pumped asymmetrically. The results show that under strong pumping conditions it is not possible to steer the beam past the centre of the device (between the electrodes) when the electrodes are symmetrically pumped because of modal instability. It is believed that the computer instability is predicting bistability, which requires further investigations.

The diffusion coefficient has also been shown to play an important role in determining the stability of the device. Unlike a single stripe laser,

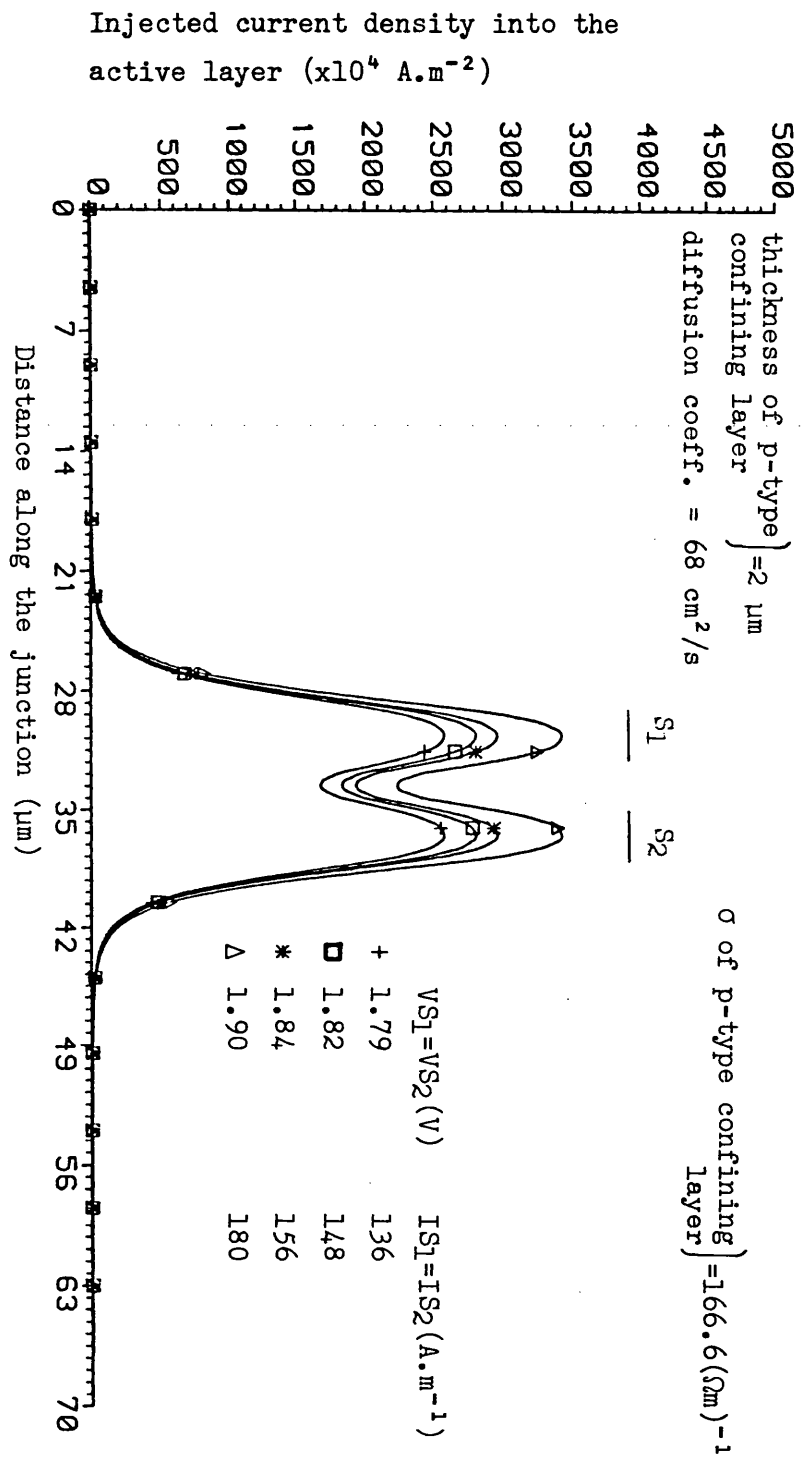

Figure 7.5.5-2a Current density distribution injected into the active layer of a twin stripe laser whose confining layer thickness and conductivity are 2.0μm and 166.6 $(ohm.m)^{-1}$ respectively, under symmetric pumping conditions.

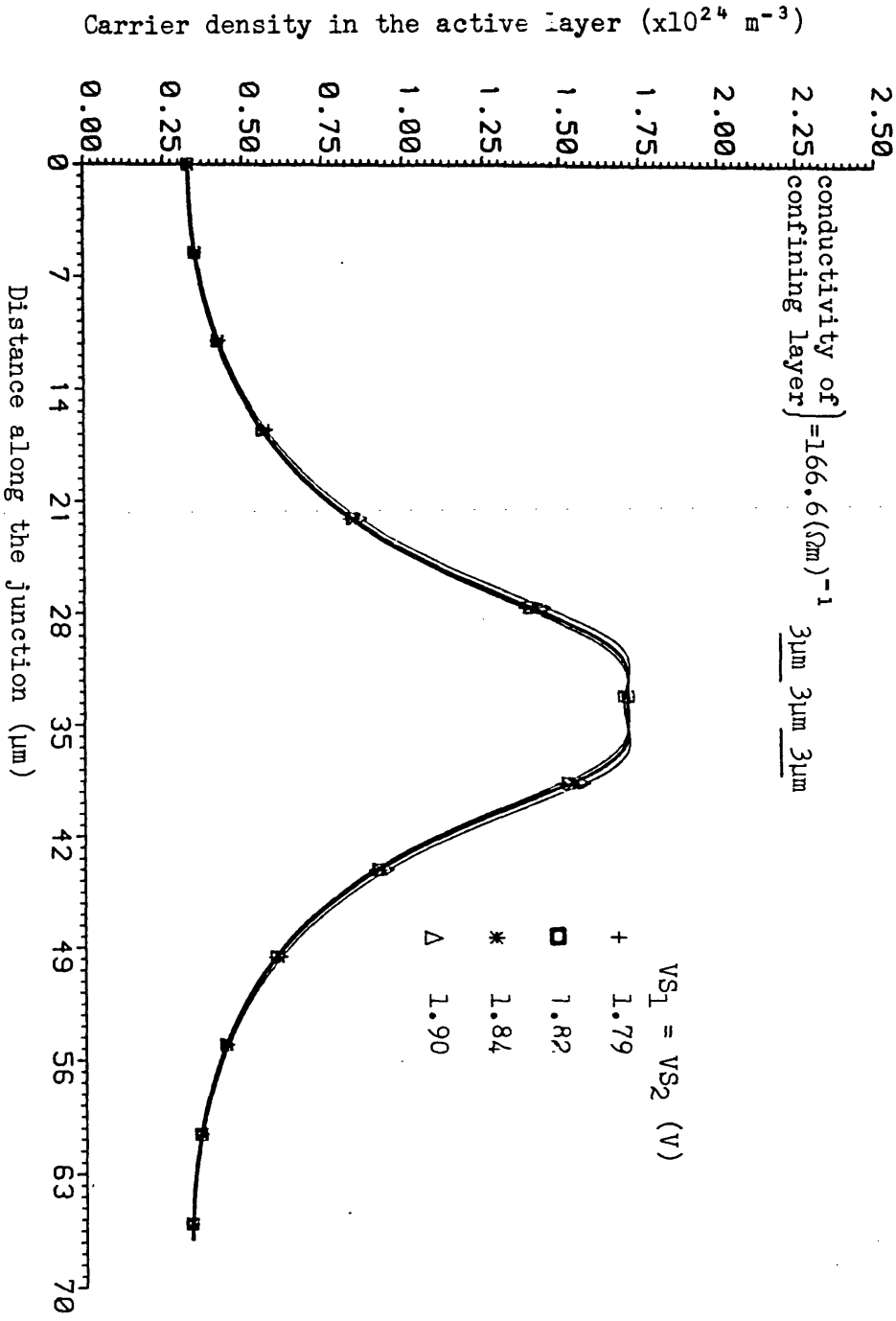

Figure 7.5.5-2b Carrier density in the active layer of a twin stripe laser whose confining layer 2.0 μm thick has conductivity 166.6 $(ohm.m)^{-1}$ and the device is symmetrically pumped.

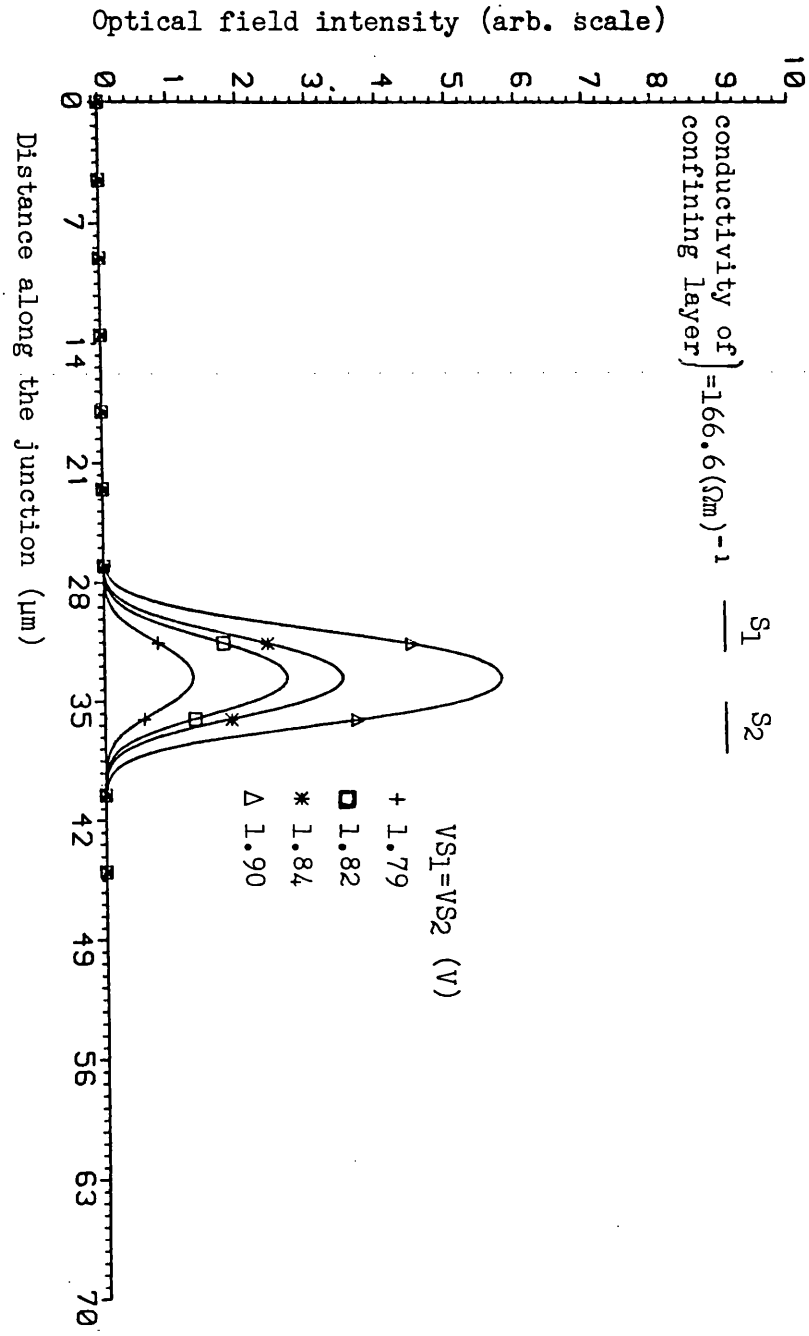

Figure 7.5.5-2c Optical field intensity distribution under symmetric pumping condition of a twin stripe laser with 2.0μm thick confining layer possessing conductivity as 166.6 $(\Omega.m)^{-1}$

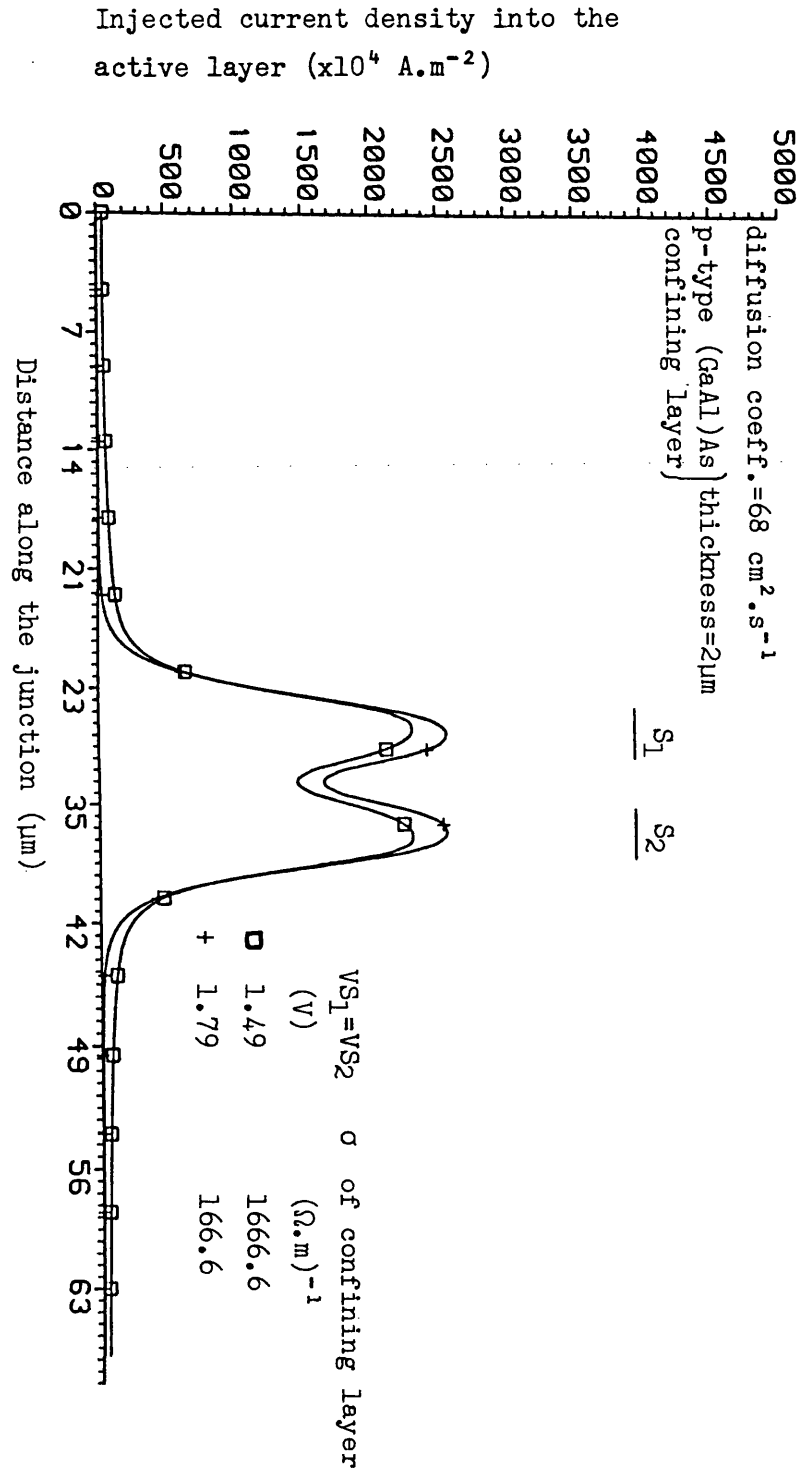

Figure 7.5.5-3a Comparison of the injected current density into the active layer of a twin stripe laser just above threshold when the conductivity of the confining layer is

(□) 1666.6 $ohm^{-1}.m^{-1}$

(+) 166.6 $ohm^{-1}.m^{-1}$

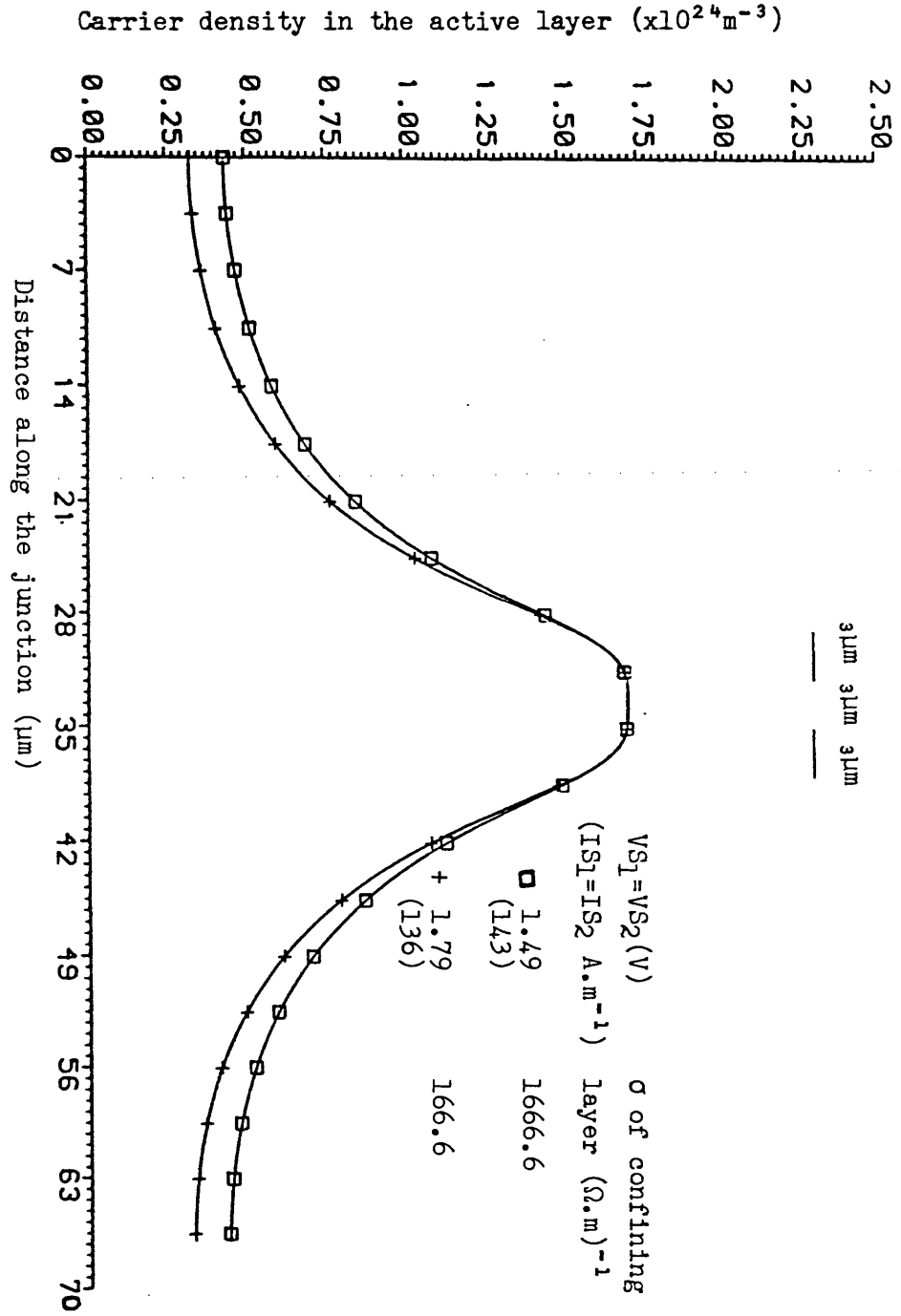

Figure 7.5.5-3b Comparison of the carrier density in the active layer of a twin stripe laser just above threshold when the conductivity of the confining layer is

(□) 1666.6 ohm^{-1}.m^{-1}

(+) 166.6 ohm^{-1}.m^{-1}

there exists a dip in the carrier density distribution corresponding to the gap in between the two electrodes. If the diffusion coefficient is low the threshold current is lower because of reduced current spreading and improved lateral carrier confinement. However, the dip in the carrier density distribution is quite significant and helps to destabilise the solution at a lower value of pumping current than for large values of diffusion coefficient.

If the device is pumped symmetrically and the spacing between the two electrodes is increased the dip in carrier density worsens and causes modal instability to occur at much reduced pumping current. However, if the device is pumped asymmetrically with the increased spacing between the electrodes the stability situation improves while the coupling between the electrodes weakens due to reduced injection of carriers from the low pumped electrode. It is also shown that the resistivity of the confining layer not only affects the current spreading in the confining layer but also plays an important role in stabilising the device behavicur. The parameter R is also seen to have an important effect on stability.

References

1. K.A. Shore, T.E. Rozzi and G.H. In'tVeld: "Semiconductor laser analysis: general method for characterising devices of various cross-sectional geometries", IEE Proc., Vol.127, Pt. I, No.5, pp.221-229, 1980.

2. J. Buus: "Models of the static and dynamic behaviour of stripe geometry lasers", IEEE J. Quantum Electron., Vol. QE-19, pp.953-960, 1983.

3. S. Wang, C. Chen, A. Liao and L. Figueroa: "Control of mode behaviour in semiconductor lasers", IEEE J. Quantum Electron., Vol. QE-17, pp.453-467, 1981.

4. W. Sreifer, R.D. Burnham, and D.R. Scifres: " Channeled substrate non-planar laser analysis part I- formulation and the plano-convex waveguide laser", IEEE J. Quantum Electron., Vol QE-17, pp.736-744, 1981.

5. R.P. Brouwer, C.H.F. Velzel and B.S. Yeh: "Lateral modes and self-oscillations in narrow stripe double heterostructure GaAl-As injection lasers", IEEE J. Quantum Electron., Vol. QE-17, pp.694-700, 1981.

6. C.Z. Guo and K.G. Wang: "Intrinsic pulsation in stripe-geometry DH semiconductor lasers", IEEE J. Quantum Electron., Vol. QE-18, pp.1728-1737, 1982.

7. R. Lang: "Lateral transverse mode instability and its stabilisation in stripe geometry injection lasers", IEEE J. Quantum Electron., Vol. QE-15, pp.718-726, 1979.

8. M. Ueno, R. Lang, S. Matsumoto, H. Kawano, T. Furuse, and I. Sakuma: "Optimum designs for InGaAsP/InP (λ = 1.3μm) planoconvex waveguide lasers under lasing conditions", IEE Proc., Vol.129, Pt.I, No.6, pp.218-228, 1982.

9. P.M. Asbeck, D.A. Cammack, J.J. Daniele and V. Klebanoff: "Lateral mode behaviour in narrow stripe lasers", IEEE J. Quantum Electron., Vol. QE-15, pp.727-733, 1979.

10. D.P. Wilt and A. Yariv: "A self-consistent static model of the double heterostructure laser", IEEE J. Quantum Electron., Vol. QE-17, pp.1941-1979, 1981.

11. K.A. Shore and T.E. Rozzi: "Near field control in multistripe geometry injection lasers", IEEE J. Quantum Electron., Vol. QE-17, pp.718-722, 1981.

12. W.B. Joyce: "Carrier transport in double-heterostructure active layers", J. Appl. Phys. Vol.53(11), pp.7235-7239, 1982.

13. T. Kumar, R.F. Ormondroyd and T.E. Rozzi: "Interstripe coupling and current spreading in a sub-threshold double heterostructure twin-stripe laser", IEEE J. Quantum Electron., Vol. QE-20, pp.364-373, 1984.

14. T. Kumar, R.F. Ormondroyd and T.E Rozzi: "Numerical solution of lateral current spreading and diffusion in near threshold DH twin-stripe lasers", IEEE J. Quantum Electron., May, 1985 (in press).

15. W.B. Joyce: "Analytic approximations for the Fermi energy of an ideal Fermi gas", Appl. Phys. Lett., Vol.31, No.5, pp.354-356, 1977.

16. A. Wexler: "Computation of electromagnetic fields" IEEE Trans. on Microwave Theory and Techniques, MTT-17, pp.416-439, 1969.

17. R.S. Martin and J.H. Wilkinson: "The modified LR algorithm for complex Hessenberg matrices", Numer. Math. 12, pp.369-376, 1968.

18. J.H. Wilkinson: "The algebric eigenvalue problem", Oxford University Press, London, 1965.

19. G. Lengyel, P. Meissner, E. Patzak and K.H. Zschauer: "An analytic solution of the lateral current spreading and diffusion problem in a narrow oxide stripe (GaAl)As/GaAs DH lasers", IEEE J. Quantum Electron., Vol. QE-18, pp.618-625, 1982.

20. K.A. Shore: "Above-threshold current leakage effects in stripe-geometry injection lasers", Opt. and Quantum Electron., Vol.15, pp.371-379, 1983.

21. W.B. Joyce: "Role of the conductivity of the confining layer in DH laser spatial hole burning effects", IEEE J. Quantum Electron., Vol. QE-18, No.12, pp.2005-2009, 1982.

22. D.R. Scifres, W. Streifer and R.D. Burnham: "Beam scanning with twin-stripe injection lasers", Appl. Phys. Lett., Vol.38, No.8, pp.702-704, 1978.

23. I.H. White, J.E. Carroll and R.G. Plumb: "Closely coupled twin-stripe lasers", IEE Proc., Vol.129, Pt.I, No.6, pp.291-296, 1982.

24. K.A. Shore and T.E. Rozzi: "Stability analysis of transverse modes in stripe-geometry injection lasers", IEE Proc. Pt.I, Vol.128, No.4, pp.154-159, 1981.

25. W. Streifer, R.D. Burnham and D.R. Scifres: "An analytic study of (GaAl)As gain guided lasers at threshold", IEEE J. Quantum Electron., Vol. QE-18, No.5, pp.856-864, 1982.

CHAPTER VIII

CONCLUSIONS

8.1 Introduction

In chapter (V) the problem of coupling the electrodes of a twin stripe laser via the p-type (GaAl)As confining layer was considered for the case when lateral diffusion of carriers in the active layer was absent. The model was used to give an efficient, reasonably accurate, estimate of the terminal behaviour of the device, and estimates of the current density distributions in the active layer. It was observed that symmetrical pumping of the two electrodes lowered the threshold current density of the device. It was further seen how the electrical coupling between the electrodes was affected by the interstripe spacing, thickness and conductivity of the p-type (GaAl)As confining layer. The aspect ratio of the electrode width to the thickness of the p-type (GaAl)As layer was also found to be an important parameter affecting current confinement. In particular, it was shown that only 49% of the current injected into the electrode remained confined to the electrode width at (GaAl)As/GaAs heterojunction when the aspect ratio was 1.5, for a (GaAl)As thickness of 2 μm. The model also gave the potential distributions in the confining layer for the single and twin stripe lasers which confirmed strong current crowding at the edges of the electrodes and lateral current spreading. Current density distributions of current injected into the electrodes were also calculated which showed a highly non-uniform current density distribution.

It was apparent from this relatively simple model that the assumption of uniform current injection into the active layer beneath each electrode was not realistic and that because of the coupling of the electrodes via the resistive (GaAl)As layer considerable current was injected into the active layer between the electrodes.

In chapter (VI) the model of the twin stripe laser was refined to obtain the solution of the carrier density distribution in the active layer consistently with the current spreading in the confining layer. In this model, lateral diffusion of carriers was assumed to occur, and the density of carriers in active layer was controlled by the separation of the quasi-Fermi levels in the active layer. This was used as the link between the solution to Laplace's equation in the confining layer and the diffusion equation. It was found, from this model, that the carrier density distribution and injected current density distribution were now considerably different, because of the effect of lateral diffusion.

The effects of interstripe gap, thickness of the confining layer, diffusion coefficient and resistivity of the confining layer were examined. It was found that the effects of carrier diffusion and current spreading conspired to give extremely high levels of carriers in the active layer between the electrodes. Although the effect of diffusion had only a little effect on the current density distribution and the level of current injected into the electrodes, relatively large dips in the current density distribution between the electrodes were not matched by similar dips in the carrier density. In the case of high diffusion coefficients dips in the carrier density between the electrodes were found to be absent. This corresponds to the region of maximum local gain.

A feature of the analysis concerned the current density distribution of a single stripe laser. Here, dips were found in the injected current density distribution for relatively wide electrodes (relative to the thickness of the confining layer) and high values of diffusion coefficient. It was found that this dip in current density increased as the electrode width increased, and also as the diffusion coefficient was allowed to increase. The reason for this dip is due to several reasons —

i) current crowding giving a non-uniform current distribution at the electrode, and also at the active layer, ii) non-linearities along the heterojunction and iii) carrier diffusion.

This refined model was found to give an accurate estimate of current density and carrier density distributions of the laser upto threshold, where the density of stimulated photons is small. Above threshold, however, the interaction of the optical field with the carriers in the active layer must be included. This can be inculded in the diffusion equation describing the carriers in the active layer via a stimulated recombination term.

The fully self-consistent model of the lateral behaviour of the optical modes of a twin stripe laser was presented in chapter (VII). In this chapter it was seen that under a wide variety of conditions of a symmetrically pumped twin stripe laser the optical field was strongly confined to the region between the electrodes, and of zero order fundamental mode. For the case of a single stripe laser the maximum optical intensity is directly beneath the centre of the electrode, and again for a wide range of conditions the optical field has a zero order fundamental modal shape. In this case gain guiding was seen to be a predominant wave guiding mechanism. However, although gain guiding is also a strong mechanism in the twin stripe laser, the shallow dips in carrier density corresponding to the interstripe gap – reinforced by stimulated recombination – also gave a self-focussed mode. It was seen that as the stripes were driven asymmetrically beam steering of the optical near field was observed. The optical field remained zero ordered throughout the beam movement. Under some conditions the beam was seen to move over a wide lateral distance between the electrodes. However, if the electrode potential VS_1 was varied keeping the potential VS_2 fixed

just at threshold, it was not possible to move the beam beyond the symmetrical position. For the case where $VS_1 = VS_2$ where injected current was well above threshold the zero order mode became progressively less stable as the the injected current increased due to the competing higher order mode. It was found that as the electrode spacing was increased relatively large dips in the carrier density were observed. This led to less stable fundamental mode solution and favourable conditions for higher order mode.

A well known kink in the light/current characteristic was seen to occur at a higher level of light output in a device with a larger resistivity of the confining layer but this occurred at the cost of increased ohmic loss in the confining layer. In contrast to the consistent solution of carrier and field distributions for a fixed generation rate (the solution corresponding to a fixed injected current density distribution which was responsible for the generation of carriers) the injected current density was found to increase above threshold in this model due to the stimulated recombination and therefore generation rate would increase which would raise the level of the light output at which the kink in light/current characteristic should appear.

8.2 Further Suggestions

Currently, many research workers are engaged in the research of multiple stripe lasers (1 - 6). It will be worth a while therefore to extend the model further to extract useful informations. One obvious extension of the static steady state state consistent model is to analyse the dynamic behaviour of the twin stripe laser which is believed to give a valueable information of the device behaviour. Recently Shore (7) has reported the effect of optical injection under one of the stripes for different injection currents. He has shown the rotation in the far field of the

device by the optical injection. He has used in his analysis closed form expressions for the injection current distributions based upon the approximations for the current spreading in the confining layer. It may be useful to analyse this effect fully consistently, allowing the injection of light into the active layer as a further controlling parameter. One of the obvious advantages of the beam scanning by optical injection over that of electronic injection would be the fast response of the device. Further research interests in the development of high power phase-locked laser arrays become evident from the recent publications (8 - 11). Levine et al (3) had investigated experimentally the interaction between only two lasers where each laser had its separate contact. The coupling between the two lasers was demonstrated by them by the formation of optical fringes produced by the interference of radiating modes. Kapon et al (6) have reported similar interference patterns between the two adjacent gain-guided lasers due to the interference of radiating modes. They have further pointed out that these effects are less important in the case of index-guided laser due to negligible curvature in the wavefront of the lateral radiating modes of the two adjacent lasers. Kapon et al (5) have used Cosh^{-2} gain distribution to calculate the near field of each individual laser element of the coupled array. It may be useful to extend the consistent model of the twin stripe laser to that of an array of laser elements.

Further work which needs to be done is the extension of the model to include the possibility of allowing two modes to coexist stably by including the effect of stimulated radiation and a more sophisticated solution to the optical problem. The model could also be extended to include the time dependent solution of the optical field so that a detailed investigation of modal instability can be made for a wide range of operating conditions.

References

1. D.R. Scifres, R.D. Burnham and W. Streifer: "High power coupled multiple stripe quantum well injection lasers", Appl. Phys. Lett., 42(2), pp.118-120, 1982.

2. D.R. Scifres, R.D. Burnham, C. Lindstrom, W. Streifer and T.L. Paoli: "Phase-locked (GaAl)As laser emitting 1.5W cw per mirror", Appl. Phys. Lett., 42(8), pp.645-647, 1983.

3. B.F. Levine, R.A. Logan, W.T. Tsang, C.G. Bethea and F.R. Merritt: "Optically integrated coherently coupled $Al_xGa_{1-x}As$ lasers", Appl. Phys. Lett., 42(4), pp.339-341, 1983.

4. E. Kapon, J. Katz, S. Margalit and A. Yariv: "Longitudnal-mode control in integrated semiconductor laser phased arrays by phase velocity matching", Appl. Phys. Lett., 44(2), pp.157-159, 1984.

5. E. Kapon, J. Katz, S. Margalit and A. Yariv: "Controlled fundamental supermode operation of phase-locked arrays of gain-guided diode lasers", Appl. Phys. Lett., 45(6), pp.600-602, 1984.

6. E. Kapon, C. Lindsey, J. Katz, S. Margalit and A. Yariv: "Coupling mechanism of gain-guided integrated semiconductor laser arrays", Appl. Phys. Lett., 44(4), pp.389-391, 1984.

7. K.A. Shore: "Radiation patterns for optically steered semiconductor laser-beam scanner", Appl. Opt., Vol.23, pp.1386-1390, 1984.

8. D.R. Scifres, W. Streifer and R.D. Burnham: "High-power coupled-multiple-stripe phase-locked injection lasers", Appl. Phys. Lett., 34(4), pp.259-261, 1979.

9. D.E. Ackley: "High power multiple-stripe injection lasers with channel guides", IEEE J. Quantum Electron., Vol. QE-18, pp.1910-1917, 1982.

10. J. Katz, E. Kapon, C. Lindsey, S. Margalit and A. Yariv: "Far-field distributions of semiconductor phase-locked arrays with multiple contacts", Electron. Lett., Vol.19, pp.660-662, 1983.

11. J. Katz, E. Kapon, C. Lindsey, S. Margalit, U. Shreter and A. Yariv: "Phase-locked semiconductor laser array with separate contacts", Appl. Phys. Lett., 43(6), pp.521-523, 1983.

APPENDICES

Appendix A

The finite difference technique was used to solve the non-linear diffusion equation in chapter (VI). The set of non-linear algebric equations obtained was solved using the Newton-Raphson over-relaxation method. In this iterative technique, consider a set of non-linear equations $f_\ell(N) = 0$. Representing equation (6.3-4) for each node, the solution for the carrier density, N , is found using:

$$N^{i+1} = N^i - \theta' \left[\frac{f_\ell(N^i)}{\partial f_\ell(N^i)/\partial N} \right] \qquad \text{(A-1)}$$

where θ' denotes the over-relaxation parameter, whose value can be adjusted between 1 and 2 in order to optimize the number of iterations. The actual value of θ' is dependent to a large extent on the degree of non-linearity in the problem. If θ' is equal to 1 it becomes an ordinary Newton-Raphson technique. i represents the i^{th} iteration and ℓ represents the node number along the junction.

Equation (A-1) is solved iteratively for each node until an acceptably small error ($\Delta_1 = 10^{-4}$) is achieved for the absolute global change between successive iterations.

Having determined the carrier density at the heterojunction using this technique, equation (6.2-12) is used to find the potential distribution along the heterojunction, $V(\ell)|_{new}$. This potential is then compared with the estimated potential distribution found in step 1 (chapter VI). The estimated potential at each node along the junction is now modified to form a new estimate using the relationship:

$$V(\ell)|_{nest} = V(\ell)|_{est} + \Theta V(\ell)|_{new} \qquad \text{(A-2)}$$

where Θ is the under-relaxation parameter whose value is adjusted between 0.5-0.6 in order to obtain a stable numerical solution. With the improved estimates of potential along the junction steps 1 and 2 (chapter VI) are repeated to obtain the self consistent solution. This process is repeated until the estimates of both $N(\ell)$ and $V(\ell,m)$ differ by only an allowed small error between successive complete iteration cycles, for all the nodes. The iterations are finally stopped when the following stringent criterion is met:

$$\sum_{\ell=0}^{\ell=L} \left| V^{i}(\ell)\big|_{nest} - V^{i+1}(\ell)\big|_{new} \right| \leq \Delta_2 \qquad \text{(A-3)}$$

where Δ_2 is the acceptable error, typically $1x10^{-4}$ or less, and i is the i^{th} iteration. Double precision computation was used throughout.

The choice of the allowable global error between iterations only shows that the solutions are accurate enough for the mesh size chosen. Prior to presenting a full set of solutions to the twin stripe problem a trial problem was solved repeatedly as a function of the mesh size to check the accuracy of the technique. It was found from this preliminary check that a mesh size of h_x = 0.3 μm and h_y = 0.1 μm provided an accurate solution, without placing unnecessary burdens on the storage requirements of the computer.

Appendix B

The "shooting method" of solution applied to boundary value problems

The optical model of the laser requires a solution to the second order differential equation.

$$d^2\psi/dx^2 + \{k^2\tilde{\varepsilon}_{eff}(x) - \tilde{\beta}^2\}\psi = 0 \qquad \text{(B-1)}$$

subject to the boundary condition $d\psi/dx = 0$ at each end nodes of the region under consideration. The problem is a standard eigenvalue problem which results in a set of solutions $\psi_1(x)$, $\psi_2(x)$, $\psi_3(x)$ etc. representing the lateral distributions of the optical modes corresponding to the discrete values of $\tilde{\beta}$ for which the solution is valid. In the technique an initial value solution technique, using the boundary conditions at one edge of the region as an initial condition, is applied iteratively until the solution at the other boundary satisfies that boundary condition.

Let the region of interest, $0 \leqslant x \leqslant h_x(M - 1)$ be discretised into $(M - 1)$ elements each of length h_x. At the boundary nodes it is assumed that the boundary conditions:

$$(d\psi/dx)\big|_{x=0} = (d\psi/dx)\big|_{x=h_x(M-1)} = 0 \qquad \text{(B-2)}$$

exist.

In this problem it is also reasonable to assume that the optical field has also decayed to a small value at the initial node corresponding to $x = 0$ i.e. $\psi_m \simeq 10^{-3}$.

If the solution of the m^{th} mode at the ℓ^{th} node is known or may be assumed to have a value, $\psi_m(\ell)$, then the solution of the m^{th} mode at the next node along, $\ell + 1$ may be obtained to a first approximation by:

$$\psi_m(\ell + 1) = \psi_m(\ell) + h_x\psi_m'(\ell) \qquad \text{(B-3)}$$

where $\psi_m'(\ell) = \{d\psi_m(\ell)/dx\}$

Equation (B-3) may be applied to each node in turn. However, it is necessary to know $\psi_m'(\ell)$ at each node. This may be evaluated from a difference version of the wave equation (B-1) as follows:

$$\frac{d^2\psi_m}{dx^2} = \frac{d\psi_m'}{dx} \simeq \frac{\psi_m'(\ell+1) - \psi_m'(\ell)}{h_x} = -\{k^2\tilde{\varepsilon}_{eff}(\ell+1) - \tilde{\beta}_{mo}^2\}\psi_m(\ell+1) \qquad \text{(B-4)}$$

where $\tilde{\beta}_{mo}$ is the initial guess of the value of $\tilde{\beta}$ appropriate to the m^{th} mode. Thus $\psi_m'(\ell+1)$ may be calculated as:

$$\psi_m'(\ell+1) = \psi_m'(\ell) - \{k^2\tilde{\varepsilon}_{eff}(\ell+1) - \tilde{\beta}_{mo}^2\}\psi_m(\ell+1)h_x \qquad \text{(B-5)}$$

The problem is started at the first node $\ell = 1$ (i.e. $x = 0$). The boundary condition assumed is that $\psi_m'(1) = 0$ and $\psi_m(1) = 1x10^{-3}$(say). $\tilde{\varepsilon}_{eff}(2)$ can be calculated from expression (7.2.2-2). As a consequence $\psi_m(2)$ may be calculated from equation (B-3) and $\psi_m'(2)$ may be calculated from expression (B-5). This is required to calculate $\psi_m(3)$ from equation (B-3). This interpolation procedure is carried out for each node. In this way at the other end node, $\ell = M$ (i.e $x = (M-1)h_x$), the calculated value of $\psi_m'(M)$ becomes:

$$\psi_m'(M) = \psi_m'(M-1) - \{k^2\tilde{\varepsilon}_{eff}(M) - \tilde{\beta}_{mo}^2\}\psi_m(M)h_x \qquad \text{(B-6)}$$

which may then be compared with the known boundary condition at this point, namely $\psi_m'(M) = 0$. This is the second of the two boundary conditions required to solve the second order differential equation.

If calculated boundary condition does not agree within the acceptable tolerance a new value of $\tilde{\beta}$ is chosen, $\tilde{\beta}_{m1}$, and the set of calculations repeated. If $\psi_m'(M)$ does not satisfy the boundary condition for this new

value of $\tilde{\beta}$ then a further estimate of $\tilde{\beta}$ is made using the following strategy:

$$\frac{\Delta\psi_m'(M)}{\Delta\tilde{\beta}} = \frac{\psi_m'(M)\big|_{\tilde{\beta}=\tilde{\beta}_{mo}} - \psi_m'(M)\big|_{\tilde{\beta}=\tilde{\beta}_{m1}}}{\tilde{\beta}_{mo} - \tilde{\beta}_{m1}} \tag{B-7}$$

and

$$\tilde{\beta}_{m2} = \tilde{\beta}_{m1} - \left[\frac{\psi_m'(M)\big|_{\tilde{\beta}=\tilde{\beta}_{m1}}}{\{\Delta\psi_m'(M)/\Delta\tilde{\beta}\}}\right] \tag{B-8}$$

From this point the new estimate of $\tilde{\beta}$ is made automatically by expression (B-8) and the entire set of calculations for $\psi_m(x)$ are repeated until the boundary condition at node M is satisfied. Clearly only discrete values of $\tilde{\beta}$ allow a solution for $\psi(x)$. The technique is insensitive to the boundary locations and is efficient. It is necessary, however, to ensure that h_x is small relative to any perturbations in $\psi(x)$ to ensure that compounding computational errors are small at the end node relative to the allowable tolerance.

The technique is applied to each mode in turn. The value of $\tilde{\beta}_{mo}$ and $\tilde{\beta}_{m1}$ required for initial conditions are estimated from the corresponding eigenvalue in the eigen spectrum of the finite difference solution discussed in section (7.3) expression (7.3-2). The modes of interest are the modes with the positive imaginary parts occuring in a decreasing order. Further, only excited modes where $2\mathrm{Im}(\tilde{\beta})$ = cavity loss, survive and these, obviously, are the ones of interest.

Appendix C

The strategy for adjusting S_o to achieve the threshold condition

In section (7.2.2) it was described how the optical model of the laser couples to the continuity equation in the active layer via the stimulated recombination term. However, optical modes are only supported if the modal gain is equal to the total cavity loss for that mode. A critical parameter in coupling of the two equations is the photon density, S_o. If the initial guess of the photon density gives value for the considered modal gain larger than the cavity loss then expression (7.2.2-6) suggests that the local gain, $g(x)$, and hence carrier density must be reduced in order that condition (7.2.2-5) is satisfied. To achieve this the value of the initial estimated photon density must be increased further so that the carrier density (and hence modal gain) is depressed by stimulated recombination. Similarly if the initial guess for S_o gives a modal gain less than the cavity loss then a new guess below the initial value must be chosen to reduce the stimulated recombination term. If the two separate guesses of photon density are S_o and S_o' and result in modal gains G_o and G_o' respectively then the new estimate for photon density S'' can be determined using the following strategy:

$$\frac{\Delta S_o}{\Delta G_o} = \frac{S_o - S_o'}{G_o - G_o'} \qquad \text{(C-1)}$$

The new estimate of the photon density thus becomes:

$$S'' = S_o - \frac{\Delta S_o}{\Delta G_o} \times (G_o - C_{loss}) \qquad \text{(C-2)}$$

where C_{loss} is the cavity loss.

Thus all that is necessary to automate the correct selection of the value S_o is to supply two initial estimates of the photon density and calculate the two corresponding modal gains from which expression (C-2) may be applied in an iterative form until the estimates of S_o relax to within a specified tolerance and $G_o \simeq C_{loss}$.